New oxide based materials for catalytic applications

Shin, Rodney Foo Kok

Award date:
2007

Awarding institution:
University of Bath

New oxide based materials for catalytic applications

Rodney Foo Kok Shin

A thesis submitted for the degree of Doctor of Philosophy

University of Bath

Department of Chemical Engineering

June 2007

ProQuest LLC
789 East Eisenhower Parkway
P.O. Box 1346
Ann Arbor, MI 48106-1346

Acknowledgements

I would like to thank my parents and family for their support throughout my studies. My PhD supervisor, Dr. Dmitry Lukyanov for his guidance and supervision. Tanya Vazhnova from the University of Bath for her invaluable advice and training in experimental techniques.

The Autocatalyst group at Johnson Matthey Technology Centre, Sonning Common for the positive and rewarding work experience to obtain the necessary catalytic data along with fruitful discussion of results and feedback. In particular, Paul Millington, Raj Rajaram, Jillian Bailie, Valerie Houel, and Stan Golunski.

Serennah Longworth and Hoi Jobson from JMTC for providing the TEM and XRD characterisation results.

The Department of Chemical Engineering, University of Bath and Johnson Matthey Plc for funding and providing the resources to conduct my research. MEL chemicals (UK) for providing the zirconium hydroxide used in this project.

I would also like to thank the staff and postgraduates at the Department of Chemical Engineering, University of Bath who tirelessly helped me with my PhD studies. Namely, Dmitry Bavykin, Chin-Chi Tai and Brendan Darragh.

Last but not least, my friends and colleagues who have put up with my questions and supported me throughout my studies.

Abstract

The development of solid acids catalysts is an active area of research in particular to synthesise solid acid catalysts that have high thermal stability and are active for various acid catalysed applications. This study identifies promising mixed oxide solid acid catalytic supports that are suitable for further development as solid acid catalysts. Tungsten oxide supported on zirconia (WO_3/ZrO_2) was selected as one of the most promising catalytic supports based on its high numbers of acid sites and good thermal stability. The WO_3/ZrO_2 support was characterised by IR spectroscopy, XRD and TEM where different zirconium hydroxide precursors were used and the tungsten oxide loading was varied. It was shown that the acidity of the WO_3/ZrO_2 support could be altered to tailor the desired catalytic application by changing the calcination temperature, tungsten oxide loading and the zirconium hydroxide precursor used.

The WO_3/ZrO_2 catalytic support was used to synthesise a new active catalyst for the selective catalytic reduction of nitrogen oxides by ammonia (NH_3 SCR of NO_x). Iron promoted tungsten oxide zirconia catalysts ($Fe/WO_3/ZrO_2$) were shown to be active for NH_3 SCR and hydrothermally stable with the activity that was comparable or better than the reference Fe/beta catalysts. The synthesis methods, tungsten oxide and iron loading as well as the calcination temperature were investigated using two different WO_3/ZrO_2 supports. The catalysts and supports were characterised by IR spectroscopy in order to investigate the origin of NH_3 SCR activity of $Fe/WO_3/ZrO_2$ catalysts. New Fe^{3+} Lewis acid sites (LAS) were identified as the active sites on the catalysts where the SCR activity of the catalysts can be linked to the number of Fe^{3+} LAS present on those catalysts. The Bronsted acidity was enhanced by the presence of iron and was also found to influence the SCR activity.

Table of Contents

List of Tables

List of tables

List of figures

List of figures

Chapter 1:
Introduction

Chapter 1: Introduction

Acidic materials can act as catalysts for a range of reactions such as isomerisation, cracking, hydrocracking, dehydration, alkylation, acylation and so on [1]. Homogenous or liquid acids have been widely used for these reactions, for example, $AlCl_3$, $FeCl_3$, H_2SO_4, $TiCl_4$ and CF_3SO_3H. However, liquid acid catalysts have several disadvantages in industrial applications primarily due to corrosion, difficulty in catalyst recovery and pollution of waste water streams [2].

The development of heterogenous or solid acid catalysts is an active area of research as the catalysts potentially have several advantages over liquid acids. Solid acid catalysts would be easier to handle and store, possibility of regeneration and reutilisation of the catalyst, less corrosive and ease of separation from the reaction mixture that allows continuous operation [1]. This creates a strong environmental and economic incentive to use solid acid catalysts in commercial processes.

Solid acids have been extensively studied and are widely used in the chemical and petrochemical industries as catalysts or sorbents. Some examples of solid acid catalysts currently in use in such reactions as isomerisation, polymerisation and alkylation are alumina silica, iron oxides and sulphated zirconia [3]. There have been several approaches to synthesis of solid acid catalysts and the most frequently used techniques are listed below [2]:

- Liquid acids mounted on solid supports
- Aluminium halide – combination with metal salt
- Sulphate ion promoted metal oxides
- Zeolites
- Mixed oxides

Studies were initially focused on either physically or chemically binding liquid acids onto solid supports. Catalysts were successfully synthesised despite the

considerable difficulties, and extensive patent literature is available in this area [1, 2]. Although the catalysts were very active, they had relatively short lifetimes and suffered from rapid deactivation [1, 4].

The second class of solid acid catalysts, mixtures of aluminium halides with metal salts such as $AlCl_3/Ti_2(SO_4)_3$, $AlCl_3/CuSO_4$, $AlBr_3/Ti_2(SO_4)_3$ and $AlCl_3/CuCl_2$ have been reported to be active for isomerisation of alkanes at room temperature up to 110 °C by Ono and co-workers [5, 6] but are limited in their applications due to their sensitivity to the presence of water. Metal oxides promoted by sulphate ions such as ZrO_2/SO_4, TiO_2/SO_4, $FeSO_4$ and $Fe_2(SO_4)$ have been shown to be good catalysts for various acid-catalysed reactions [7-11]. The addition of sulphate ion enhances the catalytic activity by generating new acid sites and the increased acidity has been proposed to be linked to the formation of covalent S = O bonds in sulphur complexes formed on metal oxides [7, 8, 12, 13].

Unfortunately, the solid acid catalysts synthesised on the basis of the methods noted above generally do not possess acidity levels that are comparable to those present in liquid acid catalysts; consequently exhibit lower catalytic activities and selectivity. A higher reaction temperature may be required for the solid acid catalysts in order to achieve similar reaction rates observed with the liquid acid catalysts. However, the thermal stability of those materials is insufficient for them to be used as catalysts in many industrial processes.

On the other hand, zeolites are both thermally stable and possess acidity similar to those of liquid acids. Furthermore, they have been shown to be very good solid acid catalysts. However, they are generally unstable in the presence of water vapour at elevated temperatures that are frequently required in catalysis. De-alumination of zeolites occurs under these conditions that permanently deactivates the catalysts [14-16]. To address these limitations, the development of mixed oxides with two or more components are of significant scientific and commercial interest. The incorporation of a minor oxide component can enhance the thermal stability of the major component thus allowing it to be used at higher temperatures [17-19]. Mixed oxides also generally display acidity that is

significantly higher than those of either of the component oxides. Finally, the combination of the two oxides can also enhance their overall catalytic activity [13]. Mixed oxide materials have the potential to be developed as solid acid catalysts that can be applied in a wide variety of catalytic processes.

There are many acid catalysed reactions that could be used to estimate the catalytic activity of the solid acid mixed oxide catalyst, ranging from cracking, alkylation to isomerisation of hydrocarbons. The selective catalytic reduction of nitrogen oxides by ammonia (NH_3 SCR of NO_x) was selected as a test reaction as it requires high numbers of strong acid sites and both thermal and hydrothermal stability. These are the main necessary properties of a potential commercial solid acid catalyst.

1.1 Aim of this project

The aim of this PhD study is to develop new mixed oxide solid acid catalysts that are thermally stable and exhibit high numbers of strong acid sites. To achieve this goal, the following objectives have been set for the catalytic support:

Thermally stable: Withstand temperatures up to at least 700 °C
High acidity : Acidity greater or equal to reference material

The catalytic support will be used to develop a catalyst that is active for the selected catalyst application which is the selective catalytic reduction of nitrogen oxides by ammonia (NH_3 SCR of NO_x) under lean conditions at temperatures between 150 °C and 550 °C. Titania doped with tungsten oxide (9 wt% WO_3/TiO_2) was selected as the reference material to be used for comparison of the acidity of the mixed oxide catalytic supports as WO_3/TiO_2 has been shown to be a promising catalyst support that possesses good acidity levels and is thermally stable. Furthermore, current commercial catalysts for NH_3 SCR of NO_x are also based on vanadium supported on tungsten titania ($V_2O_5/WO_3/TiO_2$). Various other commercial catalysts have also been synthesised from WO_3/TiO_2 catalytic supports, most notably EUROCAT [20].

1.2 Structure of the thesis

The thesis comprises of 9 main chapters that describes the development of the solid mixed oxide catalyst ($Fe/WO_3/ZrO_2$) for NH_3 SCR of NO_x. The summary below provides an outline of the structure of the thesis.

Chapter 1

- Introduction

Chapter 2

- Literature review of potential mixed oxide supports, characterisation techniques and the NH_3 SCR of NO_x reaction.

Chapter 3

- Experimental procedures

Chapter 4

- Selection of a suitable mixed oxide catalytic support based on the comparison of the acidity levels present on the supports.
- Detailed examination of the selected tungsten oxide supported on zirconia support.

Chapter 5

- Investigating the effects of precursors, tungsten oxide loading and calcination temperature on the acidic and structural properties of WO_3/ZrO_2 catalytic supports.

Chapter 6

- Detailed characterisation and catalytic testing of $Fe/WO_3/ZrO_2$ catalysts for NH_3 SCR of NO_x.
- Factors such as tungsten oxide and iron loading, synthesis procedures, effect of the calcination temperature and effect of hydrothermal aging are all investigated.

Chapter 7

- IR characterisation of $Fe/WO_3/ZrO_2$ catalysts with CO to examine the active metal (Fe) component.

Chapter 8

- Concluding remarks on WO_3/ZrO_2 as a catalytic support.
- Conclusions regarding $Fe/WO_3/ZrO_2$ as a catalyst for NH_3 SCR of NO_x.

Chapter 9

- Recommendations for future research.

Chapter 2: Literature review

Chapter 2: Literature review

This chapter summarises the relevant information in the literature regarding identification and synthesis of solid acid mixed oxide catalysts. The charge imbalance theory that was used to select suitable mixed oxide supports is described along with the materials that were of particular interest for the development of new solid acid mixed oxide catalysts. The infrared characterisation that was used extensively in this work is also described along with the selected test reaction, the selective catalytic reduction of nitrogen oxides by ammonia.

2.1 Definition of acidity

A solid is said to be acidic when it changes the colour of a basic indicator or if a base is chemically adsorbed onto the solid. The acid strength of a solid is the ability of the solid surface to convert an adsorbed neutral base into its conjugate acid. Acidity is generally defined as the amount of acid on a solid which is usually expressed in terms of the number of acid sites in μmol per unit weight (μmol/g) or unit surface area (μmol/m^2) of the solid. There are two main classifications of acidity, namely Broensted and Lewis acidity.

Broensted acidity is where the acid acts as a proton donator. The reaction takes place by proton transfer from the solid surface to the adsorbate. Broensted acidity will usually exist as hydroxyl groups where the H^+ ion can be easily dissociated. On the other hand, Lewis acidity is when the acid acts as an electron pair acceptor and the reaction proceeds by means of electron pair transfer from the adsorbate to the solid surface.

2.2 Charge imbalance theory

Tanabe [21] proposed a theory that predicts which combinations of binary oxides will exhibit acidic properties (either Broensted or Lewis acidity) and also provide

insight regarding the structure of the acid sites. This hypothesis suggests that generation of acid sites are due to a charge imbalance caused by an excess of negative or positive charge generated when a dopant ion is introduced into a host oxide lattice. The total number of acid sites formed is estimated by the amount of excess charge generated and the positive or negative charge would indicate whether it will be predominantly Lewis or Broensted acidity. The structure of the binary oxide is in turn modelled according to two postulates:

- The coordination number of both the host and dopant metal ion is maintained on mixing.
- The coordination number of the oxide ion of the host is retained on mixing.

An example is given in Fig. 2.2.1 based on silica titania, SiO_2/TiO_2, where TiO_2 is the major host component and silica is the dopant ion. According to the two postulates described previously, the coordination numbers for the positive metal ions remain 6 for Ti and 4 for Si whereas the negative oxide ion will be 3. The 4 positive charges of the silicon atom are distributed across 4 bonds while the 2 negative charges of the oxygen are distributed over 3 bonds. The difference in charge for one bond would be, +4/4 – 2/3 = +1/3 and for all the bonds, +1/3 * 4 = +4/3 is the excess charge. In this example, Lewis acidity is assumed to be generated due to the presence of an excess positive charge.

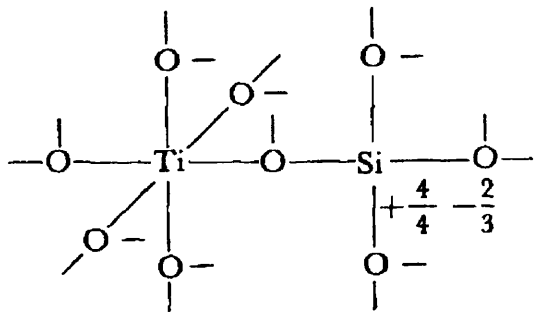

charge difference : $\left(+\frac{4}{4}-\frac{2}{3}\right)\times 4=+\frac{4}{3}$

Fig. 2.2.1. Model structures and acidity generation calculation of SiO_2/TiO_2 according to Tanabe charge imbalance theory (adapted from [22]).

Although there are other models that predict the potential acidity of binary oxides, the validity of Tanabe's hypothesis determined by experimental work was shown to have an accuracy in the region of 91% [22]. It should be noted that Tanabe's charge imbalance model can only be applied to chemically mixed binary oxides and does not hold true for mechanically mixed oxides. Furthermore, this model can only be used to determine how acidic the binary oxide mixtures will be and whether it will generate Lewis or Broensted acidity. The model cannot determine the strength of the acid sites generated.

However, the acid site strength can be predicted based on the correlation where the acid site strength has been found to increase with greater averaged electronegativities [21] as shown in Fig. 2.2.2. This correlation is useful for predicting the acid site strength of unknown binary oxides where the electronegativity controls the acid site strength.

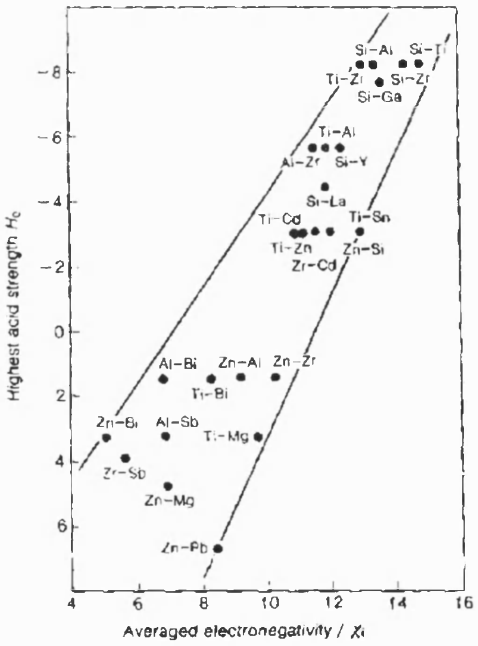

Fig. 2.2.2. Correlation between the acid site strength and averaged electronegativity for metal ions of binary oxides assuming a 1:1 molar ratio (reproduced from [21]).

The charge imbalance theory and averaged electronegativities was used to determine which mixed oxides will generate high numbers of strong acid sites. The major host components examined were silica, alumina, titania and zirconia as these materials have been shown to be very promising [1, 2, 21, 23]. A range of dopant ions were studied including WO_3, Fe_2O_3, V_2O_5, La_2O_3, Y_2O_3, MoO_3 and Mn_2O_3. Based on the calculations, the 10 most promising materials were identified and shown in Table 2.2.1.

Table 2.2.1. The ten most promising materials based on Tanabe's charge imbalance theory.

Material	Tanabe Acidity	Type	Electronegativity
WO_3/ ZrO_2	+3	L	14.5
WO_3/Al_2O_3	+3	L	14.35
WO_3/TiO_2	+2	L	14.1
V_2O_5/ZrO_2	+2.5	L	13.65
V_2O_5/TiO_2	+1.67	L	14.1
V_2O_5 /Al_2O_3	+2.5	L	13.5
TiO_2/SiO_2	-2	B	13.5
AlO_3/SiO_2	-3	B	13.25
Fe_2O_3/SiO_2	-3	B	13.25
Mn_2O_3/SiO_2	-3	B	13.25

An interesting material that was not listed in Table 2.2.1 is SiO_2/ZrO_2, as it had one of the highest Tanabe acidity values calculated (-4) but a low electronegativity value of 13.05. This would be an interesting sample as it should theoretically possess a large number of Broensted acid sites although it will most likely have weaker acid sites than the materials listed in Table 2.2.1. These results along with additional promising mixed oxide catalytic supports supplied by Johnson Matthey were used as the basis for determining promising materials for further development.

2.3 Acidity characterisation techniques

The following sections describe the common methods used to characterise the acidity levels of a sample and the results reported in the literature are often based on these techniques. Infrared spectroscopy is described in greater detail as this is

the primary technique used in this project for acidity characterisation based on the advantages provided by this method (see Section 2.4).

2.3.1 Amine titration

This method is carried out through the use of suitable indicators, which undergo a colour change as they are adsorbed onto the solid acid surface [1, 2, 24, 25]. The acid site strength can be determined by comparing the colour change of specific indicators to those reported in the literature, which will give a corresponding pK_a value thus providing an indication of acid site strength. The amount of acid sites on the solid surface can be calculated by amine titration after the acid strength has been determined.

The advantage of this methodology is that the amount of acid sites at various acid strengths can be determined. However, this method cannot differentiate between Broensted and Lewis acidity, since the acidity exhibited will be due to the sum of both Broensted and Lewis acid sites. Furthermore, this procedure is problematic with dark coloured samples as colour changes will be difficult to observe.

2.3.2 Gaseous base adsorption

The volume of gaseous base that the solid acid adsorbs measures the numbers of acid sites present [25]. The acid strength is determined by evacuation of the adsorbed bases from the acid sites at elevated temperatures. Bases that have adsorbed onto strong acid sites will be more stable than those adsorbed onto weaker sites. Thus the proportion of adsorbed bases evacuated at various temperatures will give an indication of the acid site strength.

This procedure is generally carried out by temperature programmed desorption (TPD) of basic molecules such as ammonia and pyridine. This technique can be used to determine the amount of acid sites for a solid at high temperatures or under its actual working conditions, and can be applied to coloured samples.

However, quantitative numbers of Lewis or Broensted acid sites cannot be determined and only the total number of acid sites can be calculated [22].

2.3.3 Catalytic testing

Another useful approach to get an indication of the acidity and acid site strength is through the catalytic activity of the solid acid even though the differentiation between acid site strength and number of acid sites is difficult from the measurement of catalytic activity for an acid catalysed reaction [21]. The activity for the dehydration of isopropyl alcohol or the isomerisation of butene in the presence of excess air has been reported to be a good measure of acidity [26].

A good correlation has been found between the acidity measured by gaseous adsorption and that of the catalytic activity of the two reactions described above. The catalytic activity in the reaction of skeletal isomerisation of n-butane to iso-butane has also been used to test solid acid catalysts [21].

2.3.4 General statement

All three methods described previously share a common disadvantage in that, they cannot distinguish between Broensted and Lewis acid sites (BAS and LAS). The number and strength of the acid sites determined are equivalent to that of the sum of Broensted and Lewis acid sites. In order to gain a deeper understanding of the characteristics and behaviour of solid acids, it is often necessary to distinguish between the two acid types. Characterisation using infrared spectroscopy with pyridine as the probe molecule is extensively used and considered to be one of the most reliable methods, although many other methods have been proposed to distinguish between Broensted and Lewis acid sites [22].

2.4 Infrared spectroscopy

Infrared spectroscopy is based on the absorption by the sample of energy in the form of a beam of electromagnetic radiation (EMR) in the infrared region [24, 25]. When the sample molecules absorb energy they undergo a transition from one vibrational energy state to another. These vibrational motions of a molecule occur at a certain frequency that is characteristic of the molecule and of that particular vibration. The energy involved in a particular vibration is related to several factors including the strength of the bond, mass of the atoms and type of vibrations.

The frequency of the EMR required to cause a transition for a particular vibration is equal to the frequency of that vibration, thus the vibrational frequencies can be determined by measuring the frequencies of the EMR which are absorbed by the molecule. An IR spectrum is displayed as a plot of the energy of the IR radiation in wavenumbers against the percentage of light absorbed by the sample.

The spectrum of the sample appears as a series of broad absorption peaks of variable intensity where each peak provides some piece of structural information. The absorption peak in the spectrum corresponds to a vibrational transition within the molecule, and gives a measure of the frequency at which the vibration occurs. These peaks can be assigned to their characteristic interactions and the intensities will give an indication of the quantity present on that sample.

The sample has to directly absorb energy at a particular vibrational mode; in order for IR spectroscopy to work for a given sample, it has to be associated with changes in the dipole moment. In order to overcome this limitation, probe molecules that interact with the sample are used and this allows the sample to be characterised by infrared spectroscopy. Different probe molecules are used for specific identification. For example, carbon monoxide (CO) is used to determine the presence of platinum (Pt), and pyridine is used as the probe molecule to determine the number and strength of the acid sites present.

The interaction with the probe molecule can lead to the formation of a complex between the acidic hydrogen on the catalyst surface and a base (probe molecule). The strength of this hydrogen bonding can be determined by IR spectroscopy and is taken as a measure of the acid site strength [27-29].

Infrared spectroscopy studies of the adsorption of ammonia or pyridine on solid surfaces make it possible to distinguish between Broensted and Lewis acid sites and to assess their amounts independently. The IR bands corresponding to pyridine co-ordinately bonded to Lewis acid sites are very different from that of pyridinium ion formed by adsorption onto Broensted acid sites (Table 2.4.1). This fact permits differentiation between acid types on the surface of a solid acid.

Table 2.4.1. Infrared bands of pyridine adsorption on solid acids in the 1400 – 1700 cm^{-1} region. (reproduced from E. P. Parry [30])

Hydrogen bonded pyridine	**Co-ordinately bonded pyridine**	**Pyridinium ion**
1400-1447 (vs)	1447-1460 (vs)	1485-1500 (vs)
1485-1490 (w)	1488-1503 (v)	~1540 (s)
1580-1600 (s)	~1580 (v)	~1620 (s)
	1600-1633 (s)	~1640 (s)

Band intensities: vs – very strong, s – strong, w – weak and v – variable.

2.5 Acid – base pair sites

The acidity of a sample is not the only important parameter as basic sites may also play a role in catalytic reactions. Even in reactions, which have been widely recognised to be catalysed only by acid sites on the catalytic surface, basic sites can also act more or less as active sites in cooperation with the acid sites. The catalysts that possess suitable acid – base pair sites sometimes show pronounced catalytic activity, even if the acid – base strength of that bifunctional catalyst is much weaker than the acid or base strength of a simple acid or base.

For example, zirconium oxide, ZrO_2, is both weakly acidic and basic but shows higher activity for C – H bond cleavage than highly acidic SiO_2/Al_2O_3 or highly basic MgO [22]. The cooperation of acid sites with basic sites can be quite strong for certain reactions and results in highly selective reactions. The concept of acid – base bifunctional catalytic properties of ZrO_2 has been reported by Tanabe [22] with phenol adsorption and Xu et al. [31] on formation of nitriles from alkylamines. This makes ZrO_2 an interesting metal oxide to be studied for use as a potential catalyst support.

2.6 Zirconium oxide

Zirconium oxide has attracted much attention in the past few years in particular in the field of catalysis. The catalytic applications of zirconium oxide are quite promising as it possesses both acidic and basic properties [32] as well as high thermal stability. Several authors have reported on the application of zirconium oxide as either a catalyst or catalytic support [33-35]. Specifically, zirconium oxide has been shown to be active for paraffin isomerisation [36], CO/CO_2 hydrogenation [37, 38], alcohol dehydrogenation [39, 40] and hydrogenation of carboxylic acids [41].

In order for zirconium oxide to be used commercially in catalytic applications, it has to possess high surface area, large pore-size with well developed pore structures and good thermal stability. The primary zirconium precursor used is hydrated zirconium hydroxide, $ZrO_x(OH)_{4-x}$, in the form of an amorphous powder. When it is treated in air above 450 °C hydrated zirconium hydroxide converts to crystalline zirconium oxide, ZrO_2, with 3 main structures.

- Monoclinic – stable up to 1200 °C
- Tetragonal – stable up to 1900 °C
- Cubic – stable above 1900 °C

In addition, a metastable tetragonal phase has been found that remains stable up to 650 °C [33]. There have been many proposals as to why this metastable

tetragonal form of zirconium oxide may exist at this low temperature such as matrix constraints [42], grain morphology [43], impurity effect such as due to the presence of Fe^{3+} [44], type and amount of stabilisers and crystallite size effect [45]. The last two points will be discussed with emphasis on the use of metal oxides as stabilisers.

The crystalline phase of ZrO_2 is strongly influenced by the precursors used, synthesis method and calcination temperature [46] which affects the amount of tetragonal ZrO_2 crystallites formed. Monoclinic ZrO_2 is the thermodynamically stable crystal structure for crystallites larger than 10 nm at temperatures below 1170 °C [47]. However, metastable tetragonal ZrO_2 crystallites smaller than 10 nm will often form even after oxidation at temperatures that are slightly higher than the ZrO_2 crystallisation temperature (approximately 450 °C).

ZrO_2 crystallites sinter and exist predominantly as monoclinic structures with a small percentage in the metastable tetragonal phase when treated at temperatures above 627 °C regardless of the precursor or synthesis method used [48-50]. However, pure tetragonal ZrO_2 crystallites can be stabilised by impregnating ZrO_2 with metal oxides prior to high temperature treatment and there are many metal oxides that will inhibit ZrO_2 crystallite sintering at high temperatures [33].

The metal oxides are strongly bound at the zirconium oxide surface which inhibits the intercrystallite sintering by reducing the rate of ZrO_2 surface diffusion [51]. However, at too high temperatures, the effectiveness of the metal oxides are reduced as they sinter and form bulk clusters which can decompose and desorb. The metal oxides that agglomerate into bulk clusters are in a different phase that interacts poorly with the zirconium oxide and are not catalytically active. The metal oxides used in this project to stabilise zirconium oxide are discussed in the following sections.

2.7. Sulphated zirconia

Sulphate, although not a metal oxide, is one of the most widely used dopant ions for modifying acidic and textural properties of solid oxides. The enhanced surface acidity and possible superacid catalytic properties in the case of pure zirconium oxide are widely recognised [52-54]. The effects of sulphate species on the acidic properties of silica zirconia mixed oxides [17] and transition metal promoted sulphated zirconia have also been reported [55, 56].

Furthermore, sulphation may also influence the onset temperature of crystallisation of zirconium oxide [57] that will affect its thermal stability. The main problem associated with sulphated zirconia is that the SO_4 species decomposes and desorbs at relatively low temperatures of around 600 °C to form volatile SO_2 and SO_3 products in air and H_2SO_4 when water is present. This leads to rapid sintering of the zirconium oxide support and permanent loss of acidity above 600 °C [58]. This loss of sulphate groups occurs during the process of calcination, catalysts regeneration or reduction. In addition, the relative ease of deactivation by coke formation and potential poisoning of the active metals caused by sulphate reduction under reducing environments [58] potentially make sulphated zirconia unsuitable for the intended applications of this research which requires good thermal stability up to at least 700 °C.

2.8 Silica zirconia

Zirconium oxide dispersed on high surface area and thermally stable supports such as alumina or silica have been subjected to investigation by different researchers [53-56, 59]. It was found that inexpensive high surface area and thermally stable supports that retain the unique acidic – basic properties and redox characteristics of zirconium oxide can be produced by dispersing zirconium oxide on commercially available supports.

Miller and co-workers [60-62] have shown that even the introduction of small amounts of SiO_2 into ZrO_2 (SiO_2/ZrO_2) is sufficient to prevent surface area loss

and phase transformation of zirconium oxide from the tetragonal to the monoclinic phase. In addition, silica zirconia has been proven to be active in various acid catalysed reactions such as cyclohexanol dehydrogenation [63], dehydration and dealkylation reactions [13], selective formation of isobutane from isobutene [64] and alkane isomerisation [60, 61].

There are two main methods to synthesise silica zirconia supports, either by incipient wetness impregnation or sol-gel. Regardless of synthesis method, according to the work done by Anderson et al. [65] , there is approximately a linear increase in the number of LAS as the zirconium oxide concentration is increased. This is not unexpected as pure silica exhibits no Lewis acidity whereas pure zirconium oxide does [23, 65, 66], therefore there is a linear increase in the number of LAS with higher zirconium oxide content. Broensted acidity on the other hand, was found to reach a maximum at zirconium loading around 20 mol% which then decreased to a constant number with increasing concentration of zirconium oxide. These results are in agreement with Tanabe's postulations based on the charge imbalance theory [23].

The samples prepared by incipient wetness impregnation showed higher numbers of LAS then sol-gel derived samples due to the lack of mixing thus more ZrO_2 (Zr^{4+} sites) was exposed. These LAS are relatively weak in comparison to sol-gel derived samples. Samples prepared by incipient wetness impregnation also exhibited higher numbers of BAS. There are several hypothesis as to the method of Broensted acid site generation either by changes in electron density on Si due to charge imbalances [23, 61, 66] or differences in electronegativity [67, 68]. Another possibility is the weakening of the Si – OH bond generating BAS due to the introduction of zirconium into the vicinity of the hydroxyl carrying silicon.

Anderson et al. [65] has proposed that the distribution and arrangement of components at the surface rather than in the bulk should be considered when identifying sites for the generation of BAS rather than the charge imbalance model [23]. This would explain the higher numbers of BAS exhibited by impregnated samples compared to the sol-gel derived samples.

Overall, sol-gel derived samples exhibit higher surface area, catalytic activity and lower numbers but stronger acid sites in comparison to samples prepared by incipient wetness impregnation. Furthermore, there are many parameters that can be tuned during sol-gel synthesis to produce a suitable catalyst or catalyst support.

2.9 Tungsten oxide supported on zirconia

Tungsten zirconia (WO_3/ZrO_2) was first reported to be highly acidic by Hino and Arata [69] and based on Hammett indicators to be a superacid where the acid sites are stronger than 100% sulphuric acid. However, this method of characterisation is generally unreliable [70]. It was later shown that tungsten zirconia mixed oxides were not superacidic but did possess high number of strong acid sites [69, 71-74]. Coupled with its high thermal stability, resistance under H_2 and O_2 environments and in the presence of water made tungsten zirconia an interesting catalyst or catalytic support to investigate.

WO_3/ZrO_2 was shown to be an ideal catalysts for hydrocarbon isomerisation and alkylation processes [72, 73]. Arata and Hino [71] have also reported low temperature catalytic activity for n-pentane and n-hexane isomerisation. In general, WO_3/ZrO_2 has been shown to have catalytic activity comparable to that of SO_4/ZrO_2 in butene dimerization [75]. Barton et al. [76] had shown that WO_3/ZrO_2 was thermally stable based on thermal analysis at 1000 °C where no additional features that could be attributed to decomposition or loss of WO_x species was detected.

WO_3/ZrO_2 catalysts are still studied in order to understand the reasons behind the formation of numerous strong acid sites. It is still unclear how this occurs and there have been several proposals as to the method of acid site generation on WO_3/ZrO_2. Arata and Hino [71] have proposed that the strong acidity is associated with bidentate tungstate anions coordinated to the zirconia support similar to that proposed for sulphated zirconia supports.

On the other hand, Afanasiev et al. [77] suggested that several tungsten oxoanions surround a hydrated zirconium oxide group and the OH groups that are linked to the Zr atoms are responsible for the high acidity of WO_3/ZrO_2. This is illustrated below in Fig 2.9.1.

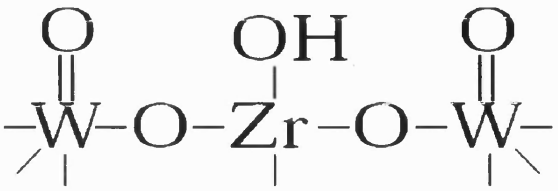

Fig. 2.9.1. Illustration of acid site generation on WO_3/ZrO_2. (adapted from [77]).

However, the above model does not agree with the results reported where tungsten oxide loadings above the monolayer coverage is required to generate highly acidic sites [73].

Barton et al. [76] have suggested that when the tungsten oxide loading exceeds that required for a single monolayer, it is assumed that domains of WO_x with distorted octahedral symmetry begin to grow [78] (based on work done using X-ray adsorption). These WO_x domains are said to be responsible for the formation of new acid sites as shown in Fig. 2.9.2.

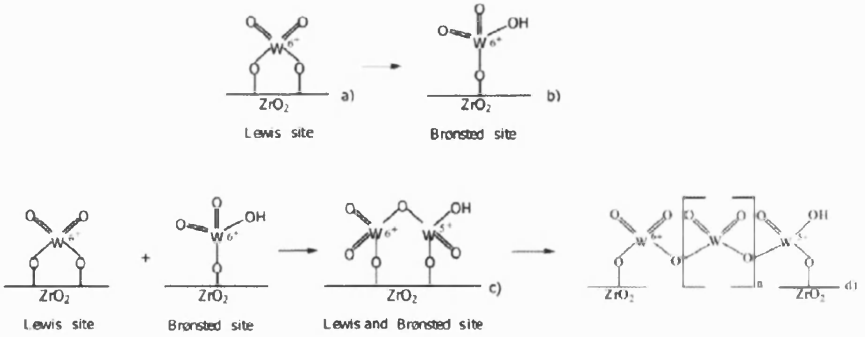

Fig. 2.9.2. Formation of acid sites on WO_3/ZrO_2, (a) Lewis acid site, (b) Broensted acid site, (c) formation of dimeric and (d) polymeric species obtained by condensation. (adapted from [79]).

It has been thought that the domain size of these centres increases with the surface density and good catalytic activity has been linked to intermediate sized WO_x domains on ZrO_2 as this size provides a compromise between reducibility and accessibility of the WO_x centres [80-82]. However, this model only considers that WO_x crystallites interact with ZrO_2 at the surface. On the other hand, Cortes-Jacome et al. [83] provided an alternative explanation that tungsten oxide and zirconium oxide form solid solutions stabilising the zirconium oxide in the tetragonal phase as seen when zirconium oxide is stabilised by Ca, Cu, Y, La or Ce [84, 85].

WO_3/ZrO_2 samples are produced using a variety of methods, most commonly, incipient wetness impregnation, co-precipitation or sol-gel. The typical calcination temperature varies from 800 – 900 °C depending on the level of tungsten oxide loading [81, 86]. It has been found that samples that are produced either by co-precipitation [73] or sol-gel [87] require higher calcination temperatures in comparison to those formed by incipient wetness impregnation of zirconium hydroxide [88].

This can be explained based on the assumption that the WO_x crystallites remain in the ZrO_2 bulk of the samples prepared by sol-gel and co-precipitation therefore stabilising the tetragonal structure, which would in turn require higher calcination temperatures in order to segregate the tungsten species from the bulk to the surface. On the other hand, it is assumed that all the tungsten species are already on the surface for impregnated catalysts. Co-precipitation and sol-gel manufactured catalysts have been shown to yield up to twice the acid site density compared to those prepared by incipient wetness impregnation [87].

Tungstate species form acid sites on the zirconium hydroxide support and inhibit zirconium oxide crystallite sintering and the tetragonal to monoclinic structural transformations by strongly influencing the $ZrO_x(OH)_{4-x}$ crystallisation into ZrO_2. Tungsten species on the surface of amorphous $ZrO_x(OH)_{4-x}$ delay crystallisation by binding to the nucleation sites and limiting the rate of ZrO_2 surface diffusion. These two factors are the key parameters required for crystallisation to occur [89].

The more nucleation sites that are blocked by increasing the tungsten oxide loading will require higher ZrO_2 surface diffusion rates in order to reach the exposed nucleation sites, which in turn raise the crystallisation temperature of ZrO_2. This has the additional effect of preventing rapid sintering of ZrO_2 crystallites and loss of surface area by the inhibition of ZrO_2 surface diffusion rates.

Barton et al. [76] studied the effect of the calcination temperature on the ZrO_2 content in the tetragonal phase. The tetragonal content of ZrO_2 decreases rapidly after calcination at temperatures above 527 °C. However, when tungsten species are present, ZrO_2 is effectively stabilised up to 800 °C (90% tetragonal for 8 wt% WO_3/ZrO_2 compared to 3% tetragonal for pure ZrO_2 at 800 °C).

The phase transition from the tetragonal to the monoclinic phase is not followed by a rapid increase in crystallite size for WO_3/ZrO_2 as both the tetragonal and monoclinic crystallites are similar and much smaller than those present in pure ZrO_2. This would suggest that the tungsten species are interacting strongly with ZrO_2 crystallites that inhibit sintering till higher temperatures. ZrO_2 crystallites size increases gradually with increasing calcination temperature till a critical crystallite size of 20 nm is reached.

Above this crystallite size, the tetragonal clusters become unstable and transform into monoclinic crystallites of the same size. However, crystallites from samples with tungsten oxide loading above 8 wt% will remain at approximately 16 nm in size. The tetragonal content of a given sample is also a function of the tungsten oxide loading. The tetragonal content increases with higher loading of tungsten and the level of monoclinic structures decrease. At 12 wt% tungsten or higher loadings no monoclinic structures can be detected and the crystallites are purely tetragonal.

Tungsten becomes ineffective at stabilising ZrO_2 after calcination at temperatures above 900 °C regardless of tungsten oxide loading [76]. This has been supported by surface area measurements where at calcination temperatures above 900 °C; the surface area reduces drastically and remains at the same constant value

regardless of tungsten oxide loading. In terms of WO_x crystallites, at high temperatures, the surface WO_x species agglomerate into monoclinic crystallites causing the reduction in the surface area. In this phase, they become less effective as sintering inhibitors and are no longer catalytic active.

The surface area of WO_3/ZrO_2 samples depends on the tungsten oxide loading. The surface area tends to increase with tungsten species concentration till a maximum is reached at tungsten oxide loadings around 8 wt% along with the tetragonal content for a given calcination temperature, which gives a tungsten surface density value of 5.0 W atoms nm^{-2}. This is below the theoretical monolayer capacity of 7.3 W atoms nm^{-2}; however, increasing the tungsten oxide loading above 8 wt% does not lead to any additional increase in the surface area.

This maximum surface area at submonolayer coverage could be as suggested by Barton et al. [76] due to there being only a fixed number of strong binding sites for metatungstate ions on zirconium hydroxide ($ZrO_x(OH)_{4-x}$). Any excess metatungstate ions (>8 wt% tungsten oxide loading) will only be weakly bounded and may also form bulk WO_3 clusters that are not effective at additional stabilisation of ZrO_2 crystallites.

The samples that contain these bulk WO_3 crystallites can be identified visually by their light yellow colour as opposed to the usual white colour [90]. This proposal that there is a maximum number of strong binding sites on a given zirconium hydroxide support has been supported by the work of Fuentes [76] who had removed the weakly bound WO_x species by washing with ammonium hydroxide solution leaving a maximum tungsten oxide loading of 8 wt%.

Shimizu et al. [91] reported that the increase in tungsten oxide loading increases the number of BAS but decreases the number of LAS. The range of tungsten oxide loading explored was between 2.5 wt% to 16.6 wt%. It is thought that WO_x species generates the BAS but the LAS are mostly due to existing LAS present on zirconium oxide. As mentioned previously in Section 2.8, pure zirconium oxide exhibits Lewis acidity. Thus as the surface coverage of tungsten

is increased, a reduction in the number of LAS occurs due to the lower number of exposed Zr^{4+} sites on the surface.

2.10 Iron as a catalyst promoter and active metal

Iron would be an interesting transition metal to use both as a dopant and as the active metal for NH_3 SCR of NO_x. Iron is widely recognised as a catalytic active metal for various types of reactions [92-95] with good dispersion when supported on zirconia based supports. The dispersion of Fe ions on various supports have been ranked as ZrO_2>Al_2O_3~TiO_2>MgO based on results from XANES and EXAFS analysis [96]. It has been suggested that those findings are most likely attributed to zirconium oxide dissolving the Fe_2O_3 species to form monoclinic or cubic solid solutions.

The dispersion of the active metal is an important factor since the stabilising interaction of the iron oxide species will depend on whether it is well dispersed and in intimate contact with the support or clustered in bulk structures [97]. Furthermore, it has been reported that the introduction of iron increases the acidity levels of zirconia based catalysts [98]. Iron will increase the number of BAS but reduce the level of Lewis acidity such that the total number of acid sites remains the same but the ratio of LAS/BAS decreases [99].

Santiesteban et al. [73] have also demonstrated that the introduction of a small amount of Fe onto WO_3/ZrO_2 catalysts enhances the Broensted acid site strength. However, the effect of iron as a promoter is still widely debated [100], where Srinivasan et al. [101] have reported that no changes in the number of acid sites occurred when sulphated zirconia was impregnated with iron. Furthermore, theoretically, the introduction of iron should increase the Lewis acidity instead of the Broensted acidity.

Not only does iron have the potential to enhance the acidity of zirconia based catalysts, it is also active for NH_3 SCR. Iron based catalysts synthesised from various supports such as pillared clays, mixed oxides and zeolites have been

reported to be active for NH_3 SCR of NO_x [102-112]. Furthermore, iron based catalysts are an environmentally benign and economical alternative to current NH_3 SCR catalysts that are based on vanadium supported on WO_3/TiO_2.

Indovina et al. [113] reported that FeO_x/ZrO_2 and $FeO_x/SO_4/ZrO_2$ catalysts were active for NO abatement with propene under lean conditions. The activity of the catalysts were found to be dependent on the reducibility of Fe^{3+} to Fe^{2+} and the sulphate species help stabilise Fe^{3+} species in $FeO_x/SO_4/ZrO_2$ catalysts. It is possible that tungsten species that are supported on zirconium oxide may have a similar role as the sulphate species.

It would be of significant interest to develop an iron promoted tungsten oxide supported on zirconia catalyst for NH_3 SCR of NO_x as iron interacts strongly with the zirconium oxide support that is stabilised by tungsten. Iron may also interact with tungsten based on the results reported for sulphated zirconia. The tungsten oxide supported on zirconia support is likely to possess good hydrothermal stability which is the primary problem encountered by new promising catalysts for NH_3 SCR of NO_x.

2.11 Selective catalytic reduction of nitrogen oxides by ammonia

Atmospheric pollutants like sulphur oxides (SO_x), nitrogen oxides (NO_x) and volatile organic compounds (VOCs) are of great environmental concern and a lot of work has been done to limit their emissions. Nitrogen oxide emissions are mainly produced from combustion processes by the oxidation of atmospheric nitrogen at high temperatures. The overall chemical reaction can be expressed as:

$$N_2 + O_2 \rightarrow 2NO$$

$$NO + \tfrac{1}{2} O_2 \rightarrow NO_2$$

The use of traditional technology such as wet sorption is limited in its use commercially for NO_x abatement due to its high costs. Therefore catalytic methods are used based on their low cost and high efficiency. To efficiently convert NO to N_2 a reducing agent has to be used where CO, hydrocarbons and ammonia have been used a reductant [114].

Selective catalytic reduction process offers the potential to remove NO_x species (NO and NO_2) in the presence of high concentrations of oxygen. The SCR process requires the use of nitrogen containing reducing agent such as ammonia (NH_3) or urea (NH_2CONH_2) or a hydrocarbon. The selective catalytic reduction of NO_x by ammonia is one of the best and most common method for NO_x abatement [115]. The overall NH_3 SCR of NO_x reaction can be described by the following reaction [116]:

$$4NO + 4NH_3 + O_2 \rightarrow 4N_2 + 6H_2O$$

Currently, the chemical aspects and, in particular, the reaction mechanism of NH_3 SCR of NO_x are still widely discussed and debated in the scientific literature. So far, research has been focused on titania based catalysts with V_2O_5, WO_3 and/or MoO_3 and many results have been published in the literature [117-123]. However, these studies occasionally do not permit comparisons with industrial NH_3 SCR catalysts since commercial working conditions are often not studied.

The catalysts developed in this PhD project will be tested under lean conditions that are identical to those used in industry at reaction temperatures between 150 °C and 550 °C. Fresh and aged catalysts will be tested to investigate the stability of those catalysts. Finally, the catalysts will also be characterised and analysed to identify the active sites.

Chapter 3: Experimental Procedures

Chapter 3: Experimental procedures

This chapter describes the experimental procedures used in the preparation and characterisation of the catalysts. There are two main sections, the first part regarding the materials and methods of synthesis. The second section contains details of characterisation techniques and catalytic testing of the catalytic supports and catalysts.

3.1 Catalyst Synthesis

The following section describes the preparation of the tungsten oxide supported on zirconia catalytic supports and iron promoted tungsten oxide supported on zirconia catalysts.

3.1.1 Preparation of hydrated zirconium hydroxide

Hydrated zirconium hydroxide, $ZrO_x(OH)_{4-x}$, is the most frequently used precursor for preparation of zirconium based mixed oxides and is commonly synthesised from two zirconium salt precursors, either zirconyl chloride or zirconium oxynitrate. In this project, zirconyl chloride, $ZrOCl_2.8H_2O$, was used as the procedure using zirconyl chloride was more widely used and better described in the literature [73, 80, 124].

The required mass of zirconyl chloride was weighed out in a beaker and the appropriate volume of water was added. In a typical preparation, 50g of zirconyl chloride was dissolved in 750ml of deionised water. This will synthesise approximately 25g of zirconium hydroxide. The solution was stirred using a magnetic stirrer and the pH of the solution was measured at regular intervals. The solid white zirconyl chloride powder dissolves readily into a colourless solution.

$$ZrOCl_2.8H_2O(s) + H_2O \rightarrow ZrOCl_2.8H_2O(aq)$$

pH: ~1

Stirrer Speed: 350 rpm

Temperature: Ambient

Ammonium hydroxide was added dropwise into the $ZrOCl_2.8H_2O$ solution until the pH reached 9.5. Generally around 60-80ml of NH_4OH was required per 50g of zirconyl chloride. Cloudy white gel-like $Zr(OH)_4$ precipitates are formed as soon as NH_4OH is introduced. As the reaction proceeds, the solution turns from clear to an opaque white solution and the stirrer vortex can no longer be clearly seen. At that point, the stirrer speed was increased to 600 RPM to improve mixing.

$$ZrOCl_2.8H_2O(aq) + NH_4OH(aq) \rightarrow ZrO_x(OH)_{4-x}(s) + NH_4^+(aq) + 2Cl^-(aq) + yH_2O(aq)$$

pH: 9.5
Stirrer Speed: 350 - 600 rpm
Temperature: Ambient

The pH probe was removed and cleaned with distilled water at regular intervals to ensure that the probe was not covered by a layer of $ZrO_x(OH)_{4-x}$ precipitate which would give a false pH reading. The pH was determined from the average of 3 separate pH readings and the probe was cleaned after each reading. When the pH reached 9.5, the mixture was stirred for an additional 10 minutes before filtering and washing to ensure that hydrolysis has gone to completion. The sample now has to be washed to remove any chloride species that are present. The sample was placed in a centrifuge and spun under the following settings:

RPM: 3500
Time per cycle: 5 minutes
Total number of cycles: 10

The sample was washed with distilled water after each cycle and the effluent was collected in a beaker. Chloride species will be present from the zirconyl chloride precurors and have to be removed to obtain high purity zirconium hydroxide. To determine if there were still any undesired chloride species present, silver nitrate solution,

$AgNO_3$, was added to the effluent to test for the presence of Cl^- ions after every 3 cycles. If Cl^- ions are present, the clear solution will either turn cloudy or white/light grey silver chloride precipitate is formed. A small amount of dilute nitric acid, HNO_3, was added if the solution turned cloudy and lightly shaken to confirm that silver chloride precipitates have formed. Dilute nitric acid reacts with and removes other ions that might also form a precipitate with silver nitrate.

It required on average 10 cycles to completely remove the presence of Cl^- ions. The samples were dried overnight in a drying cabinet at 60 °C and then crushed into small particles. Finally the crushed samples were spread evenly over a petri dish and dried overnight in a muffle furnace at 85 °C.

3.1.2 Incipient wetness impregnation

Samples were primarily prepared or modified by incipient wetness impregnation. Metal salt solution was dripped drop by drop onto the sample and stirred regularly until a paste was formed. The sample is referred to as "wet" at that stage and it is important that no excess solution is added such that the sample becomes slurry-like. The sample was considered to be wet when it had become sticky and paste-like and does not flow freely as a slurry or solution would.

Prior to impregnating the samples with the desired metal salt solution, a reference run was done using distilled water in order to determine the volume of solution required to "wet" the sample. 2g of $ZrO_x(OH)_{4-x}$ was measured out in a crucible and a 5ml measuring cylinder was filled with distilled water. Using a pipette, distilled water was slowly dripped drop by drop onto $ZrO_x(OH)_{4-x}$ and mixed with a spatula until the sample was wet.

The volume of water used to wet the sample was determined using the remaining water in the measuring cylinder. This was found to be on average approximately 2.2 ml H_2O per 2.35g of $Zr(OH)_4$ or 0.94 ml per gram of zirconium hydroxide. However, this value will

vary depending on the type of zirconium hydroxide used but will be useful as an approximation for future tests. The required mass of metal salts, ammonium metatungstate and iron nitrate, were weighed out and dissolved in the appropriate volume of water to form the necessary salt solution for the desired metal loading. The $Zr(OH)_4$ were then impregnated with the metal salt solution to synthesise the catalytic supports or catalysts. An example calculation is provided in Appendix I.

3.1.3 Calcination

The final synthesis step was to calcine the prepared samples at the appropriate temperature. WO_3/ZrO_2 supports and $Fe/WO_3/ZrO_2$ catalysts were calcined at 830 °C for 3 hours under flowing dry air with heating and cooling rates of 10 °C/min with an average dry air flowrate of 60 ml/min. The calcination temperature was changed for some samples but the heating and cooling conditions remained constant. A schematic of the calcination apparatus used is illustrated in Fig. 3.1. The air used was supplied from a gas cylinder and dried by flowing through a column packed with 13X molecular sieves. The relatively high air flow rate was used to remove the gaseous species formed during calcinations of the samples primarily from the nitrates present in the metal salt solutions.

3.1.4 Commercial zirconium hydroxide supports

Two commercial zirconium hydroxides were also used to synthesise tungsten oxide supported on zirconia. The zirconium hydroxides were supplied from MEL chemicals and Daiichi Kigenso Kagaku (DKK). The commercial zirconium hydroxides used were DKK RC-100 and MEL XZO 880/01. They are referred to by the abbreviation DKK or MEL throughout this thesis.

3.1.5 Chemical specifications

The following chemicals were used in the synthesis of the catalytic supports and catalysts:

- Zirconyl chloride [$ZrOCl_2.8H_2O$] – Fisher Scientific
- Zirconium hydroxide XZO 880/01 – MEL Chemicals
- Zirconium hydroxide RC-100 – Daiichi Kigenso Kagaku (DKK)
- Ammonium hydroxide [$NH_4.OH$] 25 wt% solution in water – Fisher Scientific
  This was diluted down to 10M solutions, which is 18 wt% solution in water
- Ammonium (meta)tungstate hydrate [$(NH_4)_6W_{12}O_{39}.1H_2O$] – Fluka
  Purum $\geq$ 85% as WO_3 (gravimetric) and H_2O ~ 18 mol/mol
- Iron(III) nitrate, nonahydrate [$Fe(NO_3)_3.9H_2O$] – Fisher Scientific
- 10wt% WO_3/ZrO_2 XZO 631/01 – MEL chemicals
- 10wt% WO_3/ZrO_2 J1374 – Daiichi Kigenso Kagaku (DKK)

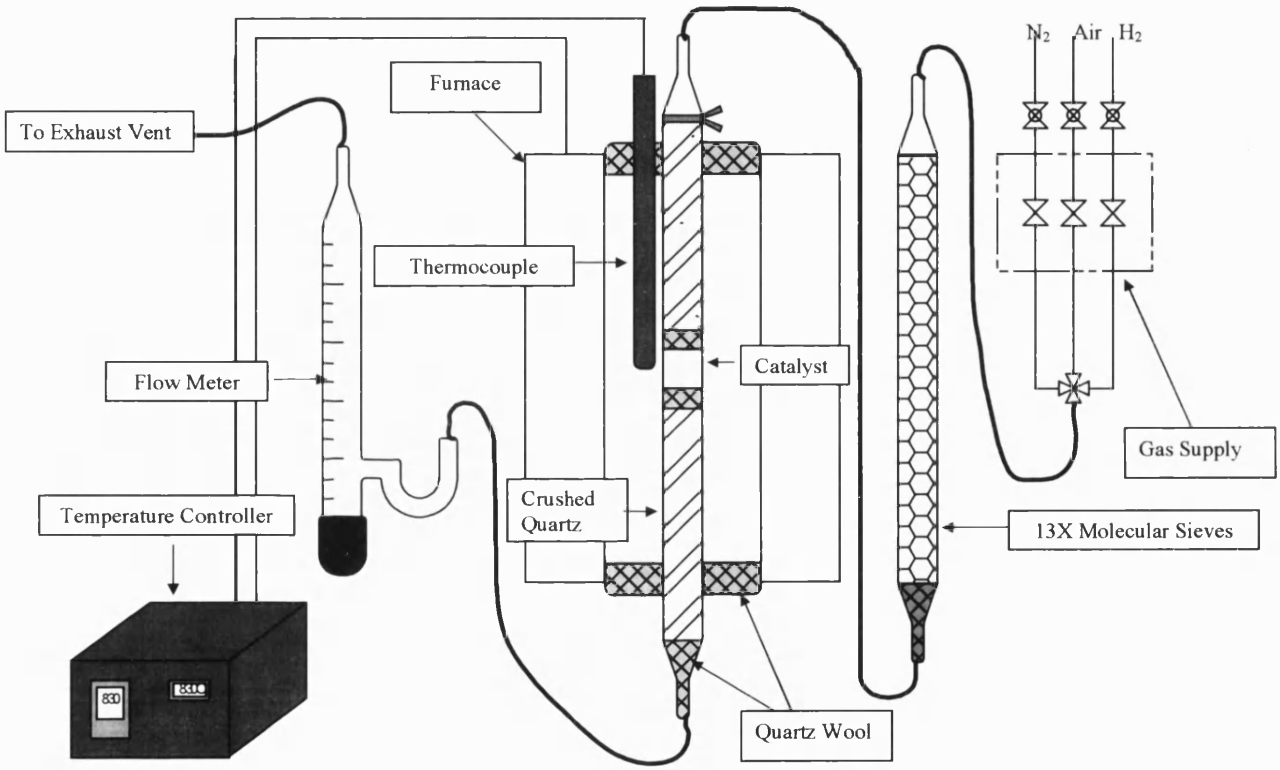

Fig. 3.1. Calcination apparatus

3.2 Samples synthesised

The WO_3/ZrO_2 supports and $Fe/WO_3/ZrO_2$ catalysts were synthesised using the procedures described previously. Flowcharts illustrating the procedures used are shown in the following pages.

3.2.1 Tungsten oxide supported on zirconia support, WO_3/ZrO_2

Preparation of zirconium hydroxide via precipitation
Zirconyl chloride [$ZrOCl_2.8H_2O$] + H_2O + 10M Ammonium hydroxide [NH_4OH]
pH = 9.5 at room temperature

↓

Synthesised or commercial zirconium hydroxide [$Zr(OH)_4$]
Dried overnight in drying cabinet at 60 °C then at 85 °C in muffle furnace

↓

Incipient wetness impregnation with ammonium (meta)tungstate hydrate
[$(NH_4)_6W_{12}O_{39}.1H_2O$]

↓

$WO_3/Zr(OH)_4$
Dried overnight at room temperature

↓

$WO_3/Zr(OH)_4$
Calcined at 830 °C for 3 hours
10 °C/min heating and cooling
60 ml/min dried air flow

↓

WO_3/ZrO_2 support
White powder

Fig. 3.2.1. Flowchart of WO_3/ZrO_2 synthesis.

3.2.2 Iron promoted tungsten oxide supported on zirconia catalysts, Fe/ WO_3/ZrO_2

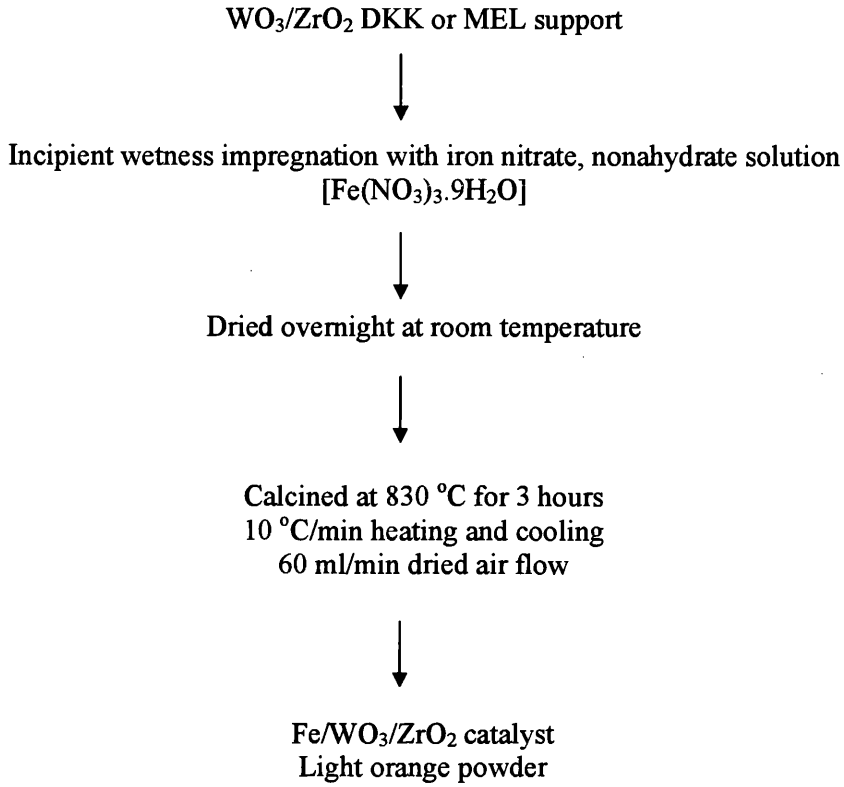

Fig. 3.2.2. Flowchart of $Fe/WO_3/ZrO_2$ synthesis.

3.3 Characterisation by infrared spectroscopy

The catalytic supports and catalysts were characterised by infrared spectroscopy using either pyridine or carbon monoxide as probe molecules. Pyridine was used to determine the acidity of the samples and carbon monoxide was used to characterise the active metal (iron). The IR spectra were obtained with a Bruker Equinox 55 spectrometer in the 4000 to 370 cm^{-1} range with 50 scans at a resolution of 2 cm^{-1}. After each pyridine adsorption experiment, the IR cell was charged with beta zeolite for a minimum of 6 hours to remove any remaining pyridine in the IR system. All experiments were carried out under high vacuum (10^{-6} Torr).

The infrared system available at the University of Bath was capable of heating the samples in-situ thus allowing both pyridine adsorption and desorption experiments to be carried out. This in turn makes it possible to determine quantitatively the number of Lewis and Broensted acid sites (LAS and BAS) as well as their respective acid site strengths. Furthermore, various gases such as oxygen, hydrogen and carbon monoxide can be introduced into the IR cell at different pressures for changing the sample pre-treatment conditions or as probe molecules. A schematic of the IR system is displayed in Fig. 3.3.2.

Before any experiments were carried out, the samples were activated at 350 °C under vacuum in order to remove any physisorbed impurities such as water vapour that may be present (Fig. 3.3.1). The sample was pressed into disks weighing between 8 – 15 mg before it was loaded into the IR cell. The pressed disk weight is based on previous experience in the catalysis and reaction engineering group (CARE) at the University of Bath, which showed that these sample disk weights provided good signal to noise ratio and, therefore, better quality spectra.

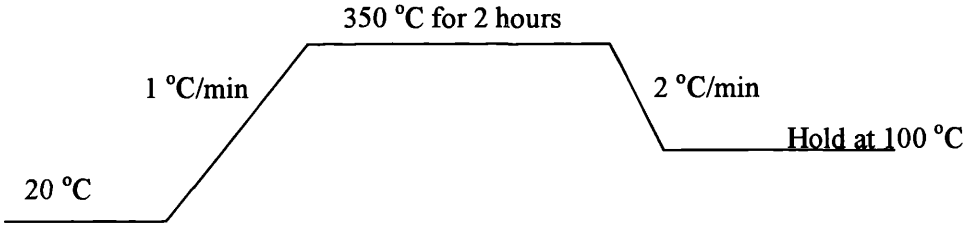

Fig. 3.3.1. Illustration of the IR sample activation programme.

In addition, the sample disk also has to be free from any cracks or deformities. The disk was loaded into the IR cell by placing it in the disk holder, then the IR cell was placed into the IR spectrometer. A diagram of the IR cell is illustrated in Fig. 3.3.3. Once the sample has been loaded a quick check was carried out to ensure that the IR cell was positioned correctly and the sample can be lowered and raised smoothly. The sample was lowered towards the IR beam and observed if there was any tension or slack on the gold chain.

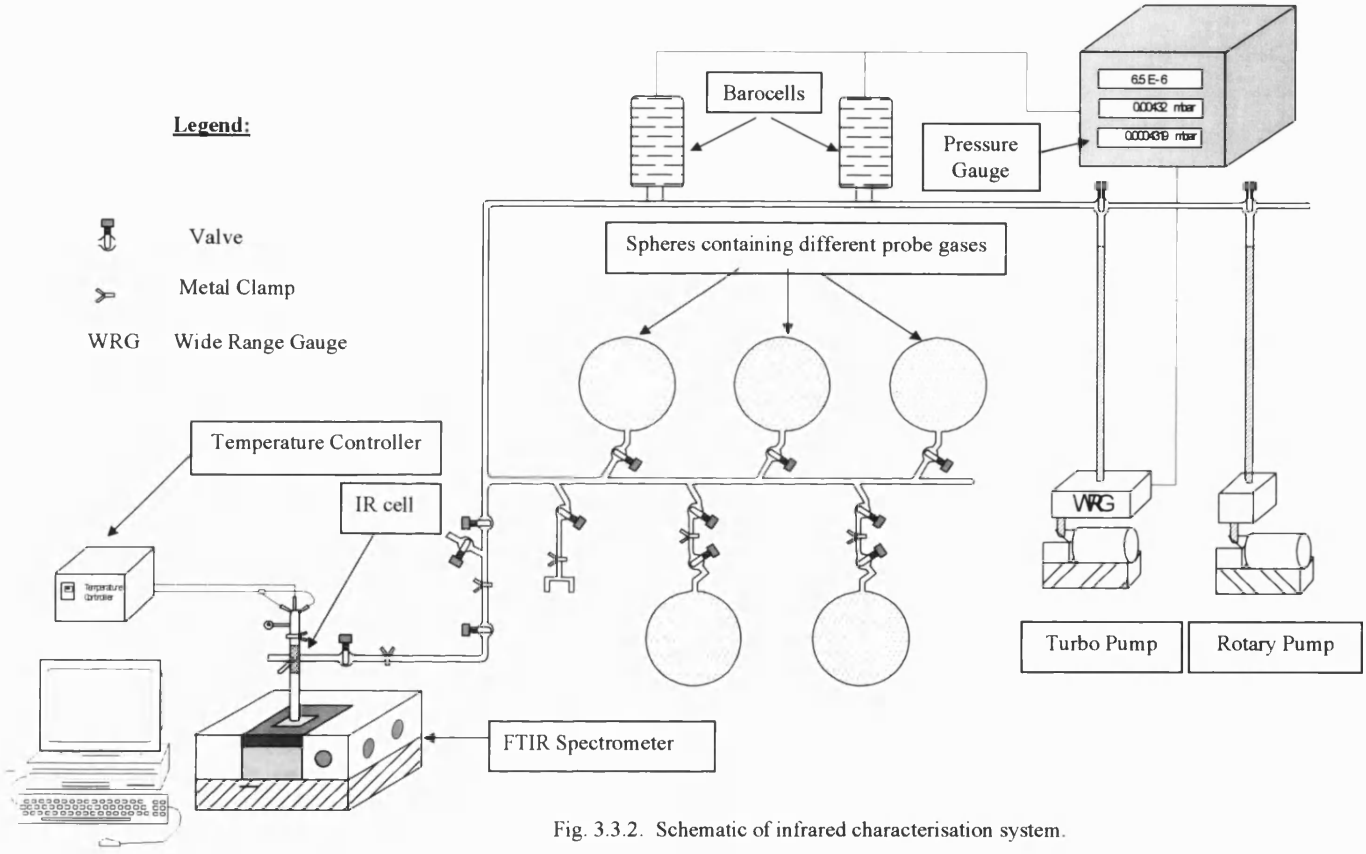

Fig. 3.3.2. Schematic of infrared characterisation system.

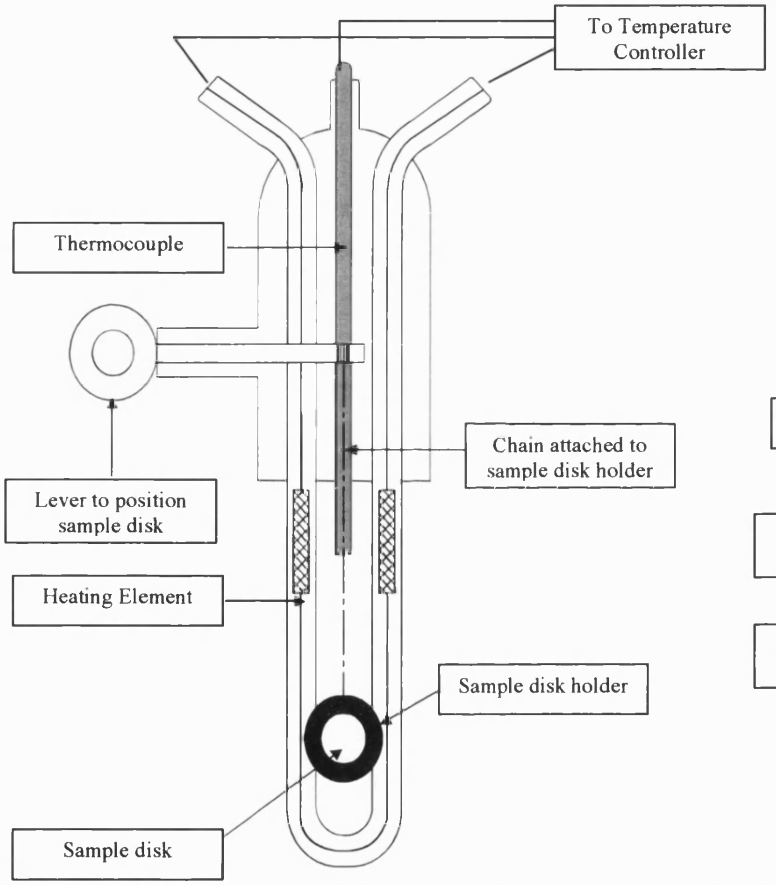

Fig. 3.3.3A. Schematic of the IR cell.

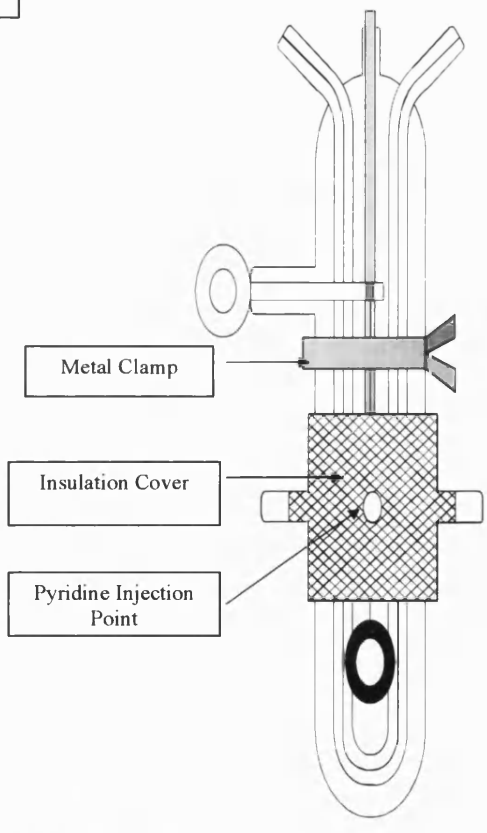

Fig. 3.3.3B. Schematic of the IR cell with cover attached.

After the sample had been activated, the IR spectrum of the sample was taken before any experiments were started, referred to as the initial spectrum. Two initial spectra were normally taken and compared to ensure that they are both identical.

Pyridine adsorption experiments were carried out at 100 °C with pyridine injections in 0.02 μL step sizes until the sample was saturated with pyridine and no further adsorption was detected. The IR cell was kept at 100 °C throughout the experiment to prevent any pyridine from physisorbing onto the sample therefore ensuring that only chemisorbed pyridine is measured. Pyridine desorption experiments were carried out by heating the sample from 100 °C to 200 °C at 5 °C/min and holding at this temperature for 30 minutes before a spectrum was taken. This was then repeated at 250 °C, 300 °C and 350 °C. The CO adsorption experiments are described separately in Section 3.5.

3.4 Analysis of the IR spectra

For each sample a series of spectra have been collected covering the initial spectra, pyridine adsorption and pyridine desorption experiments. These spectra contain essential data on the catalyst active sites and several careful analyses have to be carried out in order to extract relevant information. An outline of the analysis procedure used is given in this section. There are 4 key IR vibrational frequency ranges that are examined which are listed below:

OH region:	3800 – 3200 cm^{-1}
Py region:	1700 –1400 cm^{-1}
Framework region:	2200 – 1500 cm^{-1}
Tungstate region:	1700 – 600 cm^{-1}

The framework region refers to the frequencies at which zeolite framework vibrations occur. These framework vibrations are characteristic for different types of zeolites and generally remain constant as long as no changes to the zeolite framework take place. The tungstate region is a range of frequencies that are of particular interest for tungsten containing samples.

The IR characterisation results of 9 wt% WO_3/ZrO_2 DKK support are used as an example of how the analysis was carried out. For both the OH and Py region, the initial spectra and the spectra after pyridine adsorption at various pyridine concentrations are compared using the baseline. Each spectrum was labelled with the pyridine concentration and relevant peaks are also noted. Lastly, a brief description of the sample was entered at the bottom. Fig. 3.4.1 shows the spectra after the said manipulations where the baseline chosen was located just before the 3675 cm^{-1} peak.

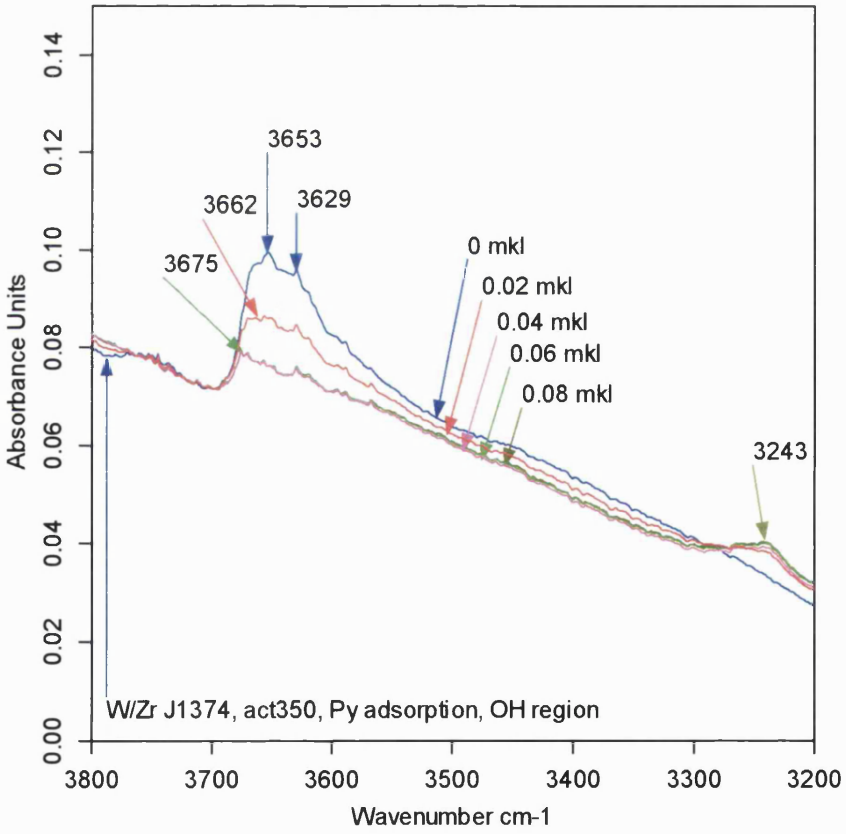

Fig. 3.4.1. IR spectra (OH region) after pyridine adsorption of 9 wt% WO_3/ZrO_2 DKK support.

The same process was carried out for the IR spectra in the pyridine region (Fig. 3.4.2). These spectra give a qualitative examination of the level of acidity present on the sample, as generally, the higher the peak intensities assigned to Py adsorption onto acid sites, the more acidic that sample is. The spectra in the OH region can also give an indication of the initial level of acidity as these hydroxyl groups are replaced or the stretching vibrational frequencies are changed by pyridine during the adsorption experiments.

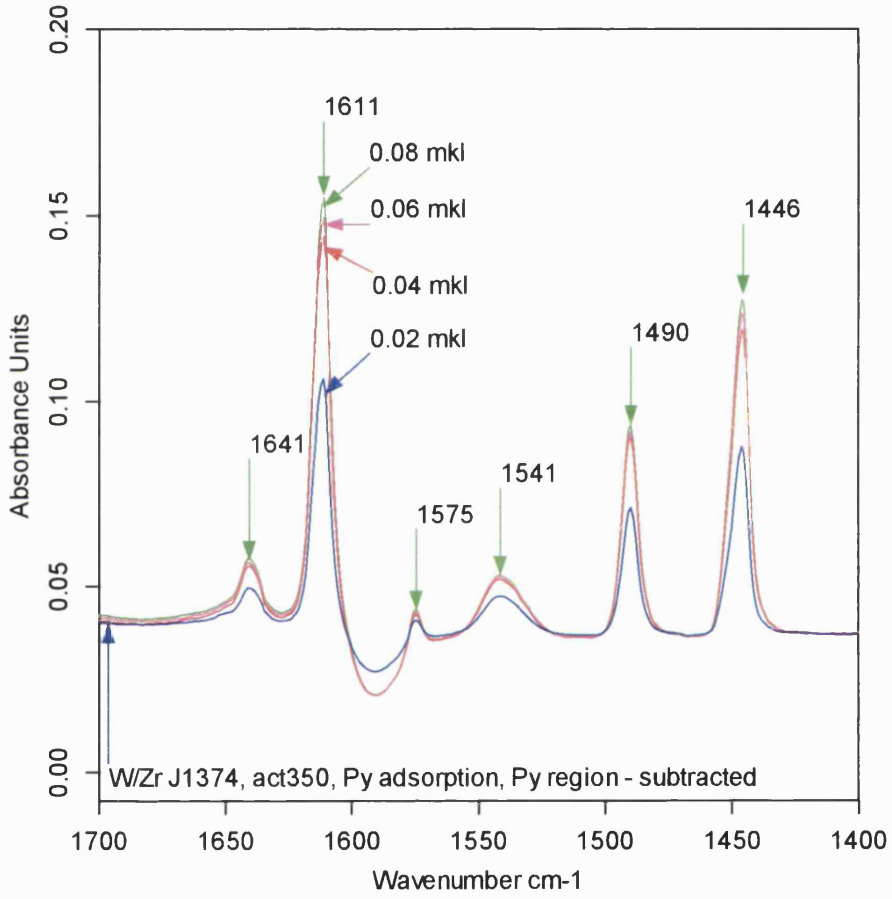

Fig. 3.4.2. IR spectra (Py region) of 9 wt% WO_3/ZrO_2 DKK support after adsorption experiments and subtraction of the initial spectrum.

In order to calculate quantitative numbers of acid sites present on a given sample, a few further steps have to be done. The spectra after pyridine adsorption and

desorption are subtracted by the initial spectrum. This will remove any peaks characteristic of that sample and highlight the peaks that are formed due to pyridine adsorption onto various acid sites. The spectra after subtraction are shown in Fig. 3.4.2 for pyridine adsorption experiments.

The five peaks in Fig. 3.4.2 representing either pyridine adsorption on LAS or BAS, ~1640 cm^{-1}, ~1611 cm^{-1}, ~1540 cm^{-1}, 1490 cm^{-1} and 1446 cm^{-1} are integrated. The peak areas calculated by integration can now be used to determine quantitative values for the total number of acid sites. The adsorption and desorption data are analysed differently since the adsorption experiments will determine the number of acid sites and the desorption results will give the relative acid site strengths.

3.4.1 Pyridine adsorption experiments

A graph of pyridine adsorbed in μmol against the peak area (A.U.) was plotted in Fig. 3.4.1.1 and two distinct regions can be seen, a curve followed by a horizontal straight line. The intercept of the horizontal line with the tangent of the curve gives the total concentration of pyridine adsorbed by the sample.

The total concentration of pyridine adsorbed at different acid sites (represented by the peaks in the IR spectra as described previously) was added together and divided by the number of peaks to obtain the average concentration of pyridine adsorbed on a given acid site. The average was taken to improve accuracy of the results although theoretically all the acid sites should adsorb the same concentration of pyridine, as pyridine will adsorb onto the LAS and BAS simultaneously. However, due to experimental errors this is often not the case.

It is possible to carry out the calculation through analysis of a single peak but this will increase the level of experimental error. Similarly, anomalous peaks may be excluded from the analysis to improve accuracy. The average concentration of pyridine adsorbed (μmol) was divided by the sample weight to give the total number of acid sites (BAS + LAS) in μmol/g.

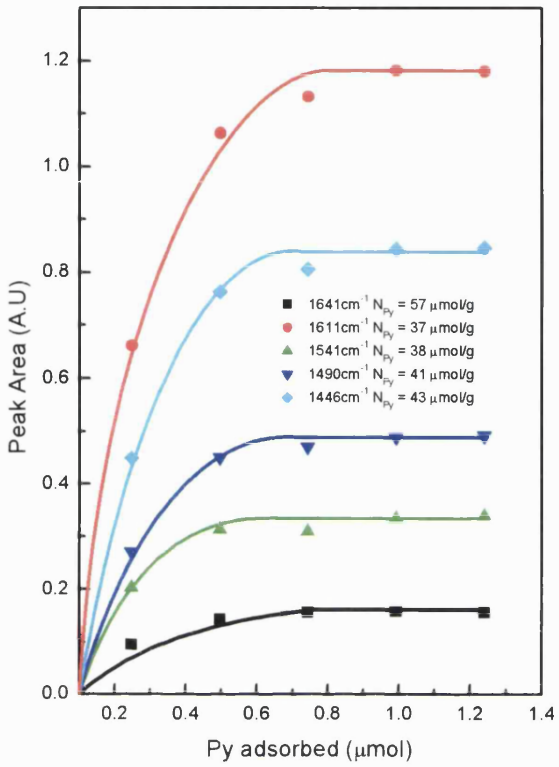

Fig. 3.4.1.1. Concentration of pyridine adsorbed against the respective peak areas for 9 wt% WO_3/ZrO_2 DKK support, used to determine quantitative numbers of acid sites.

The ratio of LAS to BAS was determined by the ratio between the peak area for the peaks corresponding to Py adsorption onto LAS (~1446 cm^{-1}) and BAS (~1540 cm^{-1}). This is based on the assumption that the molar absorption coefficient is the same for both LAS and BAS. Previous experiments carried out at the CARE laboratory, University of Bath have shown that it is possible to make this assumption. Once both the total number of acid sites and LAS/BAS ratio has been determined, the number of LAS and BAS can be calculated. Table 3.4.1.1 shows an example of the final results of the pyridine adsorption experiments.

Table 3.4.1.1. Acidity measurements of 9 wt% WO_3/ZrO_2 DKK support.

BAS + LAS (μmol/g)	Ratio LAS/BAS	LAS (μmol/g)	BAS (μmol/g)
44	1.3	25	19

Based on the results of repeated experiments, the error was found to be approximately 7%.

3.4.2 Pyridine desorption experiments

In order to plot the desorption profile, the peak areas at each desorption temperature was divided by the peak area from the IR spectra taken at 100 °C. The peak areas at different desorption temperatures were expressed relative to the peak areas at 100 °C. An example of the processed results is shown in Table 3.4.2.1. A plot of the desorption temperature against the relative peak areas will generate a pyridine temperature desorption profile.

Table 3.4.2.1. Relative peak areas against temperature for 9 wt% WO_3/ZrO_2 DKK support.

Temp (°C)	Relative peak areas				
-	1641	1611	1541	1490	1446
100	1.0	1.0	1.0	1.0	1.0
200	0.20	0.61	0.30	0.39	0.55
250	0.11	0.42	0.11	0.20	0.36
300	0	0.24	0	0.06	0.20
350	0	0.09	0	0	0.09

A graph showing the effect of temperature on the relative peak areas will give an indication of the acid site strength. An example of a pyridine desorption profile is given in Fig. 3.4.2.1.

Referring to the desorption profile for a particular sample; the relative acid site strengths can be determined. A steep curve would represent weak acid sites as pyridine rapidly desorbed from the acid sites whereas a gentle slope will be an indication of stronger acid sites that hold Py strongly. The temperature at which pyridine desorbs is also important and can be used for comparison purposes. For example, sample A is said to have weaker Lewis acidity than sample B if

pyridine has fully desorbed from the LAS present on sample A at 250 °C, whereas it only completely desorbs at 350 °C from sample B.

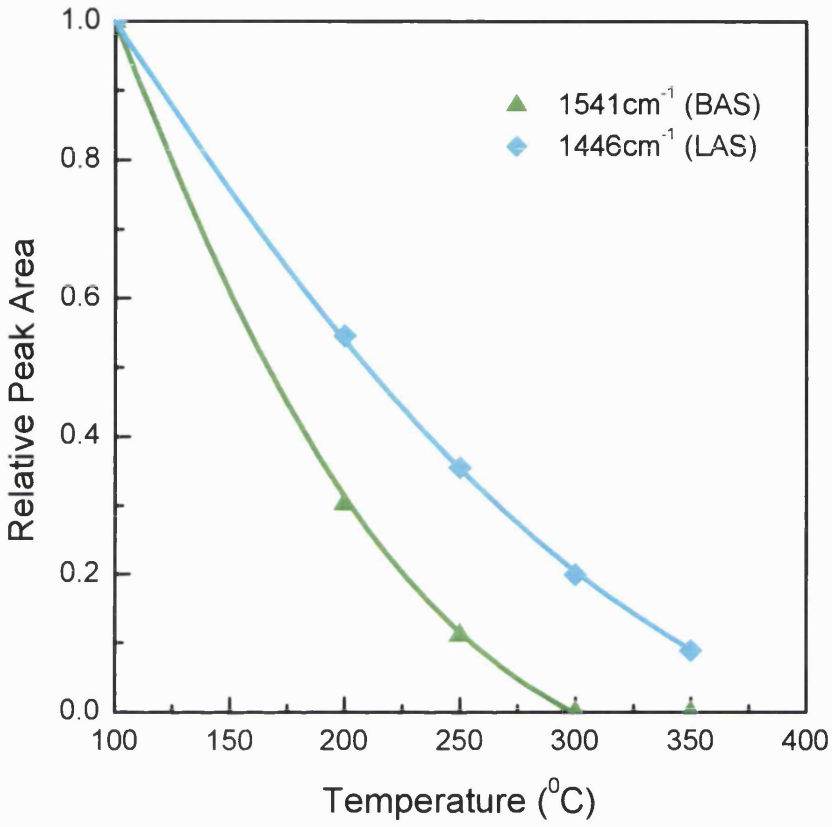

Fig. 3.4.2.1. Pyridine desorption from LAS (1449 cm^{-1}) and BAS (1541 cm^{-1}) present on 9 wt% WO_3/ZrO_2 DKK support.

3.5 CO adsorption experiments

The $Fe/WO_3/ZrO_2$ catalysts were activated under a reducing environment in the presence of 50 mbar hydrogen before CO adsorption experiments were conducted. The catalysts were reduced in order to characterise the iron species present on the $Fe/WO_3/ZrO_2$ catalysts using CO as a probe molecule. The activation procedure is outlined in Fig. 3.5.1.

After the catalyst was cleaned by heating to 350 °C under vacuum and then reduced in a hydrogen rich environment; CO was introduced in 6 mbar increments. The spectrum was collected after holding for 5 minutes at each CO pressure. Carbon monoxide was continually dosed in 6 mbar steps until the catalyst was saturated with CO and no further changes in the peak intensities took place.

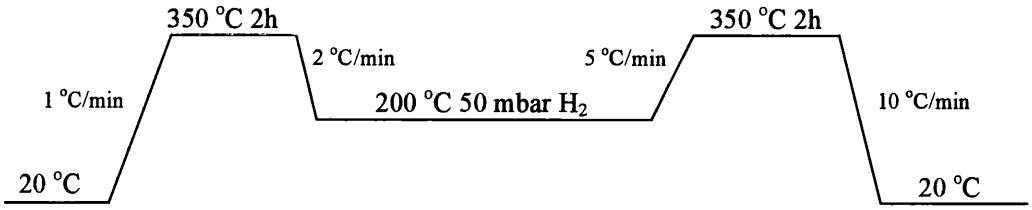

Fig. 3.5.1. Illustration of the IR sample activation procedure for CO adsorption experiments.

When the final CO adsorption spectrum was taken, the catalyst was evacuated under vacuum. Spectra were taken regularly every 15 minutes until no CO remained adsorbed on the catalysts. This provided an indication of the strength of the CO adsorption on various sites on the $Fe/WO_3/ZrO_2$ catalysts.

3.6 Comparing IR spectra from different samples

A qualitative comparison can be done across several different samples by first normalising the IR spectra either by the sample disk weight or the framework peak area. The spectra have to be normalised in order for an accurate comparison to be made, as the differences in the weight of the sample disks affect the thickness of the disk that in turn influences the signal strength. Such comparison spectra are useful to both check the accuracy of the quantitative results calculated to see if it correlates with the comparison spectra and to act as a quick visual evaluation of the acidity of several different samples.

Normalisation by the peak area in the framework vibration region is preferable as generally this would be more accurate than using the sample disk weight.

However, some samples do not have any characteristic framework peaks such as WO_3/ZrO_2. Results obtained previously in the CARE group laboratory, University of Bath have shown good agreements between the quantitative numbers of acid sites calculated and those determined from the IR spectra normalised by the sample disk weight.

3.7 Catalytic testing

Selective catalytic reduction of NO_x with NH_3 was studied in a fixed bed continuous flow reactor. Powder catalyst samples were crushed and sieved to 250-355 μm, then charged into an inconel tube (i.d. 8 mm) and fixed with quartz wool. The catalyst samples (0.3 g) were heated from 150 °C to 600 °C at a rate of 5 °C/min in reactant mixture of 12% O_2, 5% CO_2, 10% H_2O (steam), 100 ppm NH_3, 100 ppm NO and N_2 balance with a total flow of 2 L/min.

A blank test with cordierite was run before each series of samples were tested to ensure that there were no errors and the results were accurate and comparable to those obtained previously. The NH_3 was generated from a Signal Instruments NH_3 converter and the gas streams were analysed by Signal Instruments gas analysers, 4000VM NO_x analyser (NO and NH_3) and 7000FM GFC analyser (CO and CO_2). An ADC MGA-3000 series multi gas analyser was used to detect the presence of N_2O species.

3.8 XRD and TEM characterisations

The X-ray diffraction (XRD) and transmission electron microscopy (TEM) results shown in this thesis were obtained from Hoi Jobson and Serennah Longwood from Johnson Matthey Technology Centre, Sonning Common, Reading, UK.

Chapter 4: Catalytic support screening

Chapter 4: Catalytic support screening

The aim of the project was to develop new promising solid acid mixed oxide catalysts with two main objectives that the catalysts would be highly acidic and thermally stable. The catalysts will be tested for catalytic activity in the selective catalytic reduction of nitrogen oxides by ammonia (NH_3 SCR of NO_x) under lean conditions at temperatures between 150 °C and 550 °C. A series of promising mixed oxide supports was selected based on the Tanabe charge imbalance theory (Chapter 2.3) and discussions with the industrial sponsor company, Johnson Matthey.

The mixed oxide catalytic supports were characterised using IR spectroscopy with pyridine (Py) as the probe molecule to investigate the number and type of acid sites, i.e. Broensted or Lewis acid sites (BAS or LAS). The acidity of the catalytic supports was compared to the reference material, tungsten titania (WO_3/TiO_2) which is currently the catalytic support used commercially for NH_3 SCR of NO_x. A suitable mixed oxide catalytic support will be selected for further studies based on the comparison of the acidity of the supports against the reference sample. The mixed oxide catalytic supports characterised are listed below:

Zirconia silica	ZrO_2/SiO_2
Titania silica	TiO_2/SiO_2
Silica alumina	SiO_2/Al_2O_3
Tungsten oxide supported on titania	WO_3/TiO_2
Tungsten oxide supported on zirconia	WO_3/ZrO_2
Titania zirconia	TiO_2/ZrO_2
Sulphated zirconia	SO_4/ZrO_2
Silica zirconia	SiO_2/ZrO_2

4.1 Reference material, tungsten oxide supported on titania WO_3/TiO_2

Tungsten oxide supported on titania, WO_3/TiO_2, was selected as the reference material as it is currently used commercially as a catalytic support for various applications including the selective catalytic reduction of NO_x by ammonia. The acidity measurement of the WO_3/TiO_2 support is shown in Table 4.1 where it is compared to similar characterisation results obtained previously in this laboratory by Tanya Vazhnova. The results of the two characterisations are very similar and are within the acceptable range of experimental errors.

Table 4.1. Acidity measurements for the reference WO_3/TiO_2 support.

Sample	Current work	Previous work
BAS+LAS (μmol/g)	79	95
Ratio (LAS/BAS)	6.2	6.9
LAS (μmol/g)	73	83
BAS (μmol/g)	11	12

The characterisation of WO_3/TiO_2 was repeated and the second set of data was within 6% of the previous characterisation results.

4.2 Acidity measurements of the mixed oxide catalytic supports

In this section, the acidity of the various mixed oxide catalytic supports are described relative only to the other mixed oxide supports tested. For example, 30 wt% SiO_2/Al_2O_3 is said to be highly acidic with a total number of acid sites of 150 μmol/g when compared to the other 7 mixed oxide supports characterised. However, zeolite catalytic supports generally possess total number of acid sites in the region of 800 - 1000 μmol/g therefore SiO_2/Al_2O_3 would only be considered to possess low numbers of acid sites in comparison to zeolite supports.

Table 4.2 summarises the IR characterisation results for all the 8 mixed oxide catalytic supports studied. A brief description of each support is provided below and a more detailed analysis of each individual support is included in the following sections. The silica based supports was found to be unsuitable based on the low number of total acid sites present. Zirconia and titania supported on silica both had total numbers of acid sites below 20 μmol/g.

Quantitative results could not be obtained for both zirconia and titania supported on silica as the supports only adsorbed a small volume of pyridine. The samples were saturated with 0.02 μL of pyridine which was the smallest accurate unit that can be measured. As a result of this, quantitative values for the number of Lewis and Broensted acid sites (LAS and BAS) could not be determined due to the large associated experimental error on those catalysts.

Silica alumina looked promising as a potential catalytic support since it possessed one of the highest total numbers of acid sites. Furthermore, silica alumina was also one of the four supports that exhibited Broensted acidity with similar number of BAS as the reference WO_3/TiO_2 support. Tungsten titania has a lower number of LAS but a similar number of BAS in comparison to the SiO_2/Al_2O_3 support.

The TiO_2/ZrO_2 support exhibited no Broensted acidity and only possessed a high number of weak LAS as pyridine rapidly desorbed from the LAS at low temperatures. Sulphated zirconia was one of the most acidic supports tested with high numbers of LAS and BAS. This was to be expected since SO_4/ZrO_2 is known to be a highly acidic catalytic support and has been studied extensively [35, 125-130] (Chapter 2.7).

WO_3/ZrO_2 has similar numbers of BAS as that of the SO_4/ZrO_2 support however; WO_3/ZrO_2 only has a moderate number of LAS. There are approximately equal numbers of LAS and BAS present on WO_3/ZrO_2 with a LAS to BAS ratio of 1.3. The final mixed oxide support characterised, SiO_2/ZrO_2, only exhibited moderate numbers of weak LAS.

Table 4.2. Acidity measurements of the 8 mixed oxide catalytic supports characterised.

Support	2 wt% ZrO_2/SiO_2	6 wt% TiO_2/SiO_2	30 wt% SiO_2/Al_2O_3	9 wt% WO_3/TiO_2
Total acidity (μmol/g)	<20	<20	152	79
Ratio (LAS/BAS)	9	9	14.3	6
LAS (μmol/g)	-	-	143	68
BAS (μmol/g)	-	-	10	11
Pyridine Desorption	Weak LAS	Weak BAS and LAS	Moderate strength BAS Moderate to high strength LAS	Moderate strength BAS and LAS
Comment	Quantitative results not available	Quantitative results not available	-	-

Support	32 wt% TiO_2/ZrO_2	1 wt% SO_4/ZrO_2	2 wt% SiO_2/ZrO_2	9 wt% WO_3/ZrO_2
Total acidity (μmol/g)	183	162	55	44
Ratio (LAS/BAS)	-	7.5	-	1.3
LAS (μmol/g)	183	14	55	25
BAS (μmol/g)	0	19	0	19
Pyridine Desorption	Weak LAS	Strong BAS and LAS	Weak to moderate strength LAS	Moderate strength BAS Moderate to high strength LAS

The SiO_2/Al_2O_3, WO_3/TiO_2, SO_4/ZrO_2 and WO_3/ZrO_2 supports were repeated and the results were found to vary from 8 - 10%.

Based on the results in Table 4.2 and using WO_3/TiO_2 as the reference material; three materials, SiO_2/Al_2O_3, SO_4/ZrO_2 and WO_3/ZrO_2 look promising as suitable catalytic supports based on the number and strength of the Lewis and Broensted acid sites present on those supports. This was not unexpected as both silica alumina and sulphated zirconia are widely used commercially as catalytic supports or catalysts for a large variety of applications [35, 131-135]. Similarly, WO_3/ZrO_2 has been reported to be a promising catalytic support in the literature as outlined previously in Chapter 2.9 which is supported by the results in Table 4.2.

The sulphated zirconia support looks to be very promising however, there are two problems associated with its use as a catalytic support for NH_3 SCR. SO_4/ZrO_2 supports may not be thermally stable at high temperatures due to dissociation of the sulphate groups that leads to the loss of acidity [58]. This is supported by the results reported on catalysts based on SO_4/TiO_2 catalytic supports that exhibited poor thermal stability where the activity of the catalysts was reduced significantly after aging due to the loss of acidity caused by the desorption of sulphate groups.

Furthermore, SO_4/ZrO_2 is extremely unselective in the NH_3 SCR reaction. SO_4/ZrO_2 supports can not only exhibit zero NO_x conversions but more NO_x species are actually formed rather than reduced to N_2 by NH_3 (Appendix II Fig A2.6.5). The catalytic support used for the NH_3 SCR reaction should either be active for NH_3 SCR or completely unreactive so it does not inhibit the SCR activity of the catalyst.

The decision was made to focus initially on tungsten oxide supported on zirconia over the silica alumina support. The WO_3/ZrO_2 support is a more interesting catalytic support to investigate due to its unique properties and it is also less well studied in comparison to silica alumina. However, if the WO_3/ZrO_2 catalytic support is found to be unsuitable for NH_3 SCR of NO_x then the focus of the research may switch to the development of SiO_2/Al_2O_3 as a catalytic support.

4.3 IR analysis of the 8 mixed oxide catalytic supports

This section describes the mixed oxide catalytic supports characterised (Table 4.2) in more depth, focusing on 3 major aspects, the IR spectra of pyridine adsorption in the OH and Py regions along with the pyridine desorption profile. The IR spectra for all the 8 supports are shown in Appendix II with the exception of the WO_3/ZrO_2 support. The WO_3/ZrO_2 support is examined in detail in Section 4.4 as it has been selected as the most promising catalytic support for further development as a catalyst for NH_3 SCR.

4.3.1 2 wt% ZrO_2/SiO_2

The IR peak at 3743 cm^{-1} in the OH region is assigned to OH stretching in the Si – OH group (Fig. A2.1.1). There was a slight reduction in the peak intensity after pyridine adsorption which is most likely due to the interaction between pyridine and acidic OH groups. There were no new peaks formed in the OH region after pyridine adsorption although there is the possibility that a broad peak was forming in the region of 3700 – 3500 cm^{-1}, which increases very slightly in intensity with pyridine adsorption.

In the pyridine region, the 6 peaks that are associated with pyridine adsorption on LAS and BAS can be clearly seen (Fig. A2.1.2). There is either only a tiny number of (or no) BAS present on the ZrO_2/SiO_2 support because the peaks at 1637 cm^{-1} and 1539 cm^{-1} are poorly defined and are possibly attributed to signal noise instead. There was a small number of LAS present but quantitative numbers could not be determined as the support was saturated with a low volume of pyridine.

Pyridine had fully desorbed from both the LAS and BAS at 350 °C. A large amount of pyridine had already desorbed at 200 °C with only approximately 1/5 of the initial peak intensity remaining visible at 200 °C. Furthermore, due to the low peak intensities after pyridine desorption, it is difficult to differentiate between actual IR peaks and signal

noise. It can be concluded that there is only a small number of very weak LAS present on the 2wt% ZrO_2/SiO_2 support.

4.3.2 6 wt% TiO_2/SiO_2

The results are very similar to that of the 2 wt% ZrO_2/SiO_2 support with the distinctive peak at 3743 cm^{-1} in the OH region assigned to Si – OH groups (Fig. A2.2.1). There was no discernable change in the peak intensity after pyridine adsorption as the slight reduction can not be easily differentiated from an actual change in the peak intensity or due to experimental errors associated with IR spectroscopy.

There are some LAS and BAS present on the support; however, quantitative values for both the numbers of LAS and BAS could not be determined accurately (Fig. A2.2.2). The TiO_2/SiO_2 support was saturated with a similar volume of pyridine (0.04 μL) as the ZrO_2/SiO_2 support. No pyridine remained adsorbed on either the LAS or BAS at desorption temperatures of 350 °C. The majority of the pyridine had already desorbed at 200 °C with only approximately 1/6 of the initial peak intensity remaining at 200 °C. This indicates that the acid sites present are weaker than those found on the 2 wt% ZrO_2/SiO_2 support.

4.3.3 30 wt% SiO_2/Al_2O_3

The characteristic peak due to Si – OH groups at 3744 cm^{-1} along with an additional peak at 3579 cm^{-1} assigned to H-bonded OH groups in the OH region (Fig. A2.3.1). Introducing pyridine causes a gradual decrease in the 3744 cm^{-1} peak intensity and a shoulder at 3724 cm^{-1} begins to form which is most likely due to a different Si – OH vibrational frequency.

The peaks in the OH region were analysed and, based on the calculated peak areas, the total number of acid sites present was determined to be 156 μmol/g. Pyridine adsorption results in the Py region showed that the SiO_2/Al_2O_3 support possessed a high number of LAS and a small number of BAS (Fig. A2.3.2). The total number of acid sites calculated

was 153 μmol/g which matches the values obtained previously from the calculations based on the peaks in the OH region.

In the OH region, the 3744 cm^{-1} peak intensity increases but the 3576 cm^{-1} peak intensity decreases with increasing desorption temperature. The spectra steadily returns to matching the initial spectrum before pyridine adsorption as the desorption experiment progresses (Fig A2.3.3). After reaching the final desorption temperature of 350 °C, there was still some pyridine adsorbed on the LAS. Pyridine desorbed gradually from the LAS with increasing desorption temperature and had a smooth pyridine temperature desorption profile curve that indicated moderate to high strength LAS are present. On the other hand, the pyridine desorption results suggest that the BAS are comprised of weak to moderate strength BAS.

4.3.4 9 wt% WO_3/TiO_2

There are two distinct peaks at 3701 cm^{-1} and 3663 cm^{-1} in the OH region which are assigned to anatase TiO_2 (Fig. A2.4.1). Both peaks intensities decrease with increasing adsorption of pyridine until 0.08 μL of pyridine has been introduced where the peaks are no longer clearly visible. A new peak at ~3240 cm^{-1} appears after adsorption of 0.04 μL of pyridine which remains at the same peak intensity throughout the pyridine adsorption experiment (Fig. A2.4.2).

WO_3/TiO_2 possessed a high number of LAS but only a small number of BAS based on the results of the pyridine adsorption experiment. The pyridine desorption experiments showed that WO_3/TiO_2 was comprised of moderate strength LAS and weak BAS. The LAS and BAS strength was lower than those found previously on the SiO_2/Al_2O_3 support.

4.3.5 32 wt% TiO_2/ZrO_2

There was a significant level of signal noise in the OH region which made peak identification difficult even after smoothening the spectrum by 25 data points. After smoothing the IR spectra, 4 peaks can potentially be assigned at 3777, 3688, 3661 and

3640 cm^{-1} (Fig. A2.5.1). These peaks are currently unassigned however, the peaks at 3688 and 3661 cm^{-1} were also present on the 2 wt% SiO_2/ZrO_2 support (Fig. A2.8.1). This suggests that those peaks are associated with some form of interaction with zirconium oxide.

The TiO_2/ZrO_2 support only possessed a very high number of weak LAS as the support did not appear to posses any Broensted acidity based on the absence of the peak at ~1540 cm^{-1} (Fig. A2.5.2). However; there was a small peak at 1648 cm^{-1} which could possibly indicate the presence of some Broensted acidity. Pyridine rapidly desorbed from the LAS and the TiO_2/ZrO_2 support was found to have the lowest LAS strength of the 8 mixed oxide supports characterised.

4.3.6 1 wt% SO_4/ZrO_2

The IR spectrum of SO_4/ZrO_2 shows two distinct peaks at 3760 cm^{-1} and 3650 cm^{-1} in the OH region where the peaks intensities decrease steadily with increasing pyridine concentration (Fig. A2.6.1). Both peaks are most likely associated with acidic hydroxyl groups. A new broad peak at 3264 cm^{-1} begins to appear after pyridine adsorption and can only be clearly seen at high pyridine concentrations.

SO_4/ZrO_2 possessed a large number of LAS and a relatively high number of BAS (Fig. A2.6.2). The support also had the highest BAS and LAS strength of the 8 supports characterised. This made the SO_4/ZrO_2 support one of the most acidic samples characterised which was not unexpected based on the results reported in the literature [129, 130].

The SO_4/ZrO_2 support had a very distinct peak at 1383 cm^{-1} which shifts to 1333 cm^{-1} after pyridine adsorption. During the desorption experiment, the 1333 cm^{-1} peak shifts steadily back towards its original position at 1383 cm^{-1} with increasing desorption temperatures. At the final desorption temperature of 350 °C, the peak position has been shifted back to 1380 cm^{-1}. A small peak at 1226 cm^{-1} that is unassigned also appears after

pyridine adsorption which reduces in peak intensity as the desorption temperature increases (Fig. A2.6.3).

Both the 1383 cm^{-1} and 1226 cm^{-1} peaks are most likely associated with sulphate groups as the same peaks and trends were also observed on the SO_4/TiO_2 support. The sulphate groups appear to interact with pyridine, based on the peak shift from 1383 cm^{-1} to 1333 cm^{-1} after pyridine adsorption. As pyridine desorbs from the support, the sulphate group vibrational frequency begins to return to its original value (Fig. A2.6.4).

In contrast, the 1384 cm^{-1} peak present on the SO_4/TiO_2 support although undergoing a similar peak shift to 1322 cm^{-1} after Py adsorption, does not return to its original peak position after pyridine desorption. This strongly suggests there are different SO_4 interactions with titanium oxide compared to those on zirconium oxide. This could possibly account for the difference in NH_3 SCR activity between the two sulphated supports where SO_4/TiO_2 was active but SO_4/ZrO_2 was not (Fig. A2.6.5).

4.3.7 2 wt% SiO_2/ZrO_2

The IR spectra in the OH region was highly distorted due to background/signal noise and had to be smoothened by 25 data points twice. Along with the peak at 3736 cm^{-1}, two additional peaks at 3686 cm^{-1} and 3662 cm^{-1} were observed after the spectrum was smoothened (Fig. A2.7.1). None of these peaks are currently assigned but it is most likely that the peak at 3736 cm^{-1} is due to Si – OH bond vibrations and the other two peaks are associated with interactions with zirconium oxide as seen previously on the 32 wt% TiO_2/ZrO_2 support.

The SiO_2/ZrO_2 support exhibited no Broensted acidity although there was a small peak at 1644 cm^{-1} which could suggest that a very small number of BAS is present (Fig. A2.7.2). The support was found to possess only a moderate number of weak LAS. A new peak at 1536 cm^{-1} appears when the desorption temperature reaches 250 °C and increases in intensity with higher desorption temperatures. This peak is currently unassigned.

4.3.8 9 wt% WO_3/ZrO_2

The IR spectra and detailed analysis of the WO_3/ZrO_2 is shown in the following section 4.4, a brief overview is described below. The initial IR spectrum of WO_3/ZrO_2 before pyridine adsorption shows a broad peak at 1592 cm^{-1} that disappears after pyridine was introduced (Fig. 4.4.2). This peak is currently unassigned but is suspected to be due to the presence of adsorbed water or reduced tungstate species. In the OH region, a broad peak at 3653 cm^{-1} which is associated with acidic OH groups can be seen (Fig. 4.4.1). This peak shifts to 3662 cm^{-1} after adsorption of 0.02 μL of pyridine which then remains at 3675 cm^{-1} with increasing concentrations of pyridine.

A new peak at 3243 cm^{-1} also appears after adsorption of 0.04 μL of pyridine. Based on the results of the pyridine adsorption experiment, WO_3/ZrO_2 was found to possess a moderate number of LAS and a relatively high number of BAS in comparison to the other supports characterised.

The pyridine temperature programmed desorption profiles of the WO_3/ZrO_2 and WO_3/TiO_2 supports are very similar but the WO_3/ZrO_2 support had slightly weaker BAS and LAS strength compared to the reference WO_3/TiO_2 support (Fig. 4.4.5). A new peak appears at 1467 cm^{-1} when the desorption temperature reaches 250 °C and continues to increase in intensity with higher temperatures (Fig. 4.4.4). This peak is suggested to be due to either pyridine adsorbing onto LAS of different strength or nitrogen based products formed by pyridine decomposition at those temperatures.

The support was also activated at 400 °C under the same conditions and no significant differences was observed, the peak at 1592 cm^{-1} was also present in the initial spectrum. The 1467 cm^{-1} peak intensity increased slightly when heated from 350 °C to 400 °C. The sample which was initially white in colour, changes to a dark brown colour after activation under vacuum at 350 °C or 400 °C. The colour change is most likely caused by the presence of tungsten in a metallic form instead of an oxide as the support can possibly undergo auto-reduction under the reducing activation conditions used.

4.4 IR characterisation of tungsten oxide supported on zirconia catalytic support, WO_3/ZrO_2

WO_3/ZrO_2 was selected as one of the most promising catalytic supports of the 8 mixed oxide supports characterised. This section describes in detail the IR characterisation results and analysis carried out on the WO_3/ZrO_2 support. The initial IR spectrum before pyridine adsorption shows a very broad peak at 3653 cm^{-1} and 3629 cm^{-1} in the OH region (Fig. 4.4.1). The peak intensities decrease after pyridine adsorption and the peaks can be associated with acidic hydroxyl groups. A new peak at 3243 cm^{-1} also appears after pyridine adsorption that remains at approximately the same peak intensity throughout the experiment. This peak at ~3240 cm^{-1} is most likely to be due to NH_2 bonding interactions.

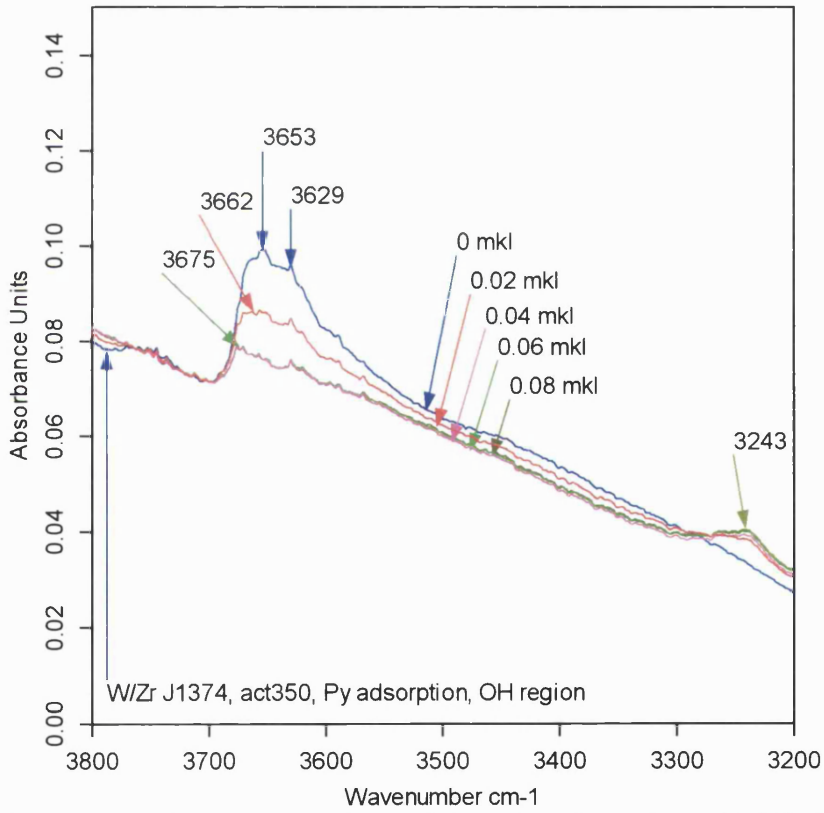

Fig. 4.4.1. IR spectra (OH region) after pyridine adsorption of 9 wt% WO_3/ZrO_2 DKK support activated at 350 °C.

In the pyridine region, a new peak at 1592 cm^{-1} was observed which has not been previously reported in the literature and is currently unassigned (Fig. 4.4.2). This peak was only visible on the initial spectrum in the Py region and disappears completely after pyridine adsorption. The 1592 cm^{-1} peak is suggested to be due to the presence of reduced tungsten species in a metallic form rather than an oxide.

The WO_3/ZrO_2 sample that was loaded into the IR cell was originally white in colour but darkens to a brown/grey colour after activation at 350 °C under vacuum; this suggests that auto-reduction may have occurred. This has not been reported previously in the literature because the IR characterisations of WO_3/ZrO_2 were generally carried out when the support was activated under an oxidising environment compared to the reducing conditions used in this study.

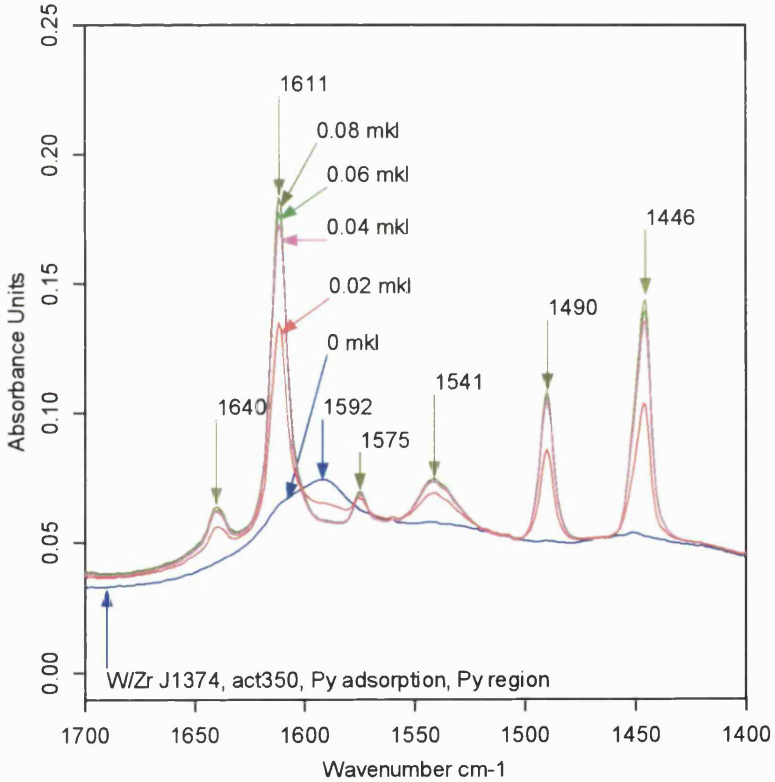

Fig. 4.4.2. IR spectra (Py region) after pyridine adsorption of 9 wt% WO_3/ZrO_2 DKK support activated at 350 °C.

Fig. 4.4.2 clearly demonstrates that WO_3/ZrO_2 has moderate numbers of BAS and LAS based on the 1541 cm^{-1} and 1446 cm^{-1} peak intensities. The WO_3/ZrO_2 support had similar numbers of BAS and LAS as shown previously in Table 4.2 where the LAS/BAS ratio was 1.3. An additional region of interest with the WO_3/ZrO_2 support is the 600 – 1100 cm^{-1} tungstate region. The peaks in the tungstate region can be assigned to specific characteristic interactions of various WO_x species as described in Table 4.3.

Table 4.3. Peak assignment in the tungstate region, 1400 - 600 cm^{-1} (adapted from [30, 136])

Wavenumbers (cm^{-1})	Assignment
1061 - 910	W – O symmetric stretching
980 - 740	W – O symmetric and W – O – W anti-symmetric stretching
830 - 300	W – O anti-symmetric stretching and bending modes
550 - 200	W – O – W symmetric stretching and bending modes
760 - 100	monoclinic and tetragonal ZrO_2

The peaks at ~990 cm^{-1}, ~1000 cm^{-1} and ~1015 cm^{-1} are present in the IR spectra of the WO_3/ZrO_2 support characterised (Fig. 4.4.3), and they have been assigned to terminal W = O bonding [137]. The shoulder present at 880 cm^{-1} has been linked to W – O – W stretching and bending modes [138]. Recently, Boyse and Ko [139] have suggested that the peak ~1020 cm^{-1} can be linked to the catalytic activity of WO_3/ZrO_2 where higher peak intensities are an indication of better catalytic activity.

Furthermore, Vaudagna et al [138] had reported that the peak at ~1020 cm^{-1} will be red shifted under reducing conditions. This is supported by the results obtained in the pyridine adsorption experiments which show a peak shift from 1023 cm^{-1} to 994 cm^{-1} after the WO_3/ZrO_2 support was reduced by pyridine (Fig. 4.4.3). There are other various

peaks between 1611 cm^{-1} and 1226 cm^{-1} that are visible in Fig. 4.4.3, which are due to pyridine adsorbing onto various acid sites on WO_3/ZrO_2.

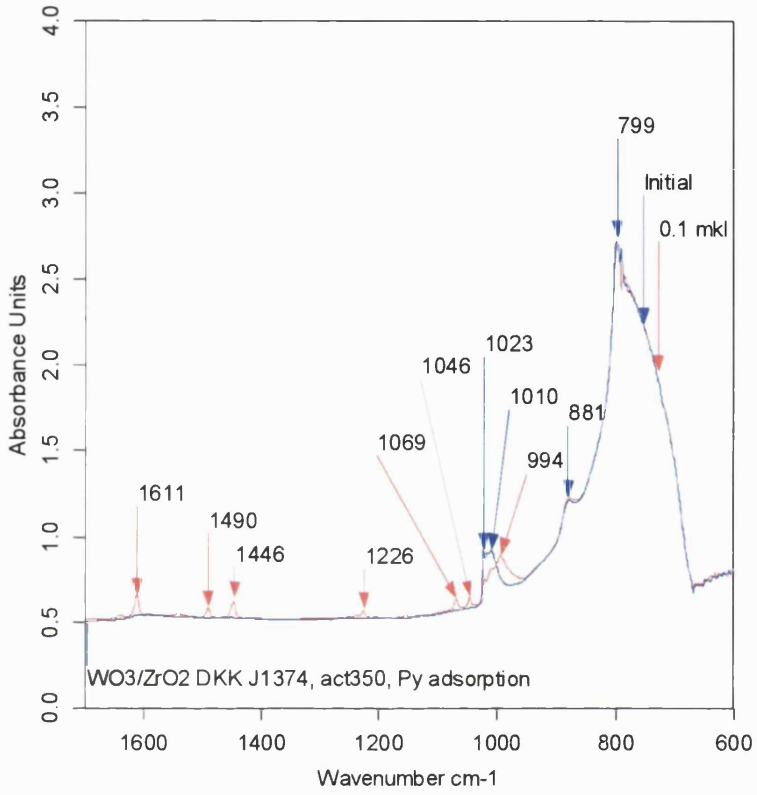

Fig. 4.4.3. IR spectra (Tungstate region) after pyridine adsorption of 9 wt% WO_3/ZrO_2 DKK support activated at 350 °C.

The pyridine desorption spectra shown in Fig. 4.4.4 produced interesting results as an additional peak at ~1467 cm^{-1} appears at 250 °C that steadily increases in peak intensity with higher temperatures. This peak is currently unassigned and is suspected to be due to either pyridine adsorbing onto a wider distribution of LAS of varying acid site strength or from interactions with nitrogen based products that are formed by the decomposition of pyridine. It is most likely to be due to the latter reason based on similar results reported on different supports.

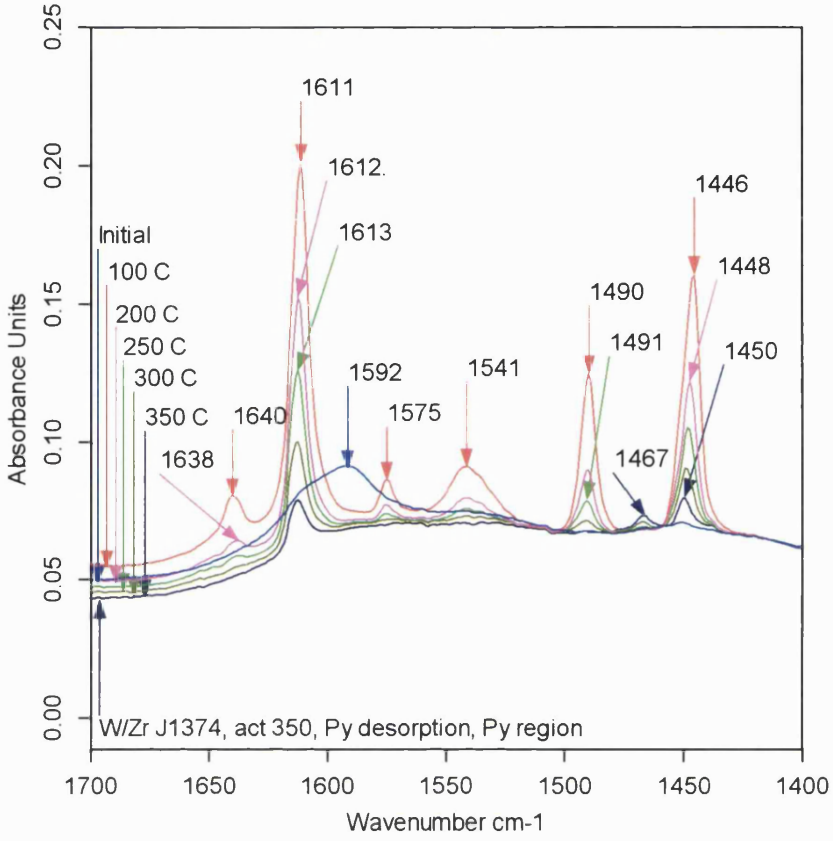

Fig. 4.4.4. IR spectra (Py region) after pyridine desorption of 9 wt% WO_3/ZrO_2 DKK support activated at 350 °C.

The LAS on WO_3/ZrO_2 was slightly weaker than those present on the reference WO_3/TiO_2 support (Fig. 4.4.5(A)). Although there were around double the number of BAS on the WO_3/ZrO_2 support, they were weaker than those found on the WO_3/TiO_2 support (Fig. 4.4.5(B)). Overall, the WO_3/ZrO_2 support has slightly weaker BAS and LAS compared to the reference WO_3/TiO_2 support with higher numbers of BAS but lower numbers of LAS.

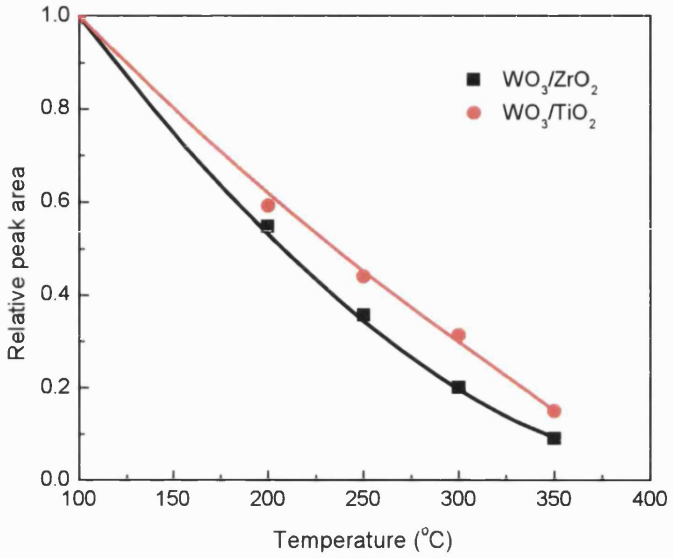

(A)

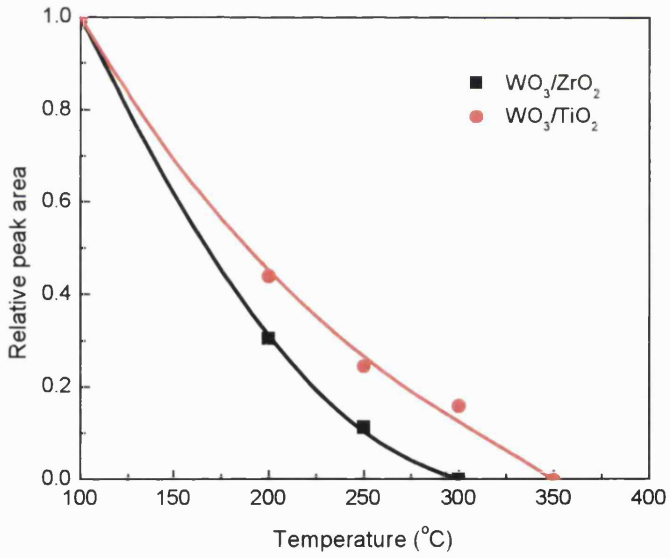

(B)

Fig. 4.4.5. Pyridine desorption from (A) LAS and (B) BAS present in the 9 wt% WO_3/ZrO_2 DKK support and the reference WO_3/TiO_2 material.

4.5 Summary

Three supports, sulphated zirconia, silica alumina and tungsten oxide supported on zirconia (SO_4/ZrO_2, SiO_2/Al_2O_3 and WO_3/ZrO_2) were shown to be the most promising catalytic supports of the 8 mixed oxide supports characterised, based on the comparison of the acidity of the supports with the reference WO_3/TiO_2 sample. WO_3/ZrO_2 was selected as the catalytic support for further studies as there were potential problems with the use of the SO_4/ZrO_2 and SiO_2/Al_2O_3 as catalytic supports for NH_3 SCR of NO_x.

The SO_4/ZrO_2 support is highly unselective in the NH_3 SCR reaction (Appendix II Fig A2.6.5) and may not be thermally stable due to loss of sulphate groups at high temperatures that was observed on SO_4/TiO_2 based catalysts. On the other hand, the SiO_2/Al_2O_3 support has already been extensively studied in the literature and has a lower number of BAS compared to the WO_3/ZrO_2 support. Therefore, it would be interesting to study further WO_3/ZrO_2, as it has a higher potential for development and gaining new understanding of the properties of WO_3/ZrO_2 as a catalytic support.

Furthermore, the WO_3/ZrO_2 support had one of the highest numbers of BAS and a moderate number of LAS compared to the other 7 supports characterised. There are approximately equal numbers of BAS and LAS present on the support where the ratio of LAS/BAS was 1.3 compared to the other supports that had significantly higher LAS/BAS ratios (ranging from 6 to 9). Although there were strong BAS and LAS present on WO_3/ZrO_2 they were slightly weaker than those found on WO_3/TiO_2. The characteristic WO_x peaks were present on the WO_3/ZrO_2 support in the tungstate region (1400 – 600 cm^{-1}) in agreement with the literature [30, 136].

The following chapter will examine the WO_3/ZrO_2 support in detail by varying the zirconium hydroxide precursors used to synthesise the support along with altering the tungsten oxide loading. The acidity, textural and structural properties of the WO_3/ZrO_2 catalytic support will be investigated through the use of IR spectroscopy, XRD and TEM.

Chapter 5: Tungsten oxide supported on zirconia catalytic support

Chapter 5: Tungsten oxide supported on zirconia catalytic support

The catalytic support selected for further development was tungsten oxide supported on zirconium oxide (WO_3/ZrO_2). This was based on the promising reports in the literature regarding tungsten oxide supported on zirconia as a catalytic support (described previously in Chapter 2.9) and the catalyst support screening experiments conducted in Chapter 4. In this chapter, WO_3/ZrO_2 was synthesised using different zirconium hydroxide precursors then characterised by IR spectroscopy, XRD and TEM to investigate the influence of the zirconium hydroxide precursor and tungsten oxide loading on the acidity, textural and structural properties of WO_3/ZrO_2.

The WO_3/ZrO_2 supports were synthesised using either DKK RC-100 or MEL XZO 880/01 zirconium hydroxide and are represented by the abbreviations DKK or MEL. For example, WO_3/ZrO_2 synthesised using DKK RC-100 zirconium hydroxide are defined as WO_3/ZrO_2 DKK supports or as WO_3/ZrO_2 MEL supports if the MEL XZO 880/01 zirconium hydroxide was used.

5.1 Zirconium hydroxide precursors

The influence of the zirconium hydroxide precursor on the properties of WO_3/ZrO_2 was investigated by comparing the acidity of the WO_3/ZrO_2 supports synthesised using three different zirconium hydroxide precursors. Zirconium hydroxide synthesised in the lab along with two commercially available zirconium hydroxides, DKK RC-100 and MEL XZO 880/01, were compared after impregnating all three supports with 10 wt% tungsten.

The zirconium hydroxide synthesis and tungsten impregnation was carried out by incipient wetness impregnation as described in Chapter 3. The different WO_3/ZrO_2 supports were characterised using IR spectroscopy with pyridine as the probe molecule to determine the number and type of acid sites present. The acidity characterisation results are shown in Fig. 5.1 and Table 5.1 which also

includes the data for two commercially available WO_3/ZrO_2, DKK J1374 and MEL XZO 631/01.

The five different WO_3/ZrO_2 supports had similar total numbers of acid sites with the exception of the sample based on the lab synthesised zirconium hydroxide which had significantly lower numbers of acid sites (Fig. 5.1 and Table 5.1). Although, the total number of acid sites was similar between tungsten supported on the MEL and DKK zirconium hydroxide supports, the ratio of LAS/BAS differed greatly. The WO_3/ZrO_2 DKK support had the highest number of LAS of all the supports tested but one of the lowest numbers of BAS. On the other hand, the WO_3/ZrO_2 MEL support had the highest number of BAS with an average number of LAS.

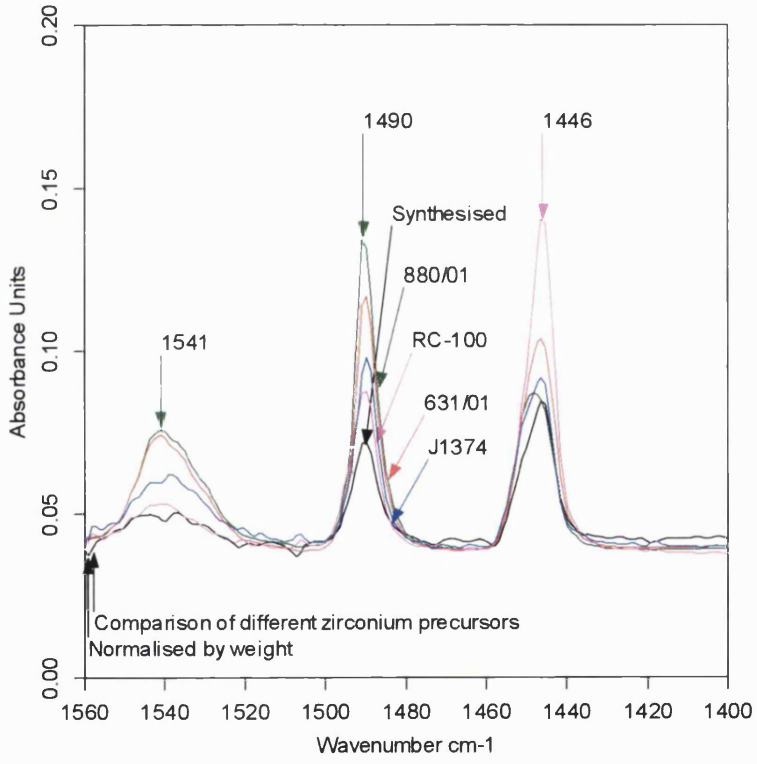

Fig. 5.1. IR spectra (Py region) after pyridine adsorption comparing 10 wt% WO_3/ZrO_2 samples synthesised using three different zirconium hydroxide precursors (Lab synthesised, MEL 880/01 and DKK RC-100) and two commercial WO_3/ZrO_2 supports (MEL 631/01 and DKK J1374).

Table 5.1. Acidity measurements for 10 wt% WO_3/ZrO_2 samples synthesised from different zirconium hydroxide precursors (DKK RC-100, MEL 880/01 and Lab synthesised) compared to commercial supports (DKK J1374 and MEL 631/01).

Support	DKK J1374	MEL XZO 631/01	DKK RC-100	MEL XZO 880/01	Lab synthesised
BAS + LAS (μmol/g)	44	44	45	47	32
Ratio LAS/BAS	1.3	1.2	4.0	1.2	2.2
LAS (μmol/g)	25	24	36	26	22
BAS (μmol/g)	19	20	9	21	10

Based on the results of repeated experiments, the error was found to be approximately 8%.

Based on the results obtained, the two commercially available zirconium hydroxides, MEL XZO 880/01 and DKK RC-100 zirconium hydroxides were selected for further studies. The lab synthesised zirconium hydroxide was not pursued further due to the low number of acid sites generated when impregnated with tungsten. The two commercial zirconium hydroxides, MEL XZO 880/01 and DKK RC-100 were used to synthesise a series of WO_3/ZrO_2 supports to investigate the effect of tungsten oxide loading on the number and strength of acid sites.

5.2 MEL XZO 880/01 zirconium hydroxide precursor

WO_3/ZrO_2 containing 5, 10, 15 and 20 wt% tungsten oxide supported on MEL zirconium hydroxide was synthesised and characterised by IR spectroscopy, XRD and TEM to examine the acidity, textural and structural properties of the WO_3/ZrO_2 MEL supports. The IR spectra in Fig. 5.2.1 demonstrate that the number of BAS gradually increases as the tungsten oxide loading was increased

from 5 wt% to 15 wt%. On the other hand, the number of LAS only increases up to 10 wt% tungsten before gradually decreasing.

At 20 wt% tungsten oxide loading, both the numbers of BAS and LAS drops slightly compared to the 15 wt% WO_3/ZrO_2 MEL support. It is interesting to note that a peak shift was observed from 1446 cm^{-1} on the 5 and 10 wt% WO_3/ZrO_2 supports to 1449 cm^{-1} present on the 15 and 20 wt% WO_3/ZrO_2 supports, which suggests a change in the type of LAS formed.

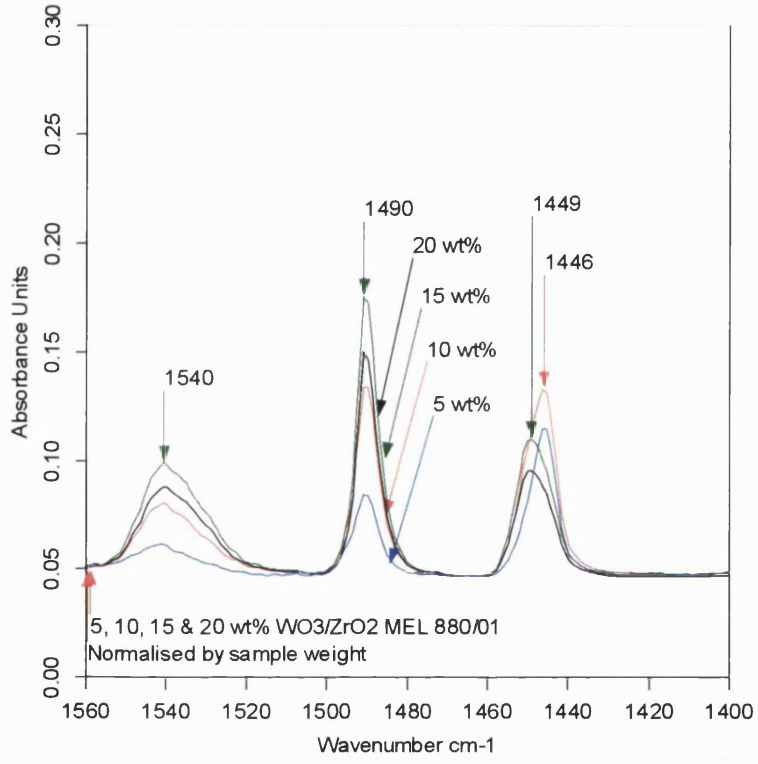

Fig. 5.2.1. IR spectra (Py region) after pyridine adsorption comparing WO_3/ZrO_2 MEL supports containing 5, 10, 15 and 20 wt% tungsten.

No clear changes to the LAS strength as the tungsten oxide loading was increased from 5 wt% to 20 wt% could be determined from the pyridine desorption profile in Fig. 5.2.2. It could be suggested that there is the possibility that the LAS strength has increased slightly when comparing the LAS strength of the 5 wt% and 15 wt% tungsten oxide supported on zirconia.

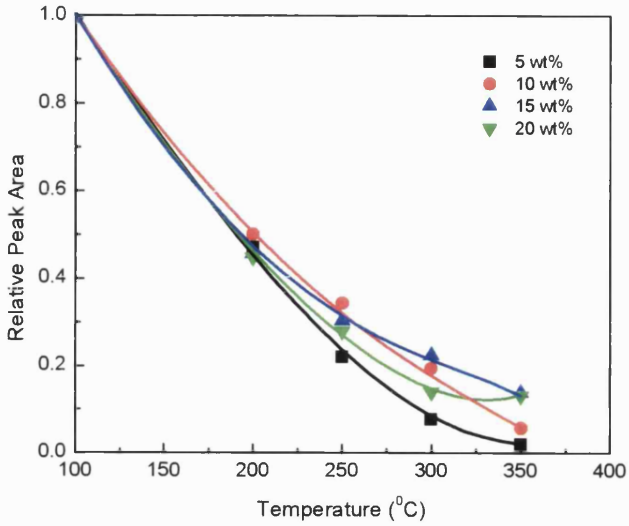

(A)

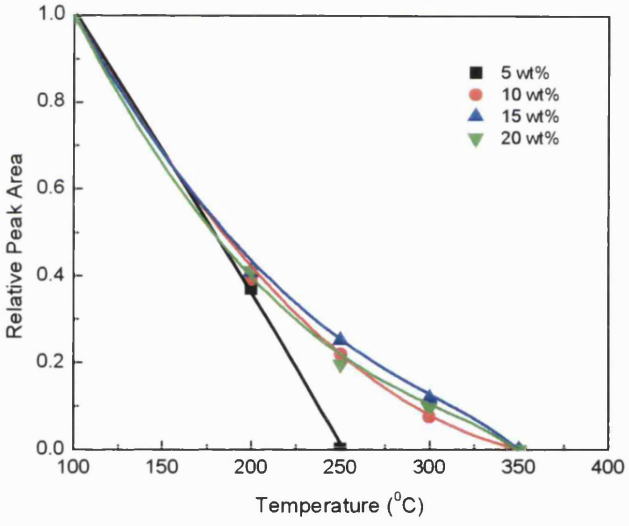

(B)

Fig. 5.2.2. Pyridine desorption from (A) LAS and (B) BAS present in the WO_3/ZrO_2 MEL supports containing 5, 10, 15 and 20 wt% tungsten oxide.

It is possible that the BAS strength increases when the tungsten oxide loading was increased above 5 wt%. The BAS strength change could be attributed to the presence of more tungsten species at higher loadings which also leads to the generation of more BAS. Any changes in the BAS and LAS strength would occur at lower tungsten oxide loadings when tungsten oxide is first introduced

and approaches the tungsten oxide saturation loading of the MEL zirconium hydroxide.

At high tungsten oxide loading, near or above the optimum tungsten oxide loading, there would be a smaller impact on the acidity of the WO_3/ZrO_2 support as the MEL zirconium hydroxide becomes saturated with tungsten oxide. Similar findings were reported in the literature by Scheithauer et al. [74].

The IR spectra are supported by the quantitative data of BAS and LAS calculated that are shown in Table 5.2. The values for the 5 wt% WO_3/ZrO_2 support in were obtained by comparing the peak intensities with those of the other supports, because accurate quantitative values could not be determined through analysis of the Py adsorption experiment results. The 5 wt% WO_3/ZrO_2 support was saturated with pyridine at a low concentration which affects the accuracy of the quantitative analysis.

Shimizu et al. [91] have suggested that new BAS are formed as more of the exposed Zr^{4+} sites that generate LAS are occupied by tungsten species. This is a possible explanation for why the number of LAS decreases with tungsten oxide loading whilst the number of BAS increases.

Table 5.2. Acidity measurements for WO_3/ZrO_2 MEL supports calcined at 830 °C containing 5, 10, 15 and 20 wt% tungsten oxide.

Loading (wt%)	**5**	**10**	**15**	**20**
BAS + LAS (μmol/g)	29*	47	51	38
Ratio LAS/BAS	3.6*	1.2	0.8	0.7
LAS (μmol/g)	23*	26	23	15
BAS (μmol/g)	6*	21	28	23

** These values were obtained by comparison of peak intensities in Fig. 5.2.1.*

Based on the results of repeated experiments, the error was found to be approximately 7%.

At 20 wt% tungsten oxide loading, bulk tungsten oxide clusters start to form as there is an excess of tungsten species present. These bulk WO_3 clusters are not acidic and cause the drop in the number of BAS and LAS observed on the 20 wt% WO_3/ZrO_2 MEL support (Fig. 5.2.1 and Table 5.2). The changes in the acidity of the WO_3/ZrO_2 supports as the tungsten oxide loading was increased could also be related to the structural changes to the zirconia support as seen in the XRD results.

The XRD results obtained from Johnson Matthey show that as the tungsten oxide loading is increased, the zirconium oxide changes from the predominantly monoclinic phase to the desired tetragonal phase. Zirconium oxide in the tetragonal phase possesses higher surface areas and exhibits better catalytic activity. The supports with 5 and 10 wt% tungsten oxide loading consist of zirconium oxide primarily in the monoclinic phase with some tetragonal zirconium oxide (Figs. 5.2.3 and 5.2.4).

In Figs 5.2.3 and 5.2.4, the red lines indicate the amount of tetragonal ZrO_2 present and the blue lines represent the level of monoclinic ZrO_2. The tetragonal content remains similar between the 5 and 10 wt% WO_3/ZrO_2 but the amount of monoclinic ZrO_2 decreases with higher tungsten oxide loadings represented by the peaks highlighted with blue lines in Figs 5.2.3 and 5.2.4.

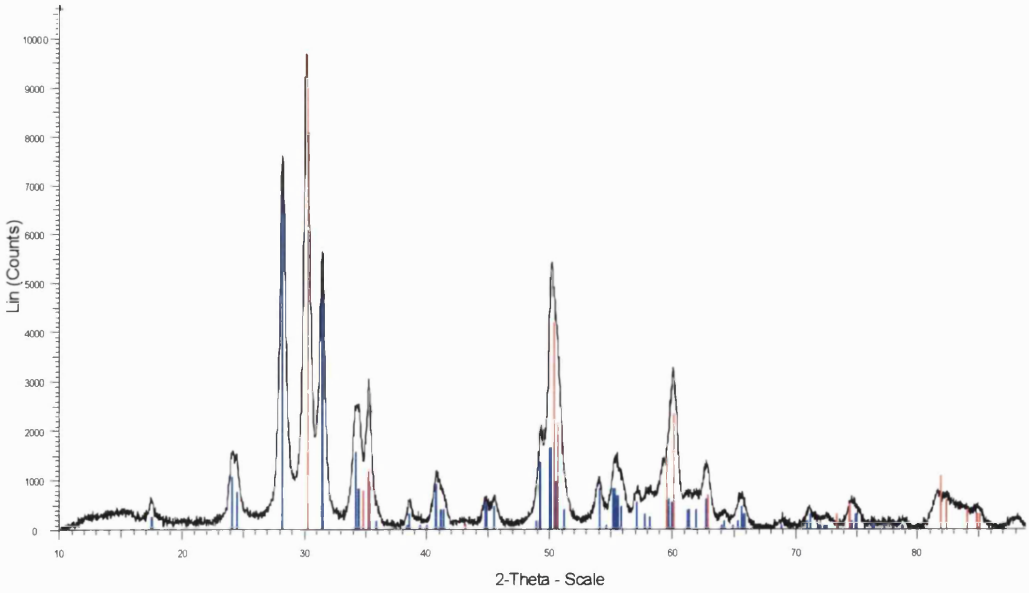

Fig. 5.2.3. X-ray diffraction pattern of 5 wt% WO_3/ZrO_2 MEL support.

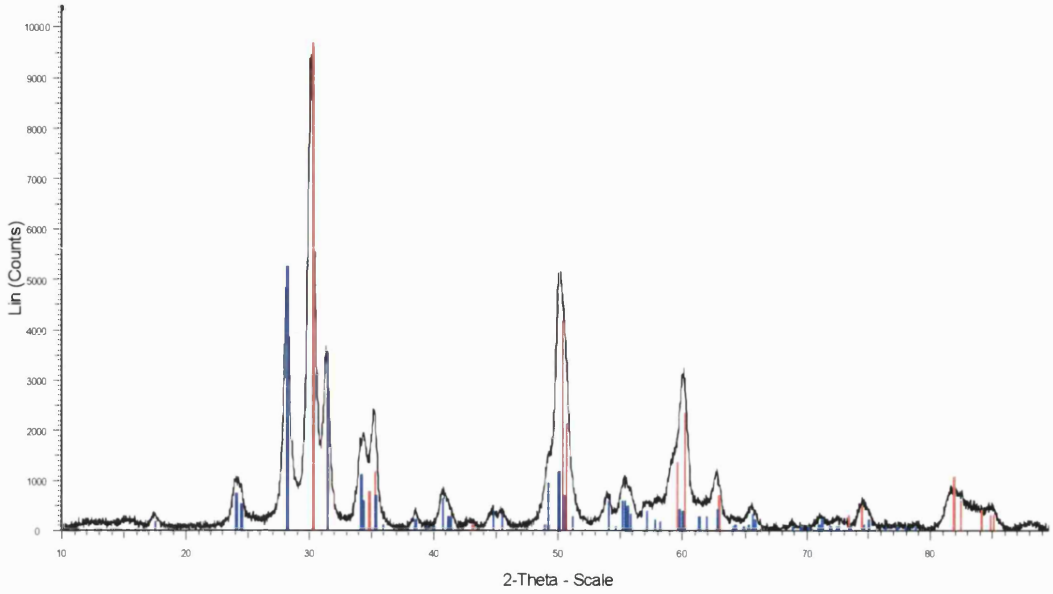

Fig. 5.2.4. X-ray diffraction pattern of 10 wt% WO_3/ZrO_2 MEL support.

However, at 15 and 20 wt% tungsten oxide loading, the MEL zirconium oxide is primarily in the tetragonal phase with a minor amount of monoclinic zirconium oxide. Shown by the increase in the intensities of the peaks assigned to tetragonal ZrO_2 species in Figs 5.2.5 and 5.2.6. The peaks assigned to tetragonal ZrO_2 are highlighted in green and those linked to monoclinic species are presented by blue lines. The XRD results indicate that at 5 and 10 wt% tungsten oxide, there is insufficient tungsten oxide present to effectively stabilise the zirconium oxide thus it remains mainly in the monoclinic phase.

At 15 and 20 wt% tungsten oxide loading, the zirconium oxide is stabilised by the tungsten species leading to the predominantly tetragonal phase. These results support those presented previously in Fig. 5.2.1 and Table 5.2 where the 15 wt% WO_3/ZrO_2 was shown to be the most acidic support.

Furthermore, the crystallite size decreases from ~16 nm to ~14 nm when the tungsten oxide loading is increased above 5 wt%. If the ZrO_2 crystallite size increases above 20 nm, the tetragonal clusters become unstable and will transform into monoclinic crystallites of the same size [76].

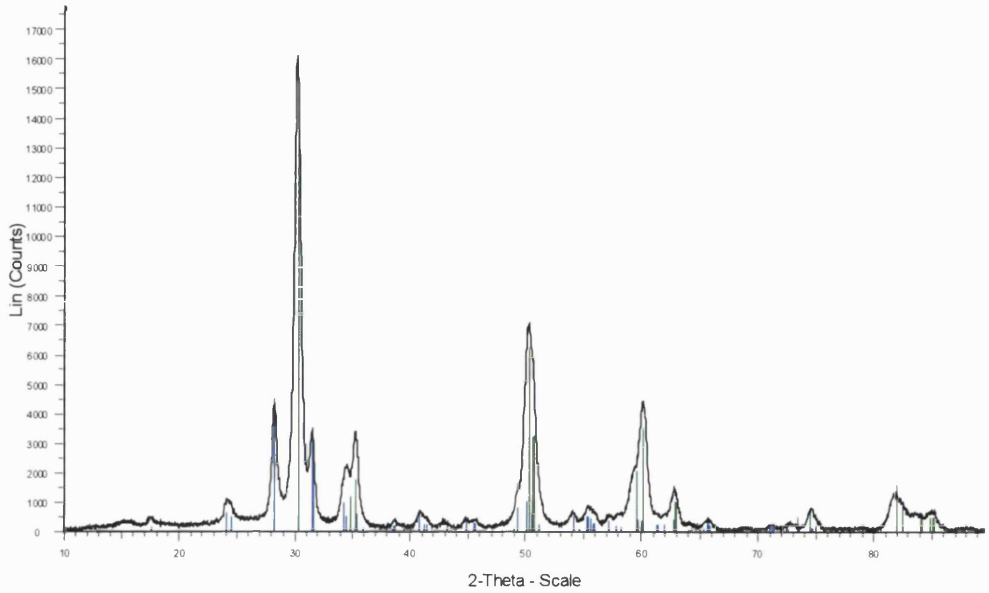

Fig. 5.2.5. X-ray diffraction pattern of 15 wt% WO_3/ZrO_2 MEL support.

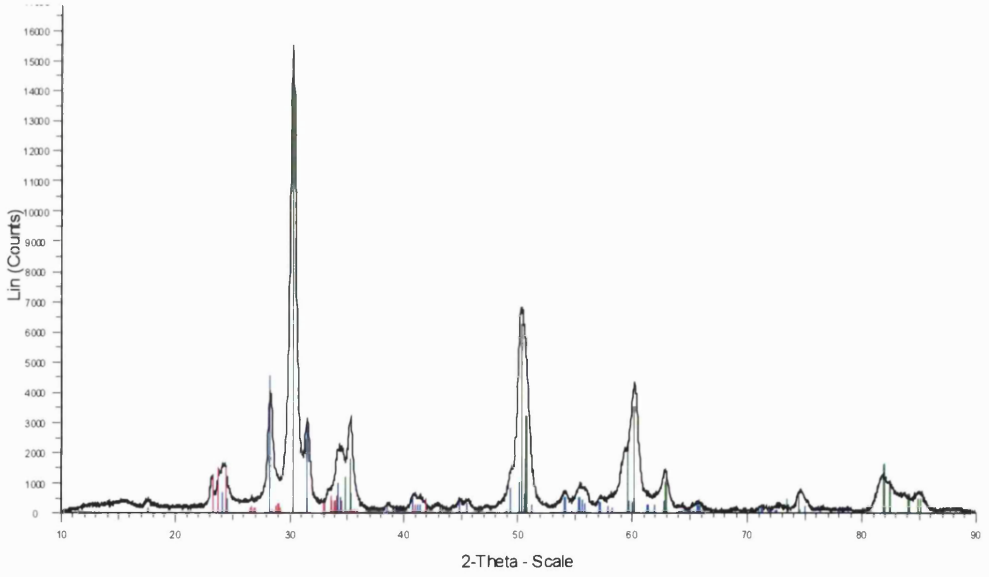

Fig. 5.2.6. X-ray diffraction pattern of 20 wt% WO_3/ZrO_2 MEL support.

At 20 wt% tungsten oxide loading, although the MEL zirconium oxide is stabilised in the tetragonal phase, the excess tungsten species will start to form bulk WO_3 clusters that are not acidic and theoretically would decrease the overall acidity of the support. This is supported by the XRD results where a minor

amount of tungsten oxide was detected on the 20 wt% WO_3/ZrO_2 represented by the peaks highlighted in red in Fig. 5.2.6.

The presence of WO_3 species coincides with the drop in the total number of acid sites (Fig. 5.2.1 and Table 5.2). There was also a noticeable colour change from white to a pale yellow colour when the tungsten oxide loading was increased from 15 to 20 wt% tungsten oxide. The pale yellow colour can be attributed to the presence of tungsten oxide, WO_3 [140].

All the WO_3/ZrO_2 MEL supports were shown to consist of large conglomerates of elongated particles in the nanoparticle size and EDX analysis confirmed the presence of both zirconia and tungsten oxide with some copper oxide impurities (Fig. 5.2.7).

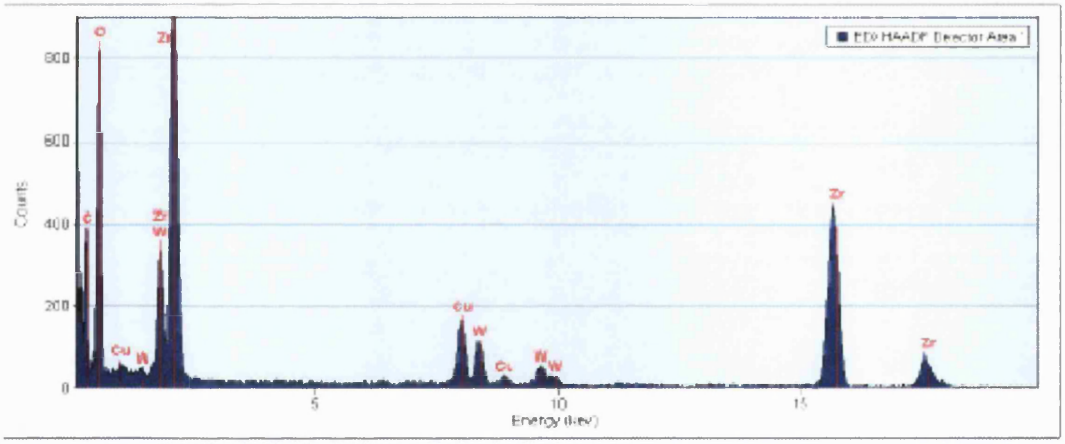

Fig. 5.2.7. EDX analysis of 20 wt% WO_3/ZrO_2 MEL support.

The supports were also characterised using TEM to examine the distribution of tungsten oxide on zirconia. The summary of the TEM characterisation report from Johnson Matthey stated that the tungsten oxide is well dispersed on zirconia and the main results are shown in Fig. 5.2.8. The darker specks shown in Fig 5.2.8 are related to denser materials (tungsten oxide) or an area where the sample was slightly thicker. It should be noted that the limitation of the TEM characterisation is the fact that it only shows the distribution in a very small area of the overall sample. This raises the possibility that the region analysed may not be characteristic of the whole sample

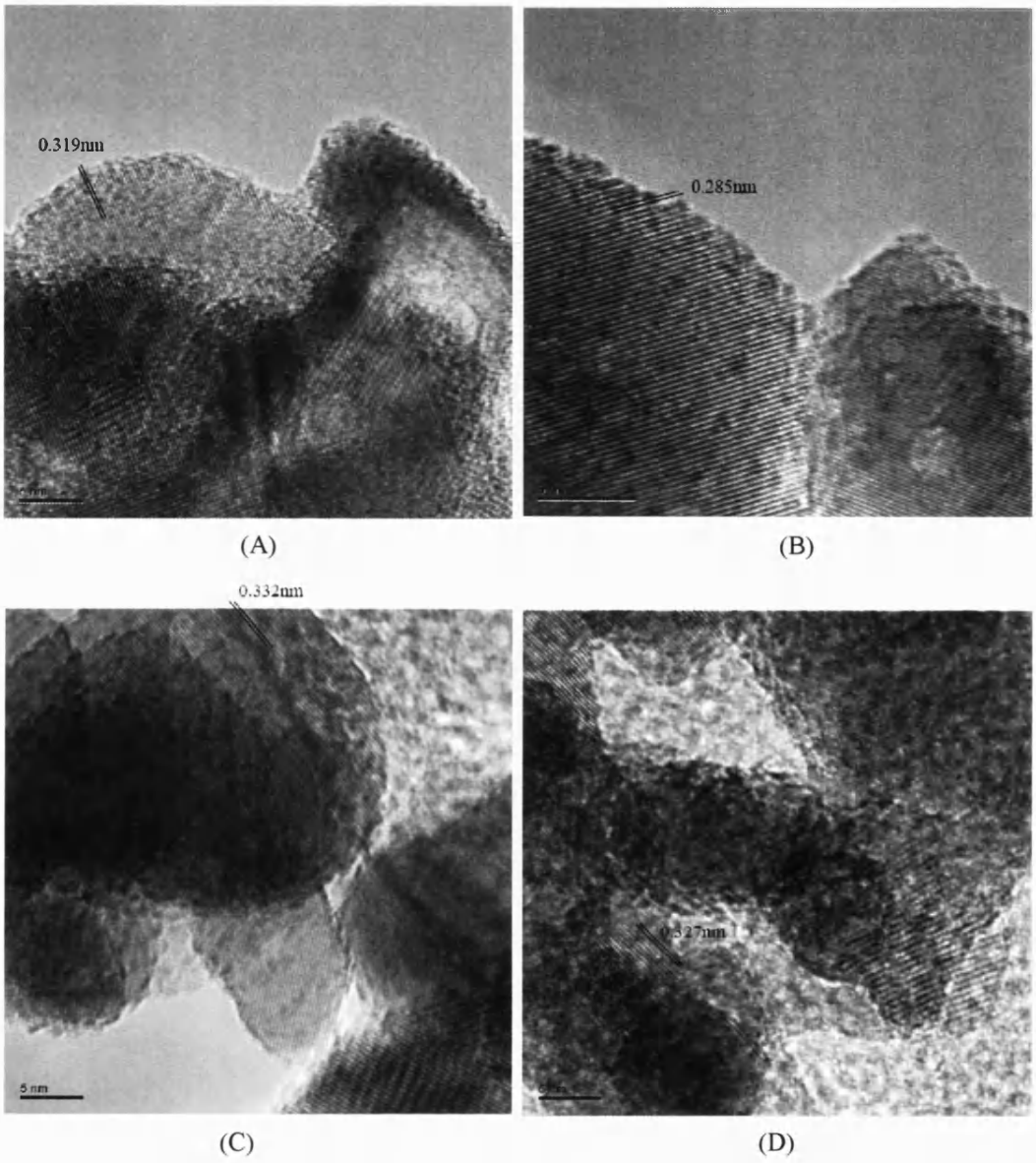

Fig. 5.2.8. TEM results for WO_3/ZrO_2 MEL supports containing (A) 5 wt%, (B) 10 wt%, (C) 15 wt% and (D) 20 wt% tungsten oxide.

The results in this section have shown that 15 wt% tungsten oxide is the optimum loading for tungsten oxide supported on MEL zirconium hydroxide. The 15 wt% WO_3/ZrO_2 MEL support exhibited the highest number and strength of BAS and LAS of the four samples tested. The zirconium oxide support was also primarily in the desired tetragonal phase.

Arata and Hino [71, 141] reported similar findings where 15 wt% tungsten oxide loading showed the best catalytic activity for the reaction of butane to isobutane. Similarly, Bordoloi et al. [142] have reported that 15 wt% WO_3/ZrO_2 calcined at 800 °C was the most active for acylation and alkylation reactions and the 20 wt% WO_3/ZrO_2 catalyst had slightly lower activity followed by the 10 wt% then 5 wt% samples. The reported results correlate well with the acidity of the samples obtained in this work (Table 5.2), where the 15 wt% tungsten oxide loading was the most acidic followed by the 20 wt%, 10 wt% and 5 wt% WO_3/ZrO_2 samples.

5.3 DKK RC-100 zirconium hydroxide precursor

Similar results were obtained with the WO_3/ZrO_2 supports synthesised using the DKK RC-100 zirconium hydroxide as the tungsten oxide loading was varied. The number of LAS steadily decreases as new BAS are formed as illustrated in Fig. 5.3.1 and Table 5.3. At 15 wt% tungsten oxide loading, the number of BAS remains similar to that of the 10 wt% WO_3/ZrO_2 support but a significant drop in the number of LAS occurs.

The results suggest that the DKK zirconium hydroxide is saturated with tungsten oxide at 10 wt% tungsten oxide loading compared to 15 wt% that was determined previously for the MEL XZO 880/01 zirconium hydroxide (Fig. 5.2.1). The changes in the number of BAS and LAS when the tungsten oxide loading was increased from 10 to 15 wt% on the WO_3/ZrO_2 DKK support is similar to the results obtained for the WO_3/ZrO_2 MEL support going from 15 wt% to 20 wt% tungsten oxide loading (Fig. 5.2.1).

The LAS strength of the WO_3/ZrO_2 DKK supports remains the same at both 10 wt% and 15 wt% tungsten oxide loading, but the BAS strength continues to increase slightly from 10 wt% to 15 wt% tungsten oxide. The changes in the LAS and BAS strength shown in Fig. 5.3.2 are similar to the results observed previously with the WO_3/ZrO_2 MEL support (Fig. 5.2.2). There was no change in the LAS strength when the tungsten oxide loading is increased above 10 wt% as all the free Zr^{4+} adsorption sites are already occupied.

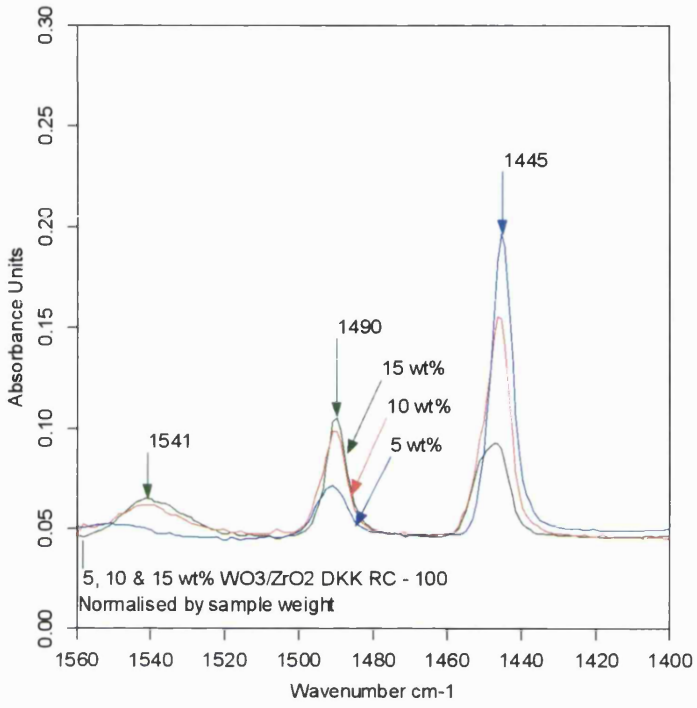

Fig. 5.3.1. IR spectra (Py region) after pyridine adsorption of WO_3/ZrO_2 DKK support containing 5, 10 and 15 wt% tungsten oxide.

Table 5.3. Acidity measurements for WO_3/ZrO_2 DKK supports calcined at 830 °C and containing 5, 10 and 15 wt% tungsten oxide.

Loading (wt%)	**5**	**10**	**15**
BAS + LAS (μmol/g)	**47***	**45**	**20**
Ratio LAS/BAS	-	**4.0**	**1.5**
LAS (μmol/g)	**47***	**36**	**12**
BAS (μmol/g)	**0***	**9**	**8**

** These values were obtained by comparison of peak intensities in Fig. 5.3.1.*

Based on the results of repeated experiments, the error was found to be approximately 9%.

There is an increase in the BAS strength due to the presence of additional tungsten species at higher tungsten oxide loading. These findings are similar to the results observed with the WO_3/ZrO_2 MEL support when the tungsten oxide loading was increased from 15 wt% to 20 wt% tungsten oxide. This supports the possibility that the DKK zirconium hydroxide is saturated at 10 wt% tungsten oxide loading.

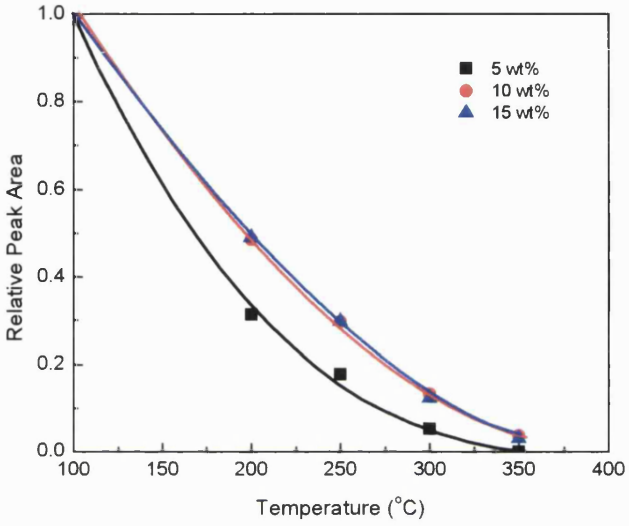

(A)

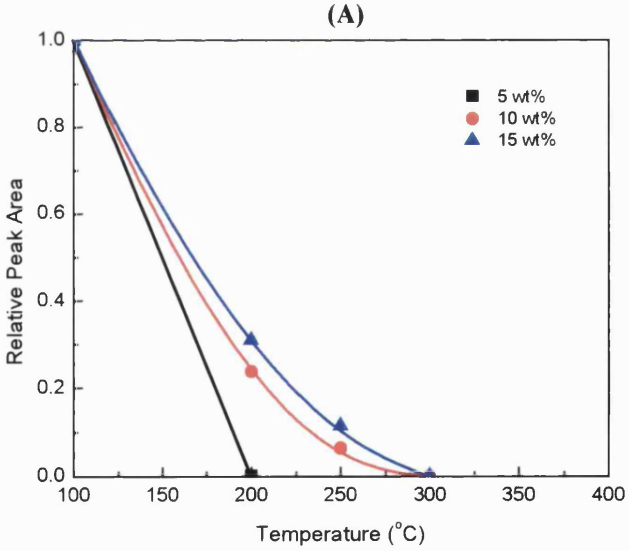

(B)

Fig. 5.3.2. Pyridine desorption from (A) LAS and (B) BAS present in the WO_3/ZrO_2 DKK support containing 5, 10 and 15 wt% tungsten oxide.

The 15 wt% WO_3/ZrO_2 DKK support was characterised using XRD where it was shown to consist primarily of zirconium oxide in the monoclinic phase with minor amounts of poorly crystalline tetragonal zirconium oxide (Fig. 5.3.3). A trace amount of tungsten oxide was also detected via XRD shown by the red peaks in Fig 5.2.6.

These results indicate that the DKK zirconium hydroxide was saturated at 10 wt% tungsten oxide. At 15 wt% there is an excess of tungsten species that form the bulk WO_3 clusters as detected by XRD analysis shown by the red peaks in Fig. 5.3.3 that leads to the drop in the number of LAS. These results are similar to the XRD results for the 20 wt% WO_3/ZrO_2 synthesised from the MEL zirconium hydroxide support.

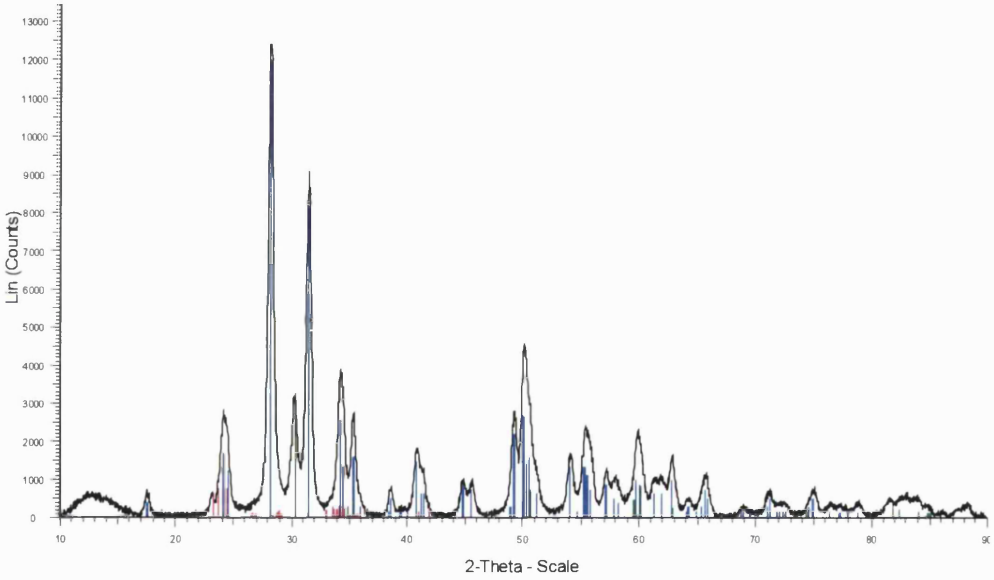

Fig. 5.3.3. X-ray diffraction pattern of 15 wt% WO_3/ZrO_2 DKK support.

The results show that 10 wt% is the optimum tungsten oxide loading for tungsten oxide supported on the DKK zirconium hydroxide. Previously, it was shown that 15 wt% tungsten oxide was the optimum loading for WO_3/ZrO_2 synthesised from the MEL zirconium hydroxide (Section 5.2). These results suggest that the optimum tungsten oxide loading varies depending on the zirconium hydroxide precursor used. This is supported by results in the literature where various

authors have reported different optimum tungsten oxide loadings ranging from 10 to 16 wt% [71, 73, 79, 140, 142-144].

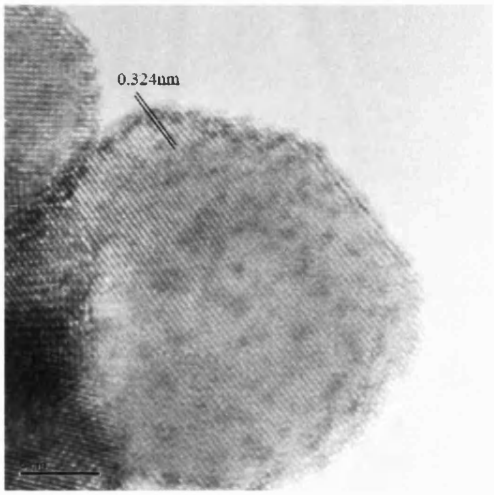

Fig. 5.3.4. TEM of 15 wt% WO_3/ZrO_2 DKK support.

5.4 Calcination temperature

The effect of the calcination temperature on the acidity of the WO_3/ZrO_2 support was investigated. 15 wt% WO_3/ZrO_2 synthesised using DKK zirconium hydroxide was calcined at five different temperatures, 650, 710, 770, 830 and 890 °C. The supports were characterised by IR spectroscopy using pyridine and the IR spectra are shown in Fig. 5.4.1.

The number of LAS decreases steadily as the calcination temperature is increased and significant drop in the number of LAS occurred when the calcination temperature was increased from 710 °C to 770 °C and from 830 °C to 890 °C. The number of BAS decreases slightly but remains fairly similar at calcination temperatures between 650 to 830 °C. There were no BAS and only a small number of LAS present when the 15 wt% WO_3/ZrO_2 DKK support was calcined at 890 °C.

High calcination temperatures are required to bring some of the tungsten oxide from the bulk to the surface of the zirconia support where it stabilises the tetragonal structures and forms new BAS. However, at too high a temperature (890 °C), the effectiveness of tungsten oxide is reduced as it sinters then agglomerates into bulk inactive clusters (Chapter 2.9). Furthermore, the WO_x species will then agglomerate into WO_3 clusters that interact poorly and are ineffective at inhibiting sintering of the zirconium oxide support. This leads to the loss of acid sites and the zirconium oxide transformation from the tetragonal to the monoclinic phase, which occurred on the support calcined at 890 °C. This is in agreement with the results reported in the literature for a WO_3/ZrO_2 support calcined at 900 °C [76].

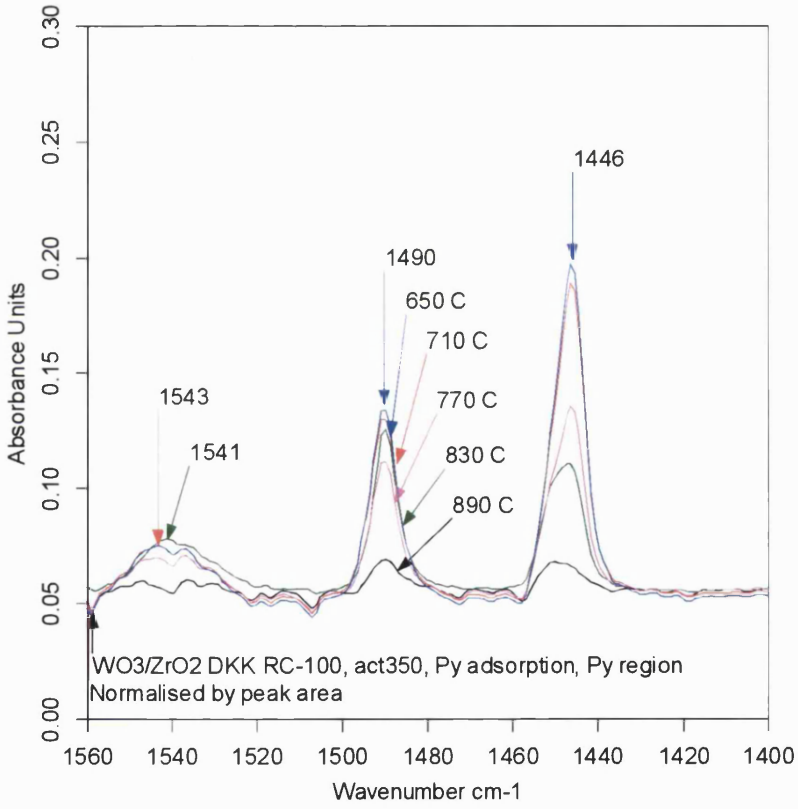

Fig. 5.4.1. IR spectra (Py region) after pyridine adsorption of 10 wt% WO_3/ZrO_2 DKK support calcined at 650, 710, 770, 830 and 890 °C.

The quantitative acidity results in Table 5.4 show that the number of BAS remains constant when the calcination temperature is increased from 650 °C to

830 °C. At the calcination temperature of 890 °C, a significant decrease in the number of BAS occurs. On the other hand, the number of LAS decreases steadily as the calcination temperature is raised. This is due to the better diffusion of tungsten species from the bulk to the surface as the calcination temperature is increased where they occupy the Zr^{4+} adsorption sites thus reducing the number of Zr^{4+} LAS.

Table 5.4. Acidity measurements for 15 wt% WO_3/ZrO_2 DKK support calcined at 650, 710, 770, 830 and 890 °C.

Calcination temperature	**650 °C**	**710 °C**	**770 °C**	**830 °C**	**890 °C**
BAS + LAS (μmol/g)	54	51	37	26	9*
Ratio LAS/BAS	3.2	2.9	2.2	1.4	0.8*
LAS (μmol/g)	41	38	25	15	4*
BAS (μmol/g)	13	13	12	11	5*

** These values were obtained by comparison of peak intensities in Fig. 5.4.1.*

Based on the results of repeated experiments, the error was found to be approximately 8%.

The number of BAS remains similar as there may only be a fixed number of adsorption sites on the DKK zirconium hydroxide where tungsten oxide will form new BAS. Similarly, Barton et. al. [76] had proposed that there are only a fixed number of strong binding sites for metatungstate ions on zirconium hydroxide. This would also account for the difference in the number of BAS present on the 10 wt% WO_3/ZrO_2 synthesised from the DKK and MEL zirconium hydroxides (Table 5.1). Different zirconium hydroxides may have different number of binding sites and, therefore, the maximum number of BAS would be dependent on the zirconium hydroxide precursor used. For example, the MEL zirconium hydroxide has a greater number of binding sites compared to the DKK zirconium hydroxide and, as a consequence, generates more BAS.

The BAS and LAS strength initially increases when the calcination temperature is raised from 650 °C to 710 °C (Fig. 5.4.2). At calcination temperatures above 710 °C, the BAS and LAS strength decreases steadily with increasing calcination temperature. The support calcined at 890 °C has a significant drop in the number and strength of both BAS and LAS.

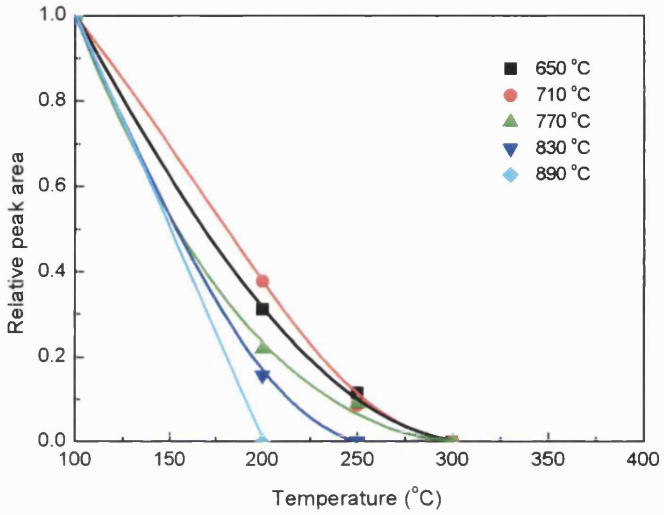

(A)

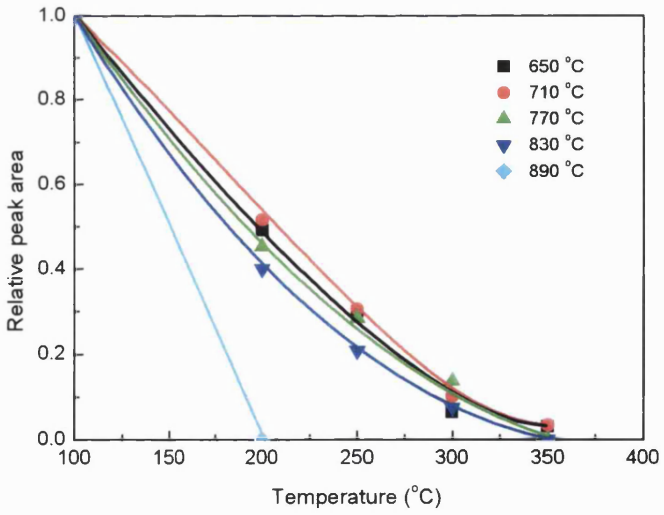

(B)

Fig. 5.4.2. Pyridine desorption from (A) LAS and (B) BAS present in 10 wt% WO_3/ZrO_2 DKK support calcined at 650, 710, 770, 830 and 890 °C.

The results of the effect of calcination temperature on the acidity of the WO_3/ZrO_2 DKK support show that the optimum calcination temperature is 710 °C. At temperatures above 710 °C a decrease in the number and strength of both the BAS and LAS occurs. Tungsten oxide is not able to effectively inhibit sintering of the zirconium oxide support when calcined above 710 °C. However, it should be noted that the support used, 15 wt% WO_3/ZrO_2 synthesised using DKK zirconium hydroxide has a tungsten oxide loading above the optimum 10 wt% tungsten oxide loading for that zirconium hydroxide, which may affect the optimum calcination temperature.

It was previously shown that the optimum tungsten oxide loading for WO_3/ZrO_2 synthesised using the DKK zirconium hydroxide was 10 wt% tungsten oxide (Section 5.3). At 15 wt% tungsten oxide loading, excess tungsten species will be present on that support. There is a strong possibility that WO_3 clusters will be formed at lower calcination temperatures due to the presence of these excess tungsten species which would decrease the acidity of the support.

The optimum calcination temperature would vary depending on the tungsten oxide saturation level of that support. Lower calcination temperatures would be suitable at tungsten oxide loadings above the saturation level and at tungsten oxide loadings below the saturation loading, it may be possible to use higher calcination temperatures. Busca [145] had reported that 900 °C was the optimum calcination temperature for the 10 wt% WO_3/ZrO_2 support he studied. That particular support was most likely not saturated with tungsten oxide at 10 wt% which allowed the support to be calcined to 900 °C.

At tungsten oxide saturation levels near or below the optimum, the ideal calcination temperature should not change. The results obtained in this study suggest that the optimum calcination temperature lies between 710 °C to 830 °C. This is supported by the results reported in the literature where calcination temperatures around 800 °C were shown to be the most favourable [142, 145, 146].

5.5 Discussion and Summary

Tungsten oxide supported on zirconia was synthesised using different zirconium hydroxide precursors and the acidity of the WO_3/ZrO_2 supports was compared to commercially available WO_3/ZrO_2. The zirconium hydroxide synthesised in this work was shown to be inferior to the commercially available samples. The two commercial zirconium hydroxides, DKK RC-100 and MEL XZO 880/01, were selected to investigate the effect of tungsten oxide loading on the acidity, textural and structural properties of the WO_3/ZrO_2 catalytic support.

The zirconium hydroxide and tungsten oxide precursors used in the synthesis of WO_3/ZrO_2 could be an important factor in the final properties of the WO_3/ZrO_2 support [29]. For example, it has been suggested that the number of zirconium adsorption sites that are required for BAS generation varies depending on the zirconium hydroxide precursor (Section 5.4). The number of BAS would change based on the zirconium hydroxide used, where the MEL precursor was shown to generate more BAS compared to the DKK precursor based on the results of the comparison of the 10 wt% WO_3/ZrO_2 DKK and MEL supports (Table 5.1).

Furthermore, it was shown that the DKK and MEL zirconium hydroxides have different tungsten oxide saturation loadings where the optimum tungsten oxide loading was found to be 10 wt% and 15 wt% tungsten oxide supported on the DKK and MEL zirconium hydroxide, respectively. Exceeding the tungsten oxide saturation loading causes a reduction in the total number of acid sites.

In addition, the synthesis method can possibly have a dramatic impact on the properties of the WO_3/ZrO_2 support. Different authors have reported that the synthesis method may or may not be important. It has been reported that the synthesis procedure can not influence the structure of the final WO_3/ZrO_2 support [71]. For example, Boyse et al. [87] had concluded that the synthesis procedure only affects the required calcination temperature of the WO_3/ZrO_2 support and does not alter the active species for the n-butane isomerisation reaction.

On the other hand, Afanasieve et al. [77] have reported that the preparation procedure appears to strongly affect the state of the tungstate species. It has also been reported that WO_3/ZrO_2 supports synthesised by co-precipitation and sol-gel procedures showed promising results in terms of the acidity of the supports that were possibly stronger than those present on the supports prepared by incipient wetness impregnation [87, 124, 147, 148]. This is an additional area that was not addressed in this thesis which could be of interest in the future. However, it should be noted that WO_3/ZrO_2 supports are primarily prepared by incipient wetness impregnation of tungsten oxide on zirconium hydroxide.

Tungsten oxide stabilises the zirconium oxide in the tetragonal phase provided there is sufficient tungsten oxide present, and also generates new BAS as the tungsten oxide loading is increased. However, at high tungsten oxide loadings where the zirconium hydroxide is saturated with tungsten oxide, bulk tungsten oxide clusters are formed as detected through the use of XRD (Figs. 5.2.6 and 5.3.3). These WO_3 clusters are not acidic and lead to a drop in the total number of acid sites and, in particular, the number of BAS.

High calcination temperatures are required to synthesise a suitable WO_3/ZrO_2 support, where the calcination temperature has to be high enough to allow tungsten oxide to diffuse from the bulk to the surface. On the other hand, if the calcination temperature is too high, the WO_x species will agglomerate into bulk WO_3 clusters and no longer inhibit the zirconium oxide support from sintering leading to the loss of surface area and acidity.

The results in Section 5.4 showed that at the calcination temperature of 890 °C there was a significant reduction in the acidity of the WO_3/ZrO_2 support due to sintering of the zirconium oxide support. This is in agreement with results reported in the literature where 900 °C was shown to be the maximum calcination temperature that can be used for WO_3/ZrO_2 supports [76]. The optimum calcination temperature was found to be dependent on the tungsten oxide saturation level of the support. Above the optimum tungsten oxide loading, lower calcination temperatures should be used to prevent the formation of WO_3 clusters that reduce the strength and number of BAS and LAS. At lower

tungsten oxide loadings, it may be possible to use higher calcination temperatures.

The results obtained in this section show that there are many variables that affect the number and strength of BAS and LAS on WO_3/ZrO_2. As a result of this, the acidity of the WO_3/ZrO_2 support can be tailored to fit the desired application. For example, if a reaction proceeds through a LAS dependent mechanism, the DKK zirconium hydroxide would be more suitable over the MEL precursor. This is because the WO_3/ZrO_2 supports synthesised from DKK zirconium hydroxide have been shown to exhibit higher numbers of LAS compared to the other precursors tested (Table 5.1).

Similarly, the MEL zirconium hydroxide would be a better choice if the number of BAS is important. The tungsten oxide loading can also be varied which will affect the number of LAS and BAS which also influences the ratio of LAS to BAS (Tables 5.2 and 5.3). The ratio of LAS/BAS could be an important factor for certain applications.

Furthermore, the calcination temperature will also affect the acidity of the WO_3/ZrO_2 support (Table 5.4). The number of BAS did not change with the calcination temperature but the number of LAS decreases with increasing calcination temperature. Thus, it is possible to change the number of LAS present and the LAS/BAS ratio on the WO_3/ZrO_2 support by controlling the calcination temperature.

The acidic properties of the WO_3/ZrO_2 catalytic support can be tailored to fit a particular application by changing the three main variables, zirconium hydroxide precursors used, tungsten oxide loading and calcination temperature. The MEL XZO 880/01 zirconium hydroxide was selected for further work based on the high number of BAS and LAS generated after impregnating with tungsten oxide.

The MEL zirconium hydroxide also has a higher tungsten oxide saturation loading compared to the DKK zirconium hydroxide which is beneficial in two different ways. This allows greater freedom to vary the tungsten oxide loading

of the WO_3/ZrO_2 support and higher calcination temperatures can be used at high tungsten oxide loading without detrimental effects on the total number of acid sites. WO_3/ZrO_2 synthesised using MEL zirconium hydroxide will be used as the catalytic support for development of a new catalyst for the selective catalytic reduction of nitrogen oxides by ammonia.

Chapter 6:
Iron promoted tungsten oxide supported on zirconia

Chapter 6: Iron promoted tungsten oxide supported on zirconia

Iron was described previously in Chapter 2 as being active for NH_3 SCR of NO_x when supported on pillared clays, mixed oxides and zeolites [102-112]. Furthermore, iron is also a non-precious metal therefore more economically viable and environmentally benign compared to existing catalysts based on vanadium supported on tungsten oxide supported on titania. It should be noted that iron supported on beta zeolite has been reported to be one of the most promising zeolite catalysts due to its high activity and good hydrothermal resistance [149].

In this chapter, iron supported on commercial tungsten oxide supported on zirconia (DKK J1374) catalysts were characterised and tested in NH_3 SCR under lean conditions at reaction temperatures between 150 and 550 °C. $Fe/WO_3/ZrO_2$ was found to be a promising catalyst for NH_3 SCR based on the comparison of the SCR activity of fresh and aged $Fe/WO_3/ZrO_2$ and Fe/beta catalysts. The $Fe/WO_3/ZrO_2$ catalysts were subsequently synthesised using MEL XZO 880/01 zirconium hydroxide to investigate the influence of the synthesis procedure. The properties of WO_3/ZrO_2 can be altered depending on the tungsten oxide loading and calcination temperature as outlined in Chapter 5.

The following sections examine the $Fe/WO_3/ZrO_2$ catalysts in more detail by investigating the effects of the synthesis procedure, iron and tungsten oxide loading on the SCR activity in order to better understand why the $Fe/WO_3/ZrO_2$ catalysts are active for NH_3 SCR of NO_x. The catalysts are defined as $xFe/yWO_3/ZrO_2$ or xFe/beta where x represents the iron loading (wt%) and y represents the tungsten oxide loading (wt%). Catalysts synthesised on the basis of DKK J1374 WO_3/ZrO_2 support are represented as $Fe/WO_3/ZrO_2$ DKK catalysts. Catalysts based on WO_3/ZrO_2 synthesised using MEL XZO 880/01 zirconium hydroxide are denoted as $Fe/WO_3/ZrO_2$ MEL catalysts.

6.1 Fresh $Fe/WO_3/ZrO_2$ DKK catalyst

Commercially available 9 wt% WO_3/ZrO_2 (DKK J1374) was used to synthesise a series of catalysts containing 0.5, 1, 2, 3 and 10 wt% iron which were tested for NH_3 SCR activity. Fig. 6.1.1 demonstrates that the WO_3/ZrO_2 DKK support without iron is not active for NH_3 SCR, in contrast to the $Fe/WO_3/ZrO_2$ DKK catalysts. The SCR activity of the $Fe/WO_3/ZrO_2$ DKK catalysts increases with iron loading up to 3 wt% where the improvement primarily occurs in the low temperature region. The differences in the high temperature activity are less pronounced.

The increase in the catalytic activity could be related to the higher numbers of well dispersed mononuclear Fe sites as the iron loading is increased from 0.5 to 3 wt% as it has been reported that mononuclear Fe sites are active for NH_3 SCR of NO_x [106]. At loadings above 3 wt%, bulk iron species are expected to be formed and these iron oligomers/clusters have been shown to be unselective for NH_3 SCR [74, 110]. This would account for the lower SCR activity exhibited by the $10Fe/WO_2/ZrO_2$ catalyst due to the formation of iron oligomers/clusters that are not active for NH_3 SCR. However, at reaction temperatures above ~450 °C, the SCR activity of all the $Fe/WO_3/ZrO_2$ DKK catalysts begins to decrease due to the catalysts becoming slightly unselective at high temperatures.

The activity of the $1Fe/WO_3/ZrO_2$ catalyst was unexpected, where initially as expected there was an improvement in the low temperature activity compared to the $0.5Fe/WO_3/ZrO_2$ catalyst. However, above 325 °C, the SCR activity of the $1Fe/WO_3/ZrO_2$ catalyst begins to level off and reaches a maximum of 50 % NO_x conversion at 425 °C in comparison to 70 % conversion seen with the $0.5Fe/WO_3/ZrO_2$ catalyst. In addition, the catalytic activity of the $1Fe/WO_3/ZrO_2$ catalyst begins to decrease dramatically above ~490 °C which was not observed with any of the other $Fe/WO_3/ZrO_2$ catalysts.

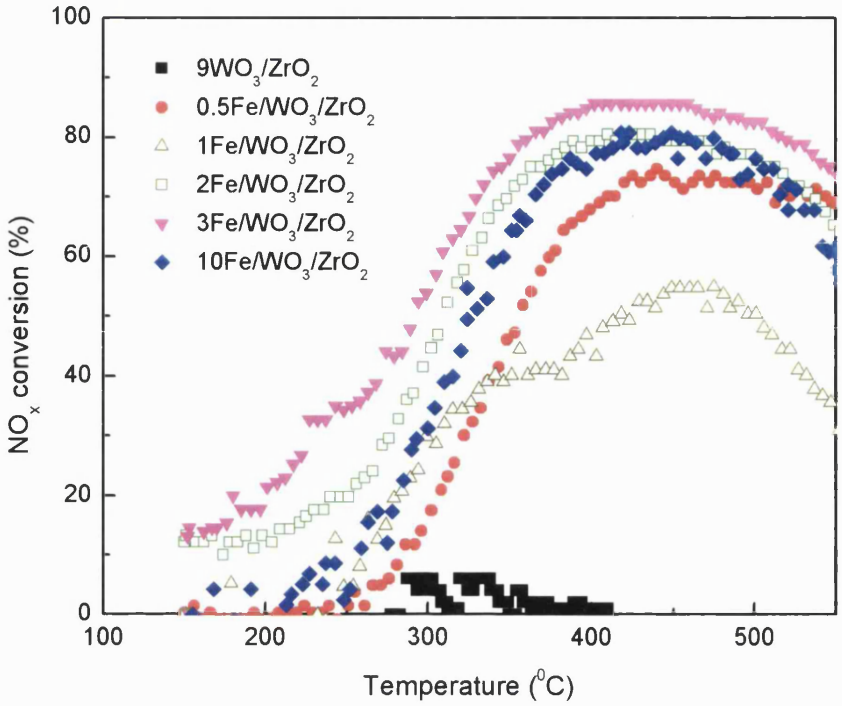

Fig. 6.1.1. Effect of temperature on NO_x conversion over $Fe/WO_3/ZrO_2$ DKK catalysts containing 0, 0.5, 1, 2, 3 and 10 wt% iron.

The NH_3 conversion over the $Fe/WO_3/ZrO_2$ DKK catalysts was examined to determine if it could provide an explanation for the poor SCR activity of the $1Fe/WO_3/ZrO_2$ catalyst (Fig. 6.1.2). Initially, there are high NH_3 conversion rates for all the $Fe/WO_3/ZrO_2$ DKK catalysts due to the adsorption of basic NH_3 molecules by the acid sites present on the catalysts. This is followed by a significant reduction in the NH_3 conversion rate as all the acid sites are occupied. The NH_3 conversion then increases steadily as the NH_3 SCR reaction proceeds and NH_3 is consumed.

The NH_3 conversion of the $Fe/WO_3/ZrO_2$ DKK catalysts with the exception of the $1Fe/WO_3/ZrO_2$ catalyst correlates well with the NO_x conversion (Fig 6.1.1) where the NH_3 and NO_x conversion increases with iron loading. The NH_3 conversion is expected to increase with the NO_x conversion as NH_3 is consumed in the NH_3 SCR reaction in reduction of NO_x to N_2.

The NH_3 conversion of the $1Fe/WO_3/ZrO_2$ (Fig. 6.1.2) suggests that the catalyst is unselective at high temperatures. The NH_3 conversion continues to increase significantly at reaction temperatures above 325 °C although the NO_x conversion rate has already begun to slow down at 325 °C. These results suggest that NH_3 is not selectively reducing NO_x to N_2 but instead converting into undesired NO_x species.

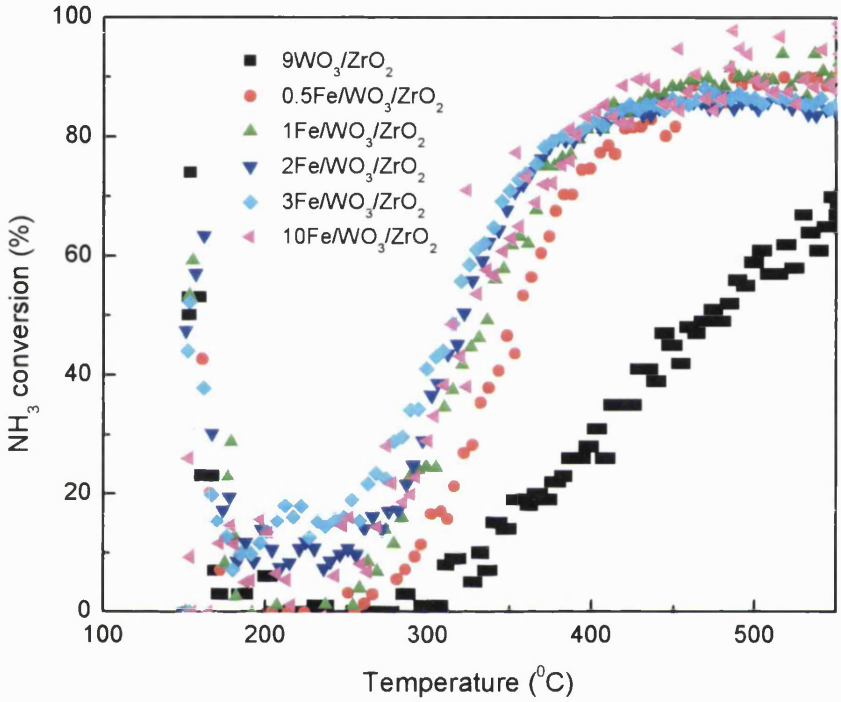

Fig. 6.1.2. Effect of temperature on NH_3 conversion over $Fe/WO_3/ZrO_2$ catalysts containing 0, 0.5, 1, 2, 3 and 10 wt% iron.

The NH_3 SCR activity is unlikely to be directly linked to the degree of iron dispersion on the $Fe/WO_3/ZrO_2$ DKK catalysts as it would not account for the poor SCR activity of the $1Fe/WO_3/ZrO_2$ catalyst. If the low SCR activity of the $1Fe/WO_3/ZrO_2$ catalyst is due to poor iron dispersion and the formation of Fe oligomers/clusters; the catalytic activity would not improve with higher iron loading that occurs with the 2 and 3 wt% catalysts. This is because at iron loadings above 1 wt%, the iron dispersion should decrease as more excess iron species will be present that will form large inactive oligomers/clusters.

The acidity of several $Fe/WO_3/ZrO_2$ DKK catalysts was investigated using IR spectroscopy in order to determine if the acidity of the catalysts are linked to the NH_3 SCR activity. The 0.5, 1 and 2 wt% $Fe/WO_3/ZrO_2$ DKK catalysts were characterised by IR using pyridine as a probe molecule and the spectra are shown in Fig. 6.1.3.

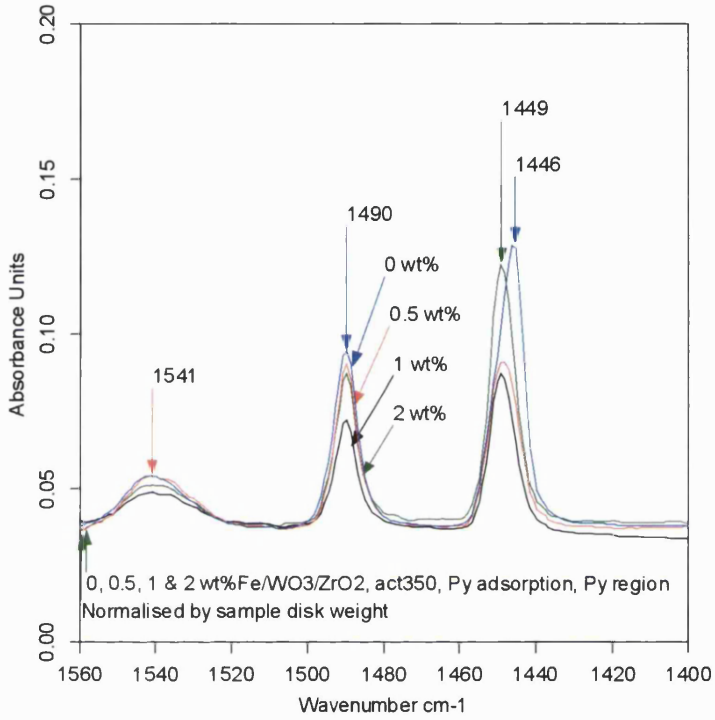

Fig. 6.1.3. IR spectra (Py region) after pyridine adsorption of $Fe/WO_3/ZrO_2$ DKK catalysts containing 0, 0.5, 1 and 2 wt% iron. The IR spectra were normalised by the sample disk weight.

The number of LAS present on the WO_3/ZrO_2 DKK support decreases significantly after 0.5 wt% iron is introduced as observed by comparing the spectra of WO_3/ZrO_2 and $0.5Fe/WO_3/ZrO_2$ (Fig. 6.1.3). The peak assigned to pyridine adsorbing onto LAS shifts from 1446 cm^{-1} on the WO_3/ZrO_2 support to 1449 cm^{-1} on the $Fe/WO_3/ZrO_2$ catalysts. This suggests that iron is generating new Fe^{3+} LAS (1449 cm^{-1}) that are replacing the Zr^{4+} LAS (1446 cm^{-1}).

This suggestion finds its support in the literature where it has been reported that new LAS will be formed when iron is introduced onto a zirconia based support [99, 100]. It should be noted that the IR peak at 1446 cm^{-1} is a combination of LAS generated from both the Zr^{4+} and Fe^{3+} LAS based on the IR peak width. It is suggested that there is a higher proportion of Fe^{3+} LAS over the Zr^{4+} LAS which leads to the observed peak shift. The 1446 cm^{-1} peak is referred to as being assigned to Fe^{3+} LAS for simplicity throughout this thesis although there maybe still be some Zr^{4+} LAS present.

The number of LAS present on the $Fe/WO_3/ZrO_2$ catalysts increases gradually with iron loading but remains below that of the WO_3/ZrO_2 support. It is possible that the new LAS generated by Fe could be linked to the NH_3 SCR activity, as the $Fe/WO_3/ZrO_2$ catalysts are active for NH_3 SCR, whereas the WO_3/ZrO_2 support is not (Fig. 6.1.1). The SCR activity of the $1Fe/WO_3/ZrO_2$ and $2Fe/WO_3/ZrO_2$ catalysts at specific reaction temperatures between 300 °C and 500 °C are compared in Table 6.1.1 against the SCR activity of the $0.5Fe/WO_3/ZrO_2$ catalyst. Furthermore, the SCR activity of the $Fe/WO_3/ZrO_2$ DKK catalysts is also compared to the relative intensities of the IR peak associated with LAS (1449 cm^{-1}).

The comparison carried out in Table 6.1.1 shows that the SCR activity of the $Fe/WO_3/ZrO_2$ DKK catalysts could be associated with the number of Fe^{3+} LAS at reaction temperatures above 350 °C. The low temperature activity (below 300 °C) does not appear to be related to the number of Fe^{3+} LAS. The higher number of LAS on the $2Fe/WO_3/ZrO_2$ catalyst could be associated with the better SCR activity of that catalyst compared to the other $Fe/WO_3/ZrO_2$ catalysts. Similarly the poor SCR activity of the $1Fe/WO_3/ZrO_2$ could be linked to the lower number of Fe^{3+} LAS present on that catalyst.

Table 6.1.1. The relative NH_3 SCR activity at temperatures between 300 °C and 500 °C of $Fe/WO_3/ZrO_2$ catalysts compared to the relative intensity of the IR peak associated with LAS (1449 cm^{-1}).

Catalyst	300 °C	350 °C	400 °C	450 °C	500 °C	Relative no. of LAS
$0.5Fe/WO_3/ZrO_2$	1.0	1.0	1.0	1.0	1.0	1.0
$1Fe/WO_3/ZrO_2$	1.4	0.9	0.7	0.8	0.7	0.9
$2Fe/WO_3/ZrO_2$	2.6	1.5	1.2	1.2	1.1	1.4

The results obtained suggest that the SCR activity can be associated with the Fe^{3+} LAS (1449 cm^{-1}). The Broensted acidity of the $Fe/WO_3/ZrO_2$ catalysts was also examined to determine if it plays a role in the NH_3 SCR activity of the catalysts (Fig. 6.1.3).

There was no change in the number of BAS when the WO_3/ZrO_2 support was impregnated with 0.5 wt% iron and a small reduction in the number of BAS was found on the $2Fe/WO_3/ZrO_2$ catalyst. However, there is a significant decrease in the number of BAS present on the $1Fe/WO_3/ZrO_2$ catalyst. This could be potentially linked to the poor catalytic activity of the $1Fe/WO_3/ZrO_2$ catalyst and suggests that the number of BAS may affect the SCR activity.

Furthermore, it was determined that the NH_3 SCR activity of the $Fe/WO_3/ZrO_2$ catalysts may also be influenced by the acid site strength. Vartuli et al. [124] have reported that iron enhances the acid site strength of WO_3/ZrO_2 supports. This effect was observed for the WO_3/ZrO_2 DKK support tested where both the LAS and BAS strength increases significantly when the WO_3/ZrO_2 support was impregnated with iron (Fig. 6.1.4).

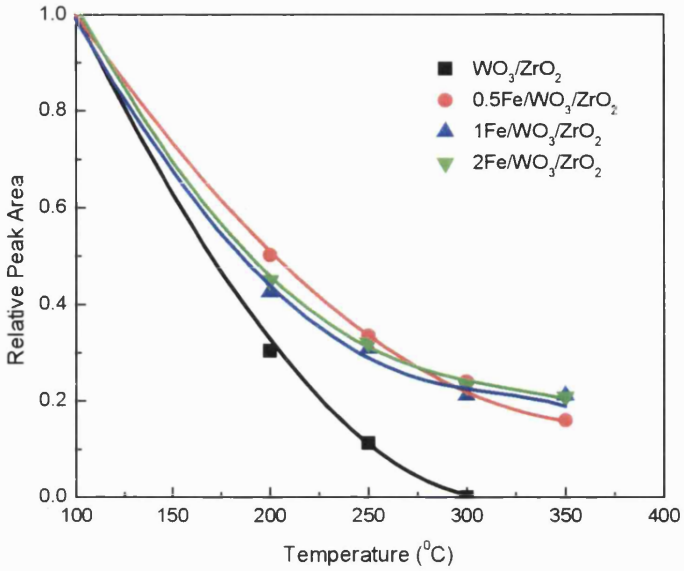

(A)

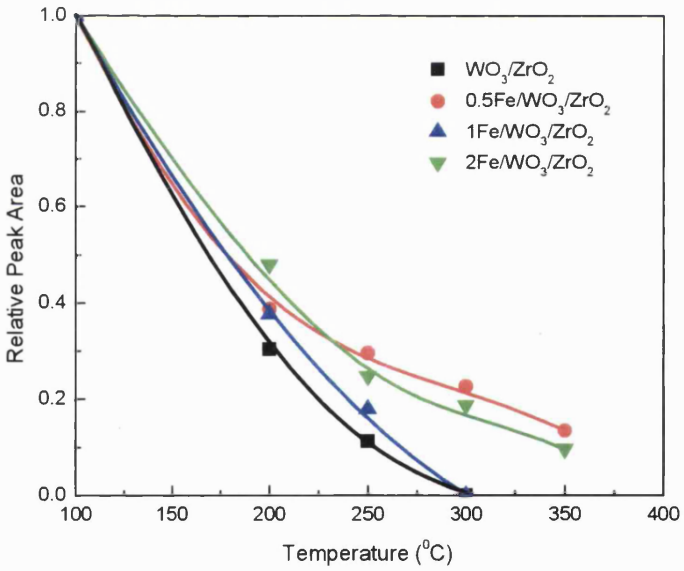

(B)

Fig. 6.1.4. Pyridine desorption from (A) LAS and (B) BAS present in $Fe/WO_3/ZrO_2$ DKK catalysts containing 0, 0.5, 1 and 2 wt% iron.

However, there was only a slight improvement in the BAS strength with the 1Fe/WO_3/ZrO_2 catalyst. The acidity results show that 1Fe/WO_3/ZrO_2 has the lowest number and strength of BAS of the Fe/WO_3/ZrO_2 catalysts characterised which can be linked to the poor catalytic activity of that catalyst. This suggests that the Broensted acidity does play an active role in the NH_3 SCR activity of Fe/WO_3/ZrO_2 DKK catalysts, predominantly in the high temperature region.

The NH_3 SCR activity could be associated with the number and type of LAS where a higher number of Fe^{3+} LAS leads to better catalytic activity. Iron generates new LAS as seen by the peak shift from 1446 cm^{-1} on the WO_3/ZrO_2 support to 1449 cm^{-1} on the Fe/WO_3/ZrO_2 catalysts (Fig. 6.1.3). These peaks are suggested to be assigned to pyridine adsorption onto Fe^{3+} LAS (1446 cm^{-1}) and Zr^4 LAS (1449 cm^{-1}) respectively.

Although the number of Fe^{3+} LAS could play a key role in the NH_3 SCR activity; some strong BAS are also required for the catalyst to be active. The 2Fe/WO_3/ZrO_2 catalyst had a slight reduction in the number of BAS compared to the 0.5Fe/WO_3/ZrO_2 catalyst but a large increase in the number of Fe^{3+} LAS (Fig. 6.1.3 and Table 6.1.2). As a result, the 2Fe/WO_3/ZrO_2 catalyst was significantly more active than the 0.5Fe/WO_3/ZrO_2 catalyst (Fig. 6.1.1). On the other hand, the 1Fe/WO_3/ZrO_2 catalyst had similar numbers of Fe^{3+} LAS as the 0.5Fe/WO_3/ZrO_2 catalyst but exhibited much lower high temperature activity due to the large drop in the number and strength of BAS.

There are more LAS present on the WO_3/ZrO_2 support compared to the Fe/WO_3/ZrO_2 catalysts based on the data in Table 6.1.2, however, it is suggested that the LAS present on WO_3/ZrO_2 are generated from Zr^{4+} LAS which are not active for NH_3 SCR. On the other hand, the Fe/WO_3/ZrO_2 catalysts have a smaller total number of LAS but a higher proportion of Fe^{3+} LAS that are active for NH_3 SCR.

Table 6.1.2. Acidity measurements for the $Fe/WO_3/ZrO_2$ DKK catalysts containing 0, 0.5, 1 and 2 wt% iron.

Catalyst	WO_3/ZrO_2	0.5Fe	1Fe	2Fe
BAS + LAS (μmol/g)	44	34	20	36
Ratio LAS/BAS	1.3	0.9	2.3	1.6
LAS (μmol/g)	25	16	14	22
BAS (μmol/g)	19	18	6	14

Based on the results of repeated experiments, the error was found to be approximately 8%.

$Fe/WO_3/ZrO_2$ catalysts showed much higher Lewis and Broensted acid site strength in comparison to the WO_3/ZrO_2 support with the exception of the $1Fe/WO_3/ZrO_2$ catalyst where only a slight increase in the BAS strength may have occurred. The differences in the BAS strength of the $1Fe/WO_3/ZrO_2$ catalyst compared to the WO_3/ZrO_2 support displayed in Fig. 6.1.4(B) could be due to experimental errors. The $1Fe/WO_3/ZrO_2$ catalyst also exhibited poor high temperature NH_3 SCR activity which suggests that a small number of strong BAS is necessary for good high temperature activity.

The results of this study support the discussions in the literature where it has been suggested by different authors that the NH_3 SCR reaction proceeds either solely through a Lewis or Broensted acid site based mechanism for iron supported on metal oxide catalysts [114, 150]. If the required strength and number of BAS is present on all the catalysts tested, the SCR activity would appear to be linked only to the number of LAS as seen with the $Fe/WO_3/ZrO_2$ DKK catalysts tested in this study except the $1Fe/WO_3/ZrO_2$ catalyst.

Changes in the strength and number of BAS would not appear to affect the SCR activity as long as the essential number of strong BAS is still present as seen on the $2Fe/WO_3/ZrO_2$ catalyst. Similarly, the SCR activity would appear to be

linked to the number of BAS if it drops below the required level of Broensted acidity and the number of LAS remains similar. This occurred with $1Fe/WO_3/ZrO_2$ catalyst.

6.2 Aged $Fe/WO_3/ZrO_2$ DKK catalysts

Iron promoted tungsten oxide supported on zirconia catalysts have been shown to be active for NH_3 SCR of NO_x. In this section, the hydrothermal stability of the $Fe/WO_3/ZrO_2$ DKK catalysts was tested as this was the weak point of other potential supports [149]. The catalysts were aged in 10 % steam at 700 °C for 65 hours and then tested for the NH_3 SCR activity under the same lean conditions as the fresh catalysts (Fig. 6.2.1). The $1Fe/WO_3/ZrO_2$ catalyst was omitted from the aging experiments based on its poor high temperature activity.

The SCR activity of all three $Fe/WO_3/ZrO_2$ DKK catalysts decreased after hydrothermal aging where the $0.5Fe/WO_3/ZrO_2$ catalyst showed the greatest difference between the fresh and aged activity at temperatures above ~350 ^{0}C. Initially, there is a slight improvement in the low temperature activity of the aged $0.5Fe/WO_3/ZrO_2$ catalyst, however, above ~350 °C, the SCR activity is ~20 % lower than the fresh catalyst.

The $2Fe/WO_3/ZrO_2$ catalyst undergoes a similar effect on the SCR activity after aging, but the overall reduction in SCR activity is ~15 % compared to ~20 % seen with the $0.5Fe/WO_3/ZrO_2$ catalyst. Interestingly, the $3Fe/WO_3/ZrO_2$ catalyst showed a larger drop in catalytic activity after aging compared to the $2Fe/WO_3/ZrO_2$ catalyst; in particular, the low temperature activity from 150 °C to 300 °C and at reaction temperatures above 450 °C.

The NH_3 conversion of the fresh $2Fe/WO_3/ZrO_2$ and $3Fe/WO_3/ZrO_2$ catalysts were very similar (Fig. 6.2.2). However, after aging, the NH_3 conversion of the two catalysts differs at temperatures above 350 °C with higher conversion rates on the $3Fe/WO_3/ZrO_2$ catalyst compared to the $2Fe/WO_3/ZrO_2$ catalyst (Fig. 6.2.2). This coincides with the decrease in the SCR activity of the aged $3Fe/WO_3/ZrO_2$ catalyst in the high temperature region (Fig. 6.2.1). These results

indicate that the aged $3Fe/WO_3/ZrO_2$ catalyst becomes unselective at high temperatures.

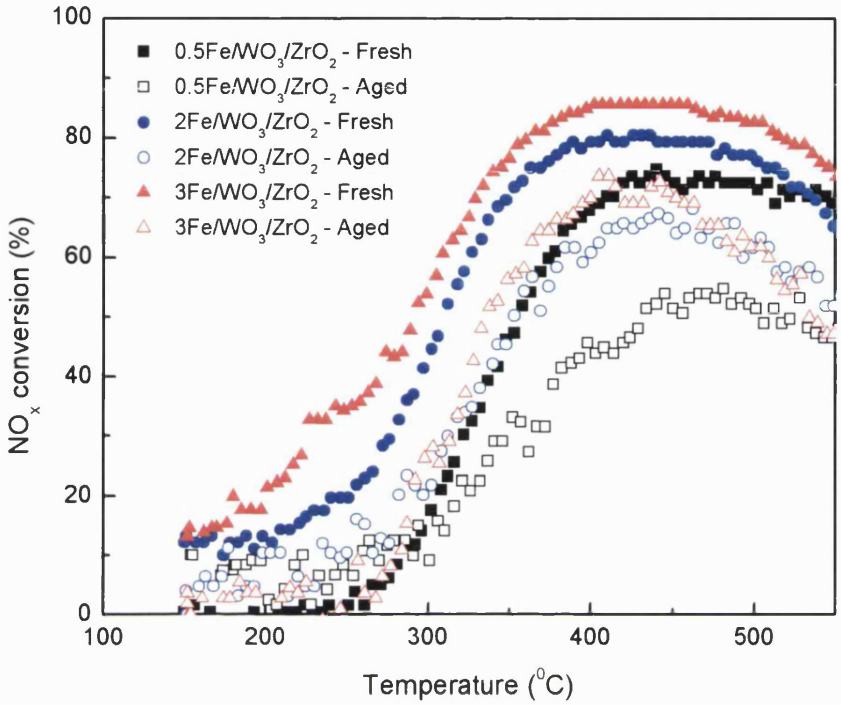

Fig. 6.2.1. Effect of temperature on NO_x conversion over fresh and aged $Fe/WO_3/ZrO_2$ DKK catalysts containing 0.5, 2 and 3 wt% iron.

The $2Fe/WO_3/ZrO_2$ catalyst displayed the best resistance to the hydrothermal aging of the three $Fe/WO_3/ZrO_2$ DKK catalysts tested. Furthermore, the catalytic activity of the fresh and aged $2Fe/WO_3/ZrO_2$ catalysts was comparable to those of the $3Fe/WO_3/ZrO_2$ catalyst. This suggests that 2 wt% may be the optimum iron loading for the WO_3/ZrO_2 DKK support based on the catalytic activity and hydrothermal resistance of the $2Fe/WO_3/ZrO_2$ catalyst.

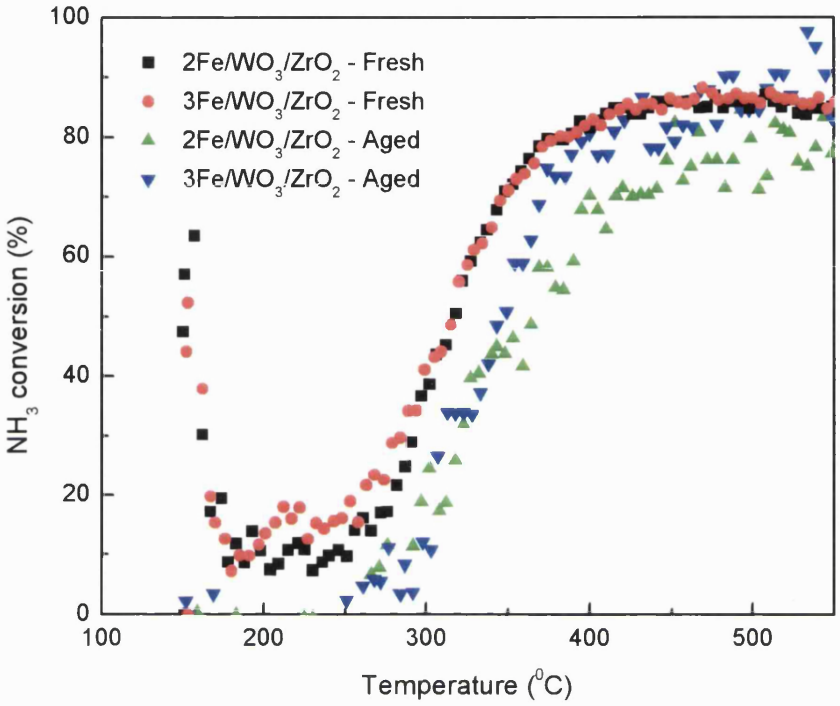

Fig. 6.2.2. Effect of temperature on NH_3 conversion over fresh and aged $Fe/WO_3/ZrO_2$ DKK catalysts containing 2 and 3 wt% iron.

6.3 Comparison of Fe/beta and $Fe/WO_3/ZrO_2$ DKK catalysts

Iron supported on H/beta zeolite has been used as a reference material for NH_3 SCR activity due to its good SCR activity and hydrothermal resistance [149]. On this basis, the activity of $Fe/WO_3/ZrO_2$ DKK catalysts was compared to that of Fe/beta. To begin with, the changes in the acidity of the H/beta zeolite support after impregnating with 2 wt% iron were investigated. This was carried out to determine if iron generated similar new Fe^{3+} LAS that are active for NH_3 SCR on the H/beta zeolite support as seen with the $Fe/WO_3/ZrO_2$ DKK catalysts (Section 6.1).

A clear peak shift from 1456 cm^{-1} on the parent H/beta to 1450 cm^{-1} on the 2Fe/beta catalyst can be seen in Fig. 6.3.1 where both peaks are associated with LAS. A similar peak shift was previously observed when the WO_3/ZrO_2 DKK support (1446 cm^{-1}) was impregnated with iron to synthesise the $Fe/WO_3/ZrO_2$ DKK catalysts (1449 cm^{-1}). The peak shift from 1446 to 1449 cm^{-1} was suggested to be due to the formation of new Fe^{3+} LAS. The spectra in Fig. 6.3.1 indicate that iron is also generating similar new Fe^{3+} LAS on the H/beta zeolite support. Furthermore, a new peak at 1609 cm^{-1} assigned to pyridine adsorption onto LAS appears after H/beta is impregnated with iron.

Iron generates a large number of new Fe^{3+} LAS when supported on H/beta where the number of LAS on Fe/beta far exceeds those present on the parent H/beta support. In comparison, the $Fe/WO_3/ZrO_2$ DKK catalysts had lower numbers of LAS than the parent WO_3/ZrO_2 support. The 2Fe/beta catalyst has a higher number of Fe^{3+} LAS compared to the $2Fe/WO_3/ZrO_2$ catalyst based on the comparison of the 1449 and 1450 cm^{-1} peak intensities (Fig. 6.3.1). It would be expected that the 2Fe/beta catalyst will be significantly more active for NH_3 SCR compared to the $2Fe/WO_3/ZrO_2$ catalyst based on the differences in the number of Fe^{3+} LAS.

The Broensted acidity was previously shown to also possibly influence the NH_3 SCR activity and an increase in the number of BAS occurred when the H/beta support was impregnated with iron based on the changes in the peak intensities at 1638 cm^{-1} and 1547 cm^{-1} (Fig. 6.3.1). This is an unusual and interesting result as it is unclear how iron generates new BAS on the H/beta zeolite support. It is possible that there are acid sites present on the iron oxide species that are located on the catalyst surface, which leads to the increase in the number of BAS.

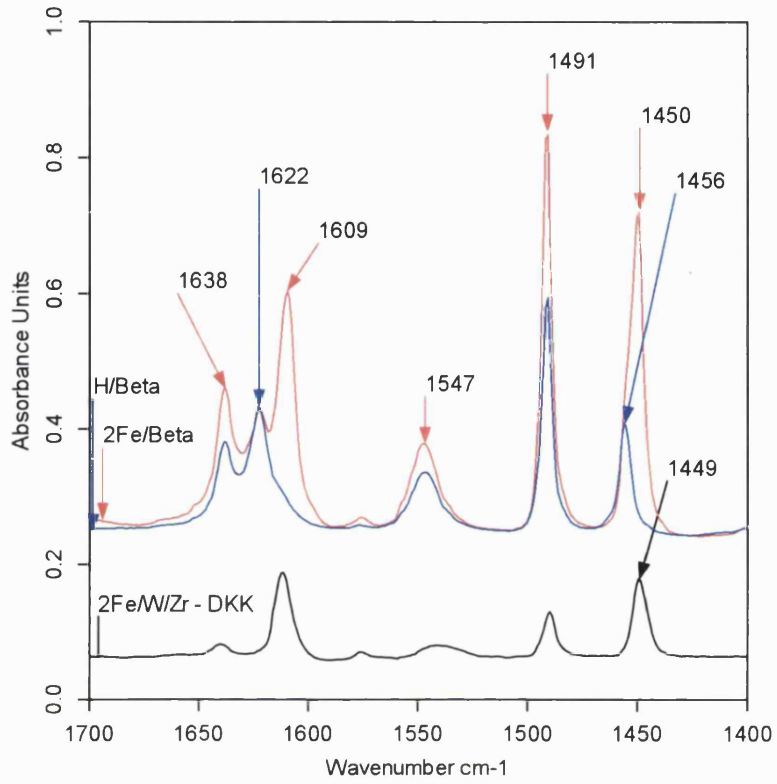

Fig. 6.3.1. IR spectra (Py region) after pyridine adsorption of H/beta support, 2Fe/beta and 2Fe/WO_3/ZrO_2 DKK catalysts. The IR spectra were normalised by the sample disk weight.

The LAS and BAS strength of the parent H/beta zeolite decreases after impregnating with iron (Fig. 6.3.2) and there was a more significant drop in the LAS strength compared to the BAS strength. The reduction in the BAS strength of the H/beta support is possibly caused by iron species interacting with the zeolite.

It should be noted that the data points in the pyridine TPD in Fig. 6.3.2(A) at 300 °C and 350 °C for the parent H/beta zeolite are inaccurate because a new shoulder appeared at ~1463 cm^{-1} (Fig. 6.3.3). The shoulder at ~1463 cm^{-1} prevents accurate integration of the peak at 1456 cm^{-1} which is assigned to pyridine adsorption onto LAS. This shoulder at ~1463 cm^{-1} is currently

unassigned and the author suggests that it is due to pyridine reacting with the strong LAS and decomposing to form new nitrogen based products based on the results and discussions at the CARE laboratory, University of Bath.

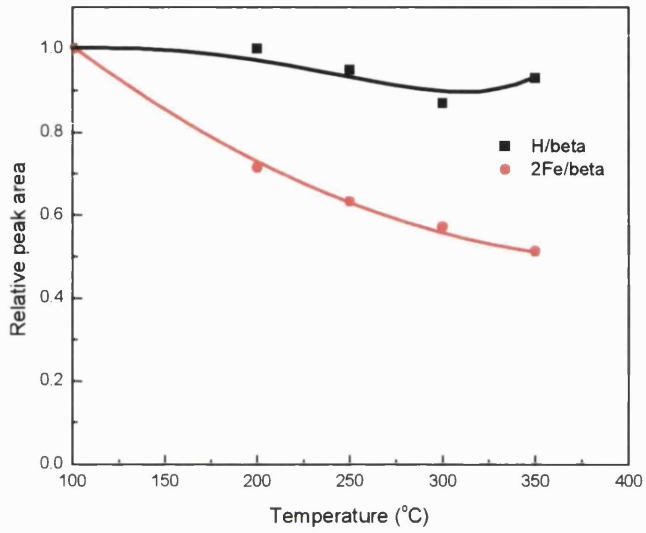

(A)

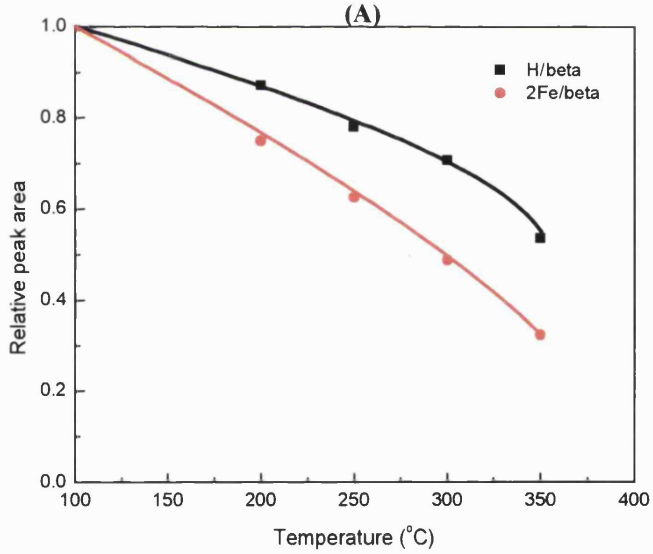

(B)

Fig. 6.3.2. Pyridine desorption from (A) LAS and (B) BAS present on H/beta support and 2Fe/beta catalyst.

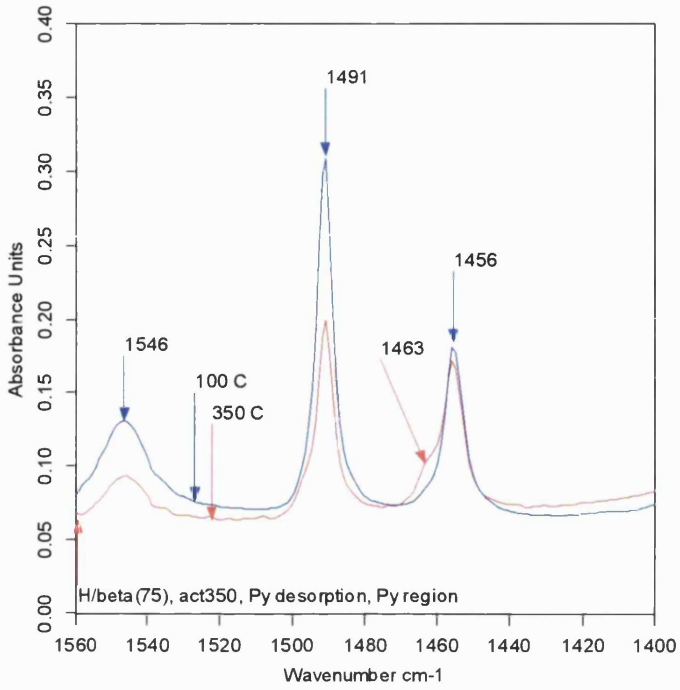

Fig. 6.3.3. IR spectra (Py region) of H/beta zeolite during pyridine desorption illustrating the appearance of the 1463 cm^{-1} peak.

The NH_3 SCR activity of the Fe/beta and $Fe/WO_3/ZrO_2$ DKK catalysts were compared and it can be seen in Fig. 6.3.4 that the Fe/beta catalysts exhibited better SCR activity at both 0.5 and 2 wt% Fe loading. This was not unexpected as it was previously suggested that the 2Fe/beta catalyst would be significantly more active than the $2Fe/WO_3/ZrO_2$ catalyst based on the higher number of Fe^{3+} LAS present.

There was no change in the low temperature activity of the Fe/beta catalysts when the iron loading was increased from 0.5 to 2 wt%. In contrast, a significant improvement in the low temperature activity can be seen when comparing the $0.5Fe/WO_3/ZrO_2$ and $2Fe/WO_3/ZrO_2$ catalysts. However, the Fe/beta catalysts exhibited significantly better low temperature activity compared to the $Fe/WO_3/ZrO_2$ DKK catalysts.

The high temperature activity of the $2Fe/WO_3/ZrO_2$ catalyst is comparable to that of 2Fe/beta. However, the SCR activity of the $2Fe/WO_3/ZrO_2$ catalyst begins to decrease at reaction temperatures above 450 °C whereas only a slight reduction occurs with the 2Fe/beta. Interestingly, the 0.5Fe/beta catalyst exhibits similar or better low temperature activity as that of 2Fe/beta up to ~325 °C but at reaction temperatures above 325 °C, the catalytic activity of 0.5Fe/beta begins to decrease steadily. This does not occur with any other Fe based catalysts tested. Furthermore, the 0.5Fe/beta catalyst has a unique increase in SCR activity that peaks at 325 °C. It is not known at this time why this occurs.

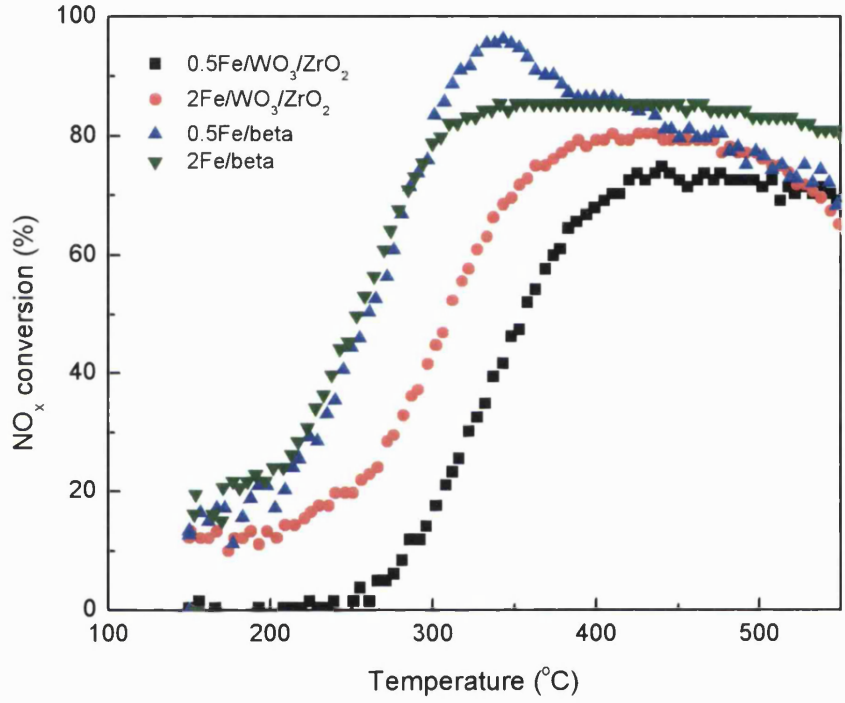

Fig. 6.3.4. Effect of temperature on NO_x conversion over $Fe/WO_3/ZrO_2$ DKK and Fe/beta catalysts containing 0.5 and 2 wt% iron.

The SCR activity of the fresh and aged 2Fe/beta and $2Fe/WO_3/ZrO_2$ catalysts was compared in Fig. 6.3.5. A significant drop in the catalytic activity of the 2Fe/beta catalyst in the low temperature region occurred after aging of this catalyst, but the high temperature activity (above 400 °C) remained comparable

to that of the fresh catalyst. A much smaller decrease in the low temperature SCR activity was observed with the aged $2Fe/WO_3/ZrO_2$ catalyst.

The difference in the NO_x conversion between the fresh and aged catalysts at 250 °C was a reduction of less than 2 times (10 vs 18 %) for the $2Fe/WO_3/ZrO_2$ catalyst compared to ~3.5 times (15 vs 54 %) with the 2Fe/beta catalyst. The activity of the aged $2Fe/WO_3/ZrO_2$ catalyst at temperatures above 325 °C is approximately 20 % lower in comparison to the fresh catalyst. These results show that the $2Fe/WO_3/ZrO_2$ catalyst shows good resistance to hydrothermal aging at the severe conditions used.

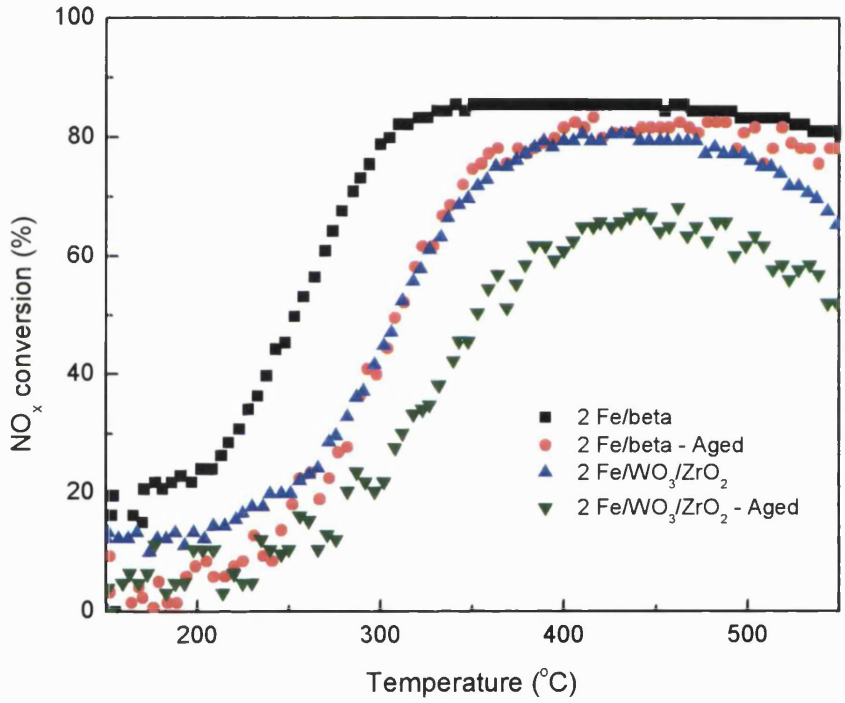

Fig. 6.3.5. Effect of temperature on NO_x conversion over fresh and aged $2Fe/WO_3/ZrO_2$ DKK and 2Fe/beta catalysts.

The results obtained previously have indicated that the acidity of the catalysts influences the NH_3 SCR activity. Therefore the acidity of the fresh and aged $2Fe/WO_3/ZrO_2$ catalysts was examined to determine if any changes to the number of LAS and BAS occurred. The spectra comparing the fresh and aged

$2Fe/WO_3/ZrO_2$ catalysts are shown in Figs. 6.3.6 and 6.3.7 examining the LAS and BAS respectively.

It can be clearly seen in Fig. 6.3.6 that there is a loss of ~18 % in the number of LAS after the $2Fe/WO_3/ZrO_2$ catalyst was aged based on the reduction in the 1449 cm^{-1} peak intensity. Similarly, referring to Fig 6.3.7, a decrease of ~ 33 % in the number of BAS was observed after the $2Fe/WO_3/ZrO_2$ catalyst was aged.

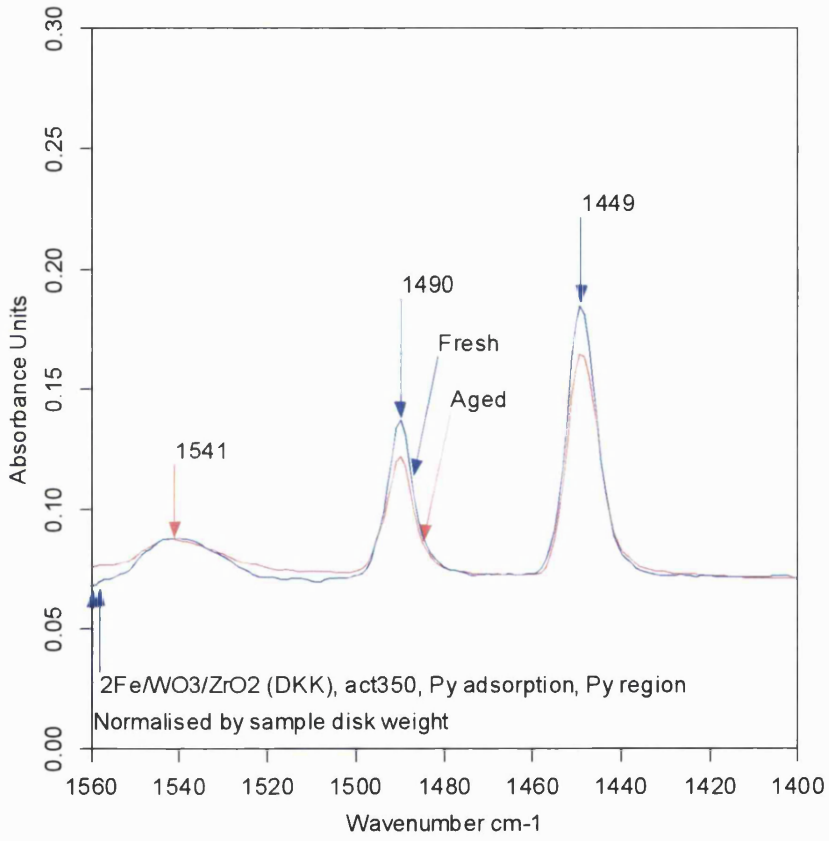

Fig. 6.3.6. IR spectra (Py region) after pyridine adsorption on fresh and aged $2Fe/WO_3/ZrO_2$ DKK catalysts examining the LAS. The IR spectra were normalised by the sample disk weight.

The reduction in the number of both LAS and BAS can be linked to the decrease in the catalytic activity of the aged $2Fe/WO_3/ZrO_2$ catalyst. The SCR activity of the $2Fe/WO_3/ZrO_2$ catalyst decreases by ~20 % after aging (Fig. 6.3.5) which

correlates with the ~18 % reduction in the number of Fe^{3+} LAS (Fig. 6.3.6). Furthermore, the decrease in the SCR activity was primarily in the high temperature region which could be linked to the loss of ~33 % in the number of BAS after aging. These results support the suggestion that the SCR activity is linked to the number of Fe^{3+} LAS and the high temperature activity can be associated with the Broensted acidity (Section 6.1).

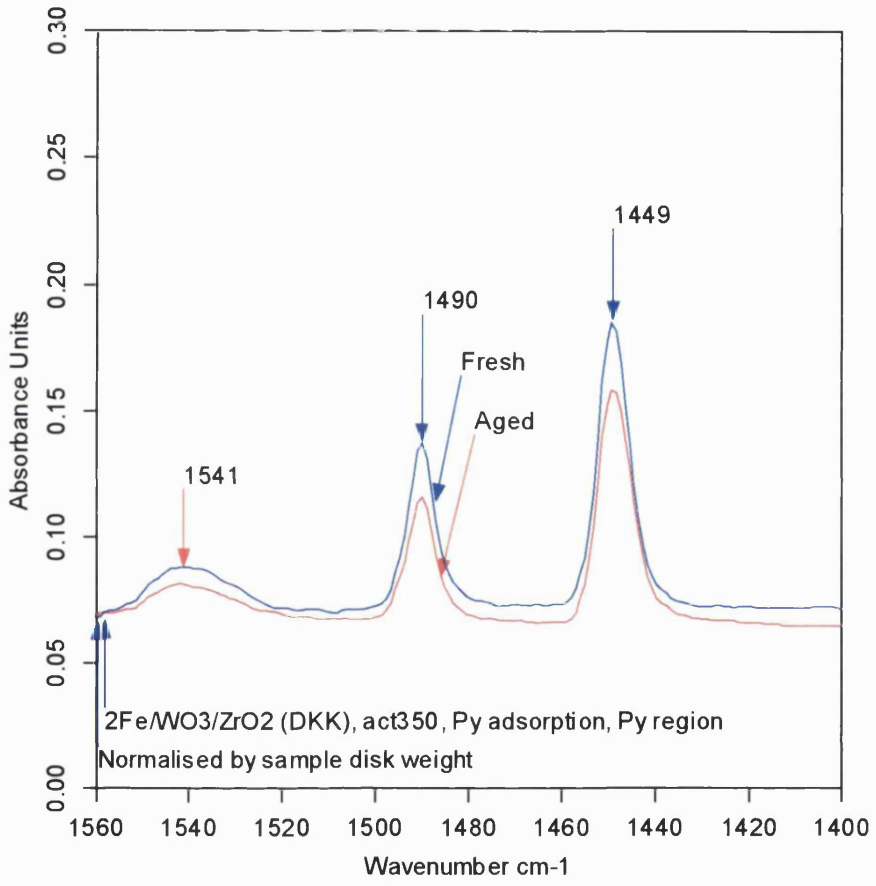

Fig. 6.3.7. IR spectra (Py region) after pyridine adsorption on fresh and aged $2Fe/WO_3/ZrO_2$ DKK catalysts examining the BAS. The IR spectra were normalised by the sample disk weight.

The LAS and BAS strength of the fresh and aged $2Fe/WO_3/ZrO_2$ catalysts was investigated in Fig. 6.3.8 however; it should be noted that some of the data points for the LAS TPD profile are inaccurate due to poor resolution of the IR peaks.

The spectra of pyridine desorption of iron based catalysts were distorted slightly at high temperatures which mainly affects the peaks assigned to pyridine adsorption on LAS (1449 cm^{-1}).

A similar effect was seen previously with the desorption spectra of H/beta zeolite (Fig. 6.3.3). From the available data obtained (Fig. 6.3.8(A)), there is no change in the LAS strength between the fresh and aged $2Fe/WO_3/ZrO_2$ catalysts. However, there is a considerable reduction in the BAS strength after the $2Fe/WO_3/ZrO_2$ catalyst was aged (Fig. 6.3.8(B)).

The acidity characterisation results of the fresh and aged $2Fe/WO_3/ZrO_2$ catalysts show a significant loss in both the number and strength of the BAS after aging. The decrease in the number and strength of BAS can be associated with the reduction in the high temperature NH_3 SCR activity. These results support the previous suggestion in Section 6.1 that the Broensted acidity influences the high temperature activity where the Broensted acidity was shown to have a major impact on the SCR activity of the $1Fe/WO_3/ZrO_2$ catalyst.

Iron supported on commercial tungsten oxide supported on zirconia (DKK J1374) shows promising results for NH_3 SCR of NO_x with good hydrothermal resistance. The $Fe/WO_3/ZrO_2$ catalysts will be studied in more detail by varying the synthesis procedure of the WO_3/ZrO_2 support to better understand the factors that affect the NH_3 SCR activity. The WO_3/ZrO_2 supports will be synthesised using MEL zirconium hydroxide instead of the commercial WO_3/ZrO_2 DKK support as this allows the synthesis of the WO_3/ZrO_2 catalytic support to be varied.

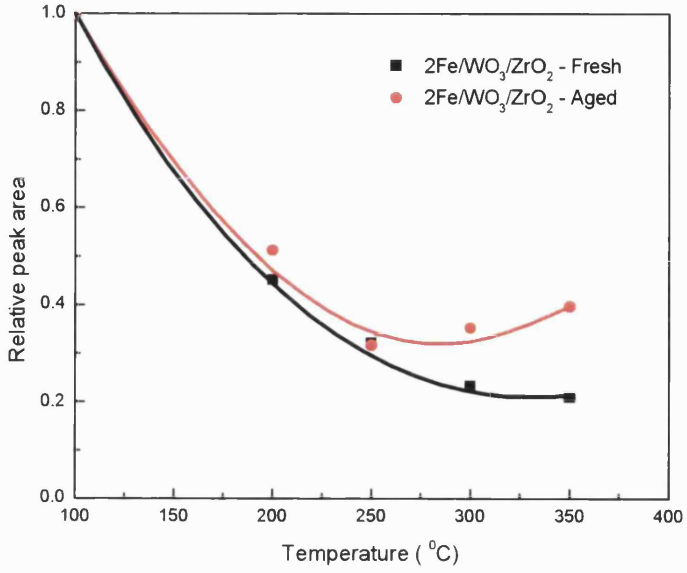

(A)

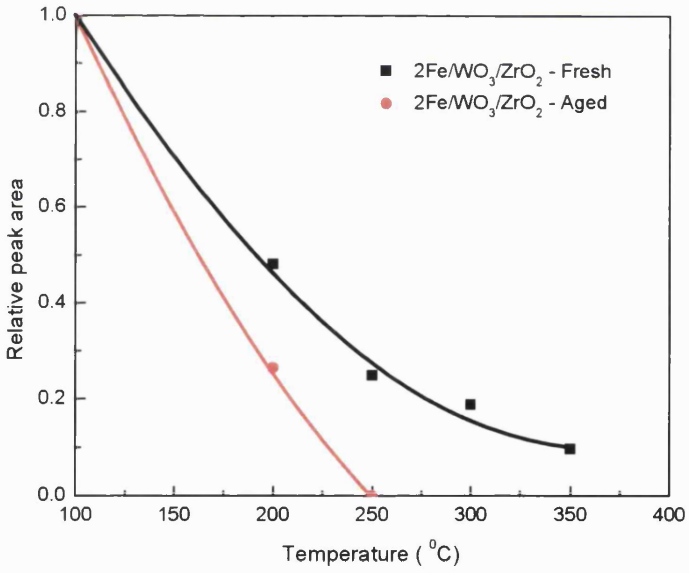

(B)

Fig. 6.3.8. Pyridine desorption from (A) LAS and (B) BAS present on fresh and aged $2Fe/WO_3/ZrO_2$ DKK catalysts.

6.4 Synthesis procedures of $Fe/WO_3/ZrO_2$ MEL catalyst

Three series of $Fe/WO_3/ZrO_2$ MEL catalysts were synthesised where the order of impregnation of iron or tungsten oxide was changed. This study was carried out to investigate the best synthesis procedure to synthesise an active $Fe/WO_3/ZrO_2$ catalyst. The iron and tungsten oxide loading was kept constant at 0.5 wt% and 15 wt% respectively, on all the catalysts supported on the MEL XZO 880/01 zirconium hydroxide.

The results in Chapter 5 have shown that 15 wt% was the optimum tungsten oxide loading for the WO_3/ZrO_2 MEL support. A low iron loading (0.5 wt%) was selected so any subtle changes in the properties of the $Fe/WO_3/ZrO_2$ catalysts will be detected which may not be apparent at higher iron loadings. A low and high calcination temperatures of 600 °C and 830 °C were also used. The three series of $Fe/WO_3/ZrO_2$ MEL catalysts with different synthesis procedures are described below:

Series 1:

A) W + Zr (830 °C) → WO_3/ZrO_2 + Fe (830 °C) → $Fe/WO_3/ZrO_2$

B) W + Zr (Uncalcined) → WO_3/ZrO_2 + Fe (600 °C) → $Fe/WO_3/ZrO_2$

C) W + Zr (Uncalcined) → WO_3/ZrO_2 + Fe (830 °C) → $Fe/WO_3/ZrO_2$

Series 2:

A) Fe + Zr (600 °C) → Fe/ZrO_2 + W (830 °C) → $Fe/WO_3/ZrO_2$

B) Fe + Zr (Uncalcined) → Fe/ZrO_2 + W (830 °C) → $Fe/WO_3/ZrO_2$

Series 3:

A) Fe + W + Zr (830 °C) → $Fe/WO_3/ZrO_2$

B) Fe + W + Zr (600 °C) → $Fe/WO_3/ZrO_2$

The catalysts are referred to by the series number and the appropriate alphabet, for example, 1A denotes the catalyst from Series 1 sample A. The catalysts were tested for NH_3 SCR activity where the results for Series 1 are shown in Fig. 6.4.1 and Series 2 and 3 in Fig. 6.4.2.

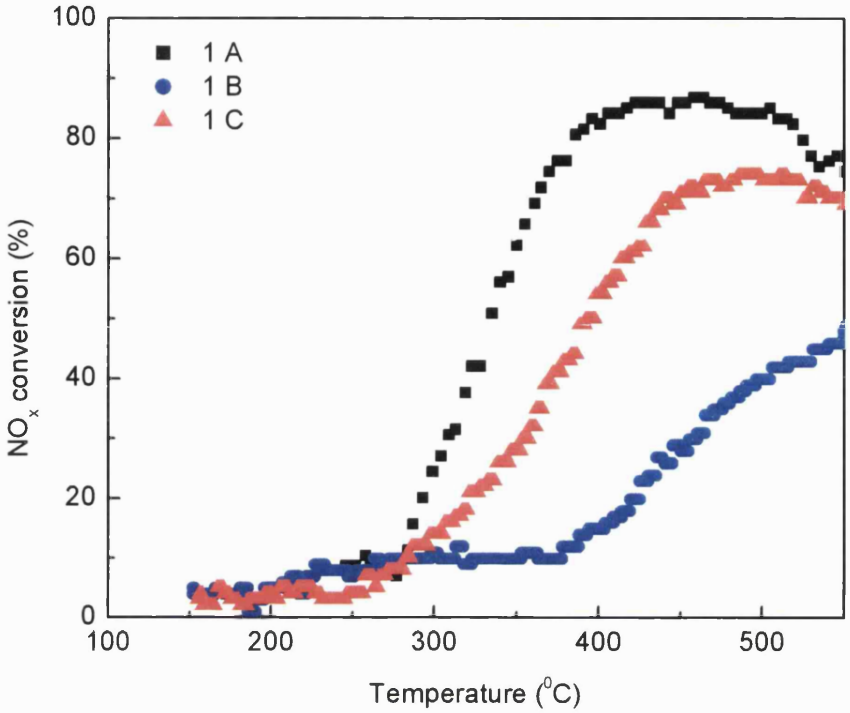

Fig. 6.4.1. Effect of temperature on NO_x conversion of $0.5Fe/15WO_3/ZrO_2$ MEL catalysts synthesised via Series 1 route.

The 1A and 1B catalysts exhibited the best and worst SCR activity of all the $Fe/WO_3/ZrO_2$ catalysts tested in the 3 different series (Figs. 6.4.1 and 6.4.2). It was not unexpected that the 1A catalyst was the most active as the synthesis procedure was based first on stabilising the zirconia support with tungsten oxide at high temperatures (830 °C) then impregnated with the active metal, iron.

The 1B catalyst had the lowest SCR activity as the WO_3/ZrO_2 support was not calcined to the high temperatures that are required to stabilise the support. The 1B catalyst was only calcined to a maximum temperature of 600 °C, however; tungsten oxide requires higher temperatures to diffuse from the bulk to the surface in order to interact with zirconium sites on the surface [145, 146] (Section 5.4).

Although the 3B catalyst was also calcined to 600 °C, the SCR activity was better than the 1B catalyst (Figs. 6.4.1 and 6.4.2). This can be explained by the

order in which the iron and tungsten oxide was introduced on these 2 catalysts. On the 1B catalyst, where tungsten oxide was introduced first, most of the zirconium adsorption sites will be occupied by tungsten oxide therefore iron can only interact with any remaining unoccupied sites. At the calcination temperature of 600 °C, tungsten oxide cannot effectively diffuse from the bulk to the surface of the zirconia support thus zirconium oxide remains in the monoclinic phase leading to poor catalytic activity (Fig. 6.4.1).

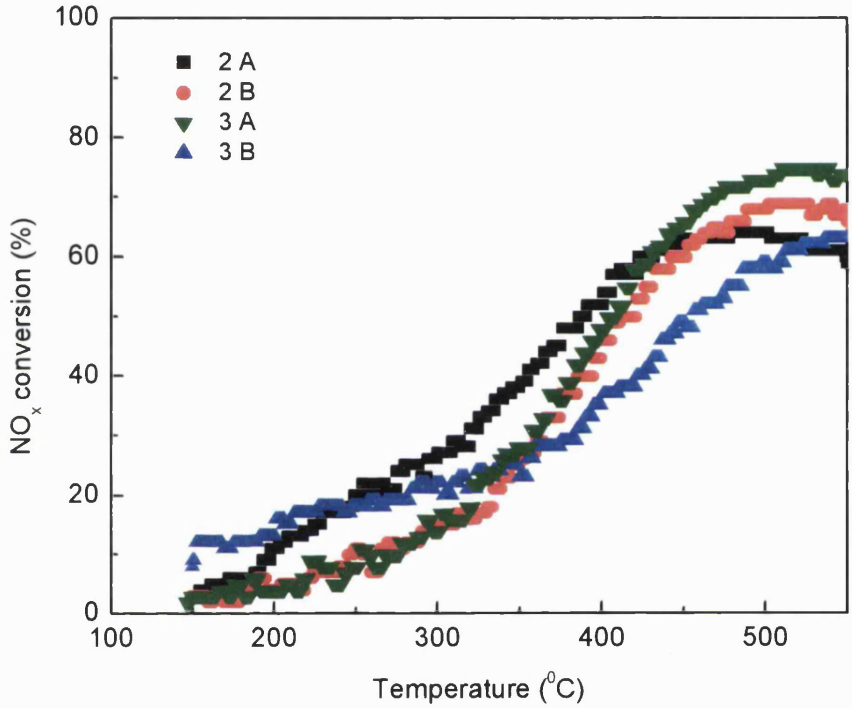

Fig. 6.4.2. Effect of temperature on NO_x conversion of $0.5Fe/15WO_3/ZrO_2$ MEL catalysts synthesised via Series 2 and 3 routes.

On the 3B catalyst, iron and tungsten oxide are introduced at the same time and, therefore, are able to interact with the zirconia support simultaneously since the iron and tungsten species will have equal access to the zirconium adsorption sites. Furthermore, iron can stabilise zirconia in the tetragonal phase when calcined to 600 °C which would account for the better catalytic activity of the 3B catalyst over the 1B catalyst.

When the 1B catalyst was calcined to 830 °C, the SCR activity increases significantly as seen with the 1C catalyst (Fig. 6.4.1). The 1C catalyst had the same synthesis procedure as the 1B catalyst except it was calcined at 830 °C instead of 600 °C. The better SCR activity of the 1C catalyst is due to the increased tungsten oxide diffusion from the bulk to the surface where it stabilises the zirconium oxide support. The SCR activity remains below that of the 1A catalyst because iron has already occupied some of the zirconium sites on the 1C catalyst therefore preventing some tungsten oxide from interacting with zirconium oxide. As a consequence of this, there will be less tungsten oxide – zirconia stabilising interaction present on the 1C catalyst, which subsequently reduces the SCR activity of that catalyst.

The 1C, 2B and 3A catalysts all exhibited comparable catalytic activity (Figs. 6.4.1 and 6.4.2). The similarity in the catalytic activity of the three catalysts can be attributed to the synthesis procedure where tungsten oxide is either introduced simultaneously or after the iron component then calcined at 830 °C. The moderate catalytic activity of these 3 catalysts is due to iron inhibiting some tungsten oxide from stabilising the zirconium oxide support. Iron will occupy some of the zirconium adsorption sites therefore preventing some tungsten oxide from interacting and stabilising the zirconium oxide in the tetragonal phase.

The poor SCR activity of the 2A and 3B catalysts (Fig. 6.4.2) can be attributed to iron occupying the bulk of the free Zr^{4+} sites before tungsten oxide is introduced. Tungsten oxide can only interact with any remaining unoccupied Zr^{4+} adsorption sites thus limiting its interaction with zirconium oxide. The 2A and 3B catalysts exhibited better low temperature activity which could be associated with better Fe – Zr interactions. It has been suggested in the literature that there is good iron dispersion when supported on zirconium oxide and a strong Fe – Zr interaction exists [113, 151]. It was also reported that NO readily adsorbs and interacts with Fe species supported on zirconium oxide.

The 1A and 1B catalyst were shown to be respectively the most and least active of the seven $Fe/WO_3/ZrO_2$ catalysts tested for NH_3 SCR. The Series 1 catalysts were studied in more detail as this series showed the highest variation in catalytic

activity with catalysts that exhibited high, moderate or low SCR activity (Fig. 6.4.3 and Table 6.4). The three Series 1 catalysts were characterised by IR spectroscopy with pyridine to examine the acidity of these catalysts as the NH_3 SCR activity was previously suggested to be linked to the acidity of the catalyst. The results obtained supports that suggestion and the SCR activity of the Series 1 catalysts was found to be linked with the number and type of LAS present on the catalyst. The 1B catalyst that exhibited the lowest SCR activity had the highest number of LAS, however, the peak position was at 1446 cm^{-1} which has been attributed to pyridine adsorbing onto Zr^{4+} LAS (Fig. 6.4.3). LAS generated from Zr^{4+} site have been shown to be inactive for NH_3 SCR of NO_x (Section 6.1).

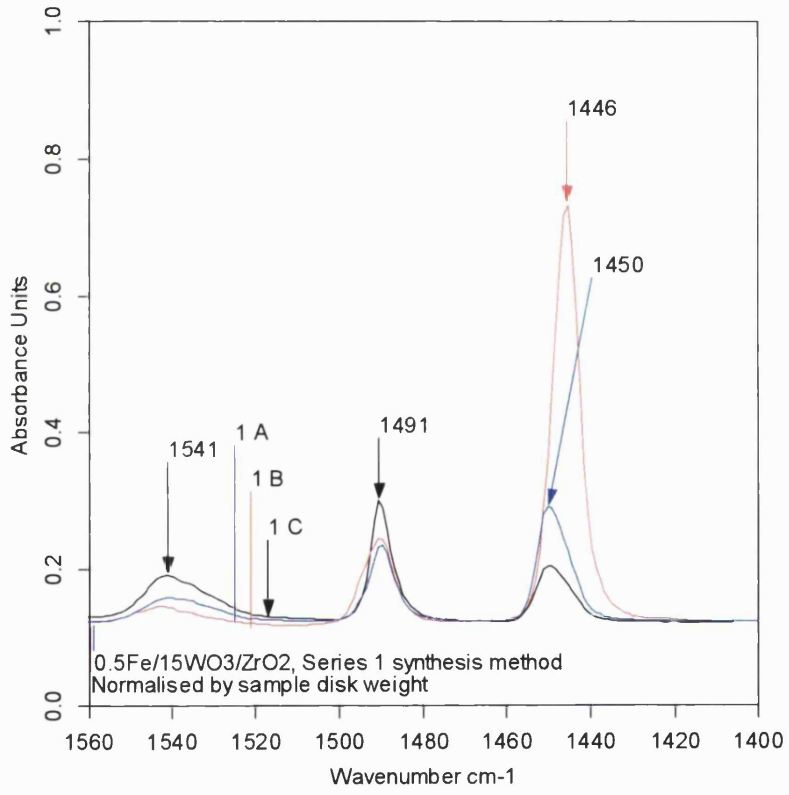

Fig. 6.4.3. IR spectra (Py region) after pyridine adsorption on $0.5Fe/15WO_3/ZrO_2$ MEL catalysts synthesised via Series 1 route. The IR spectra were normalised by the sample disk weight.

On the other hand, the 1A and 1C catalysts that were significantly more active in NH_3 SCR than the 1B catalyst have peaks at 1450 cm^{-1} which has been assigned to pyridine adsorbing onto Fe^{3+} LAS. These Fe^{3+} LAS can be linked to the NH_3 SCR activity as previously suggested in Section 6.1. The better SCR activity of the 1A catalyst can be associated with the higher number of Fe^{3+} LAS present on that catalyst compared to the 1C catalyst (Fig. 6.4.3).

Furthermore, the 1B catalyst that exhibited poor high temperature SCR activity had the lowest number of BAS of the three Series 1 catalysts. This supports the possibility that the number of BAS affects the high temperature NH_3 SCR activity. However, the 1C catalyst had almost double the number of BAS compared to the 1A catalyst but the 1A catalyst was still significantly more active in NH_3 SCR. It is most likely that the number of Fe^{3+} LAS is the key factor that influences the NH_3 SCR activity but a small number of strong BAS is also required for good SCR activity as previously suggested in Section 6.1.

Table 6.4. Acidity measurements for $Fe/WO_3/ZrO_2$ MEL Series 1 catalysts.

Catalyst	1A	1B	1C
BAS + LAS (μmol/g)	38	114	37
Ratio LAS/BAS	2.4	12.6	0.8
LAS (μmol/g)	27	106	17
BAS (μmol/g)	11	8	20

The error is estimated to be up to 10% based on the characterisation results of other samples carried out in this thesis.

The acid site strength of the Series 1 catalyst was investigated to study its effect on the SCR activity of those catalysts. As expected, the 1B catalyst had the lowest LAS and BAS strength of the three catalysts. The 1A catalyst possessed the strongest LAS followed by the 1C then 1B catalysts (Fig. 6.4.4(A)). Accurate data points at 300 °C and 350 °C for the 1A catalyst could not be

obtained due to similar reasons as that previously reported for the H/beta zeolite (Fig. 6.3.3). It is interesting to note that the 1C catalyst has a greater BAS strength compared to the 1A catalyst (Fig. 6.4.4(B)). This suggests that only a certain BAS strength is required for good SCR activity and any further increase in the BAS strength does not improve the catalytic activity.

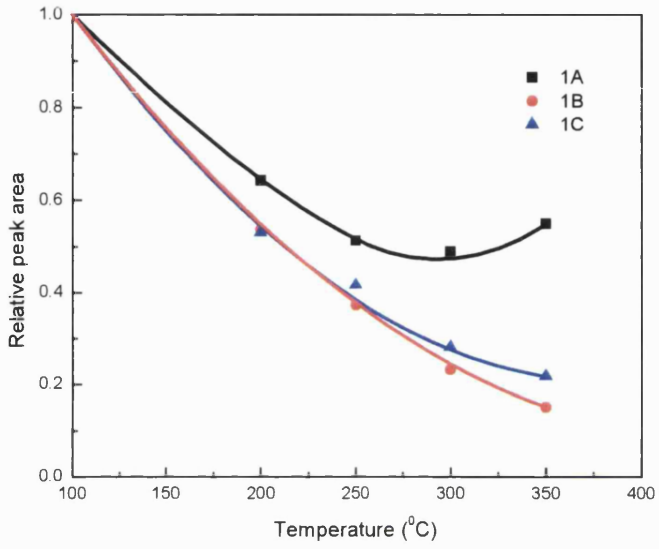

(A)

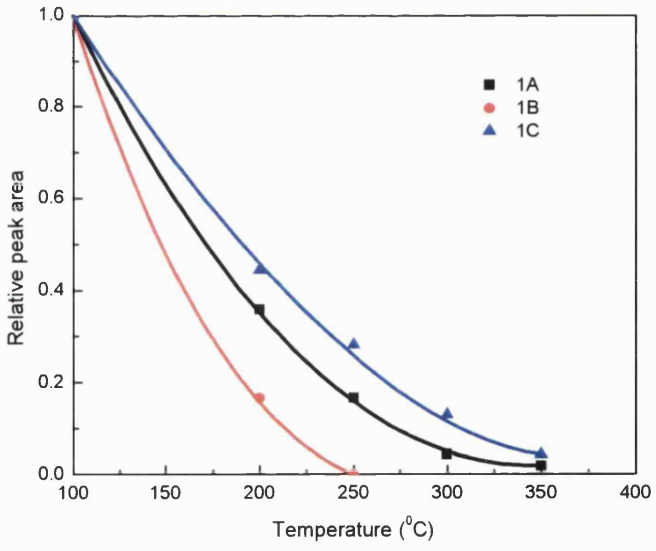

(B)

Fig. 6.4.4. Pyridine desorption from (A) LAS and (B) BAS present on $0.5Fe/WO_3/ZrO_2$ MEL catalysts synthesised via Series 1 route.

The 1C catalyst had a greater number and strength of BAS but it still exhibited lower high temperature activity than the 1A catalyst. It was previously suggested that the Broensted acidity could be linked to the high temperature activity but no improvement in the SCR activity was found when comparing the 1C catalyst with the 1A catalyst. The results suggest that only a small number of strong BAS is necessary and any additional increase in the number and strength of BAS does not significantly affect the NH_3 SCR activity. The number of Fe^{3+} LAS is the key factor in determining the NH_3 SCR activity of a catalyst although a small number of strong BAS is also required. Similar conclusions were made previously in Section 6.1 with the $Fe/WO_3/ZrO_2$ DKK catalysts.

6.5 Role of the calcination temperature of the WO_3/ZrO_2 support in the synthesis of $Fe/WO_3/ZrO_2$ MEL catalysts

The calcination temperature of the 15 wt% WO_3/ZrO_2 support synthesised using MEL zirconium hydroxide was set at 600, 710 and 830 °C before impregnating with 0.5 wt% iron then calcined at 600 °C. The $0.5Fe/15WO_3/ZrO_2$ MEL catalysts was tested for NH_3 SCR activity under lean conditions between 150 °C and 550 °C and characterised by IR spectroscopy with pyridine to determine the type and number of acid sites. The catalysts were also characterised by XRD to investigate the structural properties of the $0.5Fe/15WO_3/ZrO_2$ MEL catalysts.

The SCR activity of the $0.5Fe/15WO_3/ZrO_2$ catalysts increases with higher calcination temperatures of the WO_3/ZrO_2 support (Fig. 6.5.1). There is a significant difference between the SCR activity of the catalysts where the support was calcined at 600 °C and 710 °C. However, the SCR activity of the catalysts with supports calcined at 710 °C and 830 °C are very similar. These results are not unexpected as the WO_3/ZrO_2 support calcined at 600 °C has not been treated to sufficiently high temperatures that are required for the tungsten oxide to move from the bulk to the surface in order to stabilise the zirconium oxide in the tetragonal phase.

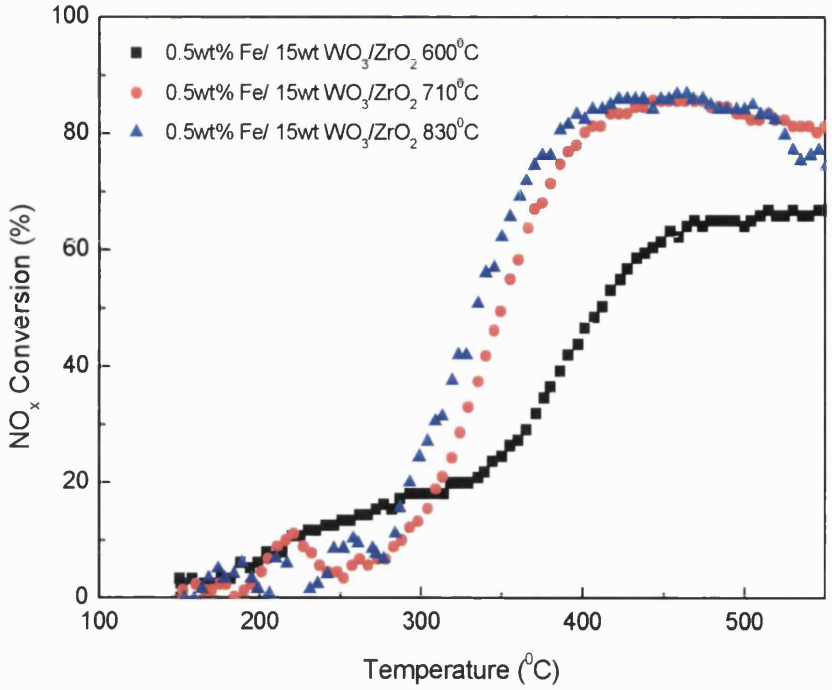

Fig. 6.5.1. Effect of temperature on NO_x conversion over $0.5Fe/15WO_3/ZrO_2$ MEL catalysts where the WO_3/ZrO_2 support has been calcined at 600, 710 and 830 °C.

The XRD results demonstrate that as the calcination temperature rises, the amount of tetragonal zirconium oxide present on the $0.5Fe/15WO_3/ZrO_2$ catalysts increases based on the increase in the peak intensities in Figs 6.5.2-4 (note: the Y axis scale changes). The red lines indicate the amount of tetragonal ZrO_2 present and the blue lines represent the level of monoclinic ZrO_2. Monoclinic zirconium oxide starts to form on the WO_3/ZrO_2 support calcined at 830 °C which suggests that 830 °C is close to the maximum calcination temperature before a drop in the level of tetragonal zirconium oxide will occur due to the formation of bulk WO_3 clusters. The XRD data are in agreement with the results obtained previously in Chapter 5.4, where there was a severe loss of acidity on the WO_3/ZrO_2 support when calcined to 890 °C that was attributed to the formation of WO_3 clusters.

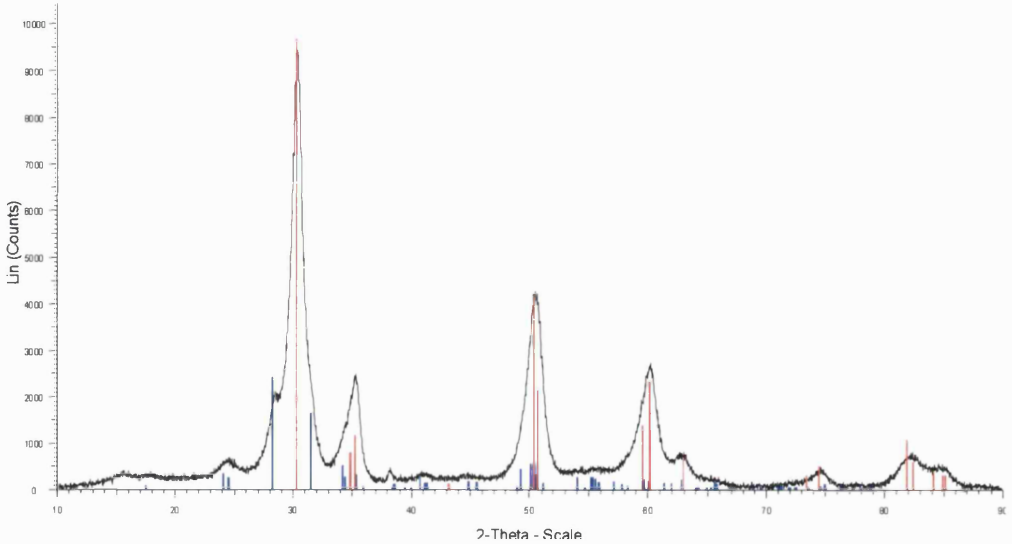

Fig. 6.5.2. X-ray diffraction pattern of $0.5Fe/15WO_3/ZrO_2$ where the WO_3/ZrO_2 MEL support was calcined at 600 °C.

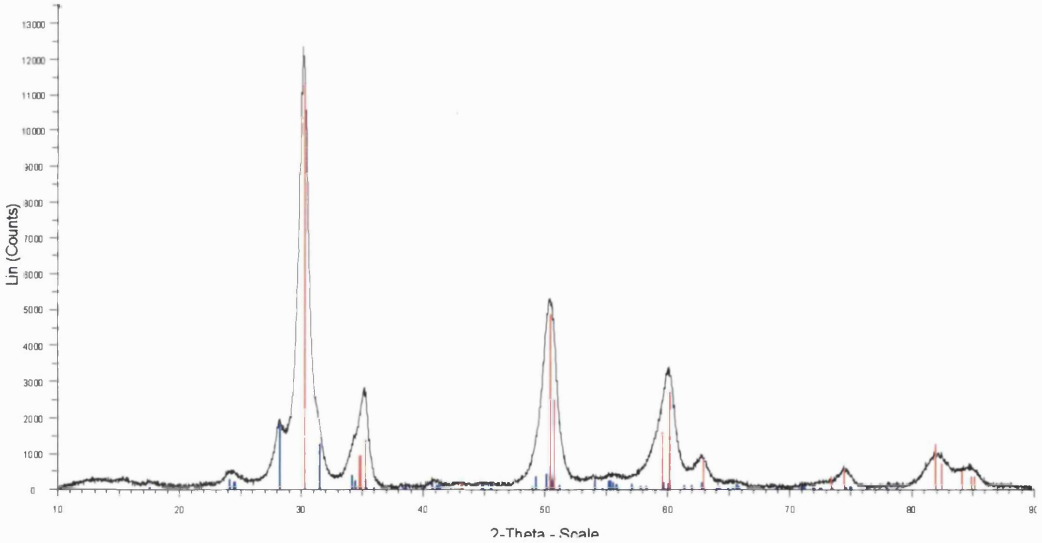

Fig. 6.5.3. X-ray diffraction pattern of $0.5Fe/15WO_3/ZrO_2$ where the WO_3/ZrO_2 MEL support was calcined at 710 °C.

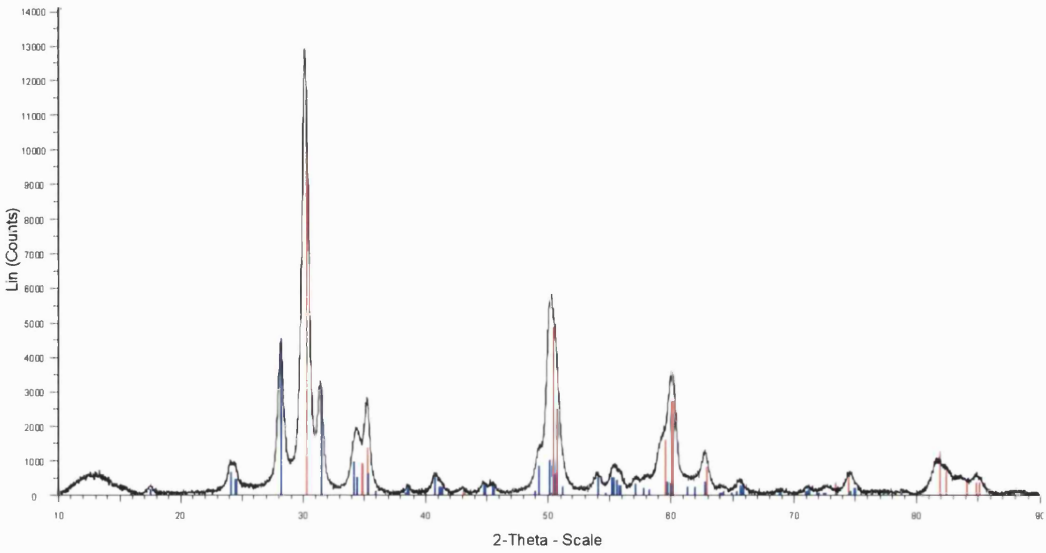

Fig. 6.5.4. X-ray diffraction pattern of $0.5Fe/15WO_3/ZrO_2$ where the WO_3/ZrO_2 MEL support was calcined at 710 °C.

The results also suggest that tungsten oxide requires at least 710 °C to have a stabilising effect on zirconium oxide which supports the work done previously in Chapters 5.4 and 6.4 and those reported in the literature [142, 145, 146]. There is only a small difference in the SCR activity of the catalyst where the WO_3/ZrO_2 support was calcined at 830 °C compared to the support calcined at 710 °C because most of the tungsten oxide has already diffused from the bulk to the surface when calcined at 710 °C. Therefore raising the calcination temperature to 830 °C does not lead to any significant increase in the level of zirconium oxide present in the tetragonal phase.

The IR spectra examining the acidity of the $0.5Fe/15WO_3/ZrO_2$ MEL catalysts where the WO_3/ZrO_2 supports were calcined at 600, 710 and 830 °C are compared in Fig. 6.5.5. The numbers of LAS present on the $0.5Fe/15WO_3/ZrO_2$ MEL catalysts decreases steadily as the calcination temperature is increased and a peak shift from 1445 cm^{-1} to 1450 cm^{-1} was observed at the calcination temperature of 830 °C.

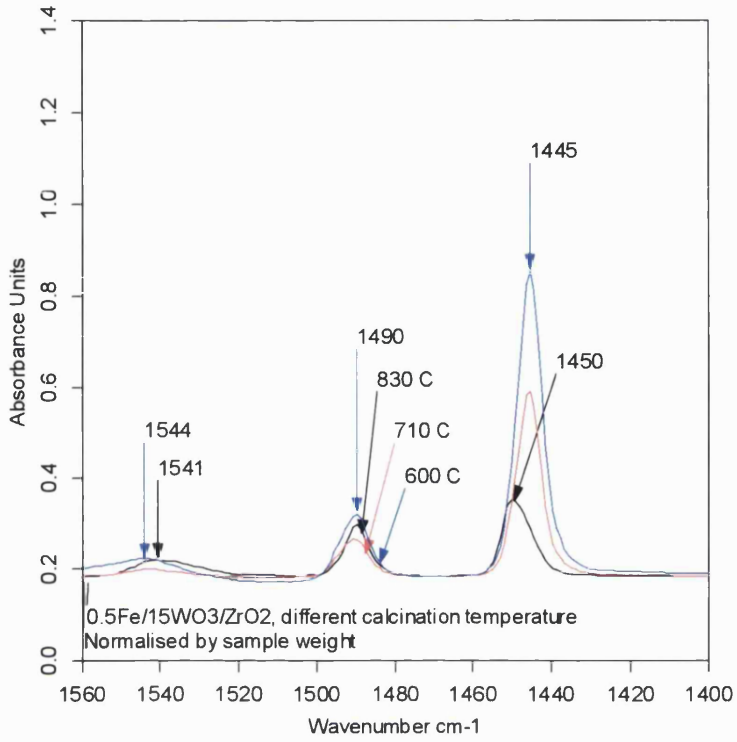

Fig. 6.5.5. IR spectra (Py region) after pyridine adsorption on $0.5Fe/15WO_3/ZrO_2$ MEL catalysts where the WO_3/ZrO_2 support was calcined at 600, 710 and 830 °C. The IR spectra were normalised by the sample disk weight.

The peaks at 1445 cm^{-1} and 1450 cm^{-1} are assigned to pyridine adsorbed onto LAS, which suggests that there is a change in the type of LAS formed on the $Fe/WO_3/ZrO_2$ MEL catalysts when the calcination temperature of the WO_3/ZrO_2 support reaches 830 °C. A similar peak shift from 1446 cm^{-1} to 1449 cm^{-1} was previously observed on the $Fe/WO_3/ZrO_2$ DKK catalysts (Fig. 6.1.3). There was also a small reduction in the number of BAS when the support is calcined above 600 °C. Quantitative values for the number of acid sites present on the $0.5Fe/15WO_3/ZrO_2$ MEL catalysts was calculated and are shown in Table 6.5.

Table 6.5. Acidity measurements for $0.5Fe/15WO_3/ZrO_2$ MEL catalysts where the WO_3/ZrO_2 support was calcined at 600, 710 and 830 °C.

Temperature	600 °C	710 °C	830 °C
BAS + LAS (μmol/g)	121	72	38
Ratio LAS/BAS	8.6	7.0	2.4
LAS (μmol/g)	108	63	27
BAS (μmol/g)	13	9	11

Based on the results of repeated experiments, the error was found to be approximately 7%.

The LAS on WO_3/ZrO_2 are generally attributed to exposed free Zr^{4+} sites on the surface and the BAS are generated by tungsten oxide. The reduction in the number of LAS at high calcination temperatures is most likely due to the increased diffusion of tungsten species from the bulk to the surface where they occupy Zr^{4+} sites therefore reducing the number of Zr^{4+} LAS.

There was no change in the number of BAS which was not unexpected as the tungsten oxide loading was kept constant at 15 wt% for all three $Fe/WO_3/ZrO_2$ MEL catalysts. This is based on the quantitative numbers calculated from analysis of the IR spectra. It should be noted that the spectra for the catalyst calcined at 710 °C shows little to no BAS. The spectra should be re-examined but the stored data was lost due to equipment failure at the laboratory.

It was expected that at higher calcination temperatures more BAS would have been generated due to the increased level of diffusion of tungsten oxide from the bulk to the surface. This did not occur and can be explained by the proposal that there are only a fixed number of suitable zirconium adsorption sites present on the zirconium hydroxide support for the formation of BAS [76].

The peak shift from 1445 cm^{1} to 1450 cm^{-1} that occurs at the calcination temperature of 830 °C is most likely caused by the formation of new Fe^{3+} LAS

on WO_3/ZrO_2 as previously reported for Fe/beta and $Fe/WO_3/ZrO_2$ DKK catalysts (Sections 6.1 and 6.3). It is possible that iron only generates a small number of Fe^{3+} LAS which is not apparent with the supports calcined at 600 °C and 710 °C (Fig. 6.5.5) because of the significantly higher number of Zr^{4+} LAS present on those catalysts.

Potentially, the catalysts calcined at 710 and 830 °C both have similar numbers of Fe^{3+} LAS therefore exhibited similar NH_3 SCR activity. However, the catalyst calcined at 710 °C also had a larger proportion of Zr^{4+} LAS present therefore the IR peak position remains at 1445 cm^{-1} instead of 1450 cm^{-1}.

The peak shift from 1445 cm^{-1} to 1450 cm^{-1} occurred when the catalytic support was calcined at 830 °C because the LAS present on that catalyst are now primarily due to Fe^{3+} LAS rather than the predominant Zr^{4+} LAS present on the supports calcined at 600 °C and 710 °C. There is also the possibility that the Fe^{3+} LAS are only formed by the interaction between iron and tetragonal zirconium oxide. Therefore the supports with greater levels of tetragonal zirconium oxide will have higher numbers of Fe^{3+} LAS thus exhibiting better NH_3 SCR catalytic activity.

The pyridine TPD profiles displayed in Fig. 6.5.6 illustrates that the LAS strength steadily increases with higher calcination temperatures. The BAS strength also increases slightly with calcination temperature. The IR spectra of the catalyst with the WO_3/ZrO_2 support calcined at 830 °C was distorted at high desorption temperatures due to the presence of nitrogen based products from the reaction between pyridine and strong LAS, similar to those reported previously on various catalysts/supports. As a result of this, the peak assigned to LAS at desorption temperatures of 300 and 350 °C could not be accurately integrated.

The pyridine desorption results indicate that although there is a high number of LAS present on the $0.5Fe/15WO_3/ZrO_2$ MEL catalysts where the supports were calcined at 600 °C and 710 °C, they are mainly composed of weak LAS. The LAS strength increases with calcination temperature as zirconium oxide is stabilised by tungsten oxide at higher calcination temperatures. The weak LAS

can be associated with the Zr^{4+} LAS present on the catalysts where the WO_3/ZrO_2 supports were calcined at 600 °C and 710 °C, whereas strong Fe^{3+} LAS are formed on the support calcined at 830 °C.

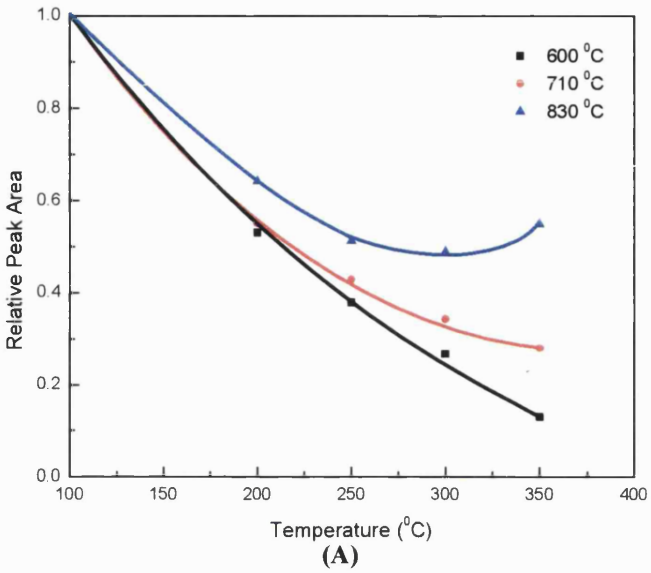

(A)

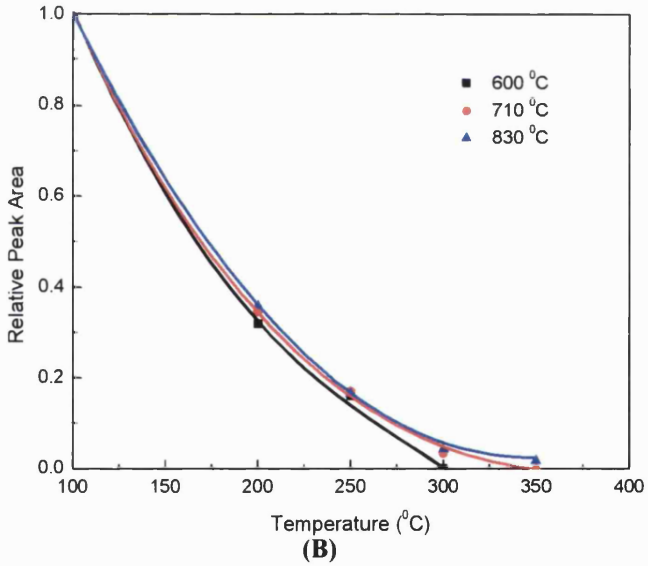

(B)

Fig. 6.5.6. Pyridine desorption from (A) LAS and (B) BAS present on $0.5Fe/15WO_3/ZrO_2$ MEL catalysts where the WO_3/ZrO_2 support was calcined at 600, 710 and 830 °C.

The results in this section support those reported in the literature and results obtained previously in Chapters 5.4 and 6.4 where it has been shown that high calcination temperatures are required for the synthesis of suitable WO_3/ZrO_2 catalytic supports [142, 145, 146]. The catalysts synthesised from supports that were calcined at temperatures equal to or above 710 °C exhibited better catalytic activity (Fig. 6.5.1). The number of BAS remained similar with a small increase in the acid site strength as the calcination temperature of the support was raised from 600 °C to 830 °C.

The number of LAS decreases with increasing calcination temperature; however, a change from Zr^{4+} to Fe^{3+} LAS occurs and the LAS strength increases with higher calcination temperatures (Figs. 6.5.5 and 6.5.6). It cannot be determined if the number of Fe^{3+} LAS increases with the calcination temperature of the WO_3/ZrO_2 support or the same number of Fe^{3+} LAS was present on all three $0.5Fe/15WO_3/ZrO_2$ MEL catalysts.

It is possible that increasing the calcination temperature only reduces the number of Zr^{4+} LAS present therefore making the smaller number of Fe^{3+} LAS visible in the IR spectra. The improvement in the NH_3 SCR activity of the catalysts with supports calcined at higher calcination temperatures could be associated with either the formation of stronger Fe^{3+} LAS or less interference from the reduced number of weak Zr^{4+} LAS.

This also creates the possibility that the NH_3 SCR activity may not be dependent on the type of LAS (Zr^{4+} or Fe^{3+}) but instead based on the strength of the LAS. There was a significant reduction in the LAS strength on the H/beta support after introducing iron which brings the Fe/beta LAS strength to similar levels to those seen on the $Fe/WO_3/ZrO_2$ catalysts (Figs 6.3.2 and 6.3.8). The WO_3/ZrO_2 support may not be active for NH_3 SCR of NO_x due to its weak LAS but introducing iron enhances the LAS strength to the required level for good SCR activity. The opposite occurs with the Fe/beta catalysts where iron decreases the LAS strength of the H/beta support to the necessary moderate LAS strength.

Furthermore, it is also possible that iron has generated numerous weak acid sites, which are not sufficiently acidic to maintain adsorbed pyridine at 100 °C and therefore, would not be accounted for in the experiments. The pyridine adsorption experiments were carried out at 100 °C to ensure that there is no physio-sorbed pyridine. These weak acid sites could be important for NH_3 SCR activity since NH_3 adsorption during SCR of NO_x reaction may require weak acid sites.

6.6 The effect of tungsten oxide loading on the acidity and NH_3 SCR activity of $Fe/WO_3/ZrO_2$ MEL catalysts

The synthesis procedure and the influence of the calcination temperature of the WO_3/ZrO_2 support of $Fe/WO_3/ZrO_2$ MEL catalysts was investigated in Sections 6.4 and 5.5. Following on from this work, the effect of tungsten oxide loading of the WO_3/ZrO_2 MEL catalytic support on the NH_3 SCR activity of the $Fe/WO_3/ZrO_2$ MEL catalysts was studied. $Fe/WO_3/ZrO_2$ catalysts were synthesised using WO_3/ZrO_2 MEL supports containing 5, 10, 15 and 20 wt% tungsten oxide before impregnating with 0.5 wt% iron. The NH_3 SCR activity of the $0.5Fe/WO_3/ZrO_2$ catalysts rises significantly as the tungsten oxide loading was increased steadily from 5 to 15 wt% (Fig. 6.6.1).

The $0.5Fe/15WO_3/ZrO_2$ catalyst had the best catalytic activity of the four catalysts tested which was slightly higher than that exhibited by the $0.5Fe/20WO_3/ZrO_2$ catalyst. The low temperature activity of the $0.5Fe/20WO_3/ZrO_2$ catalyst is very similar to the $0.5Fe/15WO_3/ZrO_2$ catalyst up the reaction temperature of 350 °C, however, above 350 °C the SCR activity of the $0.5Fe/20WO_3/ZrO_2$ catalyst is approximately 10 % lower than the $0.5Fe/15WO_2/ZrO_2$ catalyst.

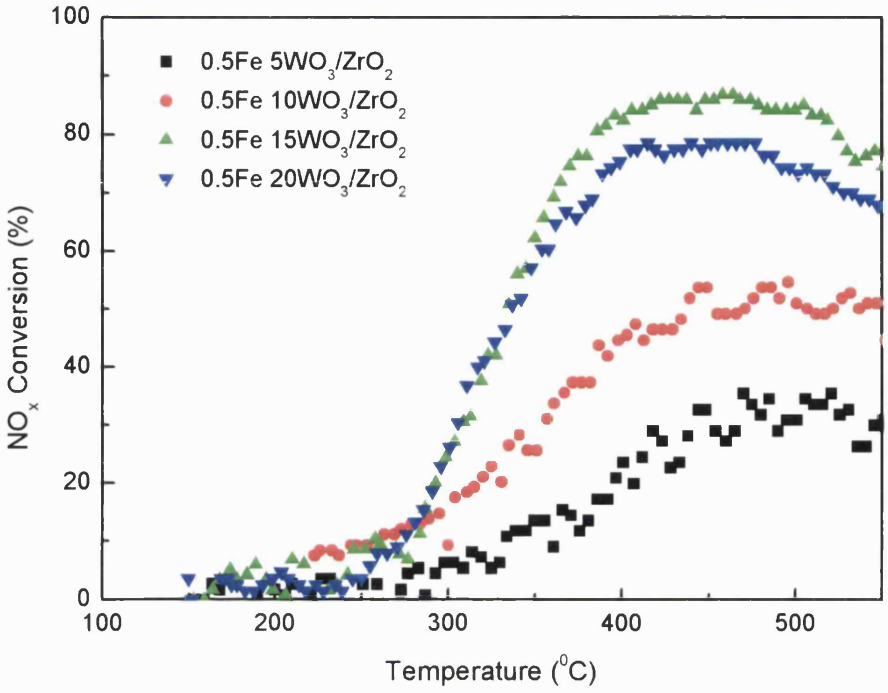

Fig. 6.6.1. Effect of temperature on NO_x conversion over $0.5Fe/WO_3/ZrO_2$ MEL catalysts containing 5, 10, 15 and 20 wt% tungsten oxide.

The SCR activity of the $0.5Fe/WO_3/ZrO_2$ MEL catalysts correlates well with the acidity of the catalysts where the SCR activity increases with the number of Fe^{3+} LAS (Figs. 6.6.1 and 6.6.2). The change from Zr^{4+} LAS to Fe^{3+} LAS occurred as seen by the peak shift from 1446 cm^{-1} on the WO_3/ZrO_2 support to 1450 cm^{-1} on the $0.5Fe/WO_3/ZrO_2$ MEL catalysts (Fig. 6.6.2).

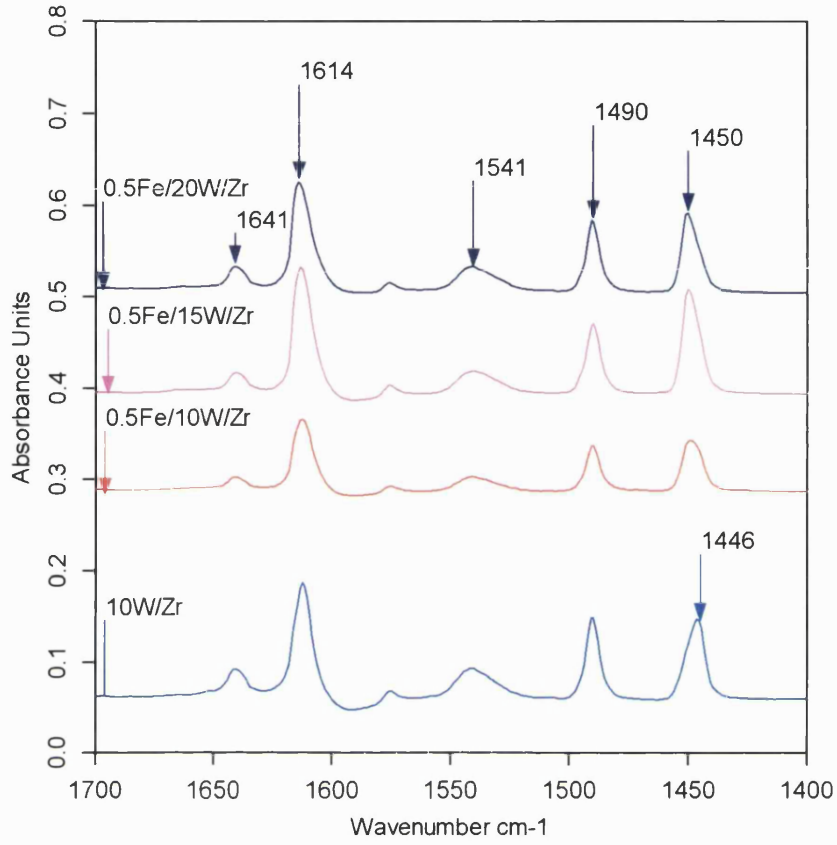

Fig. 6.6.2. IR spectra (Py region) after pyridine adsorption on $0.5Fe/WO_3/ZrO_2$ MEL catalysts containing 5, 10, 15 and 20 wt% tungsten oxide. The IR spectra were normalised by the sample disk weight.

The $0.5Fe/15WO_3/ZrO_2$ catalyst has the highest number of Fe^{3+} LAS and is also the most active of the 4 catalysts tested. The $0.5Fe/20WO_3/ZrO_2$ catalyst had a slightly lower number of Fe^{3+} LAS than the $0.5Fe/15WO_3/ZrO_2$ catalyst that can be correlated with a similar level of reduction in the SCR activity of the $0.5Fe/20WO_3/ZrO_2$ catalyst. Similarly, the $0.5Fe/10WO_3/ZrO_2$ catalyst had approximately half the number of Fe^{3+} LAS compared to the $0.5Fe/15WO_3/ZrO_2$ catalyst and a significant drop in the SCR activity was observed.

The SCR activity at specific reaction temperatures between 300 °C and 500 °C of the $0.5Fe/WO_3/ZrO_2$ MEL catalysts containing either 10, 15 or 20 wt% tungsten

oxide are compared in Table 6.6.1. Furthermore, the SCR activity of the $0.5Fe/WO_3/ZrO_2$ MEL catalysts is also compared to the relative intensities of the IR peak (1450 cm^{-1}) associated with LAS.

Table 6.6.1. The relative NH_3 SCR activity at temperatures between 300 °C and 500 °C of $0.5Fe/WO_3/ZrO_2$ MEL catalysts containing either 10, 15 or 20 wt% tungsten oxide compared to the relative intensity of the IR peak associated with LAS (1450 cm^{-1}).

Catalyst	300 °C	350 °C	400 °C	450 °C	500 °C	Relative no. of LAS
$0.5Fe/10WO_3/ZrO_2$	1.0	1.0	1.0	1.0	1.0	1.0
$0.5Fe/15WO_3/ZrO_2$	1.6	2.2	1.9	1.7	1.7	2.0
$0.5Fe/20WO_3/ZrO_2$	1.6	2.0	1.7	1.5	1.4	1.5

The SCR activity of the $0.5Fe/WO_3/ZrO_2$ MEL catalysts can be associated with the number of Fe^{3+} LAS based on the results shown in Table 6.6.1. A similar correlation between the SCR activity and the number of Fe^{3+} LAS was previously described when the $Fe/WO_3/ZrO_2$ DKK catalysts were investigated (Section 6.1). The changes in the Broensted acidity were also examined as it was previously suggested to influence the SCR activity of $Fe/WO_3/ZrO_2$ catalysts.

The numbers of BAS present on the parent 10 wt% WO_3/ZrO_2 MEL support decreases after iron impregnation compared to the $0.5Fe/10WO_3/ZrO_2$ catalyst (Fig. 6.6.2). This occurs with all the $0.5Fe/WO_3/ZrO_2$ catalysts but the IR spectra are not displayed for brevity. As anticipated, the number of BAS increases as the tungsten oxide loading of the WO_3/ZrO_2 support increases since more tungsten species will be present thus generating more BAS as reported previously in Chapter 5.

All three $0.5Fe/WO_3/ZrO_2$ MEL catalysts exhibited very similar BAS and LAS strength (Fig. 6.6.3). The data point at 350 °C for the pyridine desorption results on the LAS may not be accurate. The spectra could not be integrated

appropriately as the peak was distorted due to formation of nitrogen based products from pyridine reacting with strong LAS similar to that previously shown in Fig. 6.3.3.

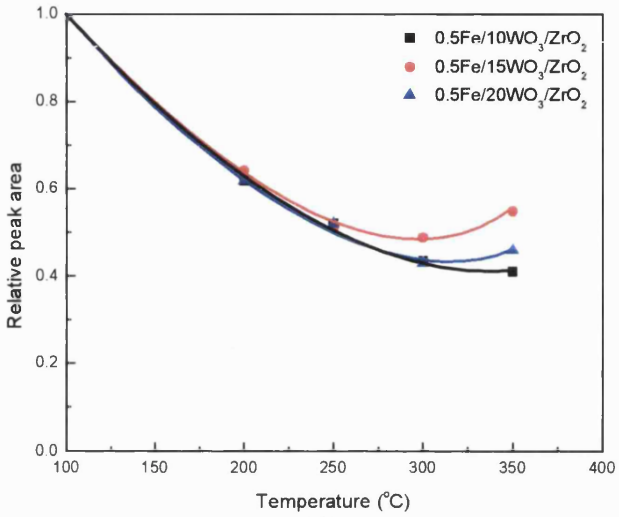

(A)

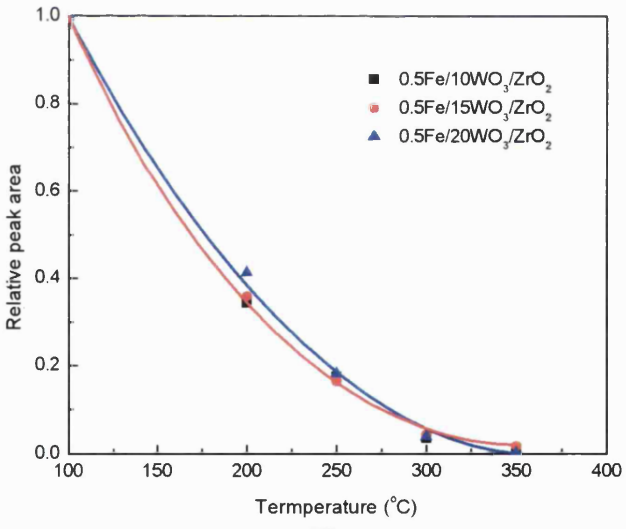

(B)

Fig. 6.6.3. Pyridine desorption from (A) LAS and (B) BAS present on $Fe/WO_3/ZrO_2$ MEL catalysts containing 10, 15 and 20 wt% tungsten oxide.

6.7 Effect of iron loading on the NH_3 SCR activity of $Fe/WO_3/ZrO_2$ MEL catalysts

The effect of iron loading on the SCR activity of $Fe/WO_3/ZrO_2$ catalysts supported on 15 wt% WO_3/ZrO_2 MEL support calcined at 830 °C was investigated. Four different $Fe/15WO_3/ZrO_2$ MEL catalysts containing 0.5, 2, 3 and 5 wt% iron were synthesised and examined. The catalysts were tested for NH_3 SCR activity under lean conditions at reaction temperature between 150 °C and 550 °C (Fig. 6.7.1).

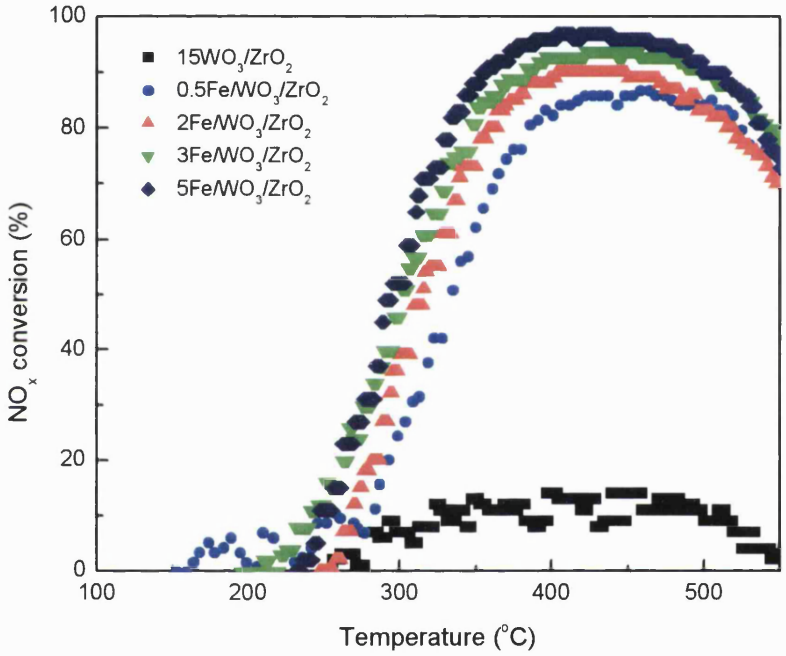

Fig. 6.7.1. Effect of temperature on NO_x conversion over $Fe/WO_3/ZrO_2$ MEL catalysts containing 0, 0.5, 2, 3 and 5 wt% iron.

The $15WO_3/ZrO_2$ MEL support is not active for NH_3 SCR with a maximum NO_x conversion of 14 %, but after impregnation with 0.5 wt% Fe, the catalyst demonstrated significant improvements and good SCR activity. The SCR activity of the $Fe/WO_3/ZrO_2$ MEL catalysts increases steadily with higher iron loading and a small drop in the SCR activity occurs at reaction temperatures

above 450 °C on all the catalysts tested. This reduction in SCR activity is most likely caused by the catalyst becoming slightly unselective at high temperatures.

There is only a small difference in the catalytic activity between the 3 wt% and 5 wt% $Fe/WO_3/ZrO_2$ catalysts whereas more significant changes were observed when increasing the iron loading from 2 wt% to 3 wt% iron. The low temperature activity of the $3Fe/15WO_3/ZrO_2$ and $5Fe/15WO_3/ZrO_2$ catalysts remains very similar and at the reaction temperatures above 275 °C, the catalytic activity of the $5Fe/15WO_3/ZrO_2$ catalyst improves only slightly by ~2-3% compared to the $3Fe/15WO_3/ZrO_2$ catalyst. These results suggest that the optimum iron loading is around 5 wt% on WO_3/ZrO_2 support synthesised using MEL zirconium hydroxide.

6.8 Comparison of the NH_3 SCR activity of Fe/beta and $Fe/WO_3/ZrO_2$ catalysts

The SCR activity of 0.5 wt% iron supported on the three different catalytic supports, $9WO_3/ZrO_2$ DKK, $10WO_3/ZrO_2$ MEL and H/beta are compared in Fig. 6.8.1. The 0.5Fe/beta catalyst exhibited significantly better SCR activity in particular in the low temperature region when compared to the $Fe/WO_3/ZrO_2$ catalysts.

However, the SCR activity of the 0.5Fe/beta catalyst decreases gradually at reaction temperatures above 350 °C that suggests the catalyst is unselective at high temperatures. The $0.5Fe/10WO_3/ZrO_2$ MEL catalyst exhibited very poor SCR activity in comparison to the other catalysts but it should be noted that the optimum tungsten oxide loading for the MEL WO_3/ZrO_2 support was shown to be 15 wt% not 10 wt% tungsten oxide (Chapter 5.2). On the other hand, 10 wt% was the optimum tungsten oxide loading for the WO_3/ZrO_2 DKK support (Chapter 5.3).

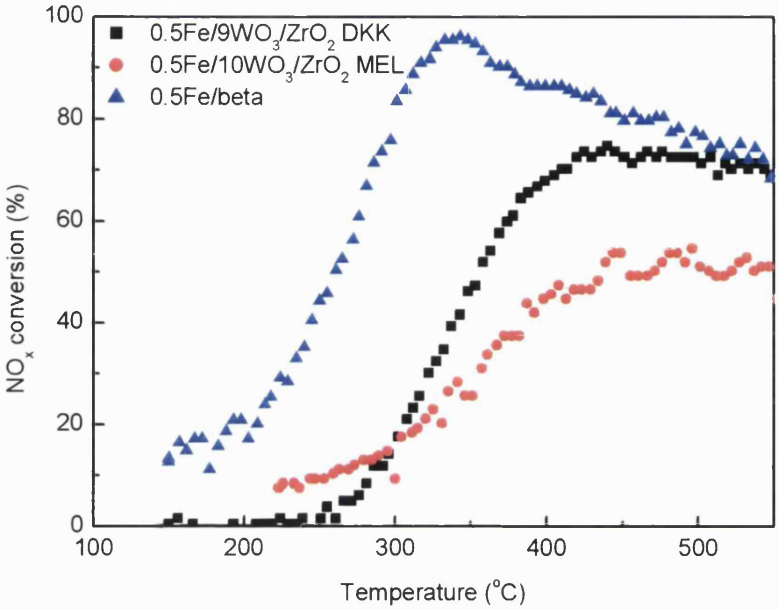

Fig. 6.8.1. Effect of temperature on NO_x conversion over $0.5Fe/9WO_3/ZrO_2$ DKK, $0.5Fe/10WO_3/ZrO_2$ MEL and 0.5Fe/beta catalysts.

The iron loading of the catalysts was increased to 2 wt% and the tungsten oxide loading of the $Fe/WO_3/ZrO_2$ MEL catalyst was changed to 15 wt% for a better comparison of the three catalysts. The NH_3 SCR activities of the three Fe – based catalysts are compared in Fig 6.8.2.

Significant improvements in the NH_3 SCR activity of the $Fe/WO_3/ZrO_2$ catalysts were made after the iron loading was increased to 2 wt%. The high temperature activities of the $Fe/WO_3/ZrO_2$ catalysts are now comparable or better than that of the 2Fe/beta catalyst. The $2Fe/15WO_3/ZrO_2$ MEL catalyst exhibited the highest SCR activity of the three catalysts at the reaction temperatures above ~350 °C.

However, better improvements in the low temperature activity of the $Fe/WO_3/ZrO_2$ catalysts are still desired. Both the $Fe/WO_3/ZrO_2$ DKK and MEL catalysts exhibited similar NO_x conversion profiles where the SCR activity begins to slowly decrease at temperatures above ~475 °C due to the catalysts becoming slightly unselective at high temperatures which does not occur with the 2Fe/beta catalyst.

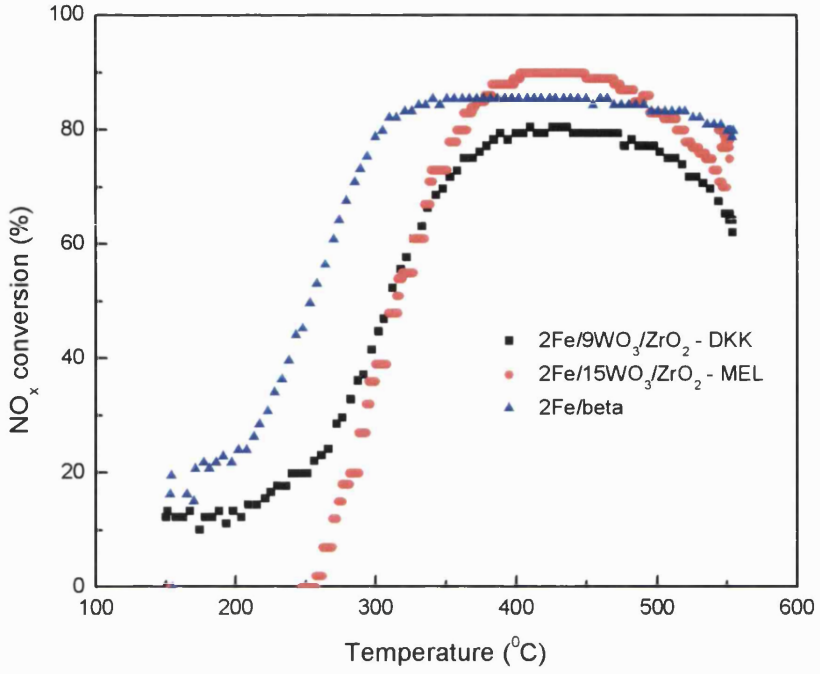

Fig. 6.8.2. Effect of temperature on NO_x conversion over $2Fe/9WO_3/ZrO_2$ DKK, $2Fe/15WO_3/ZrO_2$ MEL and 2Fe/beta catalysts.

The hydrothermal resistance of the $Fe/WO_3/ZrO_2$ and Fe/beta catalysts were previously examined in Sections 6.2 and 6.3. It was found that the $Fe/WO_3/ZrO_2$ catalysts had good hydrothermal resistance which was better than that exhibited by the Fe/beta catalyst in the low temperature region. The results obtained demonstrate that $Fe/WO_3/ZrO_2$ is a promising catalyst for NH_3 SCR of NO_x with activity comparable to that of Fe/beta.

The poor SCR activity of the $0.5Fe/10WO_3/ZrO_2$ MEL catalyst compared to the $0.5Fe/9WO_3/ZrO_2$ DKK catalyst in Fig 6.8.1 is most likely attributed to the sub-optimal tungsten oxide loading as previously suggested. It is possible that increasing the tungsten oxide loading of the $Fe/WO_3/ZrO_2$ DKK catalyst may lead to improvements in the NH_3 SCR activity. Such a comparison was not possible since the $9WO_3/ZrO_2$ DKK support used was a commercially prepared sample and the tungsten oxide loading could not be changed.

However, it is the author's opinion that the DKK RC-100 zirconium hydroxide that had an optimum tungsten oxide loading of 10 wt% was the precursor used in the synthesis of the commercial DKK $9WO_3/ZrO_2$ support. Therefore increasing the tungsten oxide loading may not improve the NH_3 SCR activity of that catalyst.

If this assumption is valid, it shows that the synthesis of a $Fe/WO_3/ZrO_2$ catalyst that is active for NH_3 SCR is highly dependent on the properties of the zirconium hydroxide precursor used. Different $Fe/WO_3/ZrO_2$ catalysts would have to be compared at their respective optimum tungsten oxide loading, and, not at the same tungsten oxide loading for an accurate evaluation of the catalysts. This may also be true when comparing the effect of iron loading of different $Fe/WO_3/ZrO_2$ catalysts on the NH_3 SCR activity of those catalysts.

6.9 Discussion and Summary

Iron promoted tungsten oxide supported on zirconia, $Fe/WO_3/ZrO_2$, was shown to be a promising catalyst for the selective catalytic reduction of nitrogen oxide by ammonia under lean conditions. In addition, the $Fe/WO_3/ZrO_2$ catalysts also demonstrated good hydrothermal resistance. Initially, the $Fe/WO_3/ZrO_2$ catalysts were synthesised using commercial $9WO_3/ZrO_2$ DKK supports (Section 6.1) where the SCR activity of the fresh and aged $Fe/WO_3/ZrO_2$ DKK catalysts was found to be promising but lower than the reference Fe/beta catalysts (Section 6.3).

The $Fe/WO_3/ZrO_2$ catalysts were subsequently produced from WO_3/ZrO_2 supports that were synthesised using MEL zirconium hydroxide where significant improvements in the SCR activity were made (Fig. 6.8.1). The $2Fe/WO_3/ZrO_2$ MEL catalyst exhibited better high temperature activity compared to the 2Fe/beta catalyst although the low temperature SCR activity is still lower. However, there is still a scope for major improvements in the development of $Fe/WO_3/ZrO_2$ catalysts.

The synthesis procedure of $Fe/WO_3/ZrO_2$ catalysts was examined in Section 6.4 where three different series of $Fe/WO_3/ZrO_2$ catalysts were synthesised and the order of impregnation with tungsten oxide or iron and the calcination temperature was varied. It was found that the best method was to first stabilise the zirconium oxide with tungsten oxide followed by calcination at 830 °C before impregnating with iron. The 1A $Fe/WO_3/ZrO_2$ catalyst synthesised using this method exhibited the best SCR activity of all the catalysts tested in Series 1, 2 and 3 (Figs. 6.4.1 and 6.4.2).

The optimum calcination temperature based on the temperature range studied was found to be 830 °C for the $Fe/WO_3/ZrO_2$ MEL catalysts (Section 6.5). At lower calcination temperatures of 600 °C, the $Fe/WO_3/ZrO_2$ catalysts exhibited poor NH_3 SCR activity due to the low diffusion of tungsten oxide from the bulk to the surface which reduces the W – Zr stabilisation effect. On the other hand, calcining the WO_3/ZrO_2 support at temperatures above 830 °C (890 °C) leads to a severe loss of acidity caused by the formation of bulk tungsten oxide, WO_3, clusters (Chapter 5.4).

Although, the 1A catalyst exhibited good overall SCR activity, the low temperature activity of that catalyst was quite poor. Interestingly, the low temperature activity improved with the 2A and 3B catalysts which were synthesised by impregnating zirconium hydroxide with iron before introducing tungsten oxide. However, the high temperature SCR activity of these catalysts was significantly reduced in comparison to the other $Fe/WO_3/ZrO_2$ catalysts (Figs 6.4.1 and 6.4.2). The improvement in the low temperature activity of the 2A and 3B catalysts could be attributed to better Fe – Zr interactions.

It has been suggested in the literature that there will be a strong Fe – Zr interaction and NO readily adsorbs and interacts with Fe species supported on zirconia oxide [113, 151]. This could also possibly account for the better low temperature SCR activity of the Fe/beta catalysts due to the strong Fe – beta zeolite interactions. The results obtained in Section 6.3 showed that it is likely that iron oxide is generating new BAS and interacting with the alumina or influencing the alumina BAS which leads to a reduction in the BAS strength.

The poor high temperature activity of the 2A and 3B catalysts is most likely caused by less W – Zr stabilising interactions which reduce the proportion of zirconium oxide in the tetragonal phase and increase the level of monoclinic zirconium oxide. The results suggest that iron has to interact directly with zirconium oxide to generate good low temperature SCR activity. The poor high temperature SCR activity is caused by the WO_3/ZrO_2 support which was not effectively stabilised because the Fe – Zr interaction inhibits the W – Zr stabilising interaction.

The H/beta support does not encounter this problem, and, therefore the Fe/beta catalyst exhibits good high and low temperature activity. This creates the possibility that iron simply requires a support that interacts strongly and provides good iron dispersion. This is supported by the results reported by Schwidder et al. [106] that the mononuclear Fe ions are the primary active sites and the SCR activity of a catalyst would decrease as iron agglomerates are formed at higher iron loading [74, 110].

Furthermore, based on discussions with the Autocatalyst group at Johnson Matthey technology centre, it appears that Fe/beta catalysts were still active despite the loss of all acid sites after severe aging. However, in this study, it was found that the NH_3 SCR activity can be correlated to the acidity of both the Fe/beta and $Fe/WO_3/ZrO_2$ catalysts. Iron generates similar new Fe^{3+} LAS on both the $Fe/WO_3/ZrO_2$ and Fe/beta catalysts based on the peak shifts observed in Figs. 6.1.3 and 6.3.1. A higher number of Fe^{3+} LAS can be linked to better SCR activity as demonstrated in Tables 6.1.1 and 6.6.1.

The correlation between the NH_3 SCR activity and the number of Fe^{3+} LAS is supported by Apostolescu et al. [150] who have reported that the NH_3 SCR reaction proceeds through a LAS based mechanism on $Fe/WO_3/ZrO_2$ catalysts. The 2Fe/beta catalyst had significantly higher numbers of LAS compared to the $2Fe/WO_3/ZrO_2$ DKK catalyst thus exhibited much better SCR activity (Fig 6.3.1). The number of Fe^{3+} LAS present on $Fe/WO_3/ZrO_2$ catalysts increases

with iron loading up to an optimum iron loading which varies depending on the WO_3/ZrO_2 support used.

Furthermore, the $Fe/WO_3/ZrO_2$ catalysts that possess a high number of weak Zr^{4+} LAS exhibited poor NH_3 SCR activity whereas catalysts with a small number of strong Fe^{3+} LAS showed good activity (Section 6.5). As the calcination temperature of the WO_3/ZrO_2 support of the $0.5Fe/15WO_3/ZrO_2$ MEL catalysts was increased, the number of weak Zr^{4+} LAS present on that catalyst decreased.

At high calcination temperatures, the LAS present on the $0.5Fe/15WO_3/ZrO_2$ MEL catalysts are predominantly generated by Fe^{3+} rather than by Zr^{4+} sites present on the supports calcined at low temperatures. However, it cannot be determined if the number of Fe^{3+} LAS increases or the IR peak assigned to Fe^{3+} LAS simply becomes clearer and more distinct as the number of Zr^{4+} LAS decreases as the calcination temperature of the WO_3/ZrO_2 MEL support increases (Fig. 6.5.3).

The improvement in the SCR activity could be due to lower interference from Zr^{4+} LAS rather than to an increase in the number of Fe^{3+} LAS. However, the results do demonstrate that a specific type of LAS (Fe^{3+}) is required for an active catalyst for NH_3 SCR.

It is also possible that iron has generated numerous weak acid sites, which are not sufficiently acidic to maintain adsorbed pyridine at 100 °C and, therefore, would not be accounted for in the experiments. The pyridine adsorption experiments were carried out at 100 °C to ensure that there is no physi-sorbed pyridine. These weak acid sites could be important for NH_3 SCR activity, however, since NH_3 adsorption during SCR of NO_x reaction may require weak acid sites.

The results have also indicated that a small number of strong BAS is required for good NH_3 SCR activity and the Broensted acidity was found to be associated with the high temperature activity (Section 6.1). This would account for the debate in the literature regarding whether the NH_3 SCR reaction proceeds via a

LAS or BAS based mechanism for iron supported on metal oxides. Most authors have reported that the reaction occurs over the LAS [114, 150] with a small number of publications stating that it requires BAS [114].

If the required number of strong BAS were present on the catalysts tested, the SCR activity would appear to be linked only to the number of LAS. The results in Section 6.4 showed that only a specific number and strength of BAS are required and any additional increase in the number and strength of the BAS does not improve the SCR activity of that catalyst. Similarly, the SCR activity would appear to be linked to the number of BAS if it drops below the required level of Broensted acidity and the number of LAS remains similar as seen on the $1Fe/WO_3/ZrO_2$ DKK catalyst.

The Fe – W interaction may also play an important role in the NH_3 SCR activity of $Fe/WO_3/ZrO_2$ catalysts. The SCR activity of the $Fe/WO_3/ZrO_2$ catalysts increased with tungsten oxide loading up to 15 wt% tungsten oxide (Section 6.6). Wong et al. had shown that Fe – O – W linkages were formed that optimised the surface reduction of WO_x species that also facilitates the formation of BAS [152]. Furthermore, the SCR activity of various Fe doped catalysts such as $Fe/WO_3/Al_2O_3$ was significantly improved by increasing the presence of tungsten oxide. The tungsten oxide loading on the $Fe/WO_3/Al_2O_3$ catalyst could not be increased any further due to physical and chemical limitations but the results suggest that such an increase would lead to improvements in the SCR activity of those catalysts.

There is the possibility that on $Fe/WO_3/ZrO_2$ catalysts synthesised from different zirconium hydroxides, the SCR activity will increase with even higher tungsten oxide loadings. Although the number of acid sites may decrease due to the presence of excess tungsten species that form inactive bulk WO_3 clusters. This would depend on whether the acidity or the strength of the Fe – W interactions influences the NH_3 SCR activity to a greater degree.

There may be an optimum tungsten oxide loading at a given specific iron loading for the highest level of Fe – W interaction on $Fe/WO_3/ZrO_2$ catalysts. The

results on the catalysts synthesised from the WO_3/ZrO_2 MEL supports coincide with the same iron and tungsten oxide loadings that generate the largest number of acid sites. This is not unexpected since the greatest level of Fe – W interaction should occur on the same optimum tungsten oxide loading on the WO_3/ZrO_2 MEL support used as that required for generation of the highest number of acid sites. This is because iron is most likely to interact better with well dispersed tungsten species compared to bulk WO_3 clusters that are formed at loadings above the optimum tungsten oxide loading.

It is the author's opinion that any improvements in the NH_3 SCR activity of the catalysts that are based on iron and tungsten oxide are actually caused by the formation of more active acid sites that are formed as a result of better Fe – W interactions. This is supported by the results in Section 6.6 where the increase in the tungsten oxide loading and the associated Fe – W interaction can be linked with an increase in the number of Fe^{3+} LAS and BAS that would account for the better SCR activity of those catalysts.

The Fe – W interaction allows the formation of the active Fe^{3+} LAS on zirconium oxide but is not necessary for the generation of Fe^{3+} LAS on H/beta zeolite. Similarly, zirconium oxide in the tetragonal phase is required for the formation of active Fe^{3+} LAS where the results in Section 6.5 have suggested that Fe^{3+} LAS do not readily form on monoclinic zirconium oxide.

The Fe/beta catalysts do not contain any tungsten oxide but exhibits good SCR activity which further supports the proposal that the acidity of the catalyst is the key parameter for good NH_3 SCR activity and not the Fe – W interactions. However, it has been reported that the SCR activity of the Fe/beta catalysts was not related to the acidity of those catalysts based on the results discussed regarding severely aged Fe/beta catalysts that were still active for NH_3 SCR despite the complete loss of acidity. Further studies on Fe/beta catalysts would have to be carried out to confirm or dispute these results. However, the results obtained in Section 6.3 indicate that the acidity of the Fe/beta catalysts can be linked to the NH_3 SCR activity of those catalysts.

The results of this PhD project strongly suggest that the NH_3 SCR activity can be linked to the formation of Fe^{3+} LAS and a small number of strong BAS. The other additional parameters such as the Fe – W interactions, synthesis procedure, and phase of the zirconium oxide support and calcination temperature are factors that will influence the generation of Fe^{3+} LAS on $Fe/WO_3/ZrO_2$ catalysts.

Iron has been identified as the key component for good NH_3 SCR activity of $Fe/WO_3/ZrO_2$ catalysts due to the generation of strong active Fe^{3+} LAS. The enhancement of the BAS strength as well as the good iron dispersion could also contribute to the SCR activity of the $Fe/WO_3/ZrO_2$ catalysts. In the following chapter, the $Fe/WO_3/ZrO_2$ catalysts were characterised with IR spectroscopy using CO as the probe molecule to investigate the iron species present on the $Fe/WO_3/ZrO_2$ catalysts.

Chapter 7:
IR characterisation of $Fe/WO_3/ZrO_2$ catalysts using CO as a probe molecule

Chapter 7: IR characterisation of $Fe/WO_3/ZrO_2$ catalysts using CO as a probe molecule

Iron was identified previously in Chapter 6 as the active metal for $Fe/WO_3/ZrO_2$ catalysts. This is in agreement with the results reported in the literature where iron has been shown to be active for NH_3 SCR of NO_x [102, 104, 106-108, 110, 153]. In order to understand further the role of Fe on $Fe/WO_3/ZrO_2$ catalysts for NH_3 SCR, carbon monoxide (CO) was used as the probe molecule in IR spectroscopy to characterise the metallic species of the $Fe/WO_3/ZrO_2$ catalysts. CO has been successfully used to investigate Fe supported on various supports along with other active metals such as platinum, palladium, nickel and copper that were used in different catalytic applications [96, 154-161].

To the author's knowledge no experiments using CO as a probe molecule have been previously reported in the literature for $Fe/WO_3/ZrO_2$ catalysts. Thus, the results of such a characterisation would be of great interest. The $Fe/WO_3/ZrO_2$ catalysts synthesised using the DKK WO_3/ZrO_2 support are referred to as $Fe/WO_3/ZrO_2$ DKK catalysts. Similarly, $Fe/WO_3/ZrO_2$ catalysts based on the MEL zirconium hydroxide are denoted as $Fe/WO_3/ZrO_2$ MEL catalysts.

7.1 IR characterisation using CO of $Fe/WO_3/ZrO_2$ catalysts

Although, $Fe/WO_3/ZrO_2$ catalysts have not been characterised previously with IR spectroscopy using CO; some characterisation work has been done on Fe/ZrO_2 catalysts [96, 113, 151] and a similar $0.5Fe/ZrO_2$ sample was synthesised and characterised to be used as a reference material for comparison with $Fe/WO_3/ZrO_2$ catalysts.

The spectrum of the reference $0.5Fe/ZrO_2$ sample shown in Fig. 7.1.1 has a major peak at 2186 cm^{-1} and a broad peak at around 2138 cm^{-1}. The spectrum is in a good agreement with those reported in the literature where the 2186 cm^{-1} peak has been assigned to CO weakly chemisorbed on Zr^{4+} sites free of water

and not covered by iron [96]. It was reported in the literature that an additional peak at 2190 cm^{-1} due to CO adsorption on a different Zr^{4+} LAS could be present. The absence of the peak at 2190 cm^{-1} would suggest that these particular Zr^{4+} LAS have been occupied by adsorbed water or iron species on the $0.5Fe/ZrO_2$ sample characterised. The second broad peak at ~ 2138 cm^{-1} is assigned to CO adsorption onto various Fe^{2+} species [96, 162].

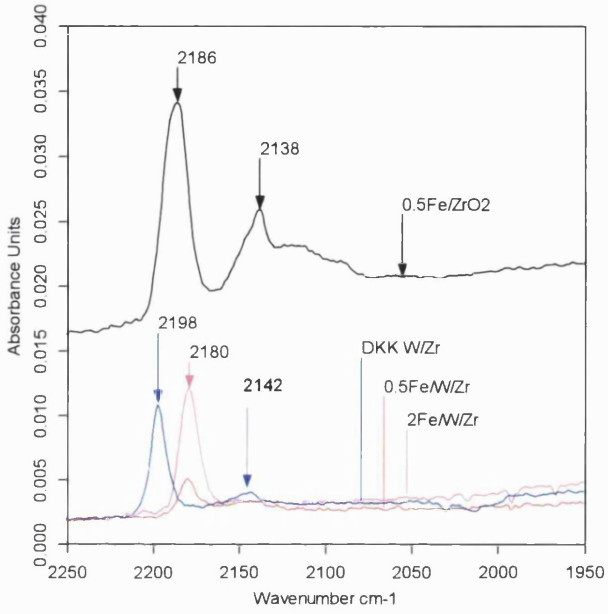

Fig. 7.1.1. IR spectra (CO region) after CO adsorption on $0.5Fe/ZrO_2$ and $Fe/WO_3/ZrO_2$ DKK catalysts containing 0, 0.5 and 2 wt% iron.

The $Fe/WO_3/ZrO_2$ catalysts containing 0, 0.5 and 2 wt% iron were characterised by IR spectroscopy after CO adsorption and the spectra are shown in Fig. 7.1.1 along with the reference $0.5Fe/ZrO_2$ sample. The WO_3/ZrO_2 DKK support has a large peak at 2198 cm^{-1} and a small peak at ~2142 cm^{-1} after CO adsorption.

No similar IR characterisation using CO as a probe molecule under the reducing conditions used in this study on WO_3/ZrO_2 have been previously carried out. CO has been used as a probe molecule to study the surface coverage and acidity of WO_3/ZrO_2 but the experiments were conducted at low temperatures around -196 °C [136, 163]. In contrast, the CO adsorption experiments in this work were

carried out at 20 °C after activating under a reducing environment with the intention to characterise the metallic function of the catalyst (iron).

The 2198 cm^{-1} peak has not been assigned in the literature but the author suggests that it is due to either CO interacting with tungsten species or with a different Zr^{4+} LAS that is formed by the presence of tungsten oxide. The minor peak at ~2142 cm^{-1} (Fig. 7.1.1) is due to CO interacting with tungsten oxide species.

A new IR peak at 2180 cm^{-1} is evident on the $Fe/WO_3/ZrO_2$ catalysts which has not been previously reported in the literature (Fig 7.1.1). The 2180 cm^{-1} peak increases in intensity with higher iron loading, indicating that the IR peak is associated with the iron component on the $Fe/WO_3/ZrO_2$ catalysts. There are several possibilities for the 2180 cm^{-1} peak assignment, mainly due to either the presence of reduced iron species or iron in a specific state due to the interaction with tungsten oxide.

There is also the lower possibility that it is linked to Zr^{4+} sites that have been influenced by the presence of nearby iron species, however, this is unlikely as the results in Chapters 5 and 6 suggests that the Zr^{4+} sites are already fully occupied by either tungsten oxide or iron.

$Fe/WO_3/Al_2O_3$ and Fe/beta catalysts were characterised by IR with CO to aid with the 2180 cm^{-1} peak assignment. If the 2180 cm^{-1} peak is due to iron interacting with tungsten oxide then it should also be present on $Fe/WO_3/Al_2O_3$ but absent from the spectrum of Fe/beta. It can be clearly seen in Fig 7.1.2, that a similar peak at 2180 cm^{-1} was present on the $Fe/WO_3/Al_2O_3$ catalyst where the peak intensity does not change with different CO concentrations.

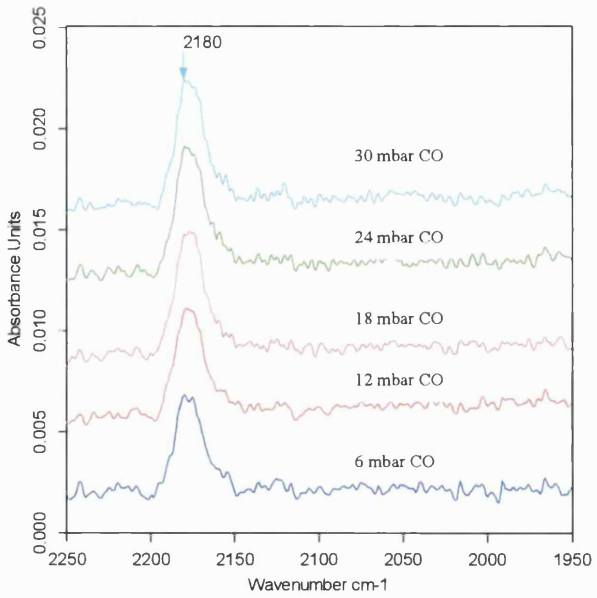

Fig. 7.1.2. IR spectra (CO region) after CO adsorption on $Fe/WO_3/Al_2O_3$ with different CO concentration.

The results of the IR characterisation of $Fe/WO_3/Al_2O_3$ supports the possibility that the new IR peak at 2180 cm^{-1} is associated with the iron species that are formed by interactions with tungsten oxide. The IR spectra of the Fe/beta sample show a different IR peak at 2188 cm^{-1} (Fig 7.1.3).

The 2188 cm^{-1} peak has a very broad base and there are 2 possible shoulders at 2200 cm^{-1} and 2176 cm^{-1}. These peaks have not been reported in the literature and are most likely due to CO interaction with a variety of different Fe groups present on Fe/beta. It is interesting to note that the same peak at 2180 cm^{-1} is present on both the iron and tungsten oxide containing catalysts which suggests that the iron species are interacting with the tungsten species. This Fe – W interaction could play an important role in the NH_3 SCR activity of the catalysts.

The $Fe/WO_3/Al_2O_3$ and $Fe/WO_3/ZrO_2$ catalysts with the same peak at 2180 cm^{-1} were both active for NH_3 SCR. However, it is interesting to note that the $0.5Fe/ZrO_2$ sample is not active for NH_3 SCR although the peak position at 2186

cm^{-1} is similar to the 2188 cm^{-1} peak present on the 0.5Fe/beta catalyst which was active (Fig. 7.1.4).

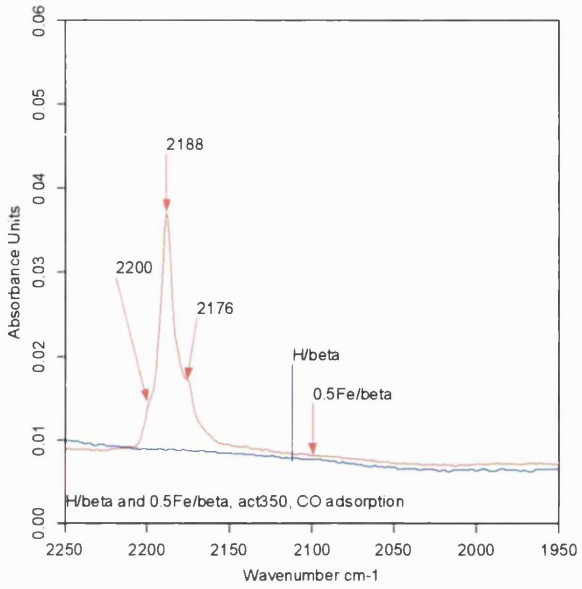

Fig. 7.1.3. IR spectra (CO region) after CO adsorption on H/beta and 0.5Fe/beta.

The 2188 cm^{-1} peak found on the 0.5Fe/beta is quite broad and has a high peak intensity when compared to the other catalysts characterised. The IR spectrum of the 0.5Fe/beta catalyst suggests that the same type of Fe species found on the Fe/ZrO_2 and $Fe/WO_3/ZrO_2$ catalyst are present on that catalyst. The shape of 2188 cm^{-1} peak and shoulder positions also suggest that there are more Fe species that are not active for NH_3 SCR present on the 0.5Fe/beta catalyst which are similar to those found on the $0.5Fe/ZrO_2$ catalyst compared to the number of Fe species that are active for NH_3 SCR seen on the $Fe/WO_3/ZrO_2$ DKK catalysts.

This could also provide an explanation as to why the high temperature activity of the 0.5Fe/beta catalyst rapidly decreases which did not occur with the other Fe/beta and $Fe/WO_3/ZrO_2$ catalysts tested (Fig. 6.3.4). Also, a similar decrease in the high temperature SCR activity was also observed on the $0.5Fe/ZrO_2$ sample (Fig. 7.1.4). The results suggest that at 0.5 wt% iron loading supported on H/beta, a large amount of iron species that are not active for NH_3 SCR similar to those present on the $0.5Fe/ZrO_2$ sample are formed in addition to the smaller

number of Fe species that are active for NH_3 SCR. It is possible that the peak at 2186 cm^{-1} can be associated with Fe species that are not active for NH_3 SCR whereas the 2180 cm^{-1} peak is linked to the catalytically active Fe species.

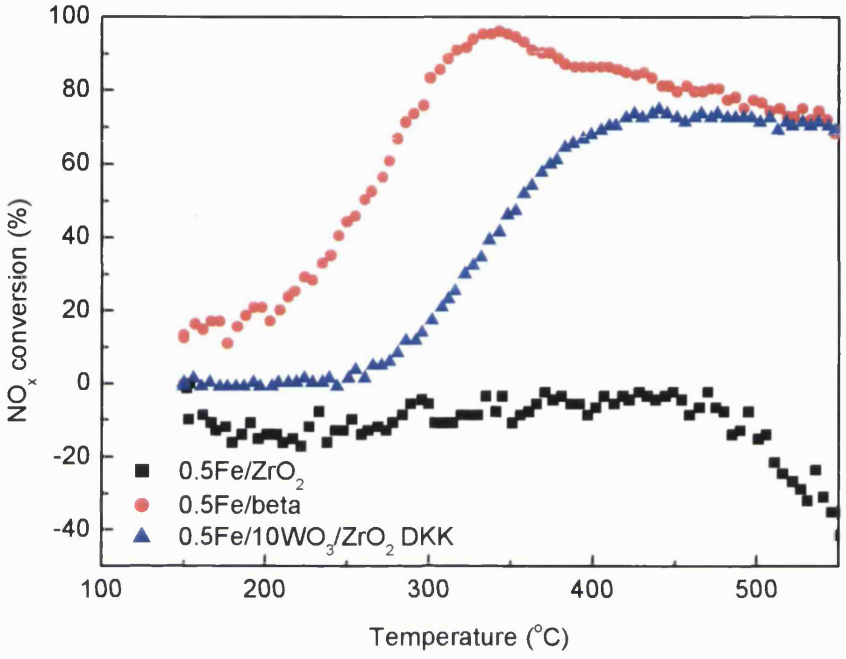

Fig. 7.1.4. Effect of temperature on NO_x conversion over $0.5Fe/ZrO_2$, 0.Fe/beta and $0.5Fe/WO_3/ZrO_2$ DKK catalysts.

7.2 Effect of iron loading on the IR spectra of $Fe/WO_3/ZrO_2$ DKK catalysts

The $Fe/WO_3/ZrO_2$ DKK catalysts containing 0.5, 1 and 2 wt% Fe were characterised using IR spectroscopy with CO as the probe molecule. This was to determine if the 2180 cm^{-1} peak intensity can be linked to the SCR activity or the acidity of the catalysts. The 2180 cm^{-1} peak intensity increases steadily with higher iron loading as expected. The peak intensity is expected to increase with iron loading due to the increased presence of Fe species and/or greater level of Fe – W interactions.

A peak at 2144 cm^{-1} was also observed on the $0.5Fe/WO_3/ZrO_2$ DKK catalyst which disappears at higher iron loadings. It was possible that a minor peak shift from 2180 to 2181 cm^{-1} occurred on the $1Fe/WO_3/ZrO_2$ catalyst. This could potentially be related to the low SCR activity of the $1Fe/WO_3/ZrO_2$ catalyst. However, it should be noted that the difference in the peak positions is within the experimental error of 4 cm^{-1} resolution of the IR spectrometer used and it has been previously suggested that the decrease in the SCR activity of $1Fe/WO_3/ZrO_2$ was related to the Broensted acidity of that catalyst (Section 6.1)

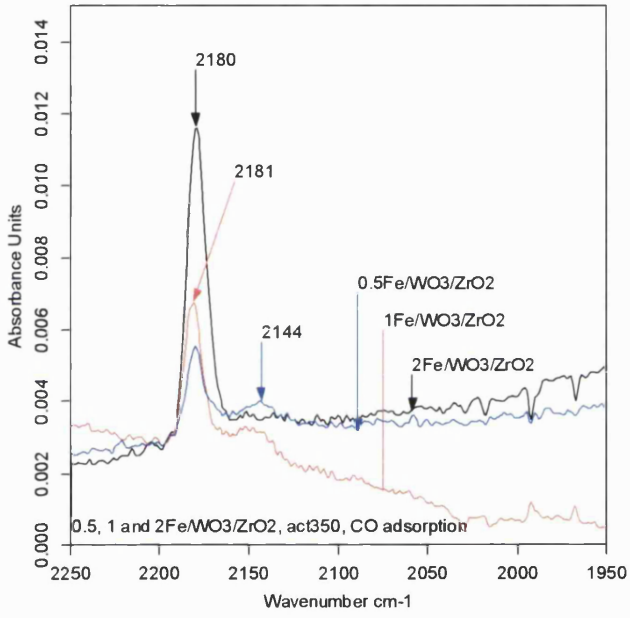

Fig. 7.2.1. IR spectra (CO region) after CO adsorption on $Fe/WO_3/ZrO_2$ DKK catalysts containing 0.5, 1 and 2 wt% iron.

It was previously suggested that the peak at 2180 cm^{-1} could be linked to the NH_3 SCR activity. To test this hypothesis, the 2180 cm^{-1} peak present on the $Fe/WO_3/ZrO_2$ DKK catalysts was integrated to obtain the peak areas which were compared to the number of LAS and the SCR activity of the $Fe/WO_3/ZrO_2$ DKK catalysts at 450 °C. The results of the comparisons are shown relative to that of $0.5Fe/WO_3/ZrO_2$ in Table 7.2.1.

There is no clear correlation between the 2180 cm^{-1} peak area and that of the SCR activity at 450 °C or the number of LAS present on $Fe/WO_3/ZrO_2$ DKK catalysts. However, there is a clear link between the numbers of LAS and the SCR activity as previously described in Chapter 6, Table 6.1.1. It should be noted that the values for the SCR activity will vary depending on the reaction temperature selected. 450 °C was chosen because the SCR activity of all the $Fe/WO_3/ZrO_2$ DKK catalysts was level at that reaction temperature.

Table 7.2.1. The relative intensities of the peak at 2180 cm^{-1} compared to the SCR activity at 450 °C and the number of LAS in $Fe/WO_3/ZrO_2$ DKK catalysts.

Catalyst	Peak area	SCR activity at 450 °C	LAS
$0.5Fe/WO_3/ZrO_2$	1.0	1.0	1.0
$1Fe/WO_3/ZrO_2$	2.2	0.74	0.9
$2Fe/WO_3/ZrO_2$	4.4	1.2	1.4

The 2180 cm^{-1} peak appears to be associated with the iron loading on the $Fe/WO_3/ZrO_2$ DKK catalysts where increasing the iron loading two-fold causes a doubling of the peak area. This is not unexpected, as the 2180 cm^{-1} peak was suggested to be due to iron interacting with tungsten oxide, and, therefore increasing the number of iron species should increase the peak intensity. It was suggested that the Fe – W interaction leads to the formation of active Fe^{3+} LAS on the $Fe/WO_3/ZrO_2$ catalysts thus this interaction could be associated with the SCR activity of those catalysts. The results in Table 7.2.1 indicate that this may not be true.

The results so far would indicate that the peak at 2180 cm^{-1} is linked to the iron species on the catalysts. However, it is still unclear whether this is due to isolated iron species or iron that is interacting with nearby tungsten species. The results obtained would suggest that it is mostly due to the latter. The tungsten oxide loading of $Fe/WO_3/ZrO_2$ catalysts was varied to examine any effects on the 2180 cm^{-1} peak.

7.3 Effect of tungsten oxide loading on the IR spectra of $Fe/WO_3/ZrO_2$ MEL catalysts after CO adsorption

The $Fe/WO_3/ZrO_2$ MEL catalysts were characterised by IR spectroscopy using CO to investigate the effect of tungsten oxide loading on the peak at 2180 cm^{-1} (Fig. 7.3.1). The CO adsorption spectra for $Fe/WO_3/ZrO_2$ MEL catalysts differ from the spectra seen previously for the $Fe/WO_3/ZrO_2$ DKK catalysts (Fig. 7.2.1). The $Fe/WO_3/ZrO_2$ MEL catalysts have two distinct peaks at 2182 cm^{-1} and at 2144 cm^{-1} instead of a single peak at 2180 cm^{-1} that was previously seen on the $Fe/WO_3/ZrO_2$ DKK catalysts.

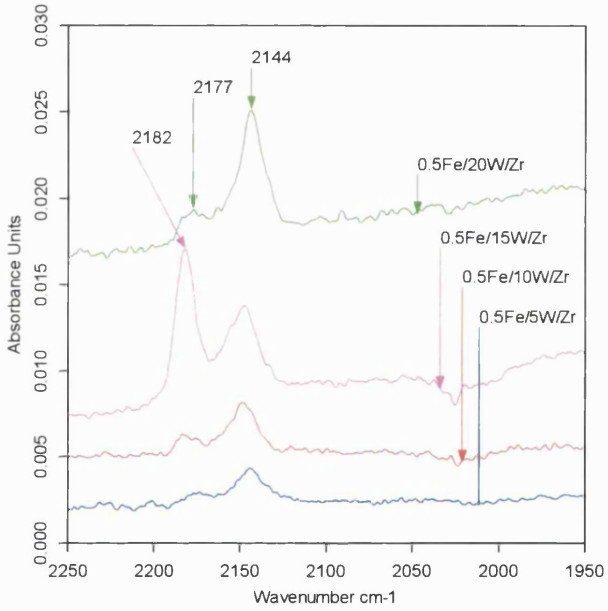

Fig. 7.3.1. IR spectra (CO region) after CO adsorption on $Fe/WO_3/ZrO_2$ MEL catalysts containing 5, 10, 15 and 20 wt% tungsten oxide.

The variation in the number of peaks observed on the $Fe/WO_3/ZrO_2$ MEL and DKK catalysts could be based on the differences in the zirconium hydroxide used. It was shown previously that the W – Zr interaction changes depending on the zirconium hydroxide support used (Chapter 5.5) which, in turn will affect the Fe – W interaction.

The 2182 cm^{-1} peak intensity rises slightly from 5 to 10 wt% tungsten oxide loading on the $Fe/WO_3/ZrO_2$ MEL catalysts. However, the 2182 cm^{-1} peak intensity increases significantly at 15 wt% tungsten oxide loading followed by a dramatic drop and a peak shift to 2177 cm^{-1} on the $0.5Fe/20WO_3/ZrO_2$ catalyst. The $0.5Fe/15WO_3/ZrO_2$ catalyst with the highest 2182 cm^{-1} peak intensity was also the most active catalyst for NH_3 SCR. The large reduction in the 2182 cm^{-1} peak intensity on the $0.5Fe/20WO_3/ZrO_2$ catalyst could be caused by the presence of bulk WO_3 species that do not interact with iron. Bulk WO_3 clusters were shown to be present on the $20WO_3/ZrO_2$ MEL support based on the XRD characterisation results in Chapter 5, Fig 5.2.6.

The 2144 cm^{-1} peak appears to be associated with tungsten species where the peak intensity increases steadily with higher tungsten oxide loading. This peak was also observed on the $0.5Fe/WO_3/ZrO_2$ DKK catalyst but was not present at higher iron loadings. It is not known why this occurs but it could be suggested that both the ~2180 cm^{-1} and 2144 cm^{-1} peaks are due to different Fe – W interactions. The tungsten oxide loading on the $0.5Fe/WO_3/ZrO_2$ DKK catalyst did not change but the iron loading did. Iron may be preferentially interacting with the specific tungsten species that leads to the formation of the peak at 2180 cm^{-1} therefore reducing the 2144 cm^{-1} peak intensity at higher Fe loading.

On the other hand, with the $Fe/WO_3/ZrO_2$ MEL catalysts, iron interacts first with tungsten species that generates the peak at 2144 cm^{-1}. This would explain why in Fig 7.3.1, the 2144 cm^{-1} peak intensity increases steadily with tungsten oxide loading but the 2182 cm^{-1} peak only increases slightly from 5 to 10 wt% tungsten oxide. At lower tungsten oxide loading, tungsten oxide exists mainly as isolated WO_x clusters however; at 15 wt% tungsten oxide loading the WO_3/ZrO_2 MEL support is saturated with tungsten oxide, increasing the tungsten oxide surface coverage.

Iron is now able to interact with more nearby tungsten species on the $15WO_3/ZrO_2$ support therefore increasing the 2182 cm^{-1} peak intensity. At 20 wt% tungsten oxide loading where bulk WO_3 clusters have formed, the surface

coverage of tungsten oxide will decrease thus causing the observed reduction in the 2182 cm^{-1} peak intensity.

The intensities of both peaks at 2182 cm^{-1} and 2144 cm^{-1} on the $Fe/WO_3/ZrO_2$ MEL catalysts were integrated and compared to the NH_3 SCR activity. Table 7.3.1 shows the 2182 cm^{-1} and 2144 cm^{-1} peak areas, SCR activity at 450 °C and the number of LAS present on the $Fe/WO_3/ZrO_2$ MEL catalysts relative to that of the $0.5Fe/5WO_3/ZrO_2$ catalyst. The results in Table 7.3.1 indicate that there is a possible correlation between the number of LAS and the SCR activity of the catalysts at 450 °C as previously described in Chapter 6, Table 6.6.1.

Similar to the results obtained with the $Fe/WO_3/ZrO_2$ DKK catalysts (Table 7.2.1), no clear links can be made between the 2182 cm^{-1} and 2144 cm^{-1} peak areas with the SCR activity of the $Fe/WO_3/ZrO_2$ MEL catalysts. However, it is possible that there may be positive correlation between the peak intensity and the SCR activity. The peak intensities increase and decrease with the SCR activity for both the $Fe/WO_3/ZrO_2$ MEL and DKK catalysts with the exception of the $1Fe/WO_3/ZrO_2$ DKK catalyst (Tables 7.2.1 and 7.3.1). Additional data points would be required to determine if a correlation exists between the peak areas and the NH_3 SCR activity of $Fe/WO_3/ZrO_2$ catalysts.

The lower SCR activity of the $1Fe/WO_3/ZrO_2$ was suggested to be attributed to a decrease in the number and strength of the BAS present. The Broensted acidity is unlikely to influence the Fe – W interaction and, therefore, will have no impact on the 2180 cm^{-1} peak intensity. The cause of the change in the Broensted acidity is not known but it can be suggested to be based on changes to the tungsten oxide species that generate the BAS.

Table 7.3.1. The relative intensities of the peaks at 2182 cm^{-1} and 2144 cm^{-1} compared to the SCR activity at 450 °C and the number of LAS in $Fe/WO_3/ZrO_2$ MEL catalysts.

Catalyst	Total Peak areas	SCR activity at 450 °C	Relative no. of LAS
$0.5Fe/5WO_3/ZrO_2$	1.0	1.0	1.0
$0.5Fe/10WO_3/ZrO_2$	2.2	1.6	1.6
$0.5Fe/15WO_3/ZrO_2$	10.3	2.7	3.0
$0.5Fe/20WO_3/ZrO_2$	7.6	2.5	2.2

7.4 Effect of calcination temperature of the tungsten oxide supported on zirconia support of the $Fe/WO_3/ZrO_2$ MEL catalysts on the IR spectra after CO adsorption

The $0.5Fe/15WO_3/ZrO_2$ MEL catalyst, where the WO_3/ZrO_2 support was calcined at 590 °C and 830 °C, was characterised by IR spectroscopy with CO to investigate the effect of the calcination temperature on the CO adsorption peaks. The calcination temperature of the WO_3/ZrO_2 support will have an effect on the state and level of tungsten oxide coverage on the zirconium oxide support. The differences in the IR spectra of the two $Fe/WO_3/ZrO_2$ catalysts where the WO_3/ZrO_2 supports have been calcined at 590 °C and 830 °C could aid in the CO adsorption peak assignments.

Fig. 7.4.1 demonstrates that when the WO_3/ZrO_2 support of the $0.5Fe/15WO_3/ZrO_2$ MEL catalyst was calcined at 590 °C, only a single peak at 2182 cm^{-1} can be seen after the CO adsorption experiment. However, when the WO_3/ZrO_2 support was calcined to the optimum 830 °C, a new peak at 2144 cm^{-1} appears. This suggests that the peaks may be associated with Fe – W interactions that are strongly affected by the state of tungsten oxide on the $Fe/WO_3/ZrO_2$ catalyst.

At the calcination temperature of 590 °C, some tungsten oxide is still present in the bulk rather than at the surface of the catalyst, therefore there are less W – Zr interactions and zirconium oxide remained primarily in the monoclinic phase. On the other hand, when the WO_3/ZrO_2 support was calcined at 830 °C, tungsten oxide diffuses to the surface and interacts strongly with any available zirconium sites stabilising zirconium oxide in the tetragonal phase. Iron should be able to interact better with the well dispersed tungsten oxide on the surface of the support calcined at 830 °C in comparison to the support calcined at 590 °C.

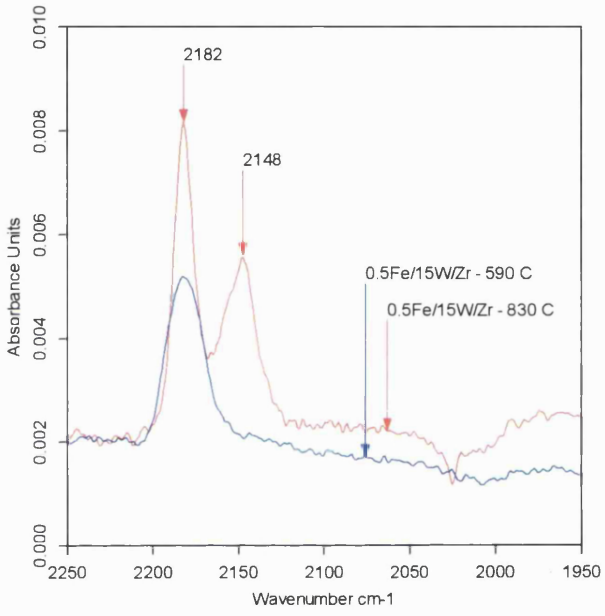

Fig. 7.4.1. IR spectra (CO region) after CO adsorption on $0.5Fe/15WO_3/ZrO_2$ MEL catalysts where the WO_3/ZrO_2 has been calcined at 590 °C or 830 °C.

The 2182 cm^{-1} peak on the $Fe/WO_3/ZrO_2$ catalyst with the WO_3/ZrO_2 support calcined at 590 °C is much broader in comparison to the peak found on the catalyst where the support was calcined at 830 °C, which has a sharp peak at 2182 cm^{-1}. This suggests a broader range of non-specific Fe – W interactions on the $Fe/WO_3/ZrO_2$ when the support was calcined at 590 °C.

Furthermore, the increased Fe – W interactions on the $Fe/WO_3/ZrO_2$ catalyst where the support was calcined at 830 °C leads to the formation of the 2144 cm^{-1}

peak and the increase in the 2182 cm^{-1} peak intensity. It is also possible that the 2144 cm^{-1} peak can be associated with the structure of the zirconium oxide, whether zirconium oxide is present in the monoclinic or tetragonal phase. This was the major difference between the $Fe/WO_3/ZrO_2$ MEL catalysts when the calcination temperature of the WO_3/ZrO_2 support was increased from 590 °C to 830 °C.

The changes in the tungsten oxide loading would also lead to variations in the level of tetragonal zirconium oxide present on the $Fe/WO_3/ZrO_2$ catalysts which in turn will affect the 2182 cm^{-1} and 2144 cm^{-1} peak intensities (Fig. 7.3.1). However, this is unlikely to have a significant impact based on the XRD results of 15 and 20 wt% WO_3/ZrO_2 MEL supports where similar levels of tetragonal zirconium oxide were present for both supports seen previously in Chapter 5, Fig. 5.2.4.

7.5 Comparison of the IR spectra after CO adsorption of $0.5Fe/ZrO_2$, $Fe/WO_3/ZrO_2$ DKK and MEL catalysts

The $Fe/WO_3/ZrO_2$ DKK and MEL catalysts were characterised by IR spectroscopy using CO with $0.5Fe/ZrO_2$ as a reference sample. The spectra of the three catalysts after CO adsorption experiments are compared in Fig 7.5.1. The distinctive peaks at ~2180 cm^{-1} and ~2148 cm^{-1} described previously due to CO adsorption can be clearly seen on all three catalysts. CO was evacuated at room temperature for 15 minutes then the spectra were collected to determine the strength of the CO interactions.

On the Fe/ZrO_2, no CO remains adsorbed on the catalyst after evacuation which suggests there is only weak Fe – CO interactions. The peak at ~2182 cm^{-1} is also no longer present after CO evacuation on the $Fe/WO_3/ZrO_2$ MEL and DKK catalysts. However, the peak at ~2148 cm^{-1} is still visible on the $Fe/WO_3/ZrO_2$ MEL catalysts although the peak intensity has been greatly reduced which indicates a stronger CO interaction than in the case with the peak at 2182 cm^{-1}.

It is interesting to note that the 2148 cm^{-1} peak intensity is much higher but the 2180 / 2184 cm^{-1} peak intensity is significantly lower on the $0.5Fe/10WO_3/ZrO_2$ MEL catalyst compared to the $0.5Fe/10WO_3/ZrO_2$ DKK catalyst. Furthermore, it can be clearly seen in Fig. 7.5.2 that the $0.5Fe/10WO_3/ZrO_2$ MEL catalyst was less active for NH_3 SCR compared to the $0.5Fe/10WO_3/ZrO_2$ DKK catalyst.

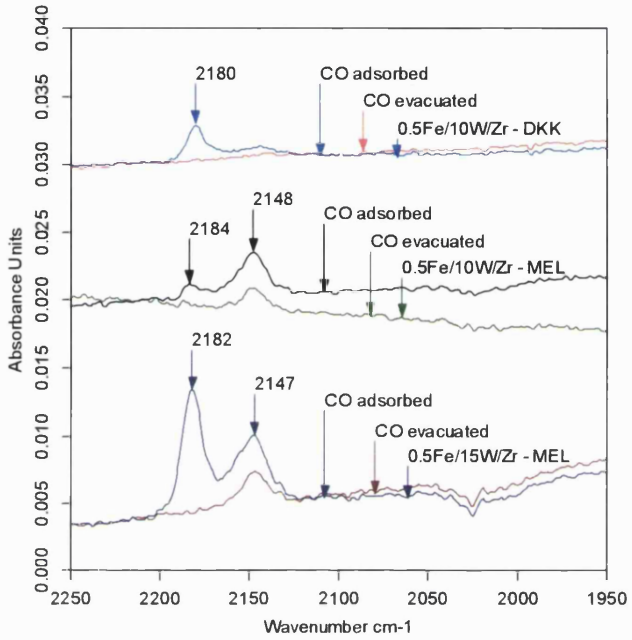

Fig. 7.5.1. IR spectra (CO region) after CO adsorption and after CO evacuation of $0.5Fe/ZrO_2$, $0.5Fe/WO_3/ZrO_2$ DKK and MEL catalysts.

Comparing the acidity of the catalysts in Table 7.5.1, it was shown that the $0.5Fe/10WO_3/ZrO_2$ DKK catalyst has a lower number of LAS but 50 % more BAS compared to the $0.5Fe/10WO_3/ZrO_2$ MEL catalyst. This can be correlated to the better high temperature SCR activity of the DKK catalyst over the MEL catalyst as it has been previously suggested that the number of BAS was associated with the high temperature SCR activity. The better low temperature SCR activity of the $0.5Fe/10WO_3/ZrO_2$ MEL catalyst can be attributed to the higher numbers of Fe^{3+} LAS.

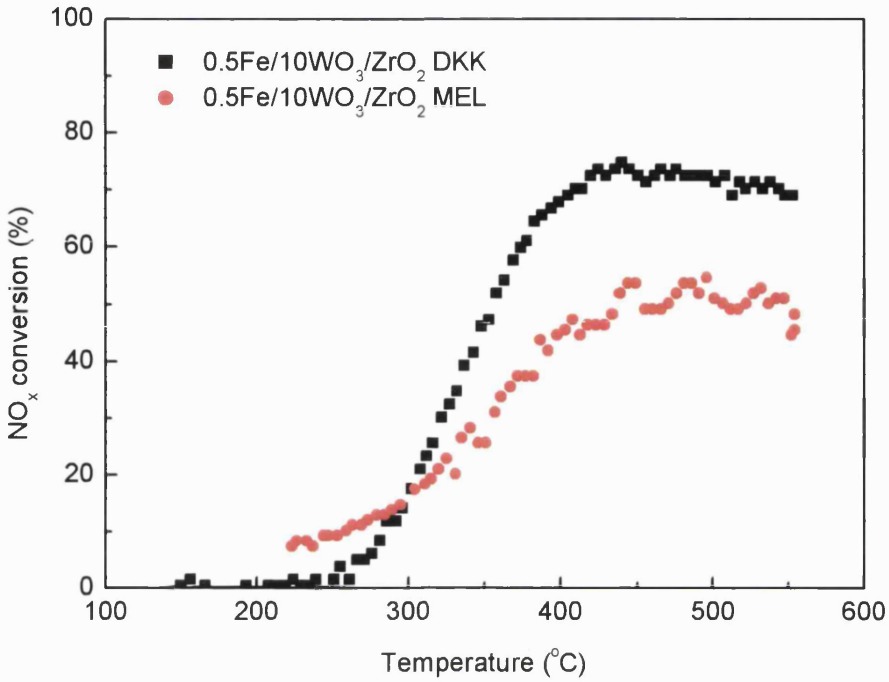

Fig. 7.5.2. Effect of temperature on NO_x conversion over $0.5Fe/10WO_3/ZrO_2$ DKK and MEL catalysts.

Table 7.5.1. Acidity measurements for $0.5Fe/WO_3/ZrO_2$ DKK and MEL catalysts.

Catalyst	DKK	MEL
BAS + LAS (μmol/g)	34	34
Ratio (LAS/BAS)	0.9	1.8
LAS (μmol/g)	16	22
BAS (μmol/g)	18	12

The error is estimated to be up to 10% based on the characterisation results of other samples carried out in this thesis.

7.6 Summary

The IR characterisation of the $Fe/WO_3/ZrO_2$ catalysts using CO as a probe molecule produced the following results. The major discovery was the presence of the two peaks at ~2180 / 2182 cm^{-1} and 2148 cm^{-1} in the IR spectra of the $Fe/WO_3/ZrO_2$ catalysts. The 2148 cm^{-1} peak is suggested to be associated with the interaction of the CO probe molecule with tungsten oxide species present on the catalysts. This was based on the results obtained by investigating the effect of tungsten oxide loading and the calcination temperature of $Fe/WO_3/ZrO_2$ MEL catalysts on the IR peaks after CO adsorption.

The peak at ~2180 / 2182 cm^{-1} was suggested to be associated with iron species present on the $Fe/WO_3/ZrO_2$ catalysts. A similar peak at 2180 cm^{-1} was shown to be also present on the $Fe/WO_3/Al_2O_3$ catalyst. This potentially indicates similar Fe species are present on $Fe/WO_3/ZrO_2$ and $Fe/WO_3/Al_2O_3$ catalysts which could possibly be linked to the presence of tungsten oxide species on the two different mixed oxide supports.

On the other hand, a different peak at 2188 cm^{-1} was seen on the Fe/beta catalyst. This difference could be due to the differences between iron species supported on mixed oxides supports ($Fe/WO_3/ZrO_2$ and $Fe/WO_3/Al_2O_3$) compared to zeolites (Fe/beta). However, it should be noted that a similar peak at 2186 cm^{-1} was also observed on the $0.5Fe/ZrO_2$ reference sample which is not a zeolite support.

The IR peaks at ~2180 cm^{-1} and 2148 cm^{-1} was suggested to be associated with Fe species present on the $Fe/WO_3/ZrO_2$ catalysts which may be linked to the NH_3 SCR activity of the catalysts. Therefore, the number of Fe^{3+} LAS and the SCR activity of the $Fe/WO_3/ZrO_2$ catalysts were compared to the ~2180 cm^{-1} and 2148 cm^{-1} peak intensities in Table 7.5.1 where no clear correlation was found. Additional infrared characterisation experiments with CO as a probe molecule would have to be carried out in order develop the suggestions made and draw any further conclusions.

Chapter 8:
Concluding remarks

Chapter 8: Concluding remarks

Several important conclusions can be drawn from the results and discussions presented in this thesis and these have been separated into 2 sections: (i) tungsten oxide supported on zirconia support and (ii) iron promoted tungsten oxide supported on zirconia catalysts for NH_3 SCR of NO_x.

8.1 Tungsten oxide supported on zirconia catalytic support

1. Tungsten oxide supported on zirconia (WO_3/ZrO_2) has been shown to be an acidic and thermally stable mixed oxide catalytic support based on comparisons with other acidic mixed oxide supports.

2. The WO_3/ZrO_2 support was shown to be stable at the calcination temperature of 830 °C but not at the temperatures above 890 °C.

3. The zirconium hydroxide precursor used in the synthesis of WO_3/ZrO_2 supports strongly affects the final properties of the support. The two main areas affected by the choice of the zirconium hydroxide precursor are the optimum/saturation tungsten oxide loading and the number of zirconium adsorption sites available for the formation of Broensted acid sites.

4. The optimum calcination temperature is dependent on the level of tungsten oxide saturation of the zirconium hydroxide precursor. Higher calcination temperatures can be used at low tungsten oxide coverage, whereas low calcination temperatures have to be used for over-saturated WO_3/ZrO_2 supports to prevent formation of bulk WO_3 clusters and loss of acidity.

5. The calcination temperature of the WO_3/ZrO_2 support affects the number of Lewis acid sites present but the number of Broensted acid sites remains constant.

6. The acidic properties, numbers of LAS and BAS and the ratio of LAS to BAS of the WO_3/ZrO_2 supports can be changed to suit the required specification by altering the zirconium hydroxide precursor, tungsten oxide loading and calcination temperature.

7. The results demonstrate that WO_3/ZrO_2 is a versatile catalytic support that could potentially be tailored for use in a wide variety of applications.

8.2 $Fe/WO_3/ZrO_2$ catalysts for NH_3 SCR of NO_x

1. $Fe/WO_3/ZrO_2$ catalysts have been shown to be active in NH_3 SCR of NO_x with catalytic activity comparable to the reference Fe/beta catalyst. Furthermore, $Fe/WO_3/ZrO_2$ catalysts have demonstrated good hydrothermal resistance which is a problem encountered by other promising NH_3 SCR catalysts.

2. The NH_3 SCR activity of the $Fe/WO_3/ZrO_2$ catalysts was suggested to be associated with the number of Fe^{3+} LAS that are formed after impregnating the WO_3/ZrO_2 support with iron. The number of Fe^{3+} LAS was the key factor in determining the NH_3 SCR activity of the catalysts although several other factors may also be important. A similar correlation was also found for the Fe/beta catalysts.

3. The reduction in the SCR activity of the $Fe/WO_3/ZrO_2$ catalysts after aging at 700 °C in 10 % steam for 65 hours could be linked to the loss of Fe^{3+} LAS and BAS.

4. The Broensted acidity of the $Fe/WO_3/ZrO_2$ catalysts was also suggsted to influence the high temperature activity of the catalysts where a small

number of strong BAS are required for good NH_3 SCR activity. If there is a reduction in the number of strong BAS, the SCR activity of that catalyst will decrease. However, any additional increase in the number of and/or strength of the BAS does not improve the SCR activity.

5. The zirconium oxide has to be stabilised by tungsten oxide in the tetragonal phase by calcination at high temperatures before iron impregnation in order to synthesise an active catalyst for NH_3 SCR.

6. The presence of iron oxide and tungsten oxide interactions were detected by IR spectroscopy using CO as a probe molecule. The peaks at ~2180 and ~2148 cm^{-1} in the IR spectra after CO adsorption are suggested to be associated with Fe species interacting with tungsten oxide that are active for NH_3 SCR.

7. Although no clear links between the Fe – W interactions could be made with the NH_3 SCR activity, it is possible that there is a positive correlation between the Fe – W interaction and NH_3 SCR activity.

8. It is the author's opinion that additional factors such as the dispersion of iron and tungsten oxide, the level of Fe – W interactions, enhancement of the acid site strength and the stabilisation of the zirconium oxide in the tetragonal phase are not directly linked to the NH_3 SCR activity but contribute to the formation of Fe^{3+} LAS that are active for NH_3 SCR.

Chapter 9: Recommendations for future work

Chapter 9: Recommendations for future Work

This PhD thesis has shown that WO_3/ZrO_2 is a promising catalytic support and iron promoted tungsten oxide supported on zirconia is an active and stable catalyst for NH_3 SCR of NO_x. There are still many points of interest and scope for improvement and development of the WO_3/ZrO_2 support and $Fe/WO_3/ZrO_2$ catalyst that are outlined in the following two sections (9.1 and 9.2)

9.1 Tungsten oxide supported on zirconia support

The tungsten oxide supported on zirconia support was described in Chapter 4 as being thermally stable and exhibited high numbers of total acid sites in comparison to other mixed oxide supports. Based on the results, the following areas would be of interest for further studies.

9.1.1 Synthesis method

The WO_3/ZrO_2 supports were synthesised by incipient wetness impregnation, however, there have been reports in the literature regarding synthesis by co-precipitation that generated promising results. Theoretically, co-precipitation synthesis procedure should form WO_3/ZrO_2 support with more homogenous distribution of tungsten oxide on zirconia. The co-precipitation technique was tried in the CARE laboratory, University of Bath with the aid of the industrial sponsor but achieved limited success.

The synthesis procedure is complicated due to the similar pH at which tungsten salt and zirconium oxide precipitate out. WO_3/ZrO_2 supports synthesised by co-precipitation should exhibit higher numbers of acid sites in comparison to those prepared by incipient wetness impregnation. The co-precipitation technique may be successful given expert instruction and resources to investigate it further.

9.1.2 Synthesis precursors

The results in Chapter 4 have shown that the zirconium hydroxide precursor used in the synthesis of the WO_3/ZrO_2 support directly influences the number of acid sites formed and, in particular, the number of Broensted acid sites. Different zirconium hydroxide precursors should be tested to select the most suitable zirconium hydroxide for the desired application of the WO_3/ZrO_2 support.

The zirconium hydroxide precursor would also be of interest to identify the properties that create suitable adsorption sites for the formation of BAS and LAS. There are additional factors that are affected by the zirconium hydroxide precursor used that could influence the final properties of the WO_3/ZrO_2 support such as the surface area and pore size distribution. The properties of the zirconium hydroxide precursor can be changed by altering the pH and synthesis conditions used.

The tungsten salt used to synthesise the WO_3/ZrO_2 support could also play an important role that affects the distribution of tungsten species on the WO_3/ZrO_2 support. It would be interesting to investigate the differences in the acidic and structural properties of WO_3/ZrO_2 synthesised from the ammonium metatungstate salt (used in this project) compared to other different tungsten oxide precursors such as tungstic and tungstophosphoric acid.

9.1.3 Additional dopants

The tungsten oxide supported on zirconia could be improved through the use of small amounts of another dopant. For example, alumina and/or silica could be used to increase the surface area of the tungsten zirconia support. Lanthanide oxides such as cerium oxide or yttrium oxide have the potential to further increase the thermal stability of the tungsten oxide supported on zirconia support. The lanthanides remain in the bulk and stabilise zirconium oxide and, therefore, will not influence or interfere with any dopants/active metals present on the surface of the support/catalyst. However, it is important that any additional

dopants do not interfere with the W – Zr interaction or Fe – W interactions on the $Fe/WO_3/ZrO_2$ catalysts.

9.2 $Fe/WO_3/ZrO_2$ catalysts

The $Fe/WO_3/ZrO_2$ catalysts are active and stable for the selective catalytic reduction of nitrogen oxides, NH_3 SCR of NO_x. This section outlines recommendations for further study on the $Fe/WO_3/ZrO_2$ catalysts and other catalysts/areas that would improve the understanding of the catalyst requirements for the NH_3 SCR of NO_x reaction.

9.2.1 Additional characterisation

Additional characterisation of the $Fe/WO_3/ZrO_2$ catalysts would be beneficial in deepening the understanding of the catalysts and, in particular, the iron species. EPR and XPS could be used to better identify the oxidation state of the iron and tungsten species.

Nitrogen (II) oxide (NO) chemisorption could be used to provide an indication of the number of accessible iron species present on the catalysts. NO chemisorption could help support the results generated by infrared spectroscopy with CO adsorption experiments in identifying and quantifying the number of active Fe sites.

Similarly, Raman spectroscopy could be a useful tool in identifying the state of tungsten species. The changes to the tungsten species could be examined by characterising a series of catalysts with different tungsten oxide loading, different zirconium hydroxide supports and calcination temperatures.

Temperature programmed reduction (TPR) can potentially be used to help determine the presence and strength of Fe – Zr and/or Fe – W interactions. The peaks in the TPR profiles could be assigned to either Fe – Zr interactions or Fe – W interactions by characterising catalysts that have been synthesised in different methods and Fe/ZrO_2. Catalysts that were synthesised by iron impregnation on

zirconium oxide before introducing tungsten should have more Fe – Zr interactions than catalysts synthesised by impregnating iron onto calcined tungsten oxide supported on zirconia.

9.2.2 NO and NH_3 adsorption

NO and NH_3 adsorption studies on $Fe/WO_3/ZrO_2$ catalysts can be used to help understand the NH_3 SCR reaction mechanism over $Fe/WO_3/ZrO_2$ catalysts. DRIFT studies of low temperature adsorption experiments of NO and NH_3 could identify the adsorption sites present on the $Fe/WO_3/ZrO_2$ catalysts. In particular, whether both the NO and NH_3 species have to adsorb onto the surface of $Fe/WO_3/ZrO_2$ therefore two different adsorption sites are required (Eley – Rideal type mechanism) or if NO remains in the gaseous phase.

However, the experimental setup and conditions would be challenging to prevent gaseous NO and NH_3 from reacting and rapidly condensing which will block the pipelines and the experimental apparatus. It may also be possible to identify weak acid sites through NH_3 adsorption that may be important for the NH_3 SCR reaction. However, these results are likely to be complicated and difficult to accurately interpret.

9.2.3 Characterisation of Fe/beta aged catalysts

Although Fe/beta catalysts are not directly related to the $Fe/WO_3/ZrO_2$ catalysts, it would be interesting to characterise the aged Fe/beta catalysts to investigate the acidity of the catalysts and how it is linked to the SCR activity of the catalysts. This would aid in the understanding of how the NH_3 SCR reaction proceeds on Fe-based catalysts, including understanding of the differences between the mechanisms for Fe supported on zeolitic supports or supported on metal/mixed oxides

9.2.4 $Fe/WO_3/Al_2O_3$ catalysts

Similarly, a more detailed analysis of the $Fe/WO_3/Al_2O_3$ catalyst would be of interest, in particular, to examine the Fe – W interaction as similar interactions were found to be present on $Fe/WO_3/ZrO_2$ catalysts. This will determine the importance of the Fe – W interaction and whether the support (zirconium oxide and/or alumina silica) plays an important role. It is possible that impregnating any metal oxide with Fe and WO_x may create an active SCR catalyst. This would also help to determine if Fe and/or WO_x have to interact with the support or not.

9.2.5 Iron precursors

The iron precursor used can potentially have a significant impact on the properties of the $Fe/WO_3/ZrO_2$ catalysts. It may be possible to achieve better distribution of Fe species on the catalysts through the use of complex salts such as ammonium iron (III) citrate or EDTA.

In addition, it may be possible to co-impregnate zirconium oxide with iron and tungsten oxide. This was tried with little success in the CARE laboratory, University of Bath however, it is the author's opinion that further studies should be carried out to fully explore the possibility of a co-impregnation synthesis of $Fe/WO_3/ZrO_2$ catalysts. This may create better iron – zirconia interactions that would improve the low temperature SCR activity of the $Fe/WO_3/ZrO_2$ catalysts although a reduction in the overall SCR activity may occur similar to the results seen in Chapter 5. However, the decrease in the SCR activity should be lower for co-impregnated catalysts.

References

References

1. Arata, K., Advances in catalysis 37 (1990) p. 165.
2. Yamaguchi, T., Applied Catalysis 61 (1990) p. 1.
3. MEL Chemicals http://www.zrchem.com. 2004.
4. Dooley, K.M. and Gates, B.C., Journal of Catalysis 96 (1985) p. 347.
5. Ono, Y., Tanabe, T., and Kitajima, N., Journal of Catalysis 56 (1979) p. 47.
6. Ono, Y., Yamaguchi, K., and Kitajima, N., Journal of Catalysis 64 (1980) p. 13.
7. Yamaguchi, T., Jin, T., and Tanabe, K., Journal of Physical Chemistry 90 (1985) p. 3148.
8. Jin, T., Yamaguchi, T., and Tanabe, K., Journal of Physical Chemistry 90 (1986) p. 4794.
9. Oudar, J., Catalysis Reviews - Science and Engineering 22 (1980) p. 171.
10. Olah, G.A., Prakash, G.K.S., and Sommer, J., *Superacids*. 1985, New York: Wiley.
11. Arata, K., Sato, K., and Toyoshima, I., Journal of Catalysis 42 (1976) p. 221.
12. Kayo, A., Yamaguchi, T., and Tanabe, K., Journal of Catalysis 83 (1983) p. 99.
13. Sohn, J.R. and Jang, H.J., Journal of Molecular Catalysis 64 (1991) p. 349.
14. Sano, T., Ikeya, H., Kasuno, T., Wang, Z.B., Kawakami, Y., and Soga, K., Zeolites 19 (1997) p. 80.
15. Sano, T., Yamashita, N., Iwami, Y., Takeda, K., and Kawakami, Y., Zeolites 16 (1996) p. 258.
16. Wang, Q.L., Giannetto, G., Torrealba, M., Perot, G., Kappenstein, C., and Guisnet, M., Journal of Catalysis 130 (1991) p. 459.
17. Handy, B.E., Baiker, A., Schraml-Marth, M., and Wokaun, A., Journal of Catalysis 133 (1992) p. 1.
18. Itoh, M., Hattori, H., and Tanabe, K., Journal of Catalysis 35 (1974) p. 225.
19. Sohn, J.R. and Jang, H.J., Journal of Catalysis 132 (1991) p. 563.
20. Coudurier, G. and Vedrine, J.C., Catalysis Today 56 (2000) p. 415.
21. Tanabe, K., Catalysis : science and technology, edited by Anderson, J.R. and Boudart, M. Editor. 1981. p. 269.
22. Tanabe, K., Misono, M., Ono, Y., Hattori, H., and Maier, W.F., Angewandte Chemie (International Edition in English) 30 (1991) p. 720.
23. Tanabe, K., Catalysis : science and technology, edited by Anderson, J.R and Boudart, M. 1981. p. 231.
24. Atkins, P.W., Physical Chemistry. 6th ed. 1998: Oxford University Press.
25. Harris, D.C., Quantitative chemical analysis. 2nd ed. 1987, New York: W.H. Freeman and Company.
26. Ali, A., Chin, Y.-H., and Resasco, D.E., Catalysis Letters 56 (1998) p. 111.
27. Armendariz, H., Sanchez Sierra, C., Figueras, F., Coq, B., Mirodatos, C., Lefebvre, F., and Tichit, D., Journal of Catalysis 171 (1997) p. 85.

28. Farcasiu, D. and Dan, H., Catalysis Letters 53 (1998) p. 3.
29. Ji, W., Hu, J., and Chen, Y., Catalysis Letters 53 (1998) p. 15.
30. Parry, E.P., Journal of Catalysis 2 (1963) p. 371.
31. Xu, B., Yamaguchi, T., and Tanabe, K., Chemistry Letters (1988) p. 281.
32. Tanabe, K., Materials Chemistry and Physics 13 (1985) p. 347.
33. Yamaguchi, T., Catalysis Today 20 (1994) p. 199.
34. Tanabe, K. and Yamaguchi, T., Catalysis Today 20 (1994) p. 185.
35. Davis, B.H., Keogh, R.A., and Srinivasan, R., Catalysis Today 20 (1994) p. 219.
36. Nakano, Y., Iizuka, T., Hattori, H., and Tanabe, K., Journal of Catalysis 57 (1979) p. 1.
37. Amenomiya, Y., Applied Catalysis 30 (1987) p. 57.
38. Suh, Y.W., Moon, S.H., and Rhee, H.K., Catalysis Today 63 (2000) p. 447.
39. Suh, Y.W., Lee, J.W., and Rhee, H.-K., Catalysis Letters 90 (2003) p. 103.
40. Davis, B.H. and Ganesan, P., Industrial and Engineering Chemistry Product Research and Development 18 (1979) p. 191.
41. Yokoyama, T., Setoyama, T., Fujita, N., Nakajima, M., Maki, T., and Fujii, K., Applied Catalysis A: General 88 (1992) p. 149.
42. Pan, L.S. and Horibe, S., Journal of Materials Science 31 (1996) p. 6523.
43. Srinivasan, R., Hubbard, C.R., Cavin, B., and Davis, B.H., Chemistry of materials 5 (1993) p. 27.
44. Labaki, M., Lamonier, J.F., Siffert, S., Zhilinskaya, E.A., and Aboukais, A., Colloids and Surfaces A: Physicochemical and Engineering Aspects 227 (2003) p. 63.
45. Garvie, R.C., Journal of Physical Chemistry 69 (1965) p. 1238.
46. Normair, C.J., Goulding, P.A., and McAlpine, I., Catalysis Today 20 (1994) p. 313.
47. Garvie, R.C. and Goss, M.F., Journal of Materials Science 21 (1986) p. 1253.
48. Matta, J., Lamonier, J.-F., Abi-Aad, E., Zhilinskaya, E.A., and Aboukaïs, A., Physical Chemistry Chemical Physics 1 (1999) p. 4975.
49. Niemantsverdriet, J.W., Spectroscopy in Catalysis: An Introduction. 1993: Wiley, John & Sons, Incorporated.
50. Markaryan, G.L., Ikryannikova, L.N., Muravieva, G.P., Turakulova, A.O., Kostyuk, B.G., Lunina, E.V., Lunin, V.V., Zhilinskaya, E., and Aboukais, A., Colloids and Surfaces A: Physicochemical and Engineering Aspects 151 (1999) p. 435.
51. Mercera, P.D.L., van Ommen, J.G., Doesburg, E.B.M., Burggraaf, A.J., and Ross, J.R.H., Applied Catalysis 71 (1991) p. 363.
52. Morterra, C., Cerrato, G., Emanuel, C., and Bolis, V., Journal of Catalysis 142 (1993) p. 349.
53. Kytokivi, A., Lakomaa, E.-L., Root, A., Osterholm, H., Jacobs, J.-P., and Brongersma, H.H., Langmuir 13 (1997) p. 2717.
54. Dang, Z., Anderson, B.G., Amenomiya, Y., and Morrow, B.A., Journal of Physical Chemistry 99 (1995) p. 14437.
55. Lopez, T., Navarrete, J., Gomez, R., Novaro, O., Figueras, F., and Armendariz, H., Applied Catalysis A: General 125 (1995) p. 217.

56. Damyanova, S., Grange, P., and Delmon, B., Journal of Catalysis 168 (1997) p. 421.
57. Mastikhin, V.M., Terskikh, V.V., Lapina, O.B., Filimonova, S.V., Seidl, M., and Knozinger, H., Solid State Nuclear Magnetic Resonance 4 (1995) p. 369.
58. Srinivasan, R., Keogh, R.A., Milburn, D.R., and Davis, B.H., Journal of Catalysis 153 (1995) p. 123.
59. Gomez, R., Lopez, T., Tzompantzi, F., Garciafigueroa, E., Acosta, D.W., and Novaro, O., Langmuir 13 (1997) p. 970.
60. Miller, J.B. and Ko, E., Advanced Catalysts and Nanostructured Materials: Modern Synthetic Methods, edited by Moser, W.R. 1996. p. 21.
61. Contescu, C., Popa, V.T., Miller, J.B., Ko, E.I., and Schwarz, J.A., Journal of Catalysis 157 (1995) p. 244.
62. Ko, E.I. and Miller, J.B., The Chemical Engineering Journal and the Biochemical Engineering Journal 64 (1996) p. 273.
63. Bosman, H.J.M., Kruissink, E.C., Vanderspoel, J., and Vandenbrink, F., Journal of Catalysis 148 (1994) p. 660.
64. Feng, Z.T., Postula, W.S., Erkey, C., Philip, C.V., Akgerman, A., and Anthong, R.G., Journal of Catalysis 148 (1994) p. 84.
65. Anderson, J.A., Fergusson, C., Rodriguez-Ramos, I., and Guerrero-Ruiz, A., Journal of Catalysis 192 (2000) p. 344.
66. Miller, J.B. and Ko, E.I., Journal of Catalysis 159 (1996) p. 58.
67. Kung, H.H., Journal of Solid State Chemistry 52 (1984) p. 191.
68. Bosman, H.J.M., Pijpers, A.P., and Jaspers, A., Journal of Catalysis 161 (1996) p. 551.
69. Hino, M. and Arata, K., Journal of the Chemical Society, Chemical Communications (1987) p. 1259.
70. Farcasiu, D., Ghenciu, A., and Miller, G., Journal of Catalysis 134 (1992) p. 118.
71. Arata, K. and Hino, M., 9th International Congress on Catalysis, Calgary, edited by Phillips, M.J and Ternan, M. 1988. p. 1727.
72. Iglesia, E., Barton, D.G., Soled, S.L., Miseo, S., Baumgartner, J.E., Gates, W.E., Fuentes, G.A., and Meitzner, G.D., 11th International Congress on Catalysis 40th anniversary proceedings of the 11th ICC, edited by Hightower, J.W., Delgass, W.N., Iglesia, E. and Bell, A.T., 1996.
73. Santiesteban, J.G., Vartuli, J.C., Han, S., Bastian, R.D., and Chang, C.D., Journal of Catalysis 168 (1997) p. 431.
74. Scheithauer, M., Cheung, T.-K., Jentoft, R.E., Grasselli, R.K., Gates, B.C., and Knozinger, H., Journal of Catalysis 180 (1998) p. 1.
75. Soled, S.L., Dispenziere, N., and Saleh, R., Progress in Catalysis: Proceedings of the 12th Canadian Symposium on Catalysis, Banff, Alberta, Canada, edited by Smith, K.J and Sandford, E.C. 1992. p. 77.
76. Barton, D.G., Soled, S.L., Meitzner, G.D., Fuentes, G.A., and Iglesia, E., Journal of Catalysis 181 (1999) p. 57.
77. Afanasiev, P., Geantet, C., Breysse, M., Coudurier, G., and Vedrine, J.C., Journal of Chemical Society, Faraday Transactions 90 (1994) p. 193.
78. Pratt, K.C., Sanders, J.V., and Christov, V., Journal of Catalysis 124 (1990) p. 416.

79. Di Gregorio, F. and Keller, V., Journal of Catalysis 225 (2004) p. 45.
80. Wilson, R.D., Barton, D.G., Baertsch, C.D., and Iglesia, E., Journal of Catalysis 194 (2000) p. 175.
81. Barton, D.G., Shtein, M., Wilson, R.D., Soled, S.L., and Iglesia, E., Journal of Physical Chemistry 103 (1999) p. 630.
82. Di Gregorio, F. and Keller, V., Journal of Catalysis 225 (2004) p. 45.
83. Cortes-Jacome, M.A., Toledo-Antonio, J.A., Armendariz, H., Hernandez, I., and Bokhimi, X., Journal of Solid State Chemistry 164 (2002) p. 339.
84. Dongare, M.K., Ramaswamy, V., Gopinath, C.S., Ramaswamy, A.V., Scheurell, S., Brueckner, M., and Kemnitz, E., Journal of Catalysis 199 (2001) p. 209.
85. Bokhimi, X., Morales, A., Garcia-Ruiz, A., Xiao, T.D., Chen, H., and Strutt, P.R., Journal of Solid State Chemistry 142 (1999) p. 409.
86. Baertsch, C.D., Soled, S.L., and Iglesia, E., Journal of Physical Chemistry B 105 (2001) p. 1320.
87. Boyse, R.A. and Ko, E.I., Journal of Catalysis 171 (1997) p. 191.
88. Vaudagna, S.R., Canavese, S.A., Comelli, R.A., and Figoli, N.S., Applied Catalysis A: General 168 (1998) p. 93.
89. German, M.R., Sintering Theory and Practice. 1996: Wiley, John & Sons, Incorporated.
90. Barton, D.G., Soled, S.L., and Iglesia, E., Topics in Catalysis 6 (1998) p. 87.
91. Shimizu, K., Venkatraman, T.N., and Song, W., Applied Catalysis A: General 224 (2002) p. 77.
92. Boutarbouch, M.N.D., Cortes, J.M.G., Begrani, M.S.E., Lecea, C.S.M.d., and Perez-Ramirez, J., Applied Catalysis B: Environmental 54 (2004) p. 115.
93. Yuranov, I., Bulushev, D.A., Renken, A., and Kiwi-Minsker, L., Journal of Catalysis 227 (2004) p. 138.
94. Perez-Ramirez, J., Journal of Catalysis 227 (2004) p. 512.
95. Neri, G., Rizzo, G., Galvagno, S., Loiacono, G., Donato, A., Musolino, M.G., Pietropaolo, R., and Rombi, E., Applied Catalysis A: General 274 (2004) p. 243.
96. Guglielminotti, E., Journal of Physical Chemistry 98 (1994) p. 4884.
97. Boot, L.A., van Dillen, A.J., Geus, J.W., and van Buren, F.R., Journal of Catalysis 163 (1996) p. 186.
98. Cheung, T.K., Ditri, J.L., and Gates, B.C., Journal of Catalysis 151 (1995) p. 464.
99. Loften, T., Gnep, N.S., Guisnet, M., and Blekkan, E.A., Catalysis Today Catalysis for a Sustainable Future, 11th Nordic Symposium on Catalysis 100 (2005) p. 397.
100. Jentoft, F.C., Hahn, A., Krohnert, J., Lorenz, G., Jentoft, R.E., Ressler, T., Wild, U., Schlogl, R., Ha[ss]ner, C., and Kohler, K., Journal of Catalysis 224 (2004) p. 124.
101. Srinivasan, R., Keogh, R.A., Ghenciu, A., Farcasiu, D., and Davis, B.H., Journal of Catalysis 158 (1996) p. 502.
102. Delahay, G., Mauvezin, M., Coq, B., and Kieger, S., Journal of Catalysis 202 (2001) p. 156.
103. Willey, R.J., Lai, H., and Peri, J.B., Journal of Catalysis 130 (1991) p. 319.

104. Long, R.Q. and Yang, R.T., Applied Catalysis B: Environmental 27 (2000) p. 87.
105. Ramis, G., Yi, L., Busca, G., Turco, M., Kotur, E., and Willey, R.J., Journal of Catalysis 157 (1995) p. 523.
106. Schwidder, M., Kumar, M.S., Klementiev, K., Pohl, M.M., Bruckner, A., and Grunert, W., Journal of Catalysis 231 (2005) p. 314.
107. Long, R.Q. and Yang, R.T., Journal of Catalysis 207 (2002) p. 274.
108. Delahay, G., Valade, D., Guzman-Vargas, A., and Coq, B., Applied Catalysis B: Environmental 55 (2005) p. 149.
109. Sjovall, H., Olsson, L., Fridell, E., and Blint, R.J., Applied Catalysis B: Environmental 64 (2006) p. 180.
110. Kumar, M.S., Schwidder, M., Grunert, W., and Bruckner, A., Journal of Catalysis 227 (2004) p. 384.
111. Qi, G. and Yang, R.T., Applied Catalysis B: Environmental 60 (2005) p. 13.
112. Long, R.Q. and Yang, R.T., Journal of Catalysis 186 (1999) p. 254.
113. Indovina, V., Campa, M.C., Pepe, F., Pietrogiacomi, D., and Tuti, S., Applied Catalysis B: Environmental 60 (2005) p. 23.
114. Busca, G., Lietti, L., Ramis, G., and Berti, F., Applied Catalysis B: Environmental 18 (1998) p. 1.
115. Hums, E., Catalysis Today 42 (1998) p. 25.
116. Bosch, H., Janssen, F.J., van den Kerkhof, F., Oldenziel, J., van Ommen, J.G., and Ross, J., Applied Catalysis 25 (1986) p. 239.
117. Gasior, M., Haber, J., Machej, T., and Czeppe, T., Journal of Molecular Catalysis 43 (1988) p. 359.
118. Alemany, L.J., Berti, F., Busca, G., Ramis, G., Robba, D., Toledo, G.P., and Trombetta, M., Applied Catalysis B: Environmental 10 (1996) p. 299.
119. Hilbrig, F., Goebel, H.E., Knoezinger, H., Schmelz, H., and Lengeler, B., J. Phys. Chem. 95 (1991) p. 6973.
120. Deo, G. and Wachs, I.E., J. Phys. Chem. 95 (1991) p. 5889.
121. Chen, J.P. and Yang, R.T., Applied Catalysis A: General 80 (1992) p. 135.
122. Topsoe, N.Y., Topsoe, H., and Dumesic, J.A., Journal of Catalysis 151 (1995) p. 226.
123. Topsoe, N.Y., Dumesic, J.A., and Topsoe, H., Journal of Catalysis 151 (1995) p. 241.
124. Vartuli, J.C., Santiesteban, J.G., Traverso, P., Cardona-Martinez, N., Chang, C.D., and Stevenson, S.A., Journal of Catalysis 187 (1999) p. 131.
125. Arata, K. and Hino, M., Materials Chemistry and Physics 26 (1990) p. 213.
126. Tran, M.-T., Gnep, N.S., Szabo, G., and Guisnet, M., Applied Catalysis A: General 171 (1998) p. 207.
127. Melada, S., Ardizzone, S.A., and Bianchi, C.L., Microporous and Mesoporous Materials 73 (2004) p. 203.
128. Farcasiu, D. and Li, J.Q., Applied Catalysis A: General 128 (1995) p. 97.
129. Song, X. and Sayari, A., Catalysis Reviews - Science and Engineering 38 (1996) p. 329.

130. Yadav, G.D. and Nair, J.J., Microporous and Mesoporous Materials 33 (1999) p. 1.
131. Figueras, F., Coq, B., Ensuque, E., Tachon, D., and Delahay, G., Catalysis Today 42 (1998) p. 117.
132. Loften, T. and Blekkan, E.A., Applied Catalysis A: General 299 (2006) p. 250.
133. Bautista, P., Faraldos, M., Yates, M., and Bahamonde, A., Applied Catalysis B: Environmental 71 (2007) p. 254.
134. Miller, J.M. and Lakshmi, L.J., Applied Catalysis A: General 190 (2000) p. 197.
135. Henker, M., Wendlandt, K.-P., Valyon, J., and Bornmann, P., Applied Catalysis 69 (1991) p. 205.
136. Vu, T.N., van Gestel, J., Gilson, J.P., Collet, C., Dath, J.P., and Duchet, J.C., Journal of Catalysis 231 (2005) p. 453.
137. Daniel, M.F., Desbat, B., Lassegues, J.C., Gerand, B., and Figlarz, M., Journal of Solid State Chemistry 67 (1987) p. 235.
138. Vaudagna, S.R., Comelli, R.A., and Figoli, N.S., Applied Catalysis A: General 164 (1997) p. 265.
139. Boyse, R.A. and Ko, E.I., Journal of Catalysis 171 (1997) p. 191.
140. Barton D.G., S.S.L., Iglesia E., Topics in Catalysis 6 (1998) p. 87.
141. Arata, K., Applied Catalysis A: General 146 (1996) p. 3.
142. Bordoloi, A., Mathew, N.T., Devassy, B.M., Mirajkar, S.P., and Halligudi, S.B., Journal of Molecular Catalysis A: Chemical 247 (2006) p. 58.
143. De Rossi, S., Ferraris, G., Valigi, M., and Gazzoli, D., Applied Catalysis A: General 231 (2002) p. 173.
144. Barton David G, S.M., Wilson Ryan D. , Soled Stuart L. and Iglesia Enrique, Journal of physical chemistry 103 (1999) p. 630.
145. Busca, G., Physical Chemistry Chemical Physics 1 (1999) p. 723.
146. Falco, M.G., Canavese, S.A., and Figoli, N.S., Catalysis Today Selected Contributions of the XIX Ibero American Catalysis Symposium 107-108 (2005) p. 778.
147. Brei, V.V., Melezhyk, O.V., Prudius, S.V., Levchuk, M.M., and Patrylak, K.I., Studies in Surface Science and Catalysis 143 (2002) p. 387.
148. Sun, W., Xu, L., Chu, Y., and Shi, W., Journal of Colloid and Interface Science 266 (2003) p. 99.
149. Rahkamaa-Tolonen, K., Maunula, T., Lomma, M., Huuhtanen, M., and Keiski, R.L., Catalysis Today Catalysis for a Sustainable Future, 11th Nordic Symposium on Catalysis 100 (2005) p. 217.
150. Apostolescu, N., Geiger, B., Hizbullah, K., Jan, M.T., Kureti, S., Reichert, D., Schott, F., and Weisweiler, W., Applied Catalysis B: Environmental 62 (2006) p. 104.
151. Guglielminotti, E. and Boccuzzi, F., Applied Catalysis B: Environmental 8 (1996) p. 375.
152. Wong, S.-T., Li, T., Cheng, S., Lee, J.F., and Mou, C.Y., Applied Catalysis A: General 296 (2005) p. 90.
153. Long, R.Q. and Yang, R.T., Journal of Catalysis 194 (2000) p. 80.
154. Lambert, R.M., Surface Science 49 (1975) p. 325.
155. Benziger, J.B. and Larson, L.R., Journal of Catalysis 77 (1982) p. 550.

156. Anderson, J.A., Chong, F.K., and Rochester, C.H., Journal of Molecular Catalysis A: Chemical 140 (1999) p. 65.
157. Derrouiche, S. and Bianchi, D., Applied Catalysis A: General 313 (2006) p. 208.
158. Perez-Osorio, G., Castillon, F., Simakov, A., Tiznado, H., Zaera, F., and Fuentes, S., Applied Catalysis B: Environmental 69 (2007) p. 219.
159. Tanaka, K. and White, J.M., Journal of Catalysis 79 (1983) p. 81.
160. Chakarova, K., Hadjiivanov, K., Atanasova, G., and Tenchev, K., Journal of Molecular Catalysis A: Chemical 264 (2007) p. 270.
161. Hadjiivanov, K. and Dimitrov, L., Microporous and Mesoporous Materials 27 (1999) p. 49.
162. Tuti, S., Pepe, F., Pietrogiacomi, D., and Indovina, V., Catalysis Today 75 (2002) p. 373.
163. Ferraris, G., De Rossi, S., Gazzoli, D., Pettiti, I., Valigi, M., Magnacca, G., and Morterra, C., Applied Catalysis A: General 240 (2003) p. 119.

Appendices

Appendix I: Example calculations for synthesis of $Fe/WO_3/ZrO_2$ catalysts.

The following describes the calculations carried out to determine the quantities of precursors necessary to synthesise $Fe/WO_3/ZrO_2$ catalysts of different iron and tungsten oxide loading. The tungsten oxide and iron species were introduced by incipient wetness impregnation on zirconium hydroxide support. The example given below is the steps taken to synthesise a $0.5Fe/15WO_3/ZrO_2$ catalyst.

Step 1: Synthesis of the WO_3/ZrO_2 support

The desired product is 2.5 grams of 15 wt% WO_3/ZrO_2. The mass of tungsten oxide (WO_3) and zirconium oxide (ZrO_2) required can be calculated as:

$$WO_3: 0.15 * 2.5 = 0.375g$$
$$ZrO_2: 0.85 * 2.5 = 2.125g$$

The precursors for WO_3 and ZrO_2 are ammonium metatungstate $[(NH_4)_6W_{12}O_{39}.xH_2O]$ and zirconium hydroxide $[Zr(OH)_4]$. From this the ratio of molecular weights of the components (WO_3 and ZrO_2) over its respective precursor salt is calculated. This ratio when multiplied by the desired mass of the respective component will give the required mass of that precursor.

Component	Molecular weight
ZrO_2	123
WO_3	232
$Zr(OH)_4$	159
$(NH_4)_6W_{12}O_{39}.4H_2O$	2956.3
$Fe(NO_3)_3.9H_2O$	404

The ratio of tungsten oxide (WO_3) would be 1.06 as calculated by:

$$\frac{(NH_4)_6W_{12}O_{39}.4H_2O}{12WO_3} \rightarrow \frac{2956.3}{(12*232)} \rightarrow 1.06$$

Ratio for zirconium oxide (ZrO_2) is 2.62.

$$\frac{Zr(OH)_4}{ZrO_2} \rightarrow \frac{159}{123} \rightarrow 1.29$$

Using these ratios, the required mass of ammonium metatungstate and zirconium hydroxide can be determined.

Tungsten oxide (WO_3) : 0.375g * 1.06 = 0.4g ammonium metatungstate
Zirconia (ZrO_2) : 2.125g * 1.29 = 2.74g zirconium hydroxide

Step 2: Synthesis of $Fe/WO_3/ZrO_2$ catalyst

The same steps are carried out to determine the mass of iron nitrate necessary to synthesise 2.5g of $0.5Fe/15WO_3/ZrO_2$.

Iron (Fe) : 0.05 * 2.5 = 0.125g
Tungsten oxide supported on zirconia (WO_3/ZrO_2) : 0.95 * 2.5 = 2.375g

Ratio for iron species (Fe) is 7.2.

$$\frac{Fe(NO_3)_3.9H_2O}{Fe} \rightarrow \frac{404}{56} \rightarrow 7.2$$

Required mass of iron nitrate:

Fe : 0.125g * 7.2 = 0.9g iron nitrate
WO_3/ZrO_2 = 2.375g

The same calculations were repeated for different iron and tungsten oxide loadings.

Appendix II: IR spectra

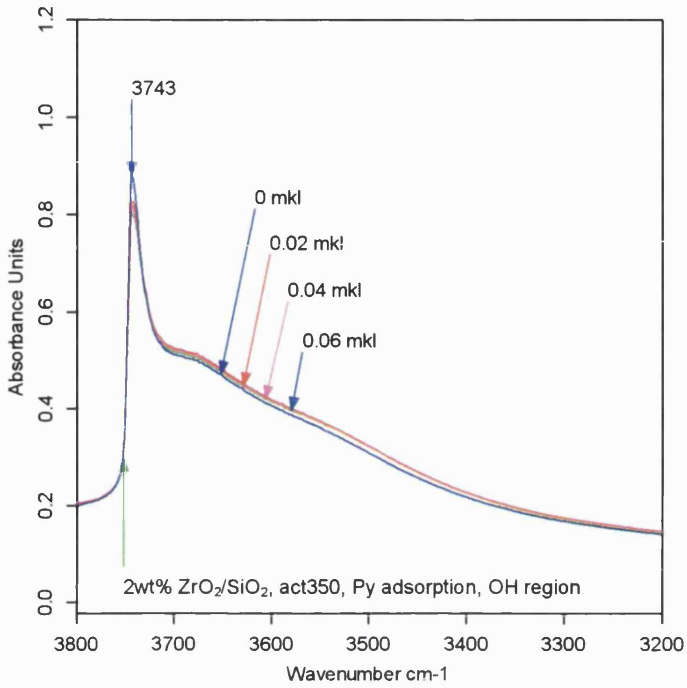

Fig. A2.1.1. IR spetra (OH region) after pyridine adsorption of 2 wt% ZrO_2/SiO_2.

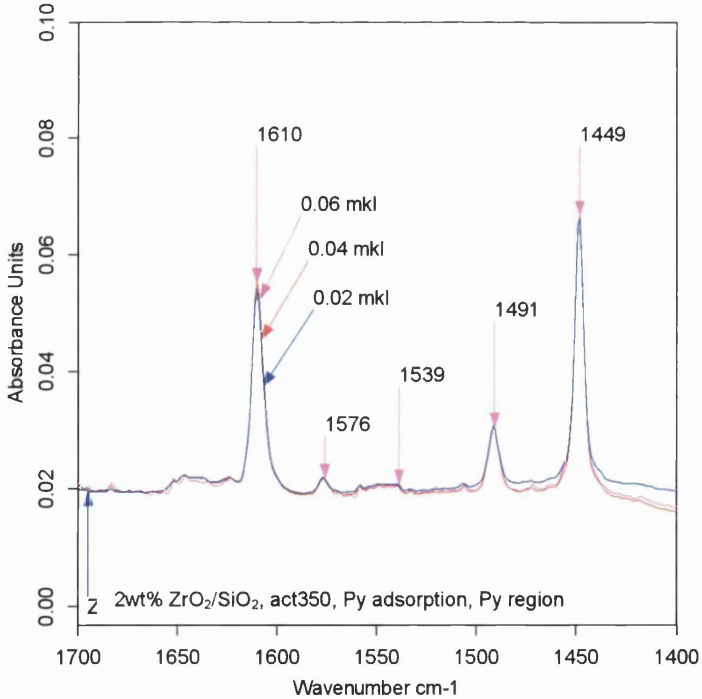

Fig. A2.1.2 IR spetra (Py region) after pyridine adsorption of 2 wt% ZrO_2/SiO_2.

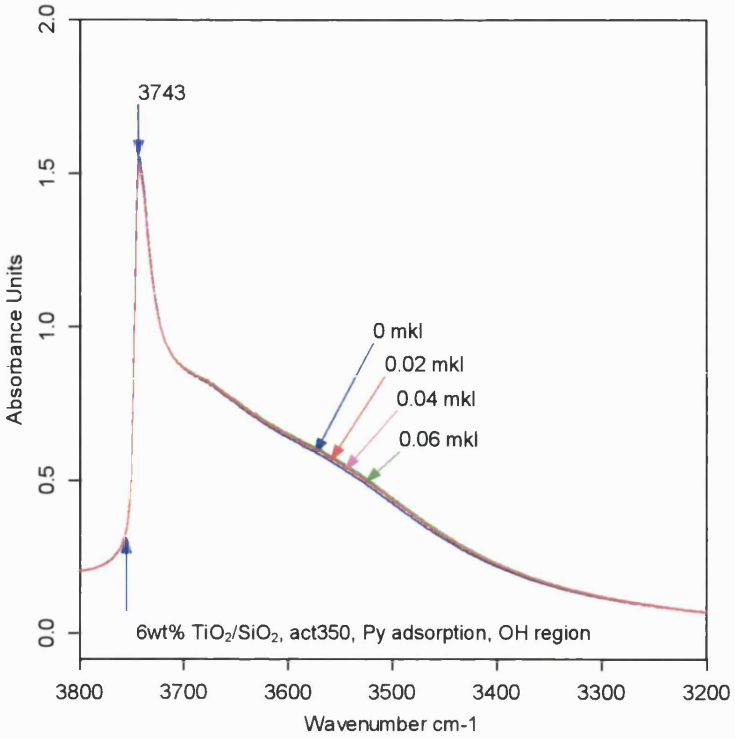

Fig A2.2.1 IR spetra (OH region) after pyridine adsorption of 6 wt% TiO_2/SiO_2.

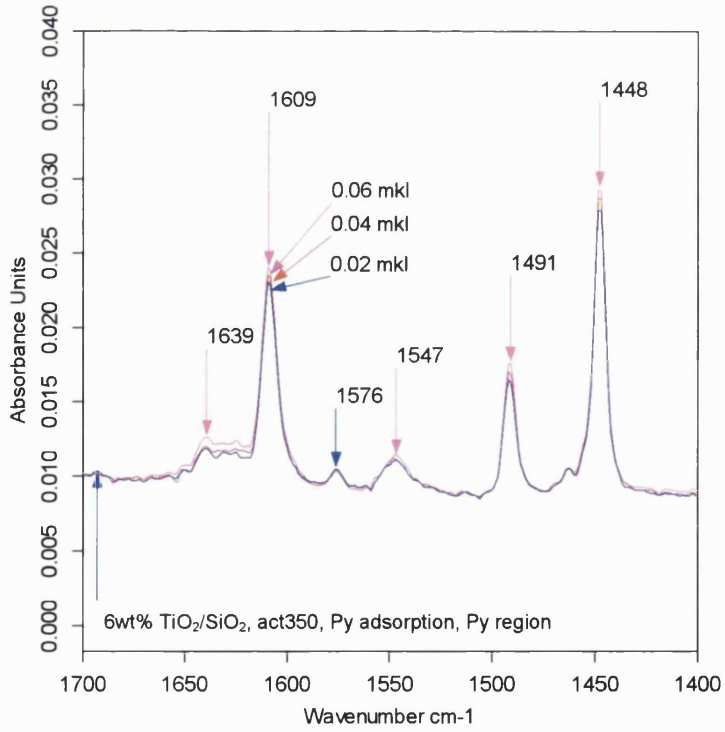

Fig A2.2.2. IR spetra (Py region) after pyridine adsorption of 6 wt% TiO_2/SiO_2.

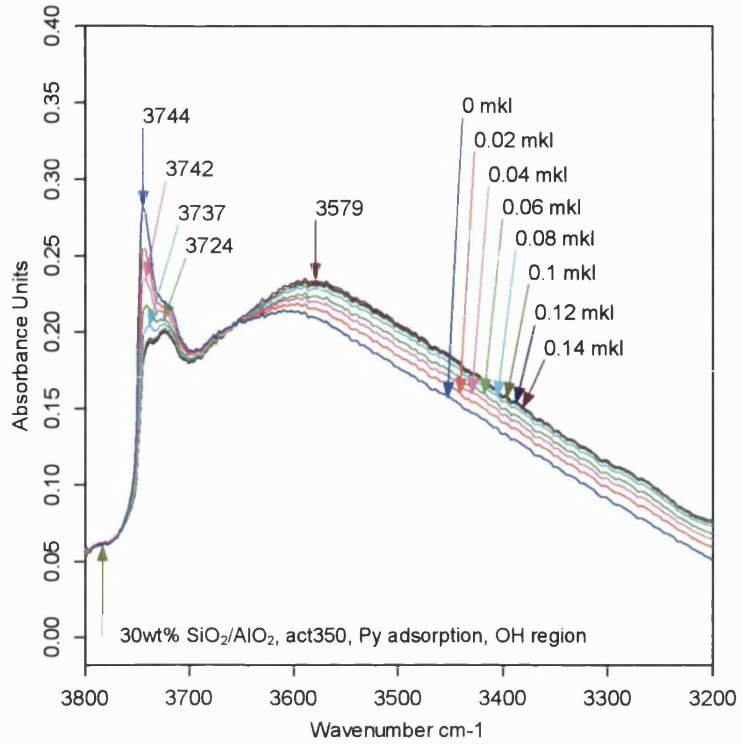

Fig. A.2.3.1. IR spetra (OH region) after pyridine adsorption of 30 wt% SiO_2/Al_2O_3.

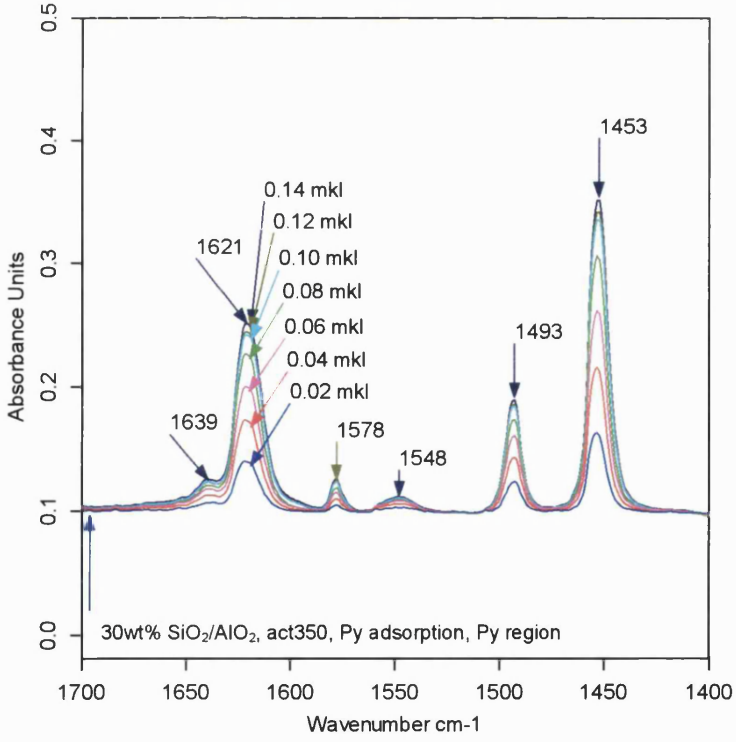

Fig. A.2.3.2. IR spetra (Py region) after pyridine adsorption of 30 wt% SiO_2/Al_2O_3.

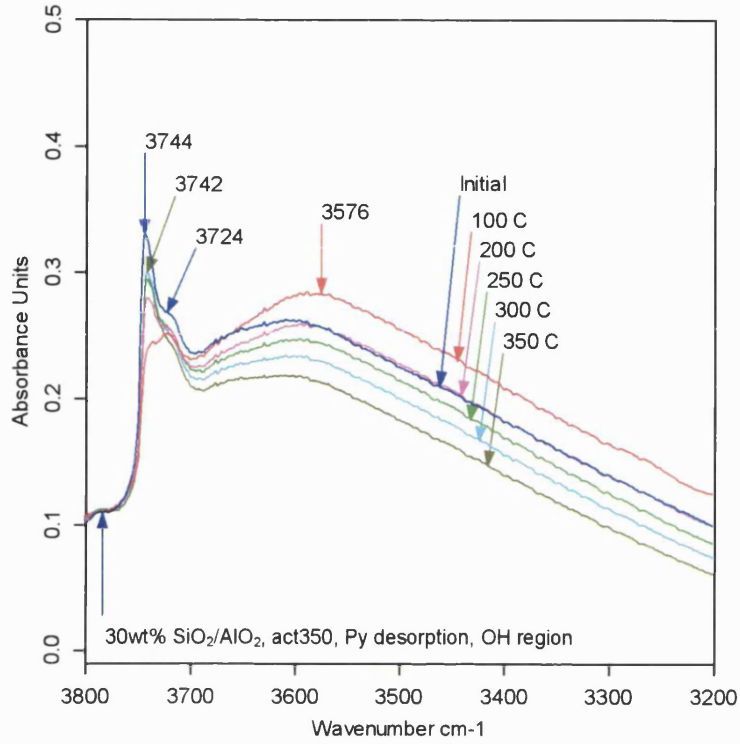

Fig. A.2.3.3. IR spetra (OH) after pyridine desorption of 30 wt% SiO_2/Al_2O_3.

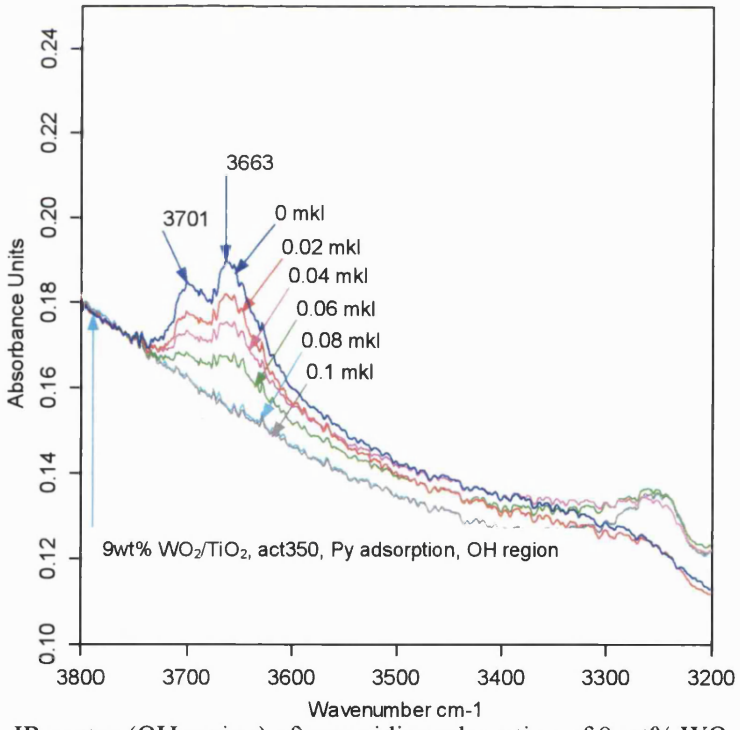

Fig. A2.4.1. IR spetra (OH region) after pyridine adsorption of 9 wt% WO_3/TiO_2.

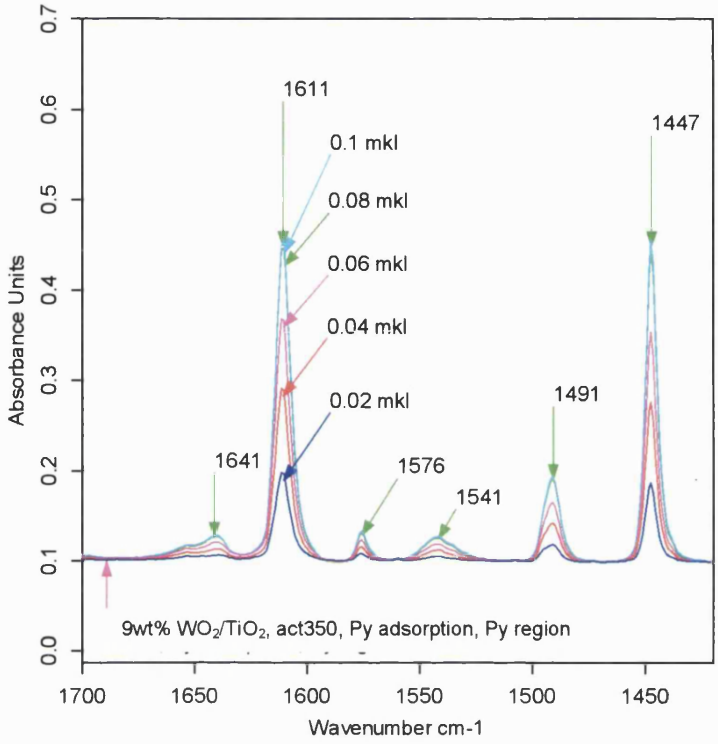

Fig. A2.4.2. IR spetra (Py region) after pyridine adsorption of 9 wt% WO_3/TiO_2.

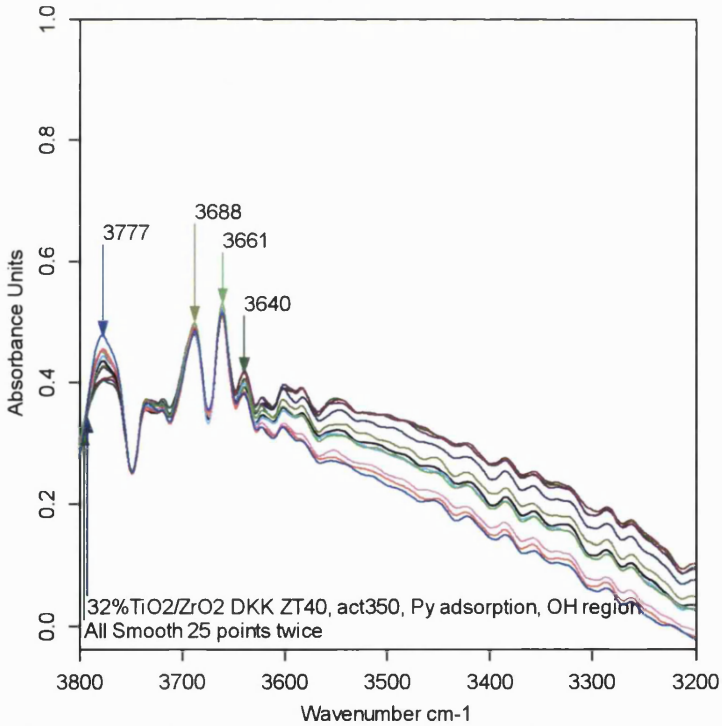

Fig. A2.5.1. IR spetra (OH region) after pyridine adsorption of 32 wt% TiO_2/ZrO_2.

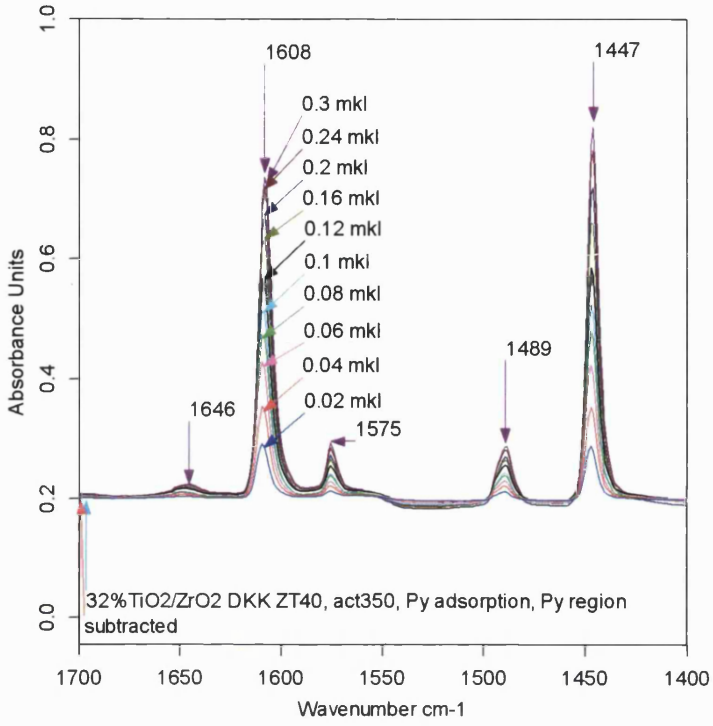

Fig. A2.5.2. IR spetra (Py region) after pyridine adsorption of 32 wt% TiO_2/ZrO_2.

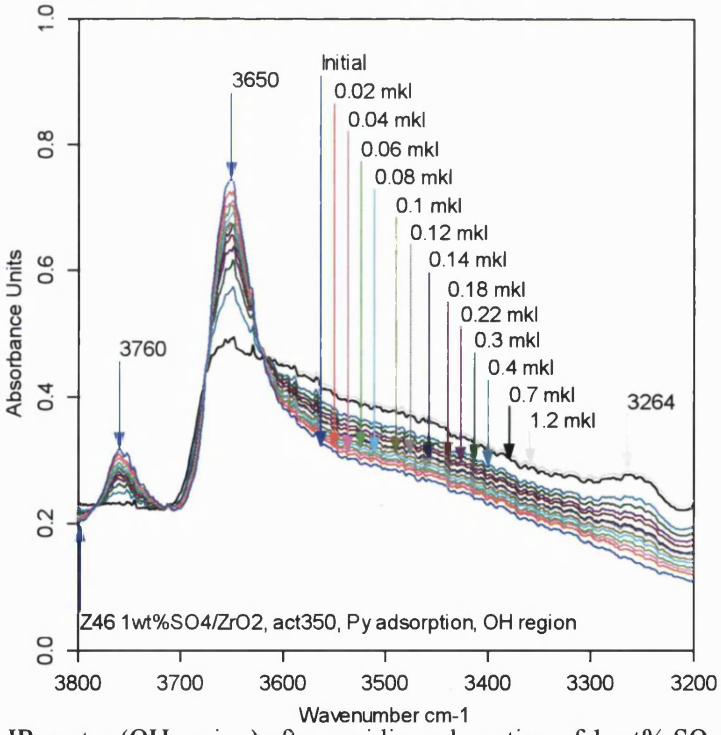

Fig. A2.6.1. IR spetra (OH region) after pyridine adsorption of 1 wt% SO_4/ZrO_2.

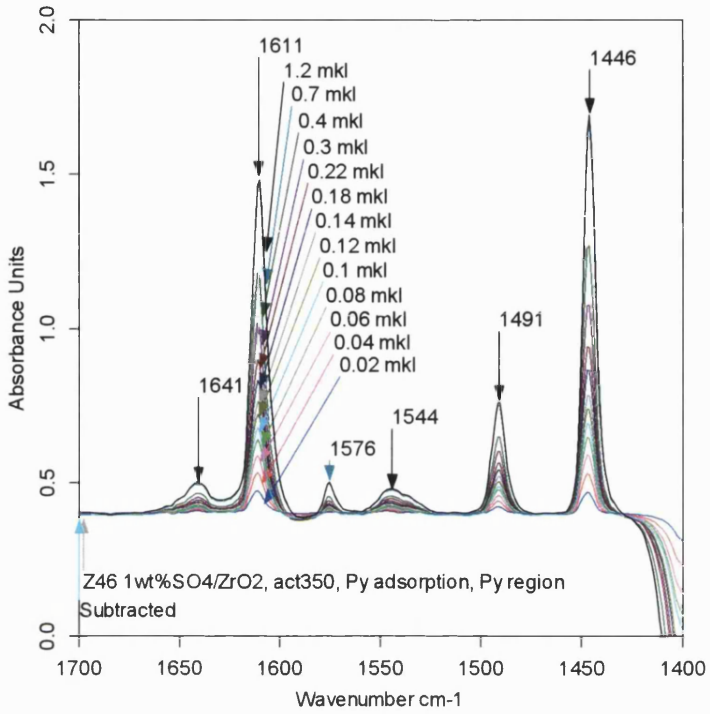

Fig. A2.6.2. IR spetra (Py region) after pyridine adsorption of 1 wt% SO_4/ZrO_2.

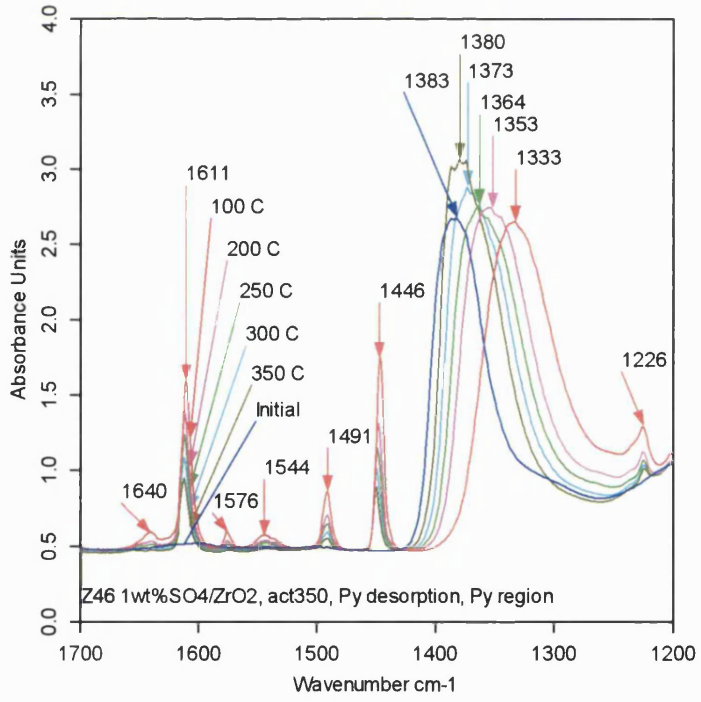

Fig. A2.6.3. IR spectra (sulphate region) after pyridine desorption of 1 wt% SO_4/ZrO_2.

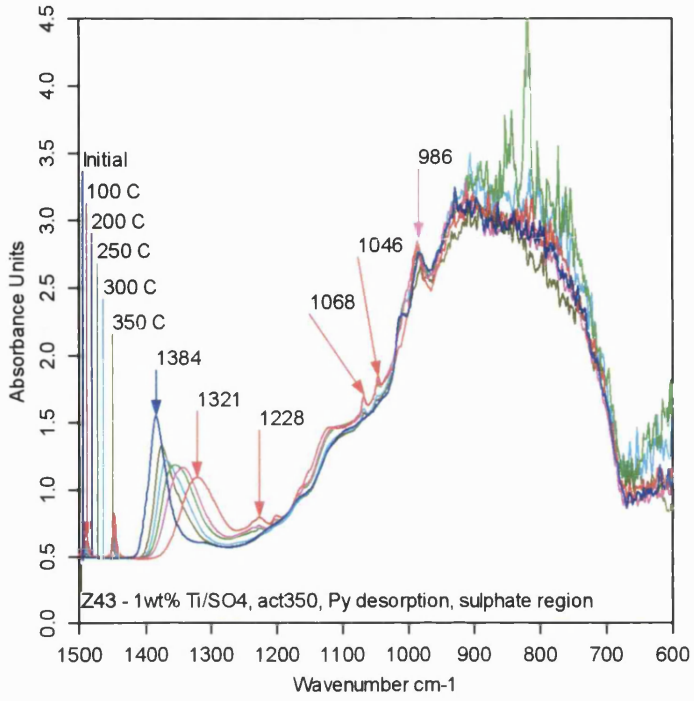

Fig. A2.6.4. IR spectra (sulphate region) after pyridine desorption of 1 wt% TiO_2/SO_4.

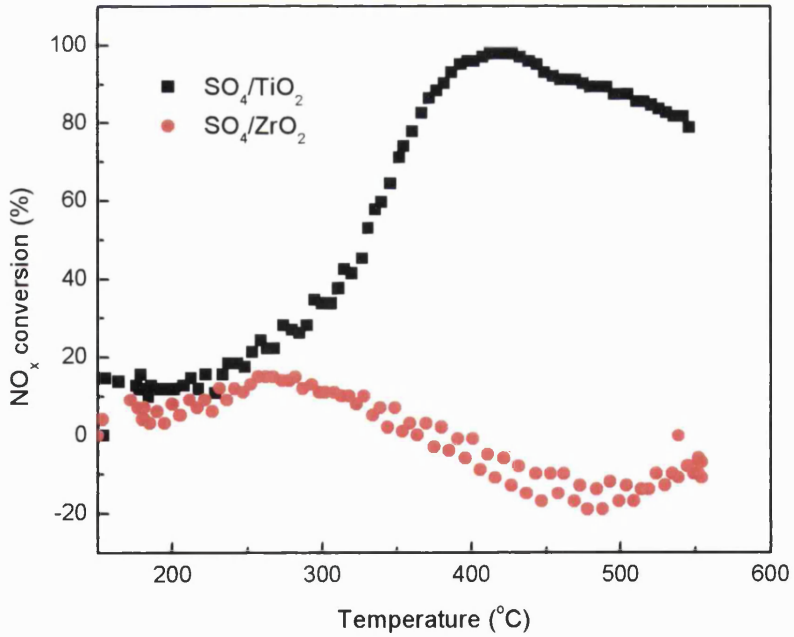

Fig. A2.6.5. Effect of temperature on NO_x conversion on SO_4/ZrO_2 catalytic supports.

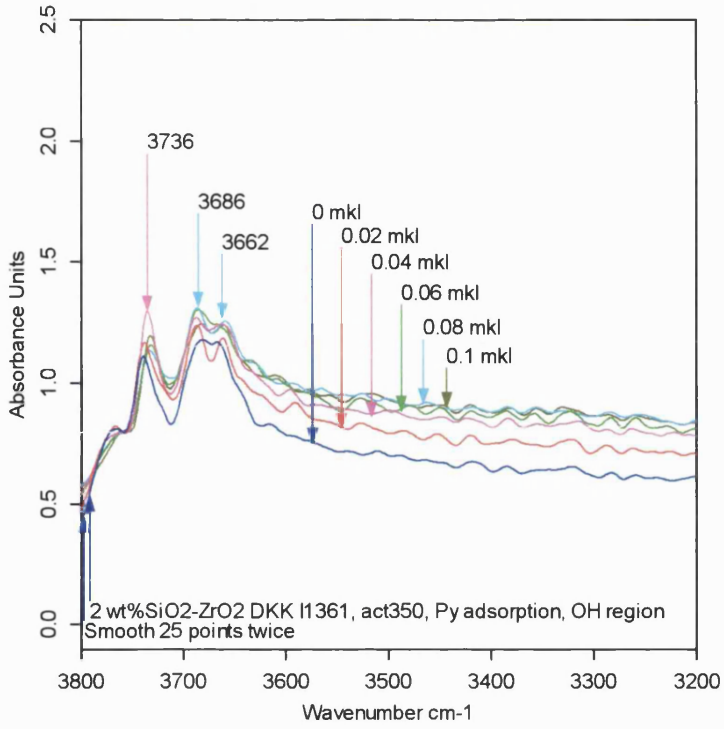

Fig. A2.7.1. IR spetra (OH region) after pyridine adsorption of 2 wt% SiO_2/ZrO_2.

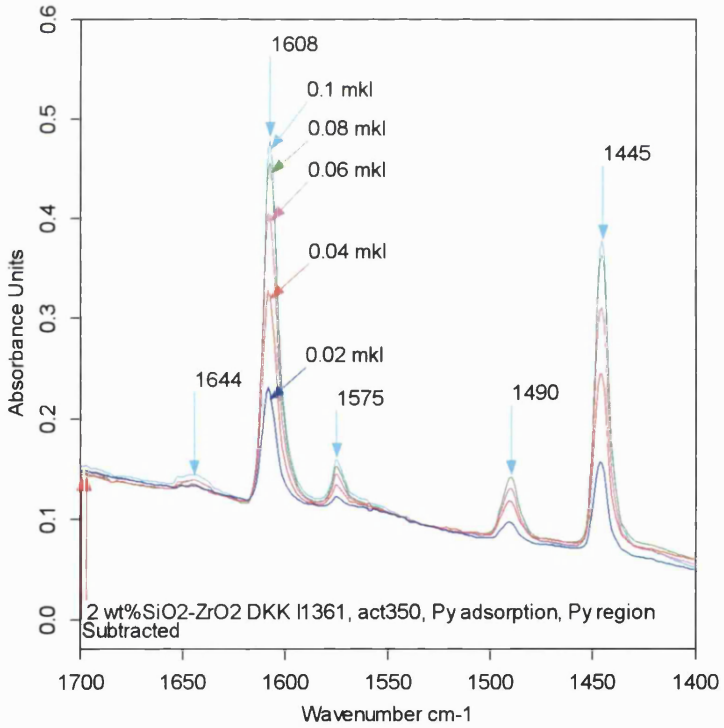

Fig. A2.7.2. IR spetra (Py region) after pyridine adsorption of 2 wt% SiO_2/ZrO_2.

Publications and presentations

Publications and presentations

1. *IR study of Zr/Si mixed oxide catalyst activated at different temperatures.* Poster presentation, Third International Taylor Conference, 5^{th} – 8^{th} September 2004, CenTACAT, Queen's University of Belfast.

2. *Developing new solid acid mixed oxide catalysts.* Departmental oral presentation, 16^{th} November 2004, Department of Chemical Engineering, University of Bath.

3. *Effect of tungsten oxide loading on acidity of WO_3/ZrO_2 mixed oxides.* Poster presentation, April 2005 Johnson Matthey symposium, University of Notthingham.

4. *Characterisation of iron promoted tungsten zirconia catalysts for selective catalytic reduction of nitrogen oxide by ammonia.* Oral presentation, June 2006, Johnson Matthey symposium, University of Notthingham. This presentation won the prize for the best presentation of the symposium.

5. Iron promoted tungsten zirconia as a potential catalyst for selective catalytic reduction of NO_x by ammonia. Paper to be submitted to Applied Catalysis B: Environmental.

IR study of Zr/Si mixed oxide catalyst activated at different temperatures

R. Foo, T. Vazhnova and D.B. Lukyanov
Catalysis and Reaction Engineering Group, Department of Chemical Engineering
University of Bath, Bath BA2 7AY, UK
r.foo@bath.ac.uk and d.b.lukyanov@bath.ac.uk

INTRODUCTION

It has been generally recognized that certain mixed oxides show much stronger acidic properties in comparison to the individual single oxides they are composed of. The generation of strong acidity in chemically mixed oxides has been attributed to the charge imbalance of the metal ions in the M-O-M[1] bonds [1]. ZrO_2-SiO_2 mixed oxides have not been studied as extensively as other systems such as Al_2O_3-SiO_2. In light of this, ZrO_2-SiO_2 oxides would be an interesting area for research. Zirconia tends to have low surface areas and poor thermal stability due to the phase transformation. However, when zirconia is combined with silica to from a mixed oxide, a high surface area and thermally stable material is obtained. This is due to the stabilizing effect of silica on zirconia. Zirconia, on the other hand, could affect the strength of the Si–OH and SiO–H bonds, which could subsequently lead to generation of Bronsted acid sites [2]. Consequently, ZrO_2-SiO_2 could be considered as a promising catalyst (or catalyst support) for acid catalyzed reactions.

In this work, a ZrO_2-SiO_2 oxide was activated over a range of temperatures to determine the effect of activation temperature on Lewis and Bronsted acidity. The samples were activated at 150, 250, 350 and 450°C. As the activation temperature is increased, it is expected that Lewis acidity should increase as adsorbed water is removed from the mixed oxide. Bronsted acidity should either remain stable or increase slightly between 150–350°C. Once the activation temperature exceeds 350°C, a drop in Bronsted acidity is expected due to dehydroxylation.

RESULTS AND DISCUSSION

Infrared spectroscopy was employed to characterize the ZrO_2-SiO_2 sample with pyridine (Py) as the probe molecule to determine Lewis and Bronsted acidity. Quantitative results could not be obtained as the sample adsorbed minute amounts of Py. 0.02μmol Py is the smallest accurate unit that could be measured and with this amount the sample was essentially saturated. Thus, due to a large associated experimental error, the exact absolute numbers for Lewis and Bronsted acid sites could not be obtained. However, indications of the maximum possible amount of acid sites and the ratio between LAS and BAS were obtained. The IR spectra were normalized based on the framework vibrations, which enabled a qualitative examination by comparing the spectra of the sample activated at different temperatures.

Lewis acid sites were present in the sample activated at all temperatures and increased steadily as temperature was raised. On the other hand, only small amounts of Bronsted acid sites existed which decreased with temperature. Similarly, there was less adsorbed water at higher temperatures. These results are in agreement with our expectations. Interestingly, Bronsted acidity was decreasing immediately above activation at 150°C, indicating that there was no stable level of BAS in the sample. Potentially, dehydroxylation was occurring at temperatures as low as 250°C. Now that the effect of the activation temperature on both Lewis and Bronsted acidity has been determined, further studies of ZrO_2-SiO_2 oxides with the different Zr:Si ratio will be carried out. The results of these studies will be presented in the paper at the conference.

REFERENCES

[1] K. Tanabe, Solids acids and bases, Academic Press, 1971.
[2] J. Anderson, C. Ferguson, I. Rodriguez, A Guerrero, J. Catal. 192 (2000) 344.

Effect of tungsten oxide loading on acidity of WO_3/ZrO_2 mixed oxides

R. Foo, T. Vazhnova and D.B. Lukyanov
Catalysis and Reaction Engineering Group, Department of Chemical Engineering
University of Bath, Bath BA2 7AY, UK
Email: r.foo@bath.ac.uk

Introduction

Tungsten zirconia was first reported to be highly acidic by Hino and Arata [162] based on use of Hammett indicators: acid sites were found to be stronger than 100% sulphuric acid. These findings were later supported by different authors [72, 73, 163]. The mechanism for acidity generation is still studied but is generally accepted to be due to the formation of intermediate WO_3 domains on ZrO_2. It would be interesting to examine the effect of tungsten oxide loading on the levels of Lewis acid sites (LAS) and Bronsted acid sites (BAS). These studies could then be used to predict the optimum tungsten oxide loading for maximum total acidity. Furthermore, samples of varying LAS to BAS ratios could potentially be synthesised to examine the effect of the LAS/BAS ratio on catalytic activity.

Experimental

Tungsten zirconia samples were synthesized by incipient wetness impregnation of zirconium hydroxide [$Zr(OH)_4$, MEL Chemicals] using ammonium (meta)tungstate salt [$(NH_4)_6W_{12}O_{39}.xH_2O$, Fluka]. Zirconium hydroxide was impregnated to the desired tungsten oxide loading and dried at room temperature overnight. The samples were then calcined at 830°C for 3 hours, heated and cooled at a rate of 10°C/min under 100 ml/min flowing dry air. The air was dried using a column packed with 13X molecular sieves. The samples were pressed into suitable disks and characterised by FT-IR spectroscopy using pyridine as the probe molecule to determine quantitative values for Lewis and Bronsted acidity. TPD was also carried out to determine the strength of the Lewis and Bronsted acid sites.

Results

Tungsten oxide loading has a significant effect on the total acidity and the ratio of LAS to BAS of tungsten zirconia mixed oxides. The results will be presented and discussed in full at the Symposium. In addition, we intend to discuss in our presentation the effect of calcination temperature on the total acidity and number of Bronsted and Lewis acid sites in tungsten zirconia.

References

1. M. Hino and K. Arata, *Synthesis of Solid Superacid of Tungsten Oxide supported on Zirconia and its Catalytic Action for Reactions of Butane and Pentane.* Journal of the Chemical Society, Chemical Communications, 1988: p. 1259.
2. E. Iglesia, D.G. Barton, S.L. Soled, S. Miseo, J.E. Baumgartner, W.E. Gates, G.A Fuentes and G.D. Meitzner, *Selective isomerisation of alkanes on supported tungsten oxide acids.* in Proceedings 11th International Congress on Catalysis, J.W. Hightower et al., Editors. 1996, Amsterdam, Elsevier, 1996.
3. J.G. Santiesteban, J.C. Vartuli, S. Han, R.D. Bastian, and C.D. Chang, *Influence of the Preparative Method on the Activity of Highly Acidic WOx/ZrO2 and the Relative Acid Activity Compared with Zeolites*. Journal of Catalysis, 1997. 168: p. 431.

Characterisation of iron promoted tungsten zirconia catalysts for selective catalytic reduction of nitrogen oxide by ammonia.

R. Foo[1], T. Vazhnova[1], D.B. Lukyanov[1], P. Millington[2], J. Bailie[2] and R. Rajaram[2]
[1]Catalysis and Reaction Engineering Group, Department of Chemical Engineering, University of Bath, Bath BA2 7AY, UK; [2]Johnson Matthey Technology Centre, Blount's Court, Sonning Common, Reading, RG4 9NH, UK
Email: r.foo@bath.ac.uk

Introduction

Tungsten zirconia has been shown to be a promising catalyst support due to its acidity and thermal stability. Previously, the effect of tungsten oxide loading on zirconia on the numbers of Lewis acid sites (LAS) and Bronsted acid sites (BAS) was investigated. We have introduced iron as the active metal into tungsten zirconia mixed oxides to develop a catalyst for selective catalytic reduction (SCR) of nitrogen oxides by ammonia. It was expected that the addition of iron will change the acidity and activity of the catalyst. In this work, acidity of tungsten zirconia oxides with and without iron was investigated as well as the role of acidity in NH_3 SCR. A detailed FT-IR investigation was undertaken on the adsorption of CO on iron in order to obtain information about the iron species and any metal/metal interactions that may occur on the catalyst.

Experimental

Tungsten zirconia samples were synthesized by incipient wetness impregnation of zirconium hydroxide [$Zr(OH)_4$, MEL Chemicals] using ammonium (meta)tungstate salt [$(NH_4)_6W_{12}O_{39}.xH_2O$, Fluka]. The samples were dried overnight then calcined at different temperatures between 590 °C to 830°C. Commercial tungsten zirconia support (DKK J1374) was also tested. Iron nonahydrate [$FeN_3O_9.9H_2O$, Fluka] was used to synthesise samples with iron loadings of 0.5wt%, 1wt% and 2wt%.

The samples were characterised by FT-IR spectroscopy using pyridine and CO as probe molecules. Pyridine was used to determine quantitative values for Lewis and Bronsted acidity. TPD was also carried out to determine the strength of the Lewis and Bronsted acid sites. CO adsorption was used to investigate the surface properties of the catalyst. Structural characterisation was carried out using XRD and BET analysis. Catalytic testing was performed with 0.3g of catalyst in reactant mixture of 12% O_2, 5%CO_2, 10% H_2O (steam), 100ppm NH_3 and 100ppm NO (Flowrate = 2 litres/min).

Results

Iron reduces total acidity of the catalysts; in particular the number of Bronsted acid sites. The effect on Lewis acidity differs depending on whether the MEL or DKK support is used. It could be expected that iron would lead to the formation of new LAS which is seen with the samples based on the MEL zirconia support. However, the DKK samples show a reduction in LAS when iron is present. No clear distinct relationship between acidity and activity was found although some links could be suggested. Overall, the results indicate that acidity of the tungsten zirconia support is not a key factor for ammonia SCR activity.

During this work, a new IR peak not reported previously in the literature was observed in iron supported on tungsten zirconia catalysts. We suggest that this IR peak is characteristic of Fe-W interactions. A clear relationship between the IR peak intensity and catalytic activity is observed i.e. a reduction in peak intensity correlates with a similar decrease in catalytic activity. The catalysts showed little or no NH_3 SCR activity when the IR peak was absent. On this basis, we propose that Fe-W interactions can be associated with NH_3 SCR activity.

Iron promoted tungsten zirconia as a potential catalyst for selective catalytic reduction of NO_x by ammonia

Rodney Foo[1], Tanya Vazhnova[1], Dmitry B. Lukyanov[1]
Authors[2] from JMTC

[1]Department of Chemical Engineering, University of Bath, Bath, BA2 7AY, UK
[2]Johnson Matthey Technology Centre, Blount's Court Sonning Common, Reading, RG4 9NH, UK

Abstract

The selective catalytic reduction (SCR) of nitrogen oxide by ammonia was studied over iron promoted tungsten zirconia catalysts under lean conditions at reaction temperatures between 150 and 550 °C. Tungsten zirconia (WO_3/ZrO_2) showed no activity in the NH_3 SCR of NO_x reaction but after impregnating tungsten zirconia with 0.5wt% iron (Fe), good SCR activity was found. The effect of iron loading was studied and four different iron promoted tungsten zirconia catalysts were synthesised with iron loadings of 0.5, 2, 3 and 10 wt%. The 3wt% $Fe/WO_3/ZrO_2$ catalyst was the most active where NO_x conversion of 80 % was observed at temperatures between 400 and 550 °C. The catalytic activity decreased slightly after aging but the catalysts remained stable and active. The catalysts were characterised by FT-IR spectroscopy in order to investigate the origin of NH_3 SCR activity of $Fe/WO_3/ZrO_2$ catalysts. New Fe^{3+} Lewis acid sites were formed that were active for NH_3 SCR and the acid site strength was also enhanced by the presence of iron. The good iron dispersion and the presence of tungsten could also contribute to the SCR activity of $Fe/WO_3/ZrO_2$ catalysts.

1. Introduction

Selective catalytic reduction of nitrogen oxides by ammonia has been a proven technology for reducing NO_x emissions of flue gases from stationary sources. Nitrogen oxides (NO, NO_2 and

N_2O) remain major air pollutants contributing to acid rains, photochemical smog and ozone depletion. Current industrial catalysts are generally based on V_2O_5/WO_3 supported on TiO_2 doped with minor additives such as sulphur and siliceous materials to improve stability and resistance [164].

There is a need to develop new catalysts active for NH_3 SCR of NO_x that are not based on toxic metals such as vanadium that is used in existing catalysts. New promising materials have been examined but with limited success due to insufficient stability or low resistance to poisoning [165-167]. There has been a strong interest in tungstate- and sulphate-doped zirconia as catalyst supports since the pioneering work of Arata and Hino [68]. Sulphated zirconia has been widely used in a variety of applications due to its high acidity and activity. However, these catalysts suffer from poor thermal stability due to the loss of sulphate groups [168-170]. Tungsten zirconia has been reported as being both highly acidic and thermally stable [75, 89, 122, 139] and has been examined as a potential catalyst or support in various applications such as hydrocarbon isomerisation and alkylation [70, 72, 141, 171-173].

Iron based materials have been shown to be active in NH_3 SCR of NO_x and studies, were conducted on Fe supported on pillared clays and mixed oxides, showed promising results. [101, 102, 110, 174]. More recently, Fe exchanged zeolites have been studied as catalysts for NH_3 SCR of NO_x [100, 105-107, 109, 175, 176]. Although high SCR activity has been reported, the hydrothermal stability of zeolitic supports is still a limiting factor. Iron supported on beta zeolite has been shown to be one of the most promising zeolite catalysts that possess good resistance to hydrothermal aging [177].

Recently, a 1.4 mol% $Fe/WO_3/ZrO_2$ catalyst was shown to be active in NH_3 SCR by [148] where the emphasis was on the effect of varying the exhaust gas mixture. Based on these findings, our aim was to investigate the possibility of using tungsten zirconia as a catalyst support with iron as the active metal for NH_3 SCR of NO_x with iron supported on beta zeolite as the reference material. The effect of iron loading on SCR activity was studied and the acidity of the samples was examined to determine if it was linked to SCR activity which has not been done for $Fe/WO_3/ZrO_2$ catalysts to date.

2. Experimental

2.1. Catalyst synthesis

The catalysts were prepared by incipient wetness impregnation method using iron nonahydrate ($FeN_3O_9{\cdot}9H_2O$, Fluka). Tungsten zirconia (9 wt% WO_3/ZrO_2) and beta zeolite (SiO_2/Al_2O_3 = 75) were used as the catalytic supports. The samples were dried for 24 h at room temperature before calcination. The samples were heated at a rate of 5 °C/min to 600 °C under 100 ml/min flowing dried air, held at 600 °C for 2 h then cooled at a rate of 5 °C/min to room temperature. Four iron promoted tungsten zirconia catalysts were synthesised with iron loadings of 0.5, 2, 3 and 10 wt% iron. These catalyst are defined as $xFe/WO_3/ZrO_2$, where x stands for Fe loading (wt%). The content of iron in beta catalysts was 0.5 wt% and 2 wt%. These catalysts are defined as 0.5Fe/beta and 2Fe/beta catalysts, respectively.

2.2. FT-IR characterization

The number and type of acid sites whether it was Broensted acid sites (BAS) or Lewis acid sites (LAS) in the catalysts was characterized by in situ Fourier transform infrared (FT-IR) spectroscopy using pyridine. The pyridine adsorption studies were carried out using a Bruker Equinox 55 FT-IR spectrometer at a resolution of 4 cm^{-1}. The samples were pressed into self supporting disks weighing 10-20 mg and placed in the sample holder. The samples were then heated in situ from room temperature to 350 °C at a heating rate of 1 °C/min under vacuum. The samples were kept at 350 °C for 2 h then cooled to 100 °C. Pyridine was introduced in 0.02 μL increments until the sample was saturated; the IR spectra were taken after each pyridine injection for assessment of the total acidity of the sample. Desorption of pyridine was studied by heating the sample to 200, 250, 300 and 350 °C.

2.3. Catalytic testing

Selective catalytic reduction of NO_x with NH_3 was studied in a fixed bed continuous flow reactor. The catalysts were pressed into pellets, crushed and sieved in a mesh size of 250-350

μm, then charged into an inconel tube (i.d. 8 mm) and fixed with quartz wool. The catalyst samples (0.3 g) were heated from 150 to 600 °C at a rate of 5 °C/min in reactant mixture of 12% O_2, 5% CO_2, 10% H_2O (steam), 100 ppm NH_3 and 100 ppm NO with a total flow of 2 L/min. A blank test with cordierite instead of the catalysts was run before each series of samples were tested.

3. Results

3.1. Fresh catalysts

Fig. 1 demonstrates that tungsten zirconia support without iron is not active for NH_3 SCR of NO_x. However, when a small amount of iron (0.5 wt%) is introduced, the iron promoted tungsten zirconia catalyst shows promising high temperature activity similar to that exhibited by 0.5Fe/beta (Fig. 1). Iron beta catalysts have been shown to be active in NH_3 SCR of NO_x and are commonly used as a reference material in comparison to other zeolite catalysts [147, 178, 179]. On this basis, the SCR activity of iron promoted tungsten zirconia is compared in this work to Fe/beta zeolite.

The 0.5Fe/WO_3/ZrO_2 catalyst has very poor low temperature activity that lights off at ~300 °C and increases to about 75 % NO_x conversion at 425 °C. In comparison, 0.5Fe/beta lights off at ~200 °C and reaches 95 % NO_x conversion at ~300 °C. However, the activity of 0.5Fe/beta catalyst gradually declines with increasing temperature and is very similar to the activity of 0.5Fe/WO_3/ZrO_2 catalyst at temperatures between 450 – 550 °C. These results possibly suggest that Fe/beta may lack selectivity at high temperatures which does not occur with 0.5Fe/WO_3/ZrO_2 catalyst. However, this could also mean that 0.5Fe/WO_3/ZrO_2 catalyst is unselective in NH_3 SCR of NO_x.

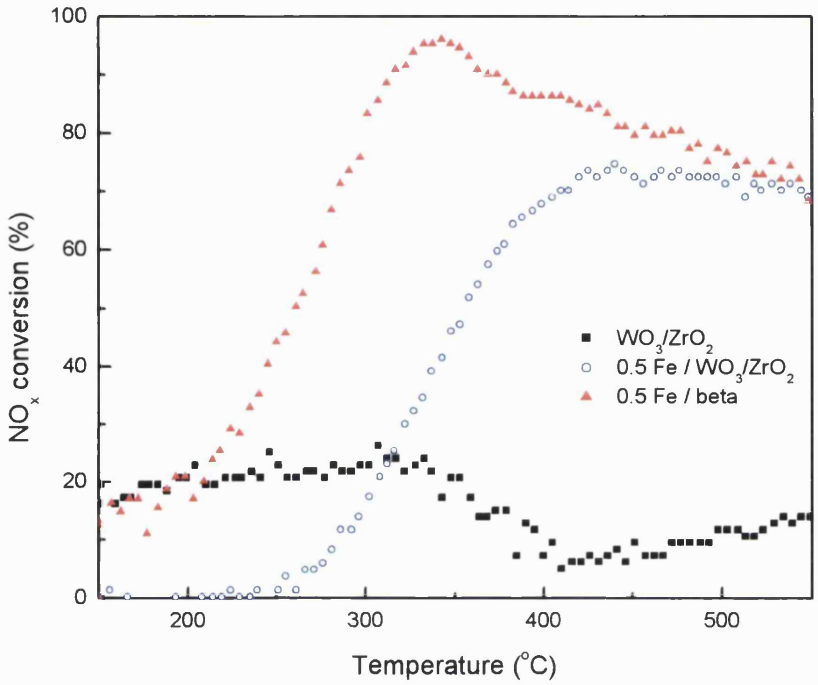

Fig. 1. Effect of temperature on NO_x conversion over WO_3/ZrO_2, $0.5Fe/WO_3/ZrO_2$ and 0.5Fe/beta catalysts.

The iron loading on WO_3/ZrO_2 support was varied to examine its effect on NH_3 SCR activity. Four different iron promoted tungsten zirconia catalysts with iron loadings of 0.5, 2, 3 and 10 wt% were tested and the results are shown in Fig. 2. The activity increased steadily as iron loading was increased from 0.5 to 3 wt%, and a drop in catalytic activity was observed with the $10Fe/WO_3/ZrO_2$ catalyst in comparison to the $3Fe/WO_3/ZrO_2$ one. The most significant difference in the SCR activity between the four $Fe/WO_3/ZrO_2$ catalysts is observed in the low temperature region, whereas the high temperature activity is quite similar for all four catalysts.

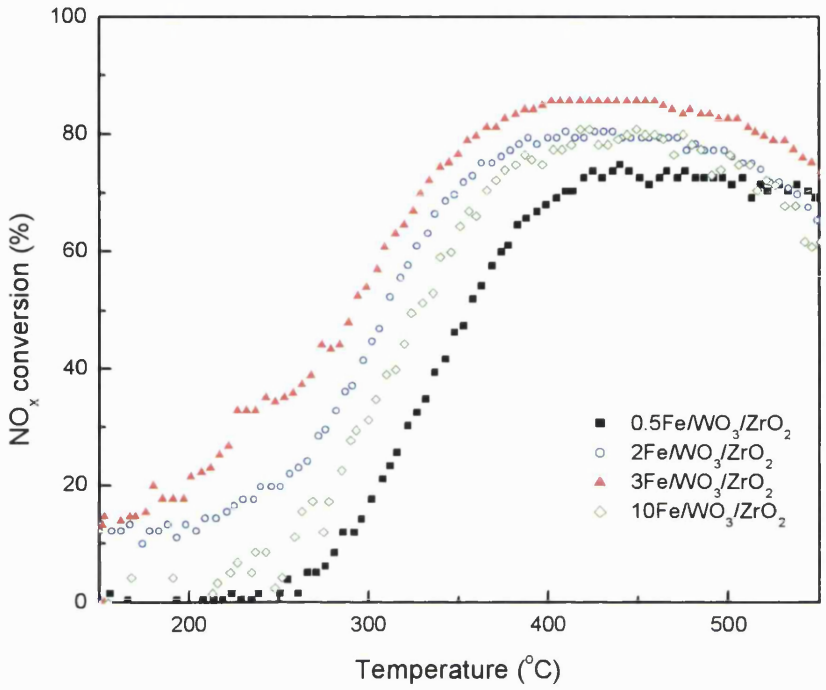

Fig. 2. Effect of temperature on NO_x conversion over four $Fe/WO_3/ZrO_2$ catalysts with different iron loading.

An essential improvement in the catalytic activity in the low temperature region was found when the iron loading was 2 or 3 wt% in comparison to the $0.5Fe/WO_3/ZrO_2$ catalyst. The improvement in SCR activity would have been due to the larger number of mononuclear Fe sites as the loading was increased from 0.5wt% to 3wt%. It has been shown that mononuclear Fe sites are active for NH_3 SCR of NO_x [104]. However, at loadings above 3 wt%, bulk iron species are expected to be formed and these iron oligomer/clusters have been shown to be unselective in NH_3 SCR [108, 180]. This expectation is supported by the lower activity exhibited by $10Fe/WO_3/ZrO_2$ catalyst in comparison to $3Fe/WO_3/ZrO_2$ one (Fig. 2).

3.2. Aged catalysts

The catalysts were aged under 10 % steam at 650 °C for 65 h and the activity was compared against the fresh catalysts. Only the results for $2Fe/WO_3/ZrO_2$ catalyst are shown in Fig. 3 for brevity, similar results were found with the other 3 catalysts with different iron loading.

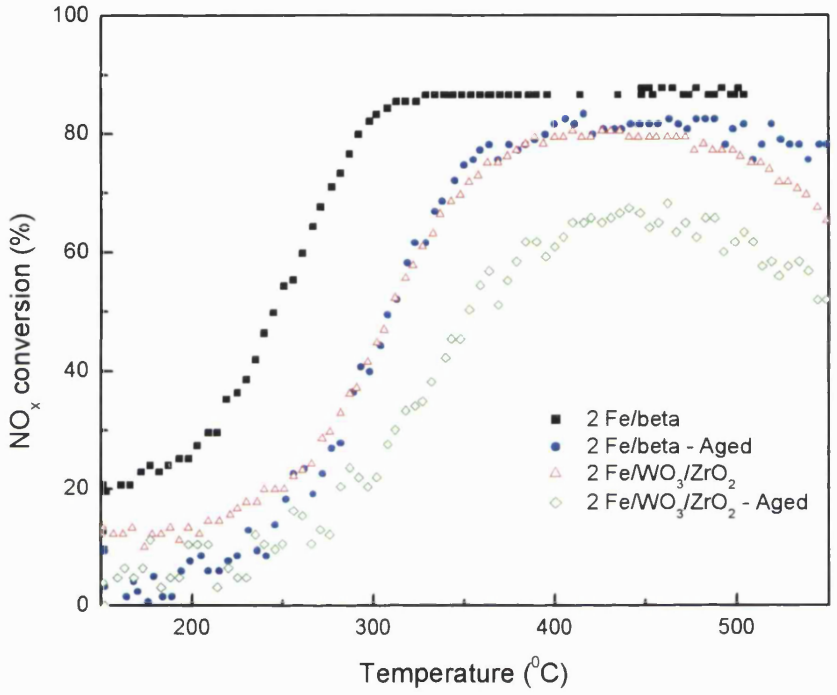

Fig. 3. Comparison of NO_x conversion over fresh and aged $2Fe/WO_3/ZrO_2$ and 2Fe/beta catalysts.

A significant drop in catalytic activity was found in the low temperature region after 2Fe/beta catalyst was aged, but the high temperature activity remains comparable to that of the fresh catalyst. Although, the activity of fresh $2Fe/WO_3/ZrO_2$ catalyst is similar to that of the aged 2Fe/beta catalyst, only a slight decrease in low temperature SCR activity was seen with $2Fe/WO_3/ZrO_2$ catalyst.

The difference in NO_x conversion between the fresh and aged catalysts at 250 °C was ~10 % for $2Fe/WO_3/ZrO_2$ compared to ~30 % with the 2Fe/beta catalyst. The activity of aged $2Fe/WO_3/ZrO_2$ at temperatures above 325 °C begins to drop uniformly by approximately 15 % in comparison to the fresh catalyst. These results show that $2Fe/WO_3/ZrO_2$ catalyst is hydrothermally stable as it is still active after the severe aging conditions used in this work.

3.3. Acidity

The IR spectra of WO_3/ZrO_2, $0.5Fe/WO_3/ZrO_2$ and $2Fe/WO_3/ZrO_2$ were recorded with pyridine as a probe molecule to investigate the acidity if the catalysts. The initial spectra are subtracted from the spectra when the catalysts have been saturated with pyridine in order for the IR peaks associated with pyridine adsorbed onto BAS or LAS to be seen clearly. The IR spectra of the three different catalysts were normalised by the catalyst disk weight and are presented in Fig. 4.

The IR peaks can be assigned to pyridine adsorbed on either BAS or LAS, 1541 cm^{-1} (BAS), 1490 cm^{-1} (BAS & LAS) and 1449 / 1446 cm^{-1} (LAS) [29, 143]. The IR peak assigned to pyridine adsorbed on LAS of WO_3/ZrO_2 is shifted from 1449 cm^{-1} to 1446 cm^{-1} after iron is introduced. This peak shift is seen with both $0.5Fe/WO_3/ZrO_2$ and $2Fe/WO_3/ZrO_2$ catalysts that indicates a change in the type of LAS has occurred due to the presence of iron.

The peak intensities of pyridine adsorbed on LAS (1446 / 1449 cm^{-1}) and BAS (1541 cm^{-1}) of $0.5Fe/WO_3/ZrO_2$ and $2Fe/WO_3/ZrO_2$ were compared against WO_3/ZrO_2. The peak intensities are shown in Table 1 relative to that of WO_3/ZrO_2. The 1541 cm^{-1} peak intensity is similar between $0.5Fe/WO_3/ZrO_2$ and WO_3/ZrO_2 catalysts but a 20 % reduction was found with the $2Fe/WO_3/ZrO_2$ catalyst. This represents a similar 20% drop in the number of BAS in $2Fe/WO_3/ZrO_2$ compared to the parent WO_3/ZrO_2 support.

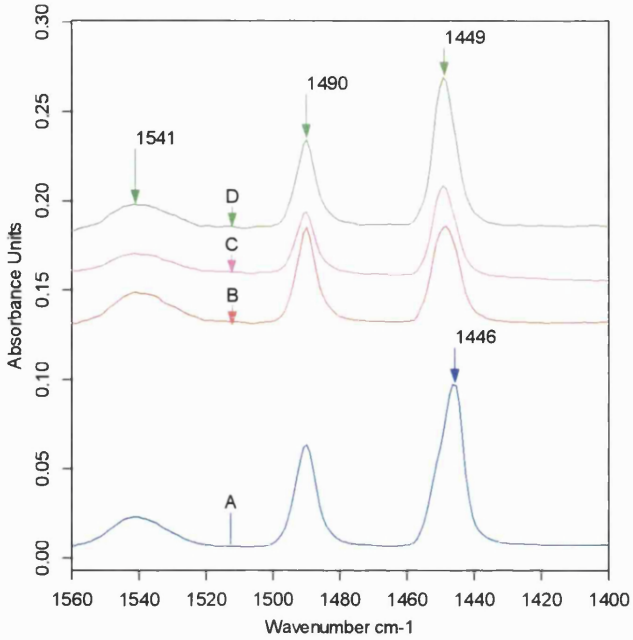

Fig. 4. IR spectra (Py region) of (A) WO_3/ZrO_2, (B) $0.5Fe/WO_3/ZrO_2$ and (C) $2Fe/WO_3/ZrO_2$ catalysts. The IR spectra were normalised by the sample disk weight.

The 1446 / 1449 cm^{-1} peak intensity associated with pyridine on LAS decreases by around 40 % when comparing the WO_3/ZrO_2 and $0.5Fe/WO_3/ZrO_2$ catalysts. However, there is a strong possibility that iron has generated new LAS as suggested in the literature [97, 98] based on the peak shift from 1446 to 1449 cm^{-1}. The new LAS generated by Fe can be linked to the NH_3 SCR of NO_x activity as the $0.5Fe/WO_3/ZrO_2$ and $2Fe/WO_3/ZrO_2$ catalysts are both active whereas WO_3/ZrO_2 is not (Fig. 1). Furthermore, an increase in the number of Fe^{3+} LAS seen with the $2Fe/WO_3/ZrO_2$ leads to a better SCR activity.

Table 1

The associated LAS and BAS peak intensities expressed as a ratio of the peak intensity of WO_3/ZrO_2 catalyst.

Catalyst	1446 / 1449 cm^{-1} (LAS)	1541 cm^{-1} (BAS)
WO_3/ZrO_2	1	1
$0.5Fe/WO_3/ZrO_2$	0.6	1.1
$2Fe/WO_3/ZrO_2$	0.9	0.8

The spectra (Fig. 5) of two tungsten zirconia with different tungsten oxide loading was compared to check if the peak shift is associated with a change in the tungsten species or due to iron. No peak shift from 1446 cm^{-1} to 1449 cm^{-1} was found when the tungsten oxide loading was increased from 9 wt% to 15 wt%.

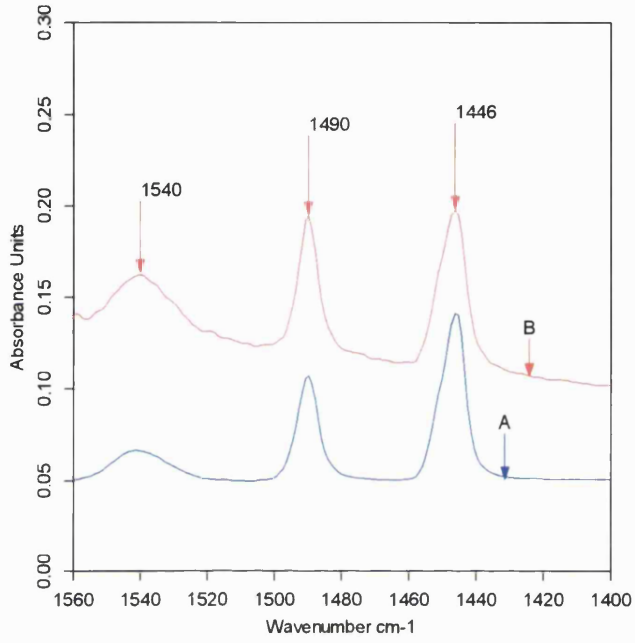

Fig. 5. IR spectra (Py region) of (A) 9 wt% WO_3/ZrO_2 and (B) 15 wt% WO_3/ZrO_2 catalysts. The IR spectra were normalised by the sample disk weight.

The pyridine TPD profiles are presented in Fig. 6 where the results show the strength of BAS and LAS are enhanced when iron is introduced. In particular, a significant increase in the BAS strength was found. These results are similar to that reported by [122] where a small amount of iron was found to enhance the acid site strength.

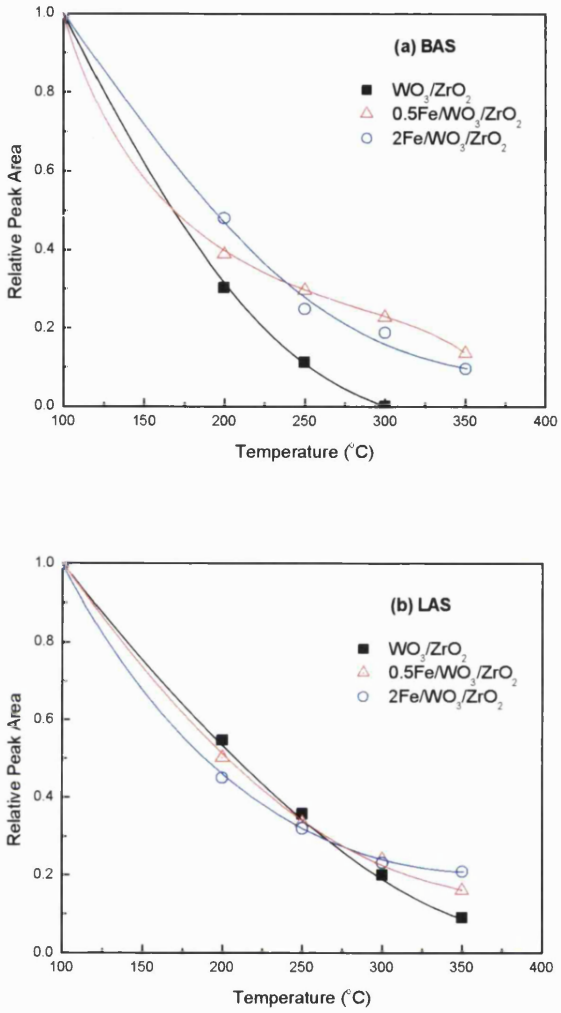

Fig. 6. Pyridine TPD profiles of WO_3/ZrO_2, $0.5Fe/WO_3/ZrO_2$ and $2Fe/WO_3/ZrO_2$ catalysts on either (a) BAS or (b) LAS.

4. Discussion

Fig. 2 clearly shows that iron promoted tungsten zirconia is both active and stable for ammonia SCR of NO_x. Tungsten zirconia is already known to be both an acidic and thermally stable support [75, 122, 181]; the results here have shown that tungsten zirconia is also hydrothermally stable which is a problem encountered by other supports. It is not immediately clear as to the

reasons why iron promoted tungsten zirconia is active, although the presence of iron will generally lead to an active catalyst. No crystalline iron phases were detected by XRD of $0.5Fe/WO_3/ZrO_2$ and only the tetragonal and monoclinic phases of zirconia was found. This would suggest that iron is well dispersed on tungsten zirconia. The NH_3 SCR activity could be due to the presence of the finely dispersed iron atoms [176]. When iron loading is too high where bulk iron species start to form, a drop in activity was found due to poorer dispersion of iron particles. This is supported by the results in Fig. 2, where a drop in activity was found with the $10Fe/WO_3/ZrO_2$ catalyst.

The acidity of the catalysts was examined to investigate if acidity played an essential role in the NH_3 SCR of NO_x activity. It has been suggested that iron can generate new LAS when introduced onto a zirconia based support [97, 98]. This is supported by the IR spectra of pyridine adsorption (Fig. 4) where a clear peak shift from 1449 cm^{-1} to 1446 cm^{-1} occurred which was not caused by changes of the tungsten species (Fig. 5). Furthermore, the pyridine TPD results (Fig. 6) suggest that new LAS were formed based on the increase in the LAS strength of iron impregnated catalysts. The LAS on tungsten zirconia are generally attributed to any remaining free Zr^{4+} sites that are not occupied by tungstate species whereas the BAS are associated with the polytungstate clusters on zirconia [73, 75, 84, 182]. When zirconium oxide is impregranted by tungsten, the tungstate species consumes the zirconium LAS generating new BAS [73, 134].

The overall effect of impregnating tungsten zirconia with iron was an increase in both the BAS and LAS strength and a drop in the number of BAS. $0.5Fe/WO_3/ZrO_2$ and $2Fe/WO_3/ZrO_2$ catalysts have similar BAS and LAS strength despite the difference in iron loading, the small variation between the two catalysts seen in Fig 6 is within the range of experimental error. Iron generated new Fe^{3+} LAS that were active for NH_3 SCR of NO_x. An improvement in catalytic activity could be linked with higher numbers of Fe^{3+} LAS, where a non-linear relationship was found. The $2Fe/WO_3/ZrO_2$ catalyst has ~50 % more LAS compared to $0.5Fe/WO_3/ZrO_2$ but there is only an improvement of around 10-15 % in SCR activity. These results support the mechanism proposed by [148] which is based on the presence of the Lewis acid Fe^{3+} sites. However, the experiments were carried out at 100 °C to eliminate any physi-sorbed pyridine. It

is possible that iron has generated numerous weak acid sites which are not sufficiently acidic to maintain adsorbed pyridine at 100 °C that would not be accounted for in our experiments.

It has been reported that there is a strong iron-zirconia interaction [183] therefore, it seems likely that iron will preferentially interact with any remaining free Zr^{4+} sites instead of the tungstate species. The results in Table 1 support this idea as the number of LAS reduces initially before any changes in the number of BAS occur. The Fe species occupies the Zr^{4+} sites that generate the LAS associated with the peak at 1446 cm^{-1} leading to the formation of a smaller number of new Fe^{3+} LAS (1449 cm^{-1}) that are active for NH_3 SCR. Increasing the iron loading generates more new Fe^{3+} LAS that in turn increases the overall catalytic activity of the catalysts.

Initially, at low iron loading (0.5 wt% Fe), there is no change in the number of BAS, however, at higher iron loadings a drop in the number of BAS occurs. This is likely to take place as all the free Zr^{4+} sites are occupied by Fe and at higher Fe loading excess free Fe species will be present. This could lead to either the excess iron interacting directly with tungsten species or iron aggregating into larger clusters that begins to interfere with nearby WO_3 sufficiently to cause a decrease in the number of BAS. This perturbation of the tungsten-zirconia interaction also leads to an increase in the BAS strength caused by the Fe species occupying nearby free Zr^{4+} LAS. The Fe species may possibly interact with the tungstate clusters as well. The presence of tungsten may also influence the SCR activity as it has been shown to play a role in SCR activity on other mixed oxide catalysts primarily by increasing the selectivity for nitrogen[119, 167].

5. Conclusions

Iron promoted tungsten zirconia has been shown to be a stable and active catalyst for NH_3 SCR of NO_x. The SCR activity can be linked to the formation of new Fe^{3+} LAS where an increase in number of LAS leads to better catalytic activity. The LAS and BAS strength were also enhanced by introducing iron on tungsten zirconia. The good iron dispersion and presence of tungsten could also contribute to the SCR activity of $Fe/WO_3/ZrO_2$ catalysts.

Acknowledgements

We thank Johnson Matthey Technology Centre and the Department of Chemical Engineering, University of Bath for financial support. Johnson Matthey Technology Centre for permission to publish the results obtained.

References

1. L.J. Alemany, F. Berti, G. Busca, G. Ramis, D. Robba, G.P. Toledo, and M. Trombetta, Applied Catalysis B: Environmental 10 (1996) p. 299.
2. J.P. Chen, R.T. Yang, M.A. Buzanowski, and J.E. Cichanowicz, Industrial & Engineering Chemistry Research 29 (1990) p. 1431.
3. P. Fabrizioli, T. Burgi, and A. Baiker, Journal of Catalysis 206 (2002) p. 143.
4. L. Singoredjo, R. Korver, F. Kapteijn, and J. Moulijn, Applied Catalysis B: Environmental 1 (1992) p. 297.
5. M. Hino and K. Arata, Journal of the Chemical Society, Chemical Communications (1987) p. 1259.
6. F.T.T. Ng and N. Horvat, Applied Catalysis A: General 123 (1995) p. L197.
7. Chen F. R., Coudurier G., Joly J. F., and Vedrine J. C., Journal of Catalysis 143 (1993) p. 616.
8. Srinivasan R., Keogh R. A., Milburn D. R., and Davis B. H., Journal of Catalysis (1995) p. 123.
9. D.G. Barton, S.L. Soled, G.D. Meitzner, G.A. Fuentes, and E. Iglesia, Journal of Catalysis 181 (1999) p. 57.
10. K. Arata, Applied Catalysis A: General 146 (1996) p. 3.
11. J.C. Vartuli, J.G. Santiesteban, P. Traverso, N. Cardona-Martinez, C.D. Chang, and S.A. Stevenson, Journal of Catalysis 187 (1999) p. 131.
12. K. Shimizu, T.N. Venkatraman, and W. Song, Applied Catalysis A: General 224 (2002) p. 77.
13. S. De Rossi, G. Ferraris, M. Valigi, and D. Gazzoli, Applied Catalysis A: General 231 (2002) p. 173.

14. D.G.B. E. Iglesia, S.L. Soled, S.Miseo, J.E. Baumgartner, W.E. Gates, G.A Fuentes and G.D. Meitzner, 11th International Congress on Catalysis 40th anniversary proceedings of the 11th ICC, Amsterdam, 1996
15. K. Arata and M. Hino, 9th International Congress on Catalysis, Calgary, Proceedings, in 9th International Congress on Catalysis, Calgary, 1988. p. 1727.
16. J.G. Santiesteban, J.C. Vartuli, S. Han, R.D. Bastian, and C.D. Chang, Journal of Catalysis 168 (1997) p. 431.
17. S. Kuba, P. Lukinskas, R.K. Grasselli, B.C. Gates, and H. Knozinger, Journal of Catalysis 216 (2003) p. 353.
18. T. Li, S.T. Wong, M.-C. Chao, H.P. Lin, C.Y. Mou, and S. Cheng, Applied Catalysis A: General 261 (2004) p. 211.
19. R.Q. Long and R.T. Yang, Applied Catalysis B: Environmental 27 (2000) p. 87.
20. R.Q. Long and R.T. Yang, Journal of Catalysis 186 (1999) p. 254.
21. Ramis G., Yi L., Busca G., Turco M., Kotur E., and Willey R. J., Journal of Catalysis (1995) p. 523.
22. R.J. Willey, H. Lai, and J.B. Peri, Journal of Catalysis 130 (1991) p. 319.
23. R.Q. Long and R.T. Yang, Journal of Catalysis 207 (2002) p. 274.
24. G. Delahay, M. Mauvezin, B. Coq, and S. Kieger, Journal of Catalysis 202 (2001) p. 156.
25. H. Sjovall, L. Olsson, E. Fridell, and R.J. Blint, Applied Catalysis B: Environmental 64 (2006) p. 180.
26. M.S. Kumar, M. Schwidder, W. Grunert, and A. Bruckner, Journal of Catalysis (2004) p. 384.
27. G. Qi and R.T. Yang, Applied Catalysis B: Environmental 60 (2005) p. 13.
28. M. Schwidder, M.S. Kumar, K. Klementiev, M.M. Pohl, A. Bruckner, and W. Grunert, Journal of Catalysis (2005) p. 314.
29. G. Delahay, D. Valade, A. Guzman-Vargas, and B. Coq, Applied Catalysis B: Environmental 55 (2005) p. 149.
30. K. Rahkamaa-Tolonen, T. Maunula, M. Lomma, M. Huuhtanen, and R.L. Keiski, Catalysis Today (2005) p. 217.
31. N. Apostolescu, B. Geiger, K. Hizbullah, M.T. Jan, S. Kureti, D. Reichert, F. Schott, and W. Weisweiler, Applied Catalysis B: Environmental 62 (2006) p. 104.

32. B. Coq, M. Mauvezin, G. Delahay, J.-B. Butet, and S. Kieger, Applied Catalysis B: Environmental (2000) p. 193.
33. R.Q. Long and R.T. Yang, Journal of Catalysis (2002) p. 274.
34. K. Rahkamaa-Tolonen, T. Maunula, M. Lomma, M. Huuhtanen, and R.L. Keiski, Catalysis Today, Catalysis for a Sustainable Future, 11th Nordic Symposium on Catalysis 100 (2005) p. 217.
35. M. Schwidder, M.S. Kumar, K. Klementiev, M.M. Pohl, A. Bruckner, and W. Grunert, Journal of Catalysis 231 (2005) p. 314.
36. M.S. Kumar, M. Schwidder, W. Grunert, and A. Bruckner, Journal of Catalysis 227 (2004) p. 384.
37. M. Scheithauer, E. Bosch, U.A. Schubert, H. Knozinger, T.-K. Cheung, F.C. Jentoft, B.C. Gates, and B. Tesche, Journal of Catalysis 177 (1998) p. 137.
38. E.P. Parry, Journal of Catalysis 2 (1963) p. 371.
39. G. Busca, Physical Chemistry Chemical Physics 1 (1999) p. 723.
40. F.C. Jentoft, A. Hahn, J. Krohnert, G. Lorenz, R.E. Jentoft, T. Ressler, U. Wild, R. Schlogl, C. Ha[ss]ner, and K. Kohler, Journal of Catalysis 224 (2004) p. 124.
41. T. Loften, N.S. Gnep, M. Guisnet, and E.A. Blekkan, Catalysis Today Catalysis for a Sustainable Future, 11th Nordic Symposium on Catalysis 100 (2005) p. 397.
42. J.H.a.Y.C. Weijie Ji, Catalysis Letters (1988) p. 15.
43. M. Scheithauer, T.-K. Cheung, R.E. Jentoft, R.K. Grasselli, B.C. Gates, and H. Knozinger, Journal of Catalysis 180 (1998) p. 1.
44. C.D. Baertsch, S.L. Soled, and E. Iglesia, Journal of Physical Chemistry B 105 (2001) p. 1320.
45. C.D. Baertsch, K.T. Komala, Y.-H. Chua, and E. Iglesia, Journal of Catalysis 205 (2002) p. 44.
46. T.N. Vu, J. van Gestel, J.P. Gilson, C. Collet, J.P. Dath, and J.C. Duchet, Journal of Catalysis 231 (2005) p. 453.
47. E. Guglielminotti, Journal of physical chemistry (1994) p. 4884.
48. J.P. Chen and R.T. Yang, Applied Catalysis A: General 80 (1992) p. 135.